Goswami, D.Y.; et. al. "Energy Conversion"
Mechanical Engineering Handbook
Ed. Frank Kreith
Boca Raton: CRC Press LLC, 1999

Energy Conversion

D. Yogi Goswami
Univeristy of Florida
Lawrence Conway
Westinghouse Electric Corporation
Steven I. Freedman
Gas Research Institute
David E. Klett
North Carolina A&T State University
Elsayed M. Afify
North Carolina State University
Roger E. A. Arndt
University of Minnesota
William B. Stine
California State Polytechnic University
Anthony F. Armor
Electric Power Research Institute
Chand K. Jotshi
University of Florida
Roberto Pagano (deceased)
University of Florida
James S. Tulenko
University of Florida
Thomas E. Shannon
University of Tennessee
Dale E. Berg
Sandia National Laboratories
Carl J. Bliem (deceased)
CJB Consulting
Gregory L. Mines
Idaho National Engineering Laboratory
Kitt C. Reinhardt
Wright Laboratory, United States Air Force

Mysore L. Ramalingam
UES, Inc.
Jean-Pierre Fleurial
Jet Propulsion Laboratory/California Institute of Technology
William D. Jackson
HMJ Corporation
Desikan Bharatban
National Renewable Energy Laboratory
Frederica Zangrando
National Renewable Energy Laboratory
William W. Bathie
Iowa State University
Howard T. Odum
University of Florida

8.1 Steam Power Plant

Lawrence Conway

Introduction

This section provides an understanding, at an overview level, of the steam power cycle. References were selected for the next level of study if required. There are noteworthy omissions in the section: site selection, fuel handling, civil engineering-related activities (like foundations), controls, and nuclear power.

Thermal power cycles take many forms, but the majority are fossil steam, nuclear, simple cycle gas turbine, and combined cycle. Of those listed, conventional coal-fired steam power is predominant. This is especially true in developing third-world countries that either have indigenous coal or can import coal inexpensively. These countries make up the largest new product market. A typical unit is shown in Figure 8.1.1.

The Rankine cycle is overwhelmingly the preferred cycle in the case of steam power and is discussed first.

Topping and bottoming cycles, with one exception, are rare and mentioned only for completeness. The exception is the combined cycle, where the steam turbine cycle is a bottoming cycle. In the developed countries, there has been a move to the combined cycle because of cheap natural gas or oil. Combined cycles still use a reasonably standard steam power cycle except for the boiler. The complexity of a combined cycle is justified by the high thermal efficiency, which will soon approach 60%.

The core components of a steam power plant are boiler, turbine, condenser and feedwater pump, and generator. These are covered in successive subsections.

The final subsection is an example of the layout/and contents of a modern steam power plant.

As a frame of reference for the reader, the following efficiencies/effectivenesses are typical of modern fossil fuel steam power plants. The specific example chosen had steam conditions of 2400 psia, 1000°F main steam temperature, 1000°F reheat steam temperature: boiler thermal 92; turbine/generator thermal 44; turbine isentropic 89; generator 98.5; boiler feedwater pump and turbine combined isentropic 82; condenser 85; plant overall 34 (Carnot 64).

Nuclear power stations are so singular that they are worthy of a few closing comments. Modern stations are all large, varying from 600 to 1500 MW. The steam is both low temperature and low pressure (~600°F and ~1000 psia), compared with fossil applications, and hovers around saturation conditions

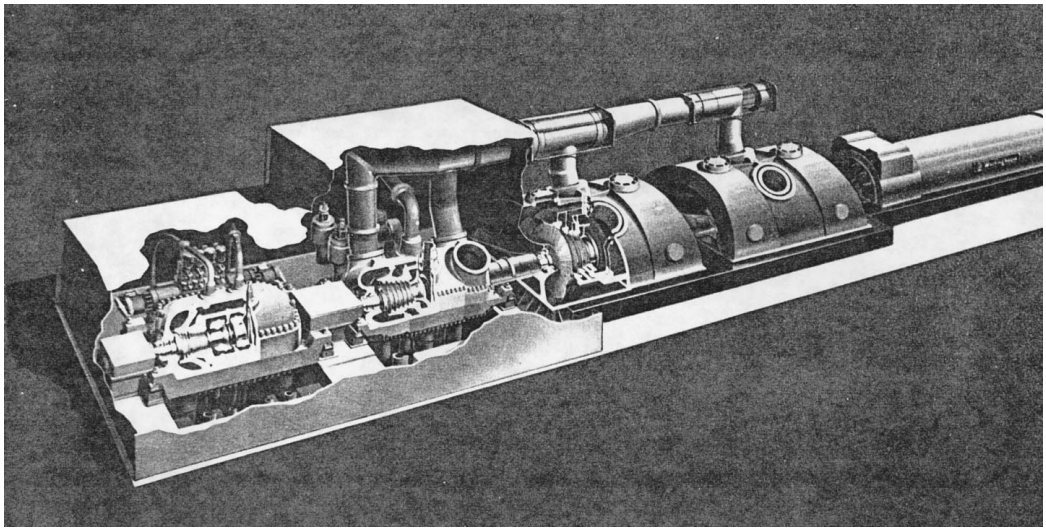

FIGURE 8.1.1 Modern steam turbine generator.

or is slightly superheated. Therefore, the boiler(s), superheater equivalent (actually a combined moisture separator and reheater), and turbines are unique to this cycle. The turbine generator thermal efficiency is around 36%.

Rankine Cycle Analysis

Modern steam power plants are based on the Rankine cycle. The basic, ideal Rankine cycle is shown in Figure 8.1.2. The ideal cycle comprises the processes from state 1:

1–2: Saturated liquid from the condenser at state 1 is pumped isentropically (i.e., $S_1 = S_2$) to state 2 and into the boiler.
2–3: Liquid is heated at constant pressure in the boiler to state 3 (saturated steam).
3–4: Steam expands isentropically (i.e., $S_3 = S_4$) through the turbine to state 4 where it enters the condenser as a wet vapor.
4–1: Constant-pressure transfer of heat in the condenser to return the steam back to state 1 (saturated liquid).

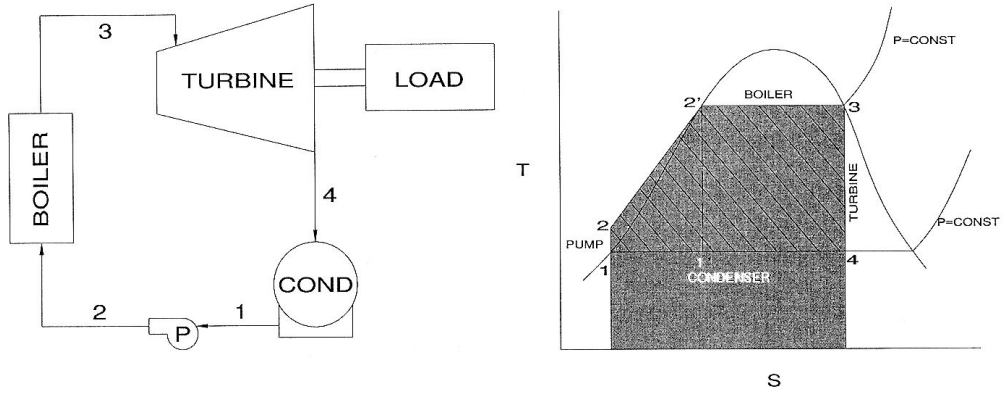

FIGURE 8.1.2 Basic Rankine cycle.

If changes in kinetic and potential energy are neglected, the total heat added to the rankine cycle can be represented by the shaded area on the T-S diagram in Figure 8.1.2, while the work done by this cycle can be represented by the crosshatching within the shaded area. The thermal efficiency of the cycle (η) is defined as the work (W_{NET}) divided by the heat input to the cycle (Q_H).

$$\eta = W_{NET}/Q_H = \left(h_3 - h_4\right)/\left(h_3 - h_2\right)$$

The Rankine cycle is preferred over the Carnot cycle for the following reasons:

The heat transfer process in the boiler has to be at constant temperature for the Carnot cycle, whereas in the Rankine cycle it is superheated at constant pressure. Superheating the steam can be achieved in the Carnot cycle during heat addition, but the pressure has to drop to maintain constant temperature. This means the steam is expanding in the boiler while heat added which is not a practical method.

The Carnot cycle requires that the working fluid be compressed at constant entropy to boiler pressure. This would require taking wet steam from point 1′ in Figure 8.1.2 and compressing it to saturated liquid condition at 2′. A pump required to compress a mixture of liquid and vapor isentropically is difficult to design and operate. In comparison, the Rankine cycle takes the saturated liquid and compresses it to boiler pressure. This is more practical and requires much less work.

The efficiency of the Rankine cycle can be increased by utilizing a number of variations to the basic cycle. One such variation is superheating the steam in the boiler. The additional work done by the cycle is shown in the crosshatched area in Figure 8.1.3.

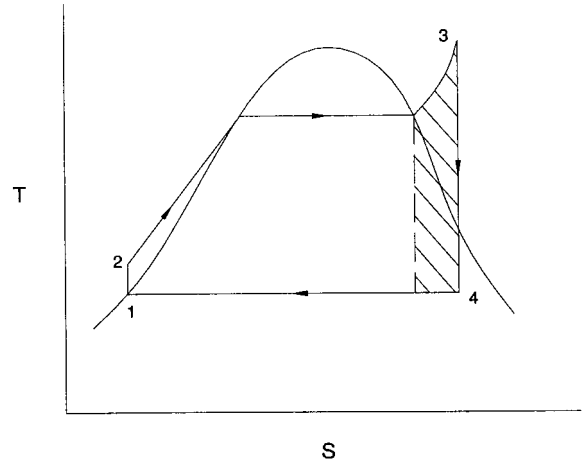

FIGURE 8.1.3 Rankine cycle with superheat.

The efficiency of the Rankine cycle can also be increased by increasing the pressure in the boiler. However, increasing the steam generator pressure at a constant temperature will result in the excess moisture content of the steam exiting the turbine. In order to take advantage of higher steam generator pressures and keep turbine exhaust moistures at safe values, the steam is expanded to some intermediate pressure in the turbine and then reheated in the boiler. Following reheat, the steam is expanded to the cycle exhaust pressure. The reheat cycle is shown in Figure 8.1.4.

Another variation of the Rankine cycle is the regenerative cycle, which involves the use of feedwater heaters. The regenerative cycle regains some of the irreversible heat lost when condensed liquid is pumped directly into the boiler by extracting steam from various points in the turbine and heating the condensed liquid with this steam in feedwater heaters. Figure 8.1.5 shows the Rankine cycle with regeneration.

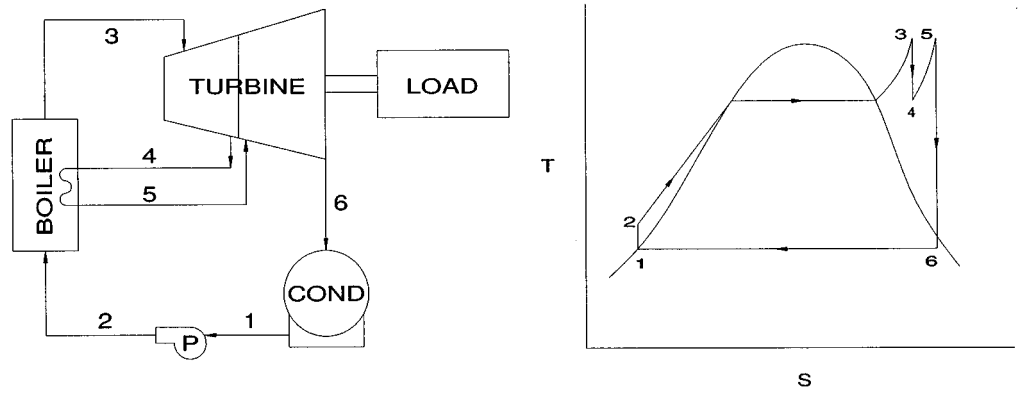

FIGURE 8.1.4 Rankine cycle with reheat.

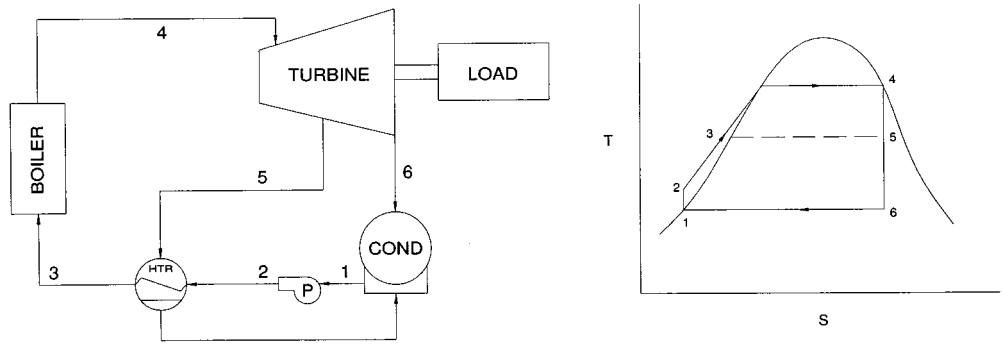

FIGURE 8.1.5 Rankine cycle with regeneration.

The actual Rankine cycle is far from ideal as there are losses associated with the cycle. They include the piping losses due to friction and heat transfer, turbine losses associated with steam flow, pump losses due to friction, and condenser losses when condensate is subcooled. The losses in the compression (pump) and expansion process (turbine) result in an increase in entropy. Also, there is lost energy in heat addition (boiler) and rejection (condenser) processes as they occur over a finite temperature difference.

Most modern power plants employ some variation of the basic Rankine cycle in order to improve thermal efficiency. For larger power plants, economies of scale will dictate the use of one or all of the variations listed above to improve thermal efficiency. Power plants in excess of 200,000 kW will in most cases have 300°F superheated steam leaving the boiler reheat, and seven to eight stages of feedwater heating.

References

Salisbury, J.K. 1950. *Steam Turbines and Their Cycles,* Reprint 1974. Robert K. Krieger Publishing, Malabar, FL.

Van Wylen, G.J. and Sonntag, R.E. 1986. *Fundamentals of Classical Thermodynamics,* 3rd ed., John Wiley & Sons, New York.

Topping and Bottoming Cycles

Steam Rankine cycles can be combined with topping and/or bottoming cycles to form binary thermodynamic cycles. These topping and bottoming cycles use working fluids other than water. Topping cycles change the basic steam Rankine cycle into a binary cycle that better resembles the Carnot cycle and improves efficiency. For conventional steam cycles, state-of-the-art materials allow peak working fluid temperatures higher than the supercritical temperature for water. Much of the energy delivered into the cycle goes into superheating the steam, which is not a constant-temperature process. Therefore, a significant portion of the heat supply to the steam cycle occurs substantially below the peak cycle temperature. Adding a cycle that uses a working fluid with a boiling point higher than water allows more of the heat supply to the thermodynamic cycle to be near the peak cycle temperature, thus improving efficiency. Heat rejected from the topping cycle is channeled into the lower-temperature steam cycle. Thermal energy not converted to work by the binary cycle is rejected to the ambient-temperature reservoir. Metallic substances are the working fluids for topping cycles. For example, mercury was used as the topping cycle fluid in the 40-MW plant at Schiller, New Hampshire. This operated for a period of time but has since been dismantled. Significant research and testing has also been performed over the years toward the eventual goal of using other substances, such as potassium or cesium, as a topping cycle fluid.

Steam power plants in a cold, dry environment cannot take full advantage of the low heat rejection temperature available. The very low pressure to which the steam would be expanded to take advantage of the low heat sink temperature would increase the size of the low-pressure (LP) turbine to such an extent that it is impractical or at least inefficient. A bottoming cycle that uses a working fluid with a vapor pressure higher than water at ambient temperatures (such as ammonia or an organic fluid) would enable smaller LP turbines to function efficiently. Hence, a steam cycle combined with a bottoming cycle may yield better performance and be more cost-effective than a stand-alone Rankine steam cycle.

Further Information

Fraas, A.P. 1982. *Engineering Evaluation of Energy Systems,* McGraw-Hill, New York.

Horlock, J.H. 1992. *Combined Power Plants, Including Combined Cycle Gas Turbine (CCGT) Plants,* Pergamon Press, Oxford.

Steam Boilers

A boiler, also referred to as a steam generator, is a major component in the plant cycle. It is a closed vessel that efficiently uses heat produced from the combustion of fuel to convert water to steam. Efficiency is the most important characteristic of a boiler since it has a direct bearing on electricity production.

Boilers are classified as either drum-type or once-through. Major components of boilers include an economizer, superheaters, reheaters, and spray attemperators.

Drum-Type Boilers

Drum-type boilers (Figure 8.1.6) depend on constant recirculation of water through some of the components of the steam/water circuit to generate steam and keep the components from overheating. Drum-type boilers circulate water by either natural or controlled circulation.

Natural Circulation. Natural circulation boilers use the density differential between water in the downcomers and steam in the waterwall tubes for circulation.

Controlled Circulation. Controlled circulation boilers utilize boiler-water-circulating pumps to circulate water through the steam/water circuit.

Once-Through Boilers

Once-through boilers, shown in Figure 8.1.7, convert water to steam in one pass through the system.

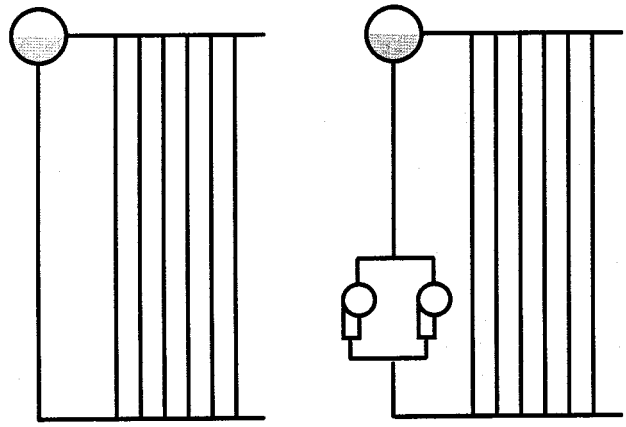

FIGURE 8.1.6 Drum boilers.

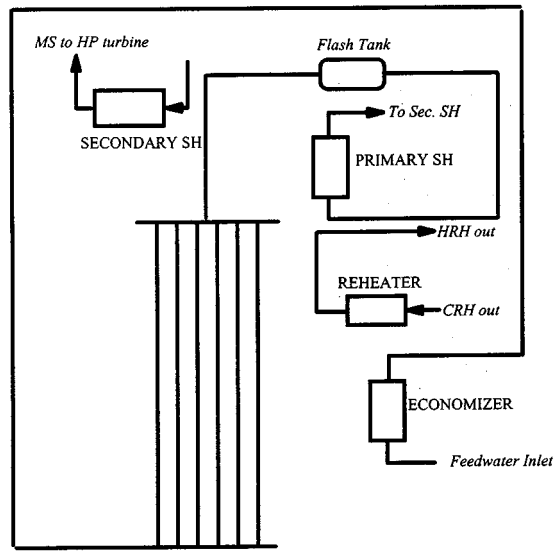

FIGURE 8.1.7 Once-through boilers.

Major Boiler Components

Economizer. The economizer is the section of the boiler tubes where feedwater is first introduced into the boiler and where flue gas is used to raise the temperature of the water.

Steam Drum (Drum Units Only). The steam drum separates steam from the steam/water mixture and keeps the separated steam dry.

Superheaters. Superheaters are bundles of boiler tubing located in the flow path of the hot gases that are created by the combustion of fuel in the boiler furnace. Heat is transferred from the combustion gases to the steam in the superheater tubes.

Superheaters are classified as primary and secondary. Steam passes first through the primary superheater (located in a relatively cool section of the boiler) after leaving the steam drum. There the steam receives a fraction of its final superheat and then passes through the secondary superheater for the remainder.

Reheaters. Reheaters are bundles of boiler tubes that are exposed to the combustion gases in the same manner as superheaters.

Spray Attemperators. Attemperators, also known as desuperheaters, are spray nozzles in the boiler tubes between the two superheaters. These spray nozzles supply a fine mist of pure water into the flow path of the steam to prevent tube damage from overheating. Attemperators are provided for both the superheater and reheater.

Steam Turbines

General

Each turbine manufacturer has unique features in their designs that impact efficiency, reliability, and cost. However, the designs appear similar to a non-steam-turbine engineer. Steam turbines for power plants differ from most prime movers in at least three ways. (1) All are extremely high powered, varying from about 70,000 to 2 million hp, and require a correspondingly large capital investment, which puts a premium on reliability. (2) Turbine life is normally between 30 and 40 years with minimal maintenance. (3) Turbines spend the bulk of their life at constant speed, normally 3600 or 1800 rpm for 60 Hz. These three points dominate the design of the whole power station, particularly of the steam turbine arrangement and materials.

In an earlier subsection it was shown that high steam supply temperatures make for more-efficient turbines. Even so, the range of steam conditions in modern service has narrowed because of these three points. Figure 8.1.8 shows the distribution of steam conditions of one manufacturer for turbines recently put in service. They are reasonably typical of the industry. This is one of the primary reasons that the steam turbines appear similar.

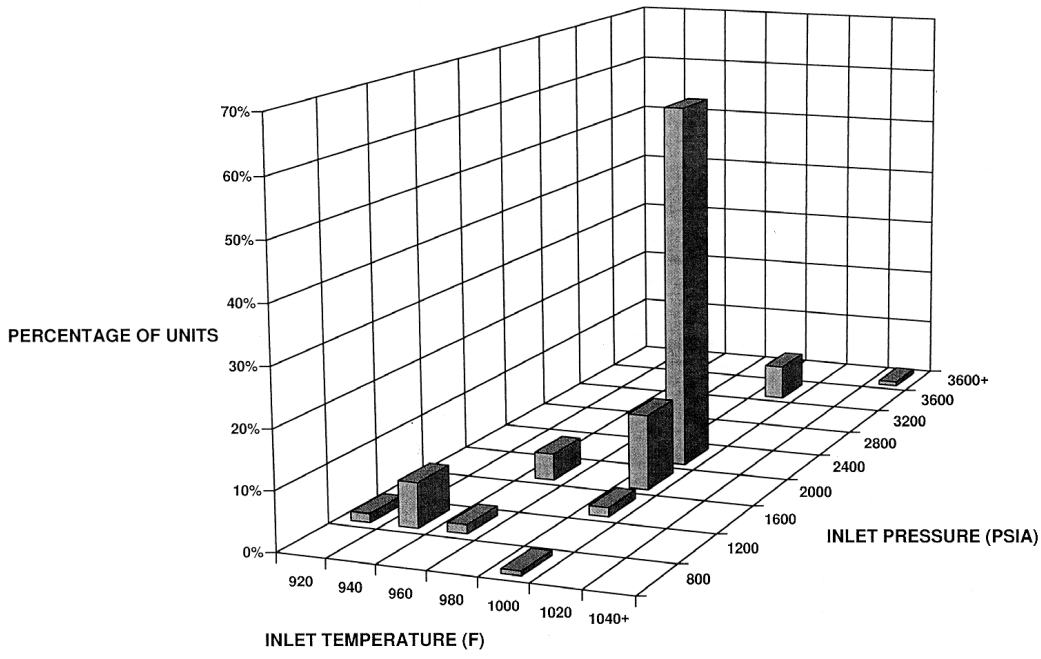

FIGURE 8.1.8 Steam turbine operating conditions.

Blading

The most highly stressed component in steam turbines are the blades. Blades are loaded by centrifugal and steam-bending forces and also harmonic excitation (from nonuniform circumferential disturbances

in the blade path). All blades are loaded by centrifugal and steam-bending loads, and, in general, blades are designed to run when the harmonic excitation is resonant with the natural modes of the blade. If harmonic excitation is permitted on very long blades, the blades become impractically big. Fortunately, as the turbine runs at constant speed, the blade modes can be tuned away from resonant conditions so that the harmonic loads are significantly reduced. This forms a split in blade design, commonly referred to as tuned and untuned blading.

Blades guide steam throughout the turbine in as smooth and collision-free a path as possible. Collisions with blades (incidence) and sudden expansions reduce the energy available for doing work. Until recently, designers would match flow conditions with radially straight blades (called parallel sided). Turbine physics does not recognize this convenience for several reasons. The most visually obvious is the difference in tangential velocity between blade hub and tip. Twisted blades better match the flow (and area) conditions. The manufacturing process was costly and this cost confined application to long blades. Now, with numerical control machine tools, twist is being spread throughout the turbine. Twisted blades are a two-dimensional adjustment for a three-dimensional steam flow. The latest blades address the full three-dimensional nature of the flow by curving in three dimensions (bowed blades). Examples of all three classes of blades are shown in Figure 8.1.9.

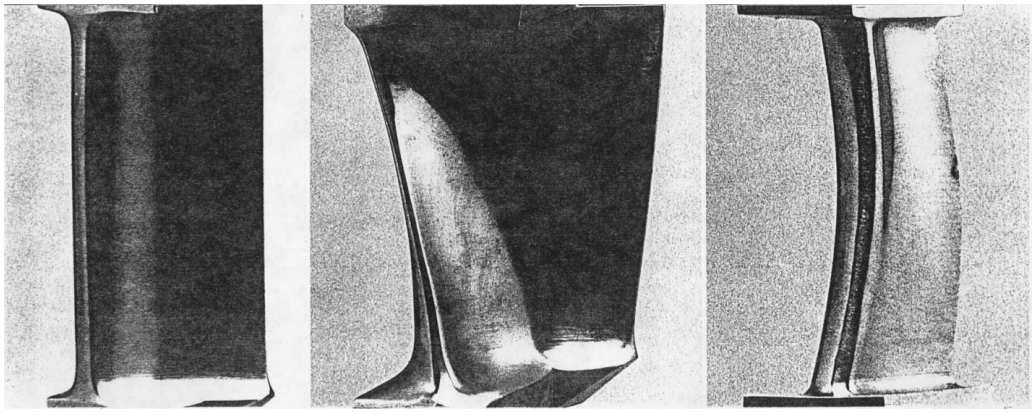

FIGURE 8.1.9 Typical steam turbine blades.

Rotors

After blades, steam turbine rotors are the second most critical component in the machine. Rotor design must account for (1) a large forging with uniform chemistry and properties in the high-strength alloys needed; (2) centrifugal force from the rotor itself and the increase from the centrifugal pull of the blades; (3) resistance to brittle fracture potentially occurring in the LP cylinder when the machine is at high speed, but the material is still not up to operational temperature; (4) creep of the high-pressure (HP) and intermediate-pressure (IP) rotors under steady high-temperature load. The life cycle is further complicated by the various transient fatigue loads occurring during load changes and start-up. Two further events are considered in rotor design: torsional and lateral vibrations caused by both harmonic steam and electrical loads. As with tuned blades, this is normally accommodated by tuning the primary modes away from running resonance.

Choosing the Turbine Arrangement

The turbine shaft would be too flexible in one piece if all the blades were to follow sequentially. It is therefore cut up into supportable lengths. The "cuts" in the shaft result in HP, IP, and LP cylinders. Manufacturers address the grouping of cylinders in many different ways, depending upon steam conditions. It is U.S. practice to combine HPs and IPs into one cylinder for the power range of about 250 to 600 MW (rare in the rest of the world). One manufacturer's grouping, shown in Figure 8.1.10, is fairly

representative of the industry. So far, the text has discussed the steam flow as though it expanded monotonically through the turbine. This is usually not the case for two reasons. The most common steam conditions, shown in Figure 8.1.10, would cause the steam exiting the last row of blades to be very wet and cause excessive erosion. Thermal efficiency can be raised by removing the steam from the turbine, reheating, and then returning it to the blade path; this increases the "average" heat supply temperature. The turbine position for reheat is normally between the HP and IP turbines.

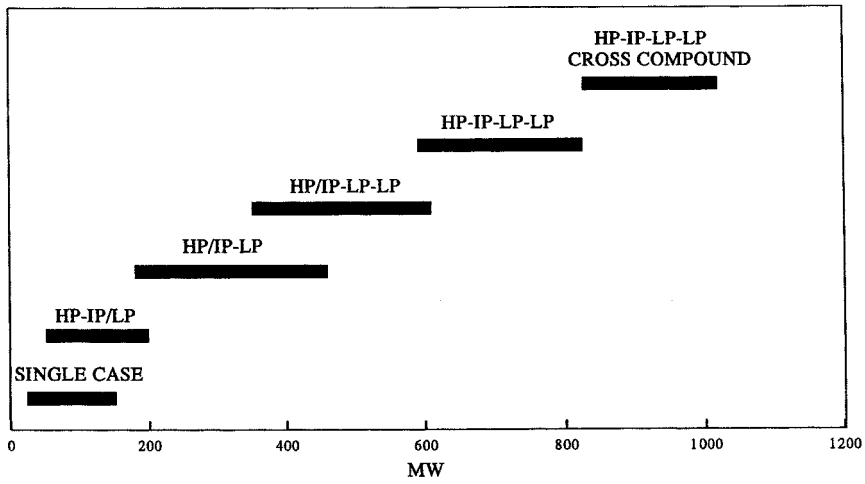

FIGURE 8.1.10 Steam turbine product combinations.

There is one further geometric arrangement. Cylinders need not be all on one shaft with a single generator at the end. A cross-compound arrangement exists in which the steam path is split into two separate parallel paths with a generator on each path. Commonly, the split will be with paths of HP-LP-generator and IP-LP-generator. Torsional and lateral vibration difficulties are more easily prevented with shorter trains, which make the foundation more compact. The primary shortcoming is the need for two generators and resultant controls.

Historically, steam turbines have been split into two classes, reaction and impulse, as explained in Basic Power Cycles. This difference in design makes an observable difference between machines. Impulse turbines have fewer, wider stages than reaction machines. As designs have been refined, the efficiencies and lengths of the machines are now about the same. For a variety of reasons, the longer blades in the LP ends are normally reaction designs. As each stage may now be designed and fabricated uniquely, the line between impulse and reaction turbines will probably disappear. Turbine blading is broadly split between machines as follows:

	Cylinder				
	HP			LP	
	Control Stage	Remainder	IP	Short Blades	End Blade(s)
Reaction turbines	Impulse	Reaction	Reaction	Reaction	Reaction
Impulse turbines	Impulse	Impulse	Impulse	Impulse	Reaction

Materials

Materials are among the most variable of all turbine parts with each manufacturer striving to improve performance by using alloying and heat-treatment techniques. It follows that accurate generalizations are difficult. Even so, the following is reasonably representative:

Item	Common Material Description								
High-temperature HP and IP blades	Moderate and cold temperature stator blades	Moderate temperature rotating blades	Cold LP rotating blades	High temperature rotors	Low temperature rotors	Hot	LP	High-temperature bolting	Cold bolting
Mod'd SS403	SS304	SS403	SS403 or 17/4 PH	1CrMoV, occasionally 12Cr	3.5 NiCrMoV	1.25Cr or 2.25Cr	Carbon, steel	SS422	B16

Cylinders and Bolting

These items are relatively straightforward, especially the LP cylinder, except for the very large sizes and precision required for the castings and fabrications. A large HP-IP cylinder has the temperature and pressure loads split between an inner and outer cylinder. In this case, finding space and requisite strength for the bolting presents a challenge for the designer.

Valves

The turbine requires many valves for speed control, emergency control, drains, hydraulics, bypasses, and other functions. Of these, there are four valves distinguished by their size and duty. They are throttle or stop, governor or control, reheat stop, and reheat interceptor.

The throttle, reheat stop, and reheat interceptor valves normally operate fully open, except for some control and emergency conditions. Their numbers and design are selected for the appropriate combination of redundancy and rapidity of action. The continuous control of the turbine is accomplished by throttling the steam through the governor valve. This irreversible process detracts from cycle efficiency. In some circumstances, the efficiency detraction is reduced by a combination of throttling and reducing the boiler pressure (normally called sliding pressure).

Further Information

Kutz, M. 1986. *Mechanical Engineers' Handbook,* John Wiley & Sons, New York.

Stodola, A. and Loewenstein, L.C. 1927. *Steam and Gas Turbines,* Reprint of 6th ed. 1945, Peter Smith, New York.

Japikse, D. and Nicholas, C.B. 1994. *Introduction to Turbomachinery,* Concepts ETI, Norwich, VT.

Heat Exchangers, Pumps, and Other Cycle Components

Heater Exchangers

Heaters. There are two classifications of condensate and feedwater heaters: the open or direct contact heater and the closed or tube-and-shell heater.

Open Heaters. In an open heater, the extraction or heating steam comes in direct contact with the water to be heated. While open heaters are more efficient than closed heaters, each requires a pump to feed the outlet water ahead in the cycle. This adds cost, maintenance, and the risk of water induction to the turbine, making the closed heater the preferred heater for power plant applications.

Closed Heaters. These employ tubes within a shell to separate the water from the heating steam (see Figure 8.1.11). They can have three separate sections where the heating of the feedwater occurs. First is the drain cooler section where the feedwater is heated by the condensing heating steam before cascading back to the next-lower-pressure heater. The effectiveness of the drain cooler is expressed as the drain cooler approach (DCA), which is the difference between the temperature of the water entering the heater and the temperature of the condensed heating steam draining from the heater shell. In the second section (condensing section), the temperature of the water is increased by the heating steam condensing around

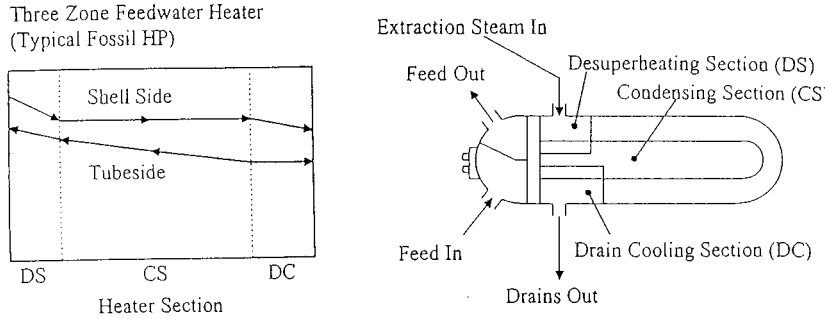

FIGURE 8.1.11 Shell and tube feedwater heater.

the tubes. In the third section (desuperheating section), the feedwater reaches its final exit temperature by desuperheating the extraction steam. Performance of the condensing and superheating sections of a heater is expressed as the terminal temperature difference (TTD). This is the difference between the saturation temperature of the extraction steam and the temperature of the feedwater exiting the heater. Desuperheating and drain cooler sections are optional depending on the location of the heater in the cycle (i.e., desuperheating is not necessary in wet extraction zones) and economic considerations.

The one exception is the deaerator (DA), which is an open heater used to remove oxygen and other gases that are insoluble in boiling water. The DA is physically located in the turbine building above all other heaters, and the gravity drain from the DA provides the prime for the boiler feed pump (BFP).

Two other critical factors considered in heater design and selection are (1) venting the heater shell to remove any noncondensable gases and (2) the protection of the turbine caused by malfunction of the heater system. Venting the shell is required to avoid air-bounding a heater, which reduces the performance or, in extreme cases, puts the heater out of service. Emergency drains to the condenser open when high water levels are present within the shell. Check valves on the heating steam line are also used, and a water detection monitor can be installed to enable operators to take prompt action when water is present.

Condenser. The steam turbines employ surface-type condensers comprising large shell-and-tube heat exchangers operating under vacuum. The condenser (1) reduces the exhaust pressure at the last-stage blade exit to extract more work from the turbine and (2) collects the condensed steam and returns it to the feedwater-heating system. Cooling water circulates from the cooling source to the condenser tubes by motor-driven pumps, which may be centrifugal, propeller, or mixed-flow type. Multiple pumps, each rated less than 100% of required pumping power, are used to allow to operation with one or more pumps out of service and operate more efficiently at part load. Cooling water is supplied from either a large heat sink water source, such as a river, or from cooling towers. The cooling in the cooling tower is assisted by evaporation of 3 to 6% of the cooling water. Airflow is natural draft (hyperbolic towers) or forced draft. The noncondensable gases are removed from the condenser by a motor-driven vacuum pump or, more frequently, steam jet air ejectors which have no moving parts.

Pumps

Condensate Pump. Condensate is removed from the hot well of the condenser and passed through the LP heater string via the condensate pump. Typically, there will be two or more vertical (larger units) or horizontal (medium and small units) motor-driven centrifugal pumps located near the condenser hot well outlet. Depending on the size of the cycle, condensate booster pumps may be used to increase the pressure of the condensate on its way to the DA.

Feedwater Booster Pump. The DA outlet supplies the feedwater booster pump which is typically a motor-driven centrifugal pump. This pump supplies the required suction head for the BFP.

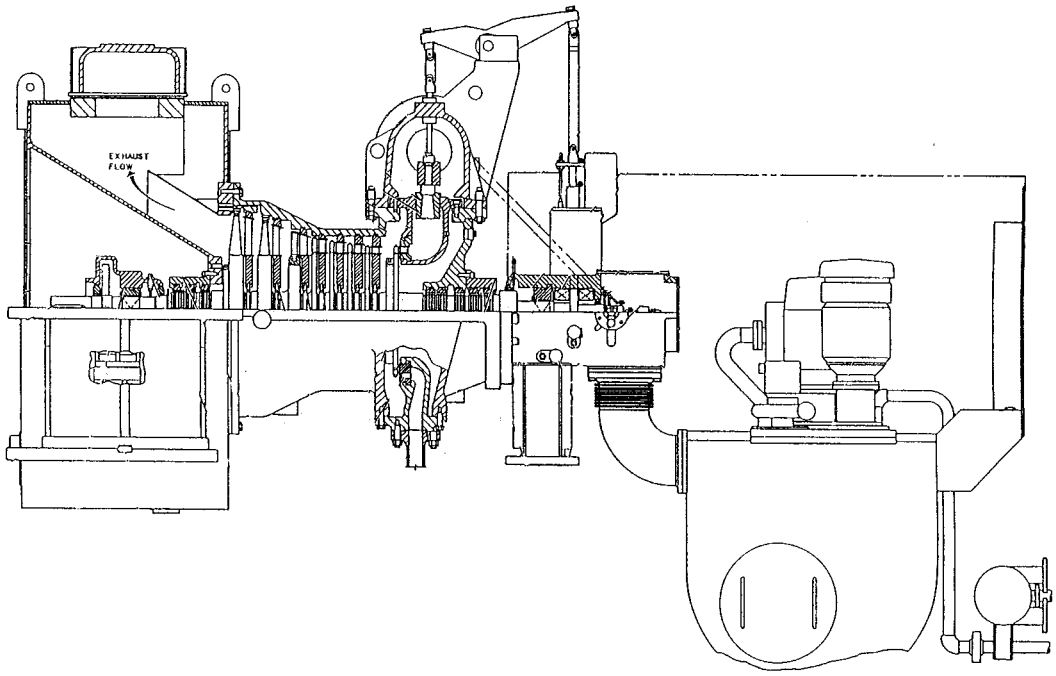

FIGURE 8.1.12 Boiler feed pump turbine.

Boiler Feed Pump. These pumps are multiple-stage centrifugal pumps, which, depending on the cycle, can be turbine or motor driven. BFP turbines (BFPT), Figure 8.1.12, are single-case units which draw steam from the main turbine cycle and exhaust to the main condenser. Typical feedpump turbines require 0.5% of the main unit power at full-load operation. Multiple pumps rated at 50 to 100% each are typically used to allow the plant to operate with one pump out of service.

Further Information

British Electricity International, 1992. *Modern Power Station Practice,* 3rd ed., Pergammon Press, Oxford.

Lammer, H.B. and Woodruff, 1967. *Steam Plant Operation,* 3rd ed., McGraw-Hill, New York.

Powell, C. 1955. *Principles of Electric Utility Operation,* John Wiley & Sons, New York.

Generators

The electric generator converts rotating shaft mechanical power of the steam turbine to three-phase electrical power at voltages of between 13.8 and 26 kV, depending upon the power rating. The generator comprises a system of ventilation, auxiliaries, and an exciter. Figure 8.1.13 shows an installed hydrogen-cooled generator and brushless exciter of about 400 MW. Large generators greater than 25 MW usually have a solid, high-strength steel rotor with a DC field winding embedded in radial slots machined into the rotor. The rotor assemblage then becomes a rotating electromagnet that induces voltage in stationary conductors embedded in slots in a laminated steel stator core surrounding the rotor (see Figure 8.1.14).

The stator conductors are connected to form a three-phase AC armature winding. The winding is connected to the power system, usually through a step-up transformer. Most steam turbines driven by fossil-fired steam use a two-pole generator and rotate at 3600 rpm in 60-Hz countries and 3000 rpm in

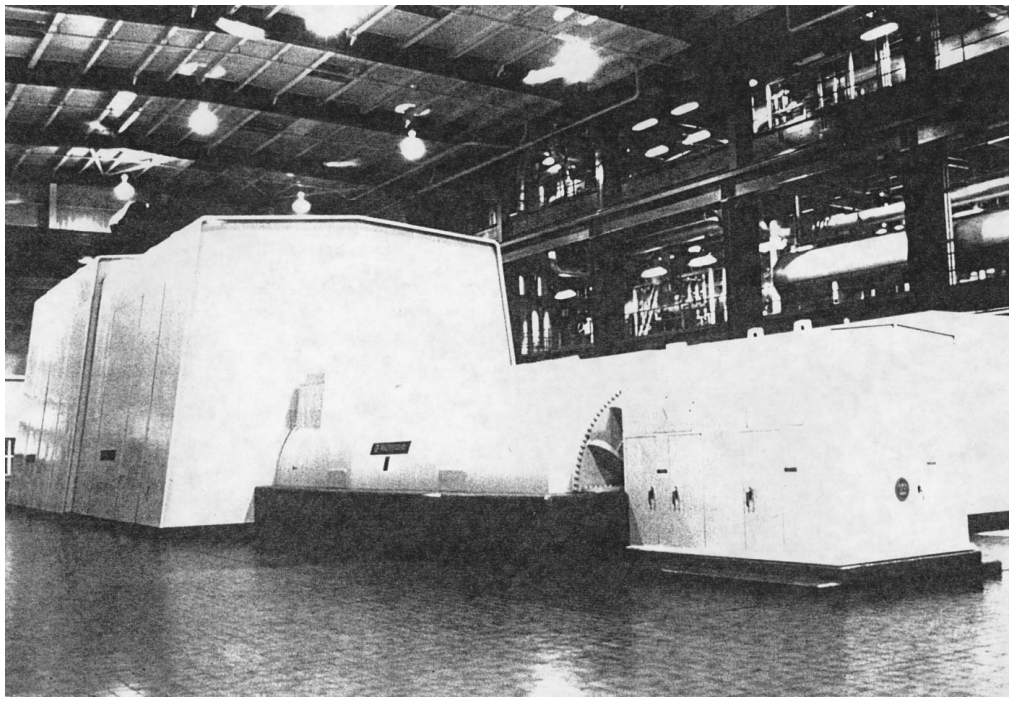

FIGURE 8.1.13 Generator and exciter.

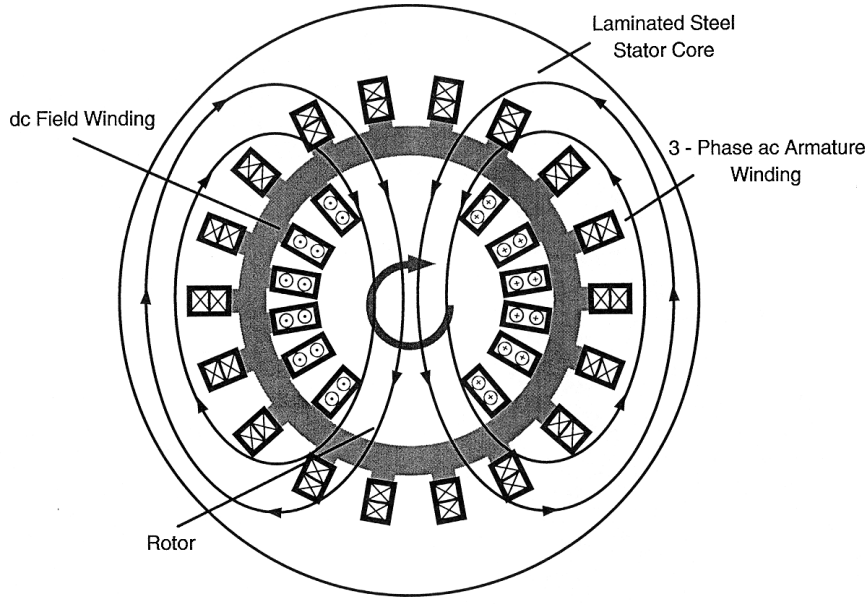

FIGURE 8.1.14 Generator magnetic paths.

50-Hz countries. Most large steam turbines driven by nuclear steam supplies use a four-pole generator and rotate at 1800 or 1500 rpm for 60 and 50 Hz, respectively.

Generator Ventilation

Cooling the active parts of the generator is so important that generators are usually classified by the type of ventilation. Air-cooled generators are used commonly up to 100 MW, though some applications exist up to 200 MW. Some use ambient air drawing air through filters and others recirculate air through air-to-water heat exchangers. Above 100 MW, most manufacturers offer hydrogen for the overall cooling, sometimes up to 1400 MW. Hydrogen has 14 times the specific heat of air and is used at lower density. This contributes to much better cooling and much lower windage and blower loss. The frame must be designed to withstand the remote circumstance of a hydrogen explosion and requires shaft seals. Hydrogen is noncombustible with purities greater than 70%. Generator purities are usually maintained well above 90%. Depending upon the manufacturer, generators with ratings above 200 to 600 MW may have water-cooled stator winding, while the remaining components are cooled with hydrogen.

Generator Auxiliaries

Large generators must have a lubrication oil system for the shaft journal bearings. Major components of this system are pumps, coolers, and a reservoir. In most cases, the turbine and generator use a combined system. For hydrogen-cooled generators, a shaft seal system and hydrogen supply system are needed. The shaft seal system usually uses oil pumped to a journal seal ring at a pressure somewhat higher than the hydrogen pressure. Its major components are pumps, coolers, and reservoir, similar to the lubrication system. The hydrogen supply system consists of a gas supply and regulators. A CO_2 supply is used to purge the generator when going from air to hydrogen or vice versa to avoid a combustible hydrogen/air mixture. The stator winding water supply again uses pumps, coolers, and a reservoir. It needs demineralizers to keep the water nonconducting and provisions to control oxygen content to avoid copper oxide corrosion which might break off and clog water passages.

Excitation

The rotor field winding must have a DC source. Many generators use rotating "collector" rings with stationary carbon brushes riding on them to transfer DC current from a stationary source, such as a thyristor-controlled "static" excitation system, to the rotor winding.

A rotating exciter, known as a brushless exciter, is used for many applications. It is essentially a small generator with a rotating rectifier and transfers DC current through the coupling into the rotor winding without the need for collectors and brushes.

Further Information

Fitzgerald, A.E., Kingsley, C.F., and Kusko, A. 1971. *Electric Machinery,* 3rd ed., McGraw-Hill, New York.

Modern Steam Power Plant — An Example

The purpose of a power plant is to generate electric power. It does so by converting chemical energy contained in fuel into thermal energy in steam; thermal energy in steam into mechanical energy in the turbine/generator; and mechanical energy in the turbine/generator into electrical energy.

Operating efficiency of a typical modern steam plant is about 35 to 45%. The primary losses result from (1) heat sink losses in the condenser, (2) boiler losses, and (3) electrical losses.

Steam plant capacities have ranges from 50 to 1600 MW; however, modern plants are being designed for more than 250 MW due to energy demands, system load requirements, and economies of scale in the larger centralized stations.

Major Steam Plant Components

Steam plants comprise three major components (1) boiler, (2) turbine, and (3) main steam condenser. The boiler and turbine are covered in earlier subsections and neither will be repeated here. A graphic of the entire fluid or work cycle is shown in Figure 8.1.15.

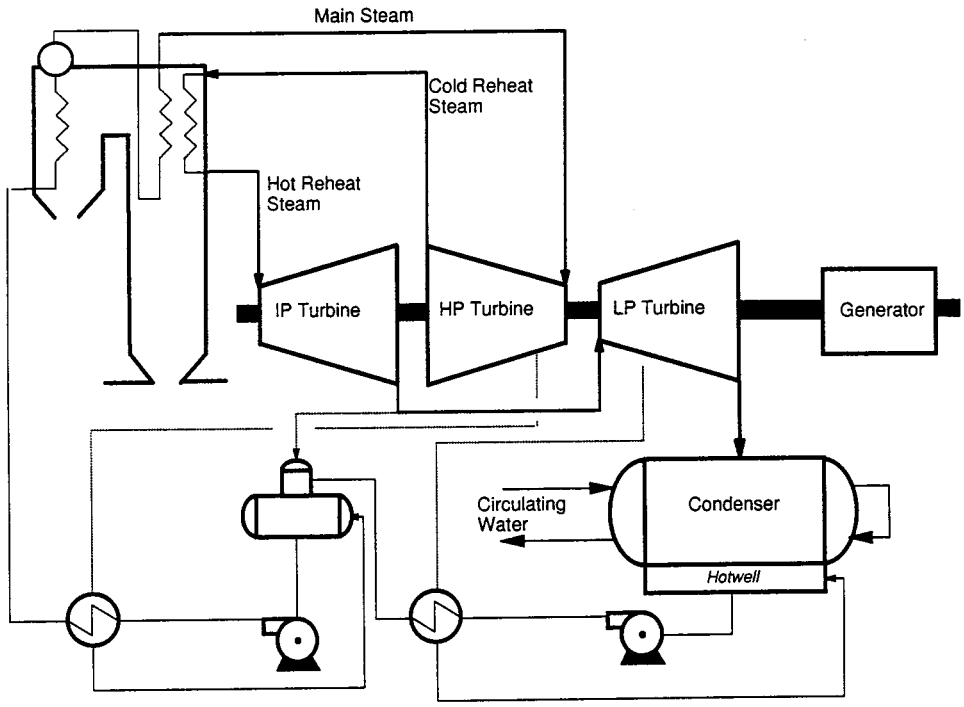

FIGURE 8.1.15 Steam power plant schematic.

Condenser. The condenser (also discussed earlier) is a large heat exchanger that takes the LP turbine exhaust steam and converts it back to water. The steam passes over a bundle of tubes located in the condenser and is cooled by the circulating water which passes through the tubes. The steam is condensed into water drops and collected in the condenser hot well. The condensate is delivered from the condenser hot well through the condensate and feedwater systems and back to the boiler where it becomes steam again.

Fuels. Coal, oil, and gas are used to fuel fossil plants. Although coal possesses the highest carbon content, it also possesses the highest sulfur, nitrogen, and ash content, thereby requiring air pollution-control equipment. Controlling these pollutants requires the installation of scrubbers for sulfur control; overfire air or gas recirculation for in-furnace nitrous oxides (NO_x) control; selective catalytic reduction (SCR) for post-combustion NO_x control; electrostatic precipitators (ESP) or baghouse for fly ash control; and pneumatic, hydraulic, or mechanical ash-handling systems for bottom ash removal. Fuel oil and natural gas are chiefly composed of compounds of hydrogen and carbon (hydrocarbons) with very low percentages of sulfur, nitrogen, and ash and do not require pollution-control equipment.

Power Plant System

Power plants comprise the following main systems: fuel handling, air handling, gas handling, main steam, reheat steam, auxiliary steam, extraction steam, condensate, feedwater, circulating water, and air removal.

Fuel-Handling System. The fuel-handling system consists of delivery, transfer, and processing. Fuel is delivered to the plant from the fuel source by truck, boat, rail (coal and oil), or pipeline (oil and gas). Once delivered, the fuel is transferred from the delivery point to various locations throughout the fuel-handling system. For coal and oil, the fuel is either transferred to storage or sent directly to the boiler. For gas, the fuel is directly transferred to the boiler without any storage. Prior to delivery to the boiler for burning, the fuel must be processed so that it will readily mix with air and burn completely. Coal must be broken down into smaller pieces by breakers and crushers. Oil requires steam, air, or mechanical atomization. Gas requires no processing.

Air/Gas-Handling Systems. Steam plants are classified as either pressurized or balance draft. Pressurized systems include forced-draft fans to provide the necessary air for fuel, an air heater to transfer heat from the exit gas to the inlet air, and a wind box where the air is stored and then directed to the individual burner ports. A balanced draft system includes all of the components of the pressurized systems and induced-draft fans to exhaust the combustion products from the boiler, thus maintaining the furnace under slightly negative pressure.

Main Steam System. The main steam system controls and regulates the flow of high-temperature, HP steam generated in the boiler furnace as it moves from the boiler to the turbine. The components in this system include main steam piping, safety valves, main steam stop valve, steam chest, and turbine control valve.

Reheat Steam System. The reheat steam system improves overall plant efficiency by increasing the energy of steam that has been exhausted from the HP turbine. Steam from the hot reheat steam system is delivered to the IP turbine. The components of the reheat steam system are cold reheat piping, the reheater section of the boiler, hot reheat piping, safety relief valves, reheat stop valves, reheater desuperheater, and intercept valves.

Auxiliary Steam System. The auxiliary steam system directs and regulates auxiliary steam from the cold reheat line to the auxiliary steam users. The auxiliary steam system users are typically steam/air preheating coils, outdoor freeze protection/heat tracing, deaerating heater pegging, turbine-driven BFP testing, turbine seals, and plant heating.

Extraction Steam System. The extraction steam system directs and regulates the flow of the extraction steam from the turbine to the feedwater heaters, BFPT, and auxiliary steam system. The extraction steam heats the feedwater that flows through the heaters, thus improving overall plant efficiency. In large steam plants, six to eight stages of feedwater heating are typical.

Condensate System. The condensate system consists of condensate pumps, LP feedwater heaters, and DA. The condensate pumps remove condensate from the main condenser hot well, increase condensate pressure, and deliver it through the LP heaters to the DA. During this process, the condensate is heated, deaerated, and chemically treated.

Feedwater System. The feedwater system consists of BFPs, HP feedwater heaters, piping, and valves. The boiler feedwater pumps deliver water from the DA storage tank, through the HP heaters, and into the boiler. Feedwater is supplied at sufficient quantities and pressure to satisfy unit demands during startups, shutdowns, and normal operation. The BFP is also the primary source of spray water for the superheater and reheater desuperheaters for control of the main and reheat steam temperatures, respectively.

BFPs can either be turbine or motor driven. Booster pumps may be required to provide additional net positive suction head (NPSH) to the main and start-up BFPs for plants designed with a low DA setting.

Circulating Water System. The circulating water system pumps cooling water through the condenser tubes at sufficient capacity, temperature, and pressure to absorb the latent heat in the LP exhaust steam.

Circulating water systems are classified as once-through systems, when a large water source is available, or recirculating systems employing cooling towers. In once-through systems, circulating water pumps deliver water from the plant water supply (river, lake, or ocean) through the condenser tubes to absorb latent heat in the exhaust steam. Water flows through the system once and is returned to its source. The major parts of this system are screens, pumps, expansion joints, valves, and piping. In recirculating systems, the cooling tower cools the heated circulating water from the main condenser by exposing it to air. The cooled water is stored in a basin located below the tower and is then circulated back through the system by the circulating water pumps.

Air Evacuation System. The air evacuation system removes air and noncondensable gases in the main steam condenser and helps maintain the vacuum created by the volume reduction of the condensing steam during normal operation. The system also establishes a normal vacuum in the condenser prior to turbine start-up.

Further Information

Baumeister, T. and Marks, L.S. 1958. *Standard Handbook for Mechanical Engineers,* 8th ed., McGraw-Hill, New York.

Singer, J.G., Ed. 1991. *Combustion Fossil Power,* 4th ed., Combustion Engineering, Inc., Windsor, CN.

8.2 Gas Turbines

Steven I. Freedman

Overview

Gas turbines are steady-flow power machines in which a gas (usually air) is compressed, heated, and expanded for the purpose of generating power. The term *turbine* is the component which delivers power from the gas as it expands; it is also called an expander. The term *gas turbine* refers to a complete power machine. The term gas turbine is often shortened to simply turbine, which can lead to confusion with the term for an expander.

The basic thermodynamic cycle on which the gas turbine is based is known as the Brayton cycle. Gas turbines may deliver their power in the form of torque or one of several manifestations of pneumatic power, such as the thrust produced by the high-velocity jet of an aircraft propulsion gas turbine engine.

Gas turbine machines vary in size from large, 250,000-hp utility machines, to small automobile, truck, and motorcycle turbochargers producing as little as 5 hp.

Gas turbines are used in electric power generation, propulsion, and compressor and pump drives. The most efficient power generation systems in commercial service are gas turbine combined cycle plants with power-to-fuel energy efficiencies of more than 50% (higher heating value basis) or 55% (lower heating value basis). Systems five points higher in efficiency are now under development and are being offered commercially, and systems of even higher efficiency are considered feasible.

History

The fourth quarter of the 19th century was one of great innovation in power machinery. Along with the spark-ignited gasoline engine, the compression-ignited diesel engine, and the steam turbine, engineers applied their skills to several hot-air engines. Charles Curtis received the first U.S. patent for a complete gas turbine on June 24, 1895. Aegidius Elling built the first gas turbine in 1903, which produced 11 hp.

The first commercial stationary gas turbine engineered for power generation was a 4000-kW machine built by the Brown Boverei Company in Switzerland in 1939.

Aviation provided the impetus for gas turbine development in the 1930s. In Germany, Hans von Ohain's first engine ran in March 1937. Frank Whittle's first engine ran in England in April 1937. The first airplane flight powered by a gas turbine jet engine was in Germany on August 27, 1939. The first British airplane powered by a gas turbine flew on May 15, 1941.

A Swiss railway locomotive using a gas turbine was first run in 1941. The first automobile powered by a gas turbine was a British Rover, which ran in 1950. And, in 1956, a gas turbine-powered Plymouth car drove over 3000 miles on a coast-to-coast exhibition trip in the United States.

Fuels and Firing

The first heat engines were external combustion steam engines. The combustion products never came in contact with the working fluid, so ash, corrosive impurities, and contaminants in the fuel or exhaust did not affect the internal operation of the engine. Later, internal combustion (piston) engines were developed. In these engines, a mixture of air and fuel burned in the space enclosed by the piston and cylinder walls, thereby heating the air. The air and combustion products formed the working fluid, and contacted internal engine parts.

Most gas turbines in use today are internal combustion engines and consequently require clean fuels to avoid corrosion and erosion of critical turbine components. Efforts were made to develop gas turbines rugged enough to burn residual or crude oil. However, due to the higher efficiencies obtainable by burning extremely clean fuel at higher temperatures, there is little current interest in using liquid fuel other than (clean) distillate oil in gas turbines. Interest in the use of residual oil is now centered on gasifying and cleaning these fuels prior to use.

A few externally heated gas turbines have been built for use with heavy oil, coal, nuclear reactor, radioisotope, and solar heat sources. However, none of these has become commercial. The added cost and pressure drop in the externally fired heater make externally fired gas turbines expensive. Because the working fluid temperature cannot be greater than that of the walls of the fired heater, externally fired gas turbines are substantially less efficient than modern internal combustion gas turbines with internally cooled blades.

The only internal combustion coal-fired gas turbine entering commercial service is the pressurized fluidized bed (PFB) combustion system. In the PFB, air discharged from the compressor of the turbine is used to fluidize a bed of limestone or dolomite in which coal is burned. The bed is maintained at modest temperature so that the ash in the coal does not form sticky agglomerates. Fortuitously, this temperature range also minimizes NO_x formation and allows capture of sulfur dioxide (SO_2) in the bed. Bed temperature is maintained in the desired range by immersed boiler tubes. Carryover fly ash is separated from gaseous combustion products by several stages of cyclone inertial separators and, in some cases, ceramic filters. The power turbine is modified to accommodate the combustion products, which after mechanical cleanup may still contain particles as large as 3 to 5 μm.

The most common gas turbine fuels today are natural gas and distillate oil. To avoid hot corrosion by alkali metal sulfates, the total sodium and potassium content of the fuel is typically limited to less than 5 ppm. Liquid fuels may also contain vanadium, which also causes corrosion. Fuels must be ash-free because particles larger than 3 to 5 μm rapidly erode blades and vanes. Experimental prototype gas turbines using pulverized coal pressurized combustors have not demonstrated adequate life. Hybrid systems — in which the moderate-temperature coal combustion products are mechanically cleaned and heated to higher temperature by use of a clean fuel such as natural gas or distillate oil — are the subject of ongoing development.

Efficiency

The term *efficiency* is applied not only to complete power generation machines but also to the individual compression, expansion, and combustion processes that make up the gas turbine operating cycle. Different definitions of efficiency apply in each case. In an **expansion process**, the **turbine efficiency** is the ratio of the actual power obtained to the maximum power that could have been obtained by expanding the gas reversibly and adiabatically between the same initial and final pressures.

Gas turbines typically involve high-speed gas flows, so appreciable differences exist between the static pressure and temperature and the total (or stagnation) pressure and temperature. Care must be taken in interpreting data to be sure that the pressure condition — static or stagnation — at each component interface is properly used.

Irreversible losses in one stage of an expansion process show up as heat (increased temperature) in later stages and add to the power delivered by such stages. Hence, a distinction exists between the polytropic efficiency (used to describe the efficiency of a process of differential pressure change) and the adiabatic (complete pressure change) efficiency. The efficiency of compressors and turbines based on their inlet and outlet pressures is called the isentropic or adiabatic efficiency. Unfortunately, both terms are reported in the literature, and confusion can exist regarding the meaning of the term *efficiency* .

Combustion efficiency in well-engineered and well-built internal combustion gas turbines is almost always close to 100%. The combustion losses appear as carbon monoxide, unburned hydrocarbons, and soot, which are typically below 100 ppm, with clean fuels.

The **gas turbine or engine efficiency** is the ratio of the net power produced to the energy in the fuel consumed. The principal gas turbine fuels are liquid and gaseous hydrocarbons (distillate oil and natural gas) which have high hydrogen content. Consequently, the term *engine efficiency* needs to be qualified as to whether it is based on the higher or the lower heat content of the fuel (the difference between the two being the latent heat of condensation of the water vapor in the products of combustion). Utility fuel transactions are traditionally based on higher heating values, and most engine publications presume the lower heating value of the fuel as the efficiency basis.

Engineers analyze gas turbine machines to evaluate improvements in component performance, in higher temperature and pressure ratio designs, and in innovative cycles. Ideal case cycle calculations generally assume the following:

- Air (with either constant or temperature-dependent specific heats) is the working fluid in both turbine and compressor (with equal mass flows);
- Air is the working fluid in both turbine and compressor but with the turbine mass flow greater by the amount of fuel used.

Components are modeled with or without frictional pressure drops, and heat transfer effectiveness may be ideal (unity) or actual, depending on the purpose of the analysis. Use of compressor air for cooling of high-temperature structure, nozzles, and blades are modeled in varying degrees of complexity. Two-dimensional temperature profiles or pattern factors exist. Component inlet and exit total pressure losses should be included in cycle analyses.

Gas Turbine Cycles

Gas turbine cycles are usually plotted on temperature-entropy (T-S) coordinates. Readers unfamiliar with entropy are referred to the chapter on thermodynamics. The T-S plot is useful in depicting cycles because in an adiabatic process — as is the case for turbines and compressors — the power produced or consumed is the product of the mass flow and the enthalpy change through the process. Thus, temperature difference, which is found on a T-S plot, is proportional to the power involved. Additionally, the heat exchange in a process involving zero power — such as a combustor or heat exchanger — is the product of the absolute temperature and the entropy change. On a T-S chart, the area under a process line for a combustor or heat exchanger is the heat exchanged.

The slope of a constant-pressure line on a T-S diagram is proportional to the absolute temperature. Consequently, lines of constant pressure become steeper, and diverge as the temperature increases. This illustrates that more work is obtained expanding a gas between fixed pressures at higher temperatures than at lower temperatures. Figure 8.2.1 shows a comparison of the process of an ideal and an actual simple cycle gas turbine on a T-S diagram. The increased compressor power consumption and the decreased turbine power generation in the actual cycle are shown to provide an understanding of the differences that component efficiencies make on machine performance.

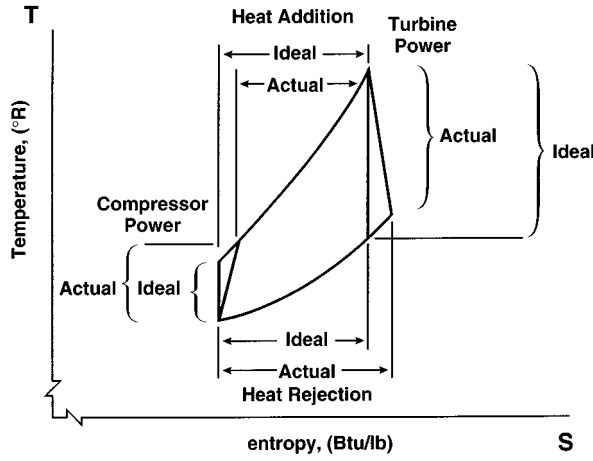

FIGURE 8.2.1 T-S diagram for a simple cycle illustrating the differences in compressor and turbine power for ideal (100% efficient) and actual components.

The incremental amount of power produced per differential pressure change in the gas is given by

$$d(\text{Power/mass flow}) = -RT\, dp/p$$

Two phenomena are illustrated by this equation. First, power is proportional to the absolute temperature of the gas. Second, power is proportional to the percent change in pressure. This latter point is important in understanding the effect of pressure losses in cycle components. In heat exchangers, the proper measure of power lost is the percent pressure drop.

Cycle Configurations

The basic Brayton cycle consists of a compressor, a combustor or burner, and an expander. This configuration is known as the simple cycle. In idealizing the actual cycle, combustion is replaced by constant-pressure heat addition, and the cycle is completed by the assumption that the exhaust to ambient pressure could be followed by a zero-pressure-loss cooling to inlet conditions.

A T-S diagram of the simple cycle gas turbine with an upper temperature limit set by metallurgical conditions is illustrated in Figure 8.2.2 for cycles of low, medium, and high pressure ratios. The heat addition is only by fuel combustion, simplified here to be without mass addition or change in specific heat of the working fluid.

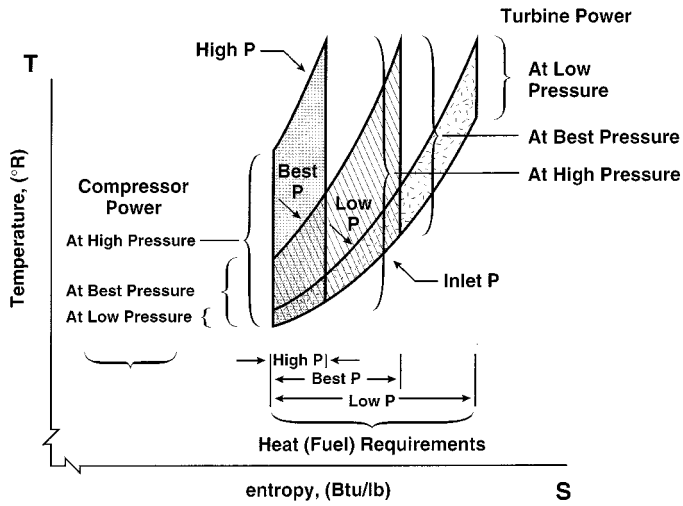

FIGURE 8.2.2 T-S diagram illustrating the power and heat (fuel) requirements at low, best, and high cycle pressures.

It is seen that the low-pressure-ratio cycle requires a large heat addition, which leads to a low efficiency, and the high-pressure-ratio cycle has turbine power output barely greater than the compressor power requirement, thereby leading to low net output and low efficiency. At intermediate pressure ratios, the turbine power output is substantially higher than the compressor power requirement, and the heat addition is modest in comparison with the difference between the turbine and compressor powers. There is an optimum pressure ratio for maximum efficiency, which is a function mainly of the maximum gas temperature in the machine, and to a lesser extent, by the component efficiencies, internal pressure losses, and the isentropic exponent. There is another optimum pressure ratio for maximum specific power (power per unit mass flow).

As the achievable turbine inlet temperature increases, the optimum pressure ratios (for both maximum efficiency and maximum specific power) also increase. The optimum pressure ratio for maximum specific power is at a lower pressure level than that for maximum efficiency for all cycles not employing a recuperator. For cycles with a recuperator, the reverse is true: maximum efficiency occurs at a lower

pressure ratio than maximum specific power. Heavy-duty utility and industrial gas turbines are typically designed to operate near the point of maximum specific power, which approximates lowest equipment cost, while aeroderivative gas turbines are designed to operate near the point of maximum efficiency, approximating highest thrust. Figure 8.2.3 shows a performance map (efficiency as a function of power per unit of air flow) for a simple cycle gas turbine for two turbine inlet temperatures. It is seen that at higher temperature, both the efficiency and specific power increase, as well as the optimum pressure ratios for both the maximum efficiency and maximum specific power conditions.

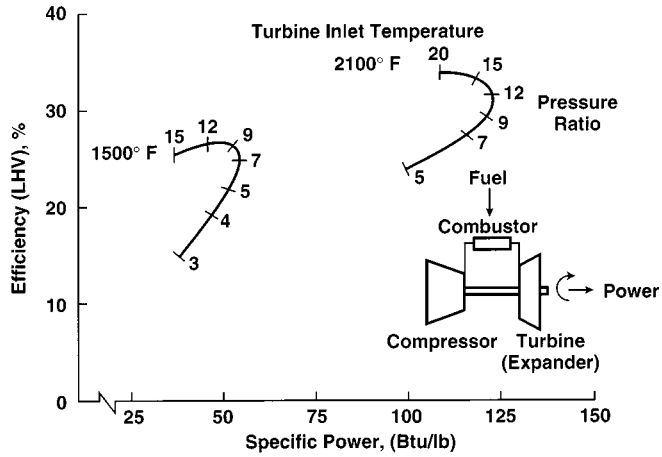

FIGURE 8.2.3 Performance map of a simple cycle gas turbine.

Aircraft gas turbines operate at temperatures above the limit of turbine materials by using blades and vanes with complex internal cooling passages. The added cost is economically justified because these machines can command high prices in the aircraft propulsion marketplace. Aeroderivative engines have higher pressure ratios, higher efficiencies, and lower exhaust temperatures than heavy-duty machines. The stationary power markets served by aeroderlvative gas turbines are principally pipeline compressor stations and oil/gas production wells. Aeroderivative gas turbines also are economically advantageous for intermediate-duty applications.

Components Used in Complex Cycles

Recuperators and **regenerators** recover heat from the turbine exhaust and use it to preheat the air from the compressor before it enters the combustor, thereby saving fuel. This heat transfer is shown in Figure 8.2.4. While recuperators and regenerators are quite similar thermodynamically, they are totally different in design. Recuperators are conventional heat exchangers in which hot and cold gases flow steadily on opposite sides of a solid (usually metal) wall.

Regenerators are periodic-flow devices. Fluid streams flow in opposite directions through passages in a wheel with heat storage walls. The wheel rotates, transferring heat from one stream to the other. Regenerators usually use a nest of very small parallel passages oriented axially on a wheel which rotates between hot and cold gas manifolds. Such regenerators are sometimes used in industrial processes for furnace heat recovery, where they are referred to as heat wheels. Because regenerators are usually more compact than recuperators, they are used in automotive gas turbines (under development). The difficulty in using regenerators on gas turbines intended for long life is that the two gas streams are at very different pressures. Consequently, the seals between the manifolds and the wheel must not leak excessively over the maintenance overhaul interval of the engine. If they do, the power loss due to seal leakage will compromise engine power and efficiency. Figure 8.2.5 shows a performance map for the regenerative

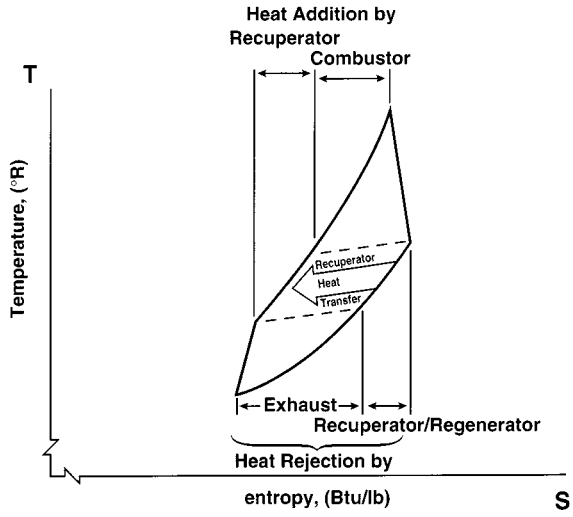

FIGURE 8.2.4 T-S diagram illustrating the heat transfer from the turbine exhaust to the compressor discharge accomplished by a recuperator/regenerator.

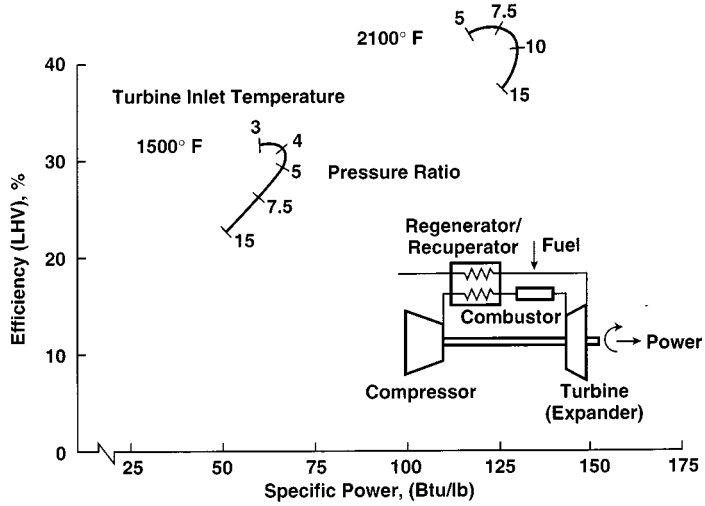

FIGURE 8.2.5 Performance map of a regenerative cycle gas turbine.

gas turbine cycle for two temperatures. It is seen that as the temperature increases, the efficiency, specific power, and optimum pressure ratio all increase.

Current research on the recovery of gas turbine exhaust heat includes examination of thermochemical recuperation, where exhaust heat is used to effect a chemical reaction (reforming) of the fuel with steam, thereby increasing the heating value of the fuel. Although this process is feasible, research is underway to determine if it is practical and economic.

Industrial process compressors frequently use **intercoolers** to reduce compressor power when the compressor has a high pressure ratio and operates for a large number of hours per year. When analyzing cycles with intercoolers, the added pressure drops in the compressor interstage entrance and exit diffuser and scroll and the pressure drop in the intercooler itself should be included.

In a similar manner, turbine reheat can be used to increase the power output of a large-pressure-ratio turbine. This is the thermodynamic principle in turbojet afterburner firing. Turbine reheat increases

power, but decreases efficiency unless the turbine exhaust heat is used for additional power generation, as is the case with a combined cycle, or is used with a recuperator to preheat combustor inlet air.

Intercoolers and reheat burners increase the temperature difference between the compressor and turbine discharges, thereby increasing the opportunity to use a recuperator to preheat the burner air with exhaust heat. An intercooled recuperated (ICR) machine is at present in development. The efficiency decrease at part load of an ICR gas turbine is much less than of conventional simple cycle machines.

Small gas turbines have uncooled turbine blades as a result of the difficulty in manufacturing extremely small cooling passages in small blades. This results in low efficiencies, making it difficult for such turbines to compete with high-volume production (low-cost) reciprocating (piston) engines. The low-pressure-ratio recuperated cycle has greater efficiency, although at higher cost. The recuperated cycle is finding favor in programs for small (under 300-kW) gas turbines used for stationary power. The recuperated cycle is efficient enough in comparison with piston engines (Otto cycles) to be of interest to automotive power plant engineers. Current designs of automotive gas turbines (AGT) have ceramic turbines and combustors and use ceramic regenerators made from a spirally wound corrugated structure with gas passages about a millimeter in diameter.

Because of their compact size, low emissions, and light weight, gas turbines are also being considered for hybrid engine-battery vehicles. Proponents are pursuing the low-pressure-ratio recuperated gas turbine as the way to obtain high efficiency and low emissions in a compact power plant.

An ingenious gas turbine cycle is the closed cycle in which the working fluid is sealed in the system. Heat is added to the fluid with an externally fired heater and extracted from the fluid through heat exchangers. The working fluid may be any gas, and the density of the gas may be varied — to vary the power delivered by the machine — by using a gas storage cylinder connected to the compressor discharge and inlet. The gas storage system is at an intermediate pressure so that it can discharge gas into the lowest pressure point in the cycle and receive gas from the highest pressure point in the cycle. About ten such units were built between 1938 and 1968; however, in spite of its sophistication, the added cost and low efficiency prevented this system from becoming economic.

The exhaust from a gas turbine is quite hot and can be used to raise steam, which can then be used to generate additional power with a steam turbine. Such a compound gas turbine-steam turbine system is referred to as a **combined cycle**. Figure 8.2.6 shows a schematic diagram of the equipment in a combined cycle. Because the exhaust of heavy-duty machines is hotter than that of aeroderivative machines, the gain in combined cycle system efficiency through use of the steam bottoming cycle described above is greater for heavy-duty machines than for aeroderivatives. Indeed, heavy-duty machines are designed with two criteria in mind: achieving lowest cost for peaking (based on the simple cycle configuration) and achieving highest efficiency in combined cycle configuration for baseload use. The optimum pressure ratios for these two system configurations are very close. Steam bottoming cycles used in combined cycles usually use steam at multiple pressure levels to increase efficiency.

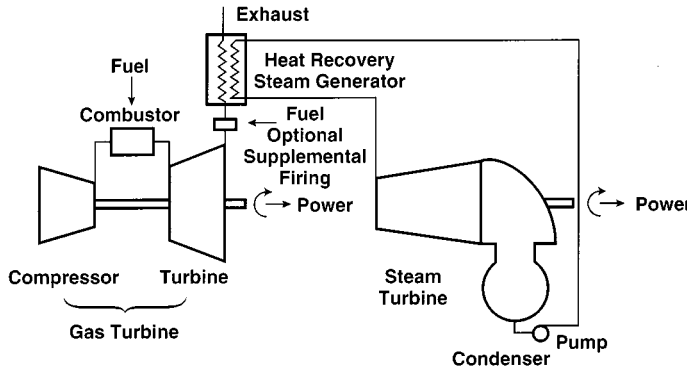

FIGURE 8.2.6 Combined (Brayton-Rankine) cycle.

Another system in which the power and efficiency of a gas turbine is increased through the use of steam is the **steam-injected gas turbine**. Figure 8.2.7 shows a schematic diagram of a steam-injected gas turbine cycle. Here the turbine exhaust flows into a heat recovery steam generator (HRSG) operating at a pressure somewhat higher than the compressor discharge pressure. The steam is introduced into the gas turbine at the combustor. The steam-air mixture then passes into the turbine, where the augmented mass flow increases the power produced by the turbine. Additional fuel is required by the combustor because the steam must be heated from the HRSG delivery temperature to the combustor discharge temperature. Typical turbines can accommodate only a limited additional mass flow — from 5 to 15%, depending on the design of the original gas turbine. Steam-injected gas turbines enable the host to use the steam for industrial purposes, space heating, or for the generation of additional power.

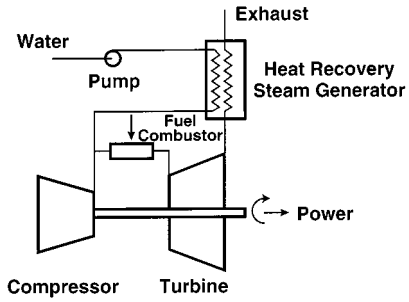

FIGURE 8.2.7 Steam-injected gas turbine.

A group of cycles under consideration for development involve the use of **adiabatic saturators** to provide steam at compressor discharge pressure to augment greatly the mass flow through the turbine, and consequently increase cycle power and efficiency. In the adiabatic saturator, water flows in a countercurrent path to the compressor discharge air in a mass transfer tower. Such equipment is often used in the chemical processing industries. The saturated air is preheated in a turbine exhaust heat recuperator. This cycle is called the **humid air turbine**, or HAT, cycle. The HAT cycle is particularly useful in using the low-temperature heat generated in coal-gasification-fueled gas turbine power plants. As the mass flow through the turbine is significantly augmented, engineers can no longer use the expansion turbine which was matched to the compressor in a conventional simple cycle gas turbine.

Figure 8.2.8 shows performance maps for the gas turbine cycles of major interest for a turbine inlet temperature typical of new products. Intercooling increases the specific power appreciably when compared with a simple cycle; however, such improvement requires an increase in pressure ratio. Recuperated cycles have considerably higher efficiency than similar cycles without recuperation. The effect of pressure ratio on the performance of recuperated cycles is opposite to that of similar cycles without recuperation. For recuperated cycles, the pressure ratio for maximum efficiency is considerably lower than for maximum specific power. Performance maps such as these are used in screening cycle alternatives for improved performance. Individual curves are generated for specific component performance values for use as a guide in developing new or improved machines.

Upper Temperature Limit

Classically, gas turbine engineers often spoke of a metallurgical limit in reference to maximum turbine inlet temperature. Later, turbine vane and blade cooling became standard on large machines. This situation creates a temperature difference between the combustion products flowing through the turbine and the turbine blade wall. Thus, because heat can be removed from the blades, the turbine can be operated with a combustion gas temperature higher than the metallurgical limit of the blade material. As a rule, the blades and vanes in new large gas turbines contain complex internal passages, through which up to 20% of compressor discharge air is directed. The cooling air first flows through internal convective cooling

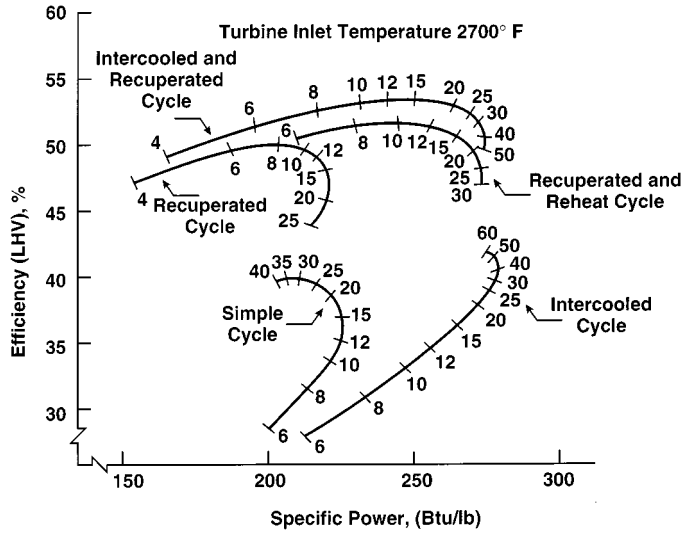

FIGURE 8.2.8 Specific power (Btu/lb).

passages, then through impingement passages, where the air is directed at the blade and vane walls, and finally through small holes in the blade, where it is used to provide a low-temperature film over the blade surface. This film cooling of the surface reduces heat transfer to the blade.

The design of blade and vane cooling passages is an extremely competitive endeavor because greater cooling enables use of higher combustion temperatures without exceeding the metallurgical limit of the blade material. However, a balance between air flow for cooling and air flow for power must be achieved; the cooling air flowing within a blade drops in pressure without producing any power within that stage (although it is available for power in later stages). In the newest gas turbines, blade cooling, the difference between turbine inlet gas temperature and blade metal temperature, is around 1000°F.

Some of the latest large gas turbines being introduced to the market in the 1997 to 2000 period are being offered for combined cycle application with closed-circuit **steam cooling** of selected hot section parts. Steam cooling reduces the need for air cooling, so that more of the compressor discharge air can be used for NO_x reduction in the combustor and for power generation. The heat transferred to the steam increases the efficiency of the bottoming cycle. The additional combustion products which flow through the high-pressure portions of the turbine generate substantially more power, thereby increasing both the power output and the efficiency of the machine. With more air for combustion, the fuel can be burned as a leaner mixture, with either less NO_x produced, or, as is preferred, with higher-temperature gases going to the turbine and the same NO_x (or a combination of these benefits).

Materials

The high-technology parts of a gas turbine are its hot section parts: blades, vanes, combustors and transition pieces. Gas turbine power, efficiency, and economics increase with the temperature of the gas flowing through the turbine blade passages. It is in the fabrication of these hot section parts that manufacturers are most competitive. Materials are selected to survive in serviceable condition for over 50,000 hr and associated numbers of thermal cycles. Ceramic coatings protect materials from oxidation and corrosion and provide thermal insulation, permitting higher gas temperatures.

Gas turbine alloys are frequently referred to as superalloys because of their extremely high strength at high temperatures. These superalloys are nickel based (such as IN 738), cobalt based (such as FSX-414), or with a nickel-iron base such as Inconel 718. Nickel resists oxidation and is creep resistant, but is subject to corrosive sulfidation. Alloy and manufacturing advancements have been led by the needs of military aircraft engines. Coating developments for corrosion resistance have been led by the needs

of stationary power for overhaul intervals as large as 50,000 hr. The developmental needs of automotive gas turbines have led to significant advances in strength and reliability of high-temperature ceramic components, including radial inflow turbines. Ceramic materials, principally silicon nitride, are expected to enter service soon in small gas turbines.

Combustion

Gas turbine combustors appear to be simple in design, yet they solve several difficult engineering challenges. Until relatively recently, gas turbine combustors employed a (turbulent) diffusion flame design approach, which created the most compact flame. European heavy-duty gas turbine manufacturers — with substantial interest in burning heavy fuel oils — preferred large, off-engine combustors, often called silo combustors because of their appearance, in order to obtain lower flame velocities and longer residence times. American heavy-duty gas turbine manufacturers use compact on-engine combustors and design for gaseous and clean (distillate) liquid fuels. Aeropropulsion gas turbines require the smallest possible frontal area and use only clean liquid fuels; hence, they use on-engine combustors.

Recently, stationary engines have been required to reduce NO_x emissions to the greatest extent possible, and combustors on stationary gas turbines first modified their diffusion flame combustors and employed water and steam injection to quench flame hot spots. Most recently, designs changed to the lean-premixed process. With the improved blade cooling, materials, and coatings now in use, the material limits on turbine inlet temperature and the NO_x emission limits on combustor temperature appear to be converging on a combustion-temperature asymptote around 2700°F (1482°C). This may be increased if catalytic combustors prove practical.

Mechanical Product Features

In view of the need to achieve all the performance features described above, one must keep in mind that a gas turbine is a high-speed dynamic machine with numerous machine design, materials, and fabrication features to consider. Major issues include the following: critical shaft speed considerations, bearing rotational stability, rotor balancing, thrust bearing design, bearing power loss, oil lubrication system, oil selection, air filter design and minimization of inlet and exhaust diffuser pressure drops, instrumentation, controls, diagnostic systems, scheduled service and inspection, overhaul, and repair. All of these topics must be addressed to produce a cost-effective, reliable, long-lived, practical gas turbine product that will satisfy users while also returning to investors sufficient profit for them to continue to offer better power generation products of still higher performance.

Defining Terms

Adiabatic saturator: A combined heat-and-mass-exchanger whereby a hot gas and a volatile liquid pass through a series of passages such that the liquid is heated and evaporates into the gas stream.

Combined cycle: An arrangement of a gas turbine and a stream turbine whereby the heat in the exhaust from the gas turbine is used to generate steam in a heat recovery boiler which then flows through a steam turbine, thereby generating additional power from the gas turbine fuel.

Combustion efficiency: Ratio of rate of heat delivered in a device which burns fuel to the rate of energy supplied in the fuel.

Expansion process: Process of power generation whereby a gas passes through a machine while going from a condition of high pressure to one of low pressure, usually the machine produces power.

Gas turbine or engine efficiency: The ratio of the net power delivered (turboexpander power minus compressor and auxiliary power) to the rate of energy supplied to the gas turbine or engine in the form of fuel, or, in certain cases such as solar power, heat.

Humid air turbine: A gas turbine in which the flow through the expander is augmented by large amounts of steam generated by use of an adiabatic saturator.

Intercooler: A heat exchanger used to cool the flow between sections of a compressor such that the high pressure section acts on a stream of reduced volumetric flow rate, thereby requiring less overall power to compress the stream to the final pressure.

Recuperator: A heat exchanger in which the hot and cold streams pass on opposite sides of a wall through which heat is conducted.

Regenerator: A heat exchanger in which the hot and cold streams alternately heat and cool a wall whose temperature rises and falls, thereby transferring heat between the streams.

Steam cooling: A process in which steam is used as the heat transfer fluid to cool a hot component.

Steam-injected gas turbine: A system in which the gas turbine flow is augmented by steam, thereby generating additional power.

Turbine efficiency: Ratio of the power delivered in an expansion process employing a turbine as the expander to the maximum power which could be produced by expanding the gas in a reversible adiabatic (isentropic) process from its initial pressure and temperature to its final pressure to the actual power.

Further Information

Wilson, D.G. 1984. *The Design of High-Efficiency Turbomachinery and Gas Turbines*, MIT Press, Cambridge, MA.

Kerrebrock, J. 1992. *Aircraft Engines and Gas Turbines*, MIT Press, Cambridge, MA.

Boyce, M.P. 1982. *Gas Turbine Engineering Handbook,* Gulf Publishing, Houston, TX.

Sawyer's Gas Turbine Engineering Handbook, Vol. 1: *Theory and Design,* Vol. 2: *Section and Application*, Vol. 3: *Accessories and Support*, Turbomachinery International Publications, Norwalk, CT, 1985.

Appendix

Equations for gas turine calculations based on the use of a perfect gas as the working fluid.

Perfect gas law	$pv = RT$
Gas constant	$R = \check{R}$/molecular weight
For air (molecule weight of 28.97)	$R = 286.96$ J/kg · K
	$= 0.06855$ Btu/lb_m · °R
	$= 53.32$ ft · lb_f/lb_m · °R
Universal gas constant	$\check{R} = 8313$ J/kg · mol · K
	$= 1.986$ Btu/lb · mol · °R
	$= 1545$ ft · lb_f/lb · mol · °R
Relationships of properties	$c_p = c_v + R$
Isentropic exponet	$\gamma = c_p/c_v$ (air, $\gamma = 1.4$)
	$(\gamma - 1)/\gamma = R/c_p$
Isentropic process	$pv^\gamma = \text{constant}$
	$P_2/P_1 = (T_2/T_1)^{\gamma/(\gamma-1)}$
Prolytropic process	$pv^n = \text{constant}$
	$P_2/P_1 = (T_2/T_1)^{n/(n-1)}$
Pressure ratio	$r = P_2/P_1$
Ratio of stagnation T° and p° to static T and p	$\frac{T^\circ}{T} = 1 + \frac{\gamma - 1}{2} M^2$
	$\frac{p^\circ}{p} = \left(1 + \frac{\gamma - 1}{2} M^2\right)^{\gamma/(\gamma-1)}$
Mach number	$M = V \Big/ \sqrt{g_c \gamma RT}$
Gravitational constant	$g_c = ma/F$
Subscripts	t = turbine
	c = compressor

f = fuel
i = inlet
e = exit

Cycle efficiency:

$$\eta = \frac{\dot{m}_t \Delta h_t - \dot{m}_c \Delta h_c}{\dot{m}_f HV}$$

where HV = heating value of fuel.
For specific heat independent of temperature and small mass flow of fuel in comparison to air:

$$\eta = \frac{\Delta T_t - \Delta T_c}{\Delta T_b}$$

Isentropic efficiency (finite pressure ratio):

$$\eta_t = \Delta T \text{ actual} / \Delta T \text{ isentropic}$$

$$\eta_t = \frac{1 - T_e/T_i}{1 - r^{(\gamma-1)/\gamma}}$$

or

$$\eta_t = \frac{1 - r^{(n-1)/n}}{1 - r^{(\gamma-1)/\gamma}}$$

and

$$\eta_c = \Delta T \text{ isentropic} / \Delta T \text{ actual}$$

$$\eta_c = \frac{r^{(\gamma-1)/\gamma} - 1}{T_e/T_i - 1}$$

or

$$\eta_c = \frac{r^{(\gamma-1)/\gamma} - 1}{r^{(\eta-1)/\eta} - 1}$$

Polytropic efficiency (differential pressure ratio):

$$\eta_t = \frac{(n-1)/n}{(\gamma-1)/\gamma}$$

and

$$\eta_c = \frac{(\gamma-1)/\gamma}{(n-1)/n}$$

Relationships between isentropic and polytropic efficencies:

$$\eta_{s,c} = \frac{r^{(\gamma-1)/\gamma} - 1}{r^{(\gamma-1)/\gamma \eta_{pc}} - 1}$$

$$\eta_{s,t} = \frac{1 - r^{(\gamma-1)/\gamma \eta_{p,t}}}{1 - r^{(\gamma-1)/\gamma}}$$

$$\eta_{p,c} = \frac{\ln r^{(\gamma-1)/\gamma}}{\ln\left[\frac{r^{(\gamma-1)/\gamma} - 1}{\eta_{s,c}} + 1\right]}$$

$$\eta_{p,t} = \frac{\ln\left[1 - \eta_{s,t}\left(1 - r^{(\gamma-1)/\gamma}\right)\right]}{\ln r^{(\gamma-1)/\gamma}}$$

8.3 Internal Combustion Engines

David E. Klett and Elsayed M. Afify

Introduction

This section discusses the two most common reciprocating internal combustion (IC) engine types in current use; the **spark ignition** (SI) and the **compression ignition** (CI or diesel) **engine**. Both the Stirling engine (technically, an external combustion engine) and the gas turbine engine are covered in other sections of this chapter. Space limitations do not permit detailed coverage of the very broad field of IC engines. For a more detailed treatment of SI and CI engines and for information on variations, such as the Wankel rotary engine and the Miller cycle engine (a variation on the reciprocating four-stroke SI engine introduced in production by Mazda in 1993), the reader is referred to the several excellent textbooks on the subject, technical papers, and other sources that are included in the list of references and the Further Information section.

Basic SI and CI engines have not fundamentally changed since the early 1900s with the possible exception of the introduction of the Wankel rotary SI engine in the 1960s (Norbye, 1971). However, major advances in the areas of materials, manufacturing processes, electronic controls, and computer-aided design have led to significant improvements in dependability, longevity, thermal efficiency, and emissions during the past decade. Electronic controls, in particular, have played a major role in efficiency gains in SI automotive engines through improved control of the fuel injection and ignition systems that control the combustion process. Electronic control of diesel fuel injection systems is also becoming more common and is producing improvements in diesel emissions and fuel economy.

This section presents the fundamental theoretical background of IC engine function and performance, including **four-stroke** and **two-stroke** SI and CI **engines**. Sections on combustion, emissions, fuels, and intake pressurization (**turbocharging** and **supercharging**) are also included.

Engine Types and Basic Operation

IC engines may be classified by a wide variety of characteristics, the primary ones being SI vs. CI, four-stroke vs. two-stroke, and reciprocating vs. rotary. Other possible categories of classification include intake type (naturally aspirated vs. turbocharged or supercharged), number of cylinders, cylinder arrangement (in-line, vee, opposed), cooling method (air vs. water), fueling system (injected vs. carbureted), valve gear arrangement (overhead cam vs. pushrod), type of **scavenging** for two-stroke engines (cross, loop, or uniflow), and type of injection for diesel engines (direct vs. indirect).

Four-Stroke SI Engine

Figure 8.3.1 is a cross-section schematic of a four-stroke SI engine. The SI engine relies on a spark plug to ignite a volatile air-fuel mixture as the piston approaches **top dead center** (**TDC**) on the compression stroke. This mixture may be supplied from a carburetor, a single throttle-body fuel injector, or by individual fuel injectors mounted in the intake port of each cylinder. One combustion cycle involves two revolutions of the crankshaft and thus four strokes of the piston, referred to as the intake, compression, power, and exhaust strokes. Intake and exhaust valves control the flow of mixture and exhaust gases into and out of the cylinder, and an ignition system supplies a spark-inducing high voltage to the spark plug at the proper time in the cycle to initiate combustion. On the intake stroke, the intake valve opens and the descending piston draws a fresh combustible charge into the cylinder. During the compression stroke, the intake valve closes and the fuel-air mixture is compressed by the upward piston movement. The mixture is ignited by the spark plug, typically somewhat before TDC. The rapid **premixed homogeneous combustion** process causes a sharp increase in cylinder temperature and pressure that forces the piston down for the power stroke. Near **bottom dead center** (BDC) the exhaust valve opens and the cylinder pressure drops rapidly to near atmospheric. The piston then returns to TDC, expelling the

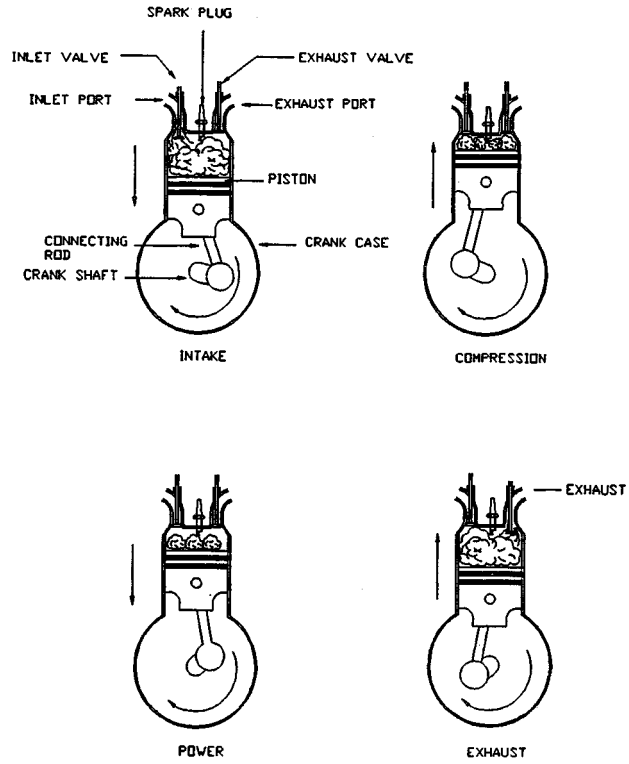

FIGURE 8.3.1 Schematic diagram of four-stroke SI engine.

exhaust products. At TDC, the exhaust valve closes and the intake valve opens to repeat the cycle again. Figure 8.3.2 is a cutaway drawing of a modern high-performance automotive SI engine. This is a fuel-injected normally aspirated aluminum alloy V-8 engine of 4.6 L displacement with dual overhead cams for each cylinder bank. Peak power output is 228 kw at 5800 rpm.

Two-Stroke SI Engine

The two-stroke SI engine completes a combustion cycle for every revolution of the crankshaft by essentially overlapping the power and exhaust functions in one downward stroke and the intake and compression processes in one upward stroke. A single-cylinder, crankcase-scavenged, two-stroke SI engine is illustrated schematically in Figure 8.3.3. The operation is as follows. On the upward stroke, the piston first covers the transfer port and then the exhaust port. Beyond this point the fresh charge is compressed and ignited near TDC. During the upward stroke, the negative pressure created in the crankcase below the piston draws in a fresh charge of fuel-air mixture through a one-way valve. On the downward power stroke, the mixture in the crankcase is pressurized. The piston uncovers the exhaust port and the high-pressure exhaust gases exit. Near BDC the transfer port is uncovered and the pressurized mixture flows from the crankcase into the cylinder and the cycle repeats. Since the crankcase is part of the induction system, it does not contain oil, and lubrication is accomplished by mixing oil with the fuel. With the cross-flow scavenging configuration illustrated in Figure 8.3.3, there will be a certain degree of mixing of the fresh charge with the combustion products remaining in the cylinder and some loss of fresh charge out the exhaust port.

Since two-stroke engines produce twice the power impulses of four-stroke engines for the same rpm, a two-stroke engine has a higher **power density** and is thus smaller and lighter than a four-stroke engine of equal output. The disadvantages of the two-stroke engine have historically been lower fuel efficiency and higher exhaust emissions because of the overlapping of the intake and exhaust processes and the

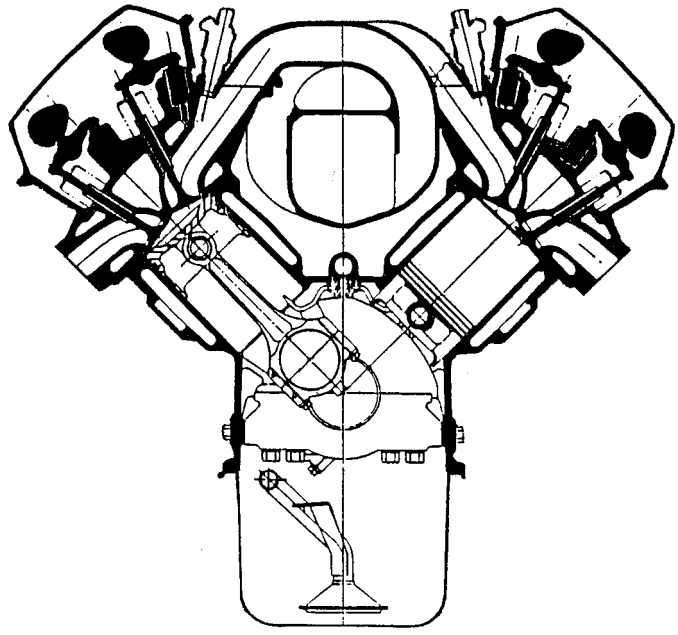

FIGURE 8.3.2 Ford 4.6-L aluminum V-8 SI engine. (Courtesy of Ford Motor Company.)

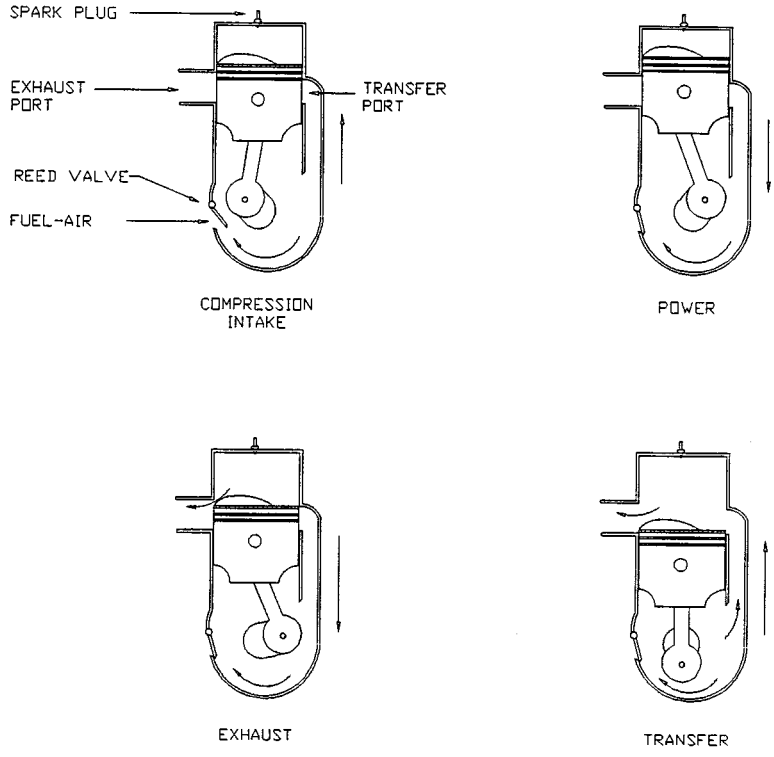

FIGURE 8.3.3 Schematic drawing of two-stroke SI engine.

loss of some fresh intake mixture with the exhaust products. For this reason, two-stroke SI engines have largely been confined to small-displacement applications, such as motorcycles, outboard marine engines, and small equipment. Several manufacturers have addressed these shortcomings in recent years and have achieved significant improvements in two-stroke engine fuel economy and emissions (Blair, 1988). The Orbital OCP (Orbital Combustion Process) engine, illustrated in Figure 8.3.4, is a modern two-stroke engine that utilizes direct injection of fuel into the cylinder in conjunction with a high-turbulence combustion chamber design and an electronically controlled exhaust port scavenging control valve to achieve very favorable fuel economy and significantly reduced levels of NO_x and hydrocarbon emissions. This engine, in three and six cylinder versions, is currently being used in automotive and marine applications.

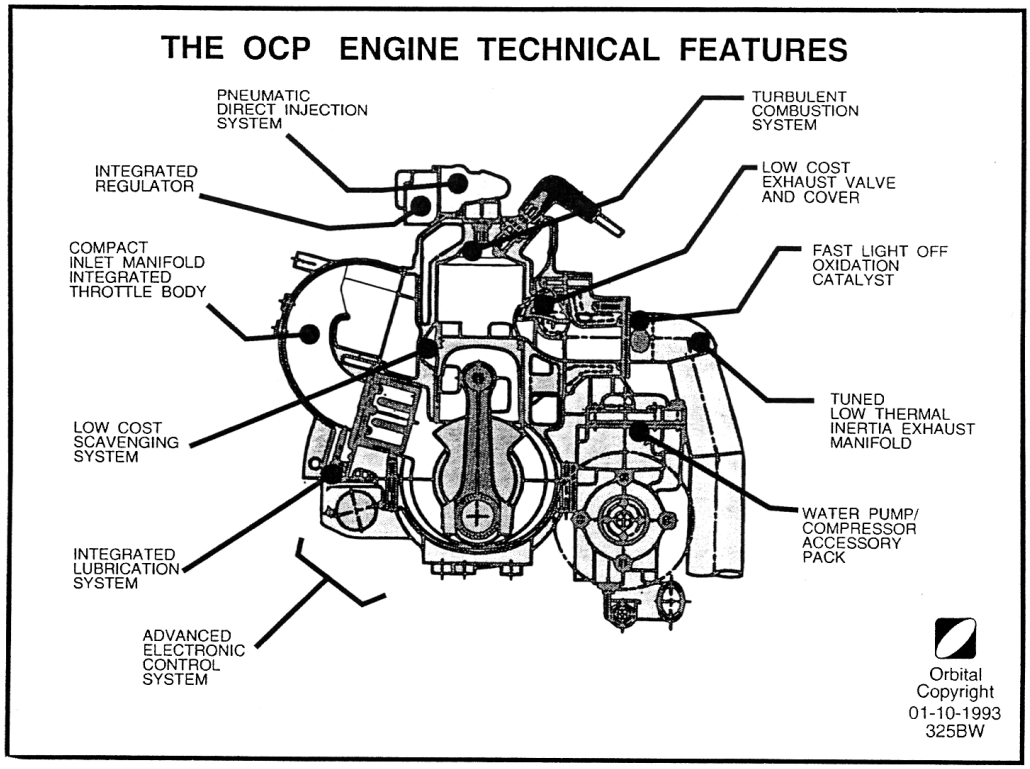

FIGURE 8.3.4 Orbital OCP two-stroke SI engine. (Courtesy of Orbital Engine Company.)

Compression Ignition Engine

The basic valve and piston motions are the same for the CI, or diesel, engine as discussed above for the SI engine. The CI engine relies on the high temperature and pressure of the cylinder air resulting from the compression process to cause **autoignition** of the fuel, which is injected directly into the combustion chamber of **direct injection (DI)** engines or into the prechamber of **indirect injection (IDI)** engines, when the piston approaches TDC on the compression stroke. The compression ratios are typically much higher for CI than for SI engines to achieve the high air temperatures required for autoignition, and the fuels used must have favorable autoignition qualities.

The time period between the start of fuel injection and the occurrence of autoignition is called the **ignition delay period**. Long ignition delay periods allow more time for fuel vaporization and fuel-air mixing, resulting in objectionable diesel knock when this larger premixed charge ignites. Combustion chambers and fuel injection systems must be designed to avoid extended ignition delay periods. Diesel

engines may be classified as DI or IDI. In DI engines, the combustion chamber consists of a bowl formed in the top of the piston and the fuel is injected into this volume. The injector tip generally has from four to eight holes to form multiple spray cones. Two variations are illustrated in Figure 8.3.5. The quiescent chamber engine utilizes a large-diameter shallow bowl shape that produces low **swirl** and low turbulence of the air during compression. Fuel is injected at high pressure through a multihole nozzle, and mixing of the fuel and air relies primarily on the energy of the injected fuel to cause air entrainment in the spray cone and diffusion of vaporized fuel into the air. This system is suited to large slow-speed engines that are operated with significant excess air.

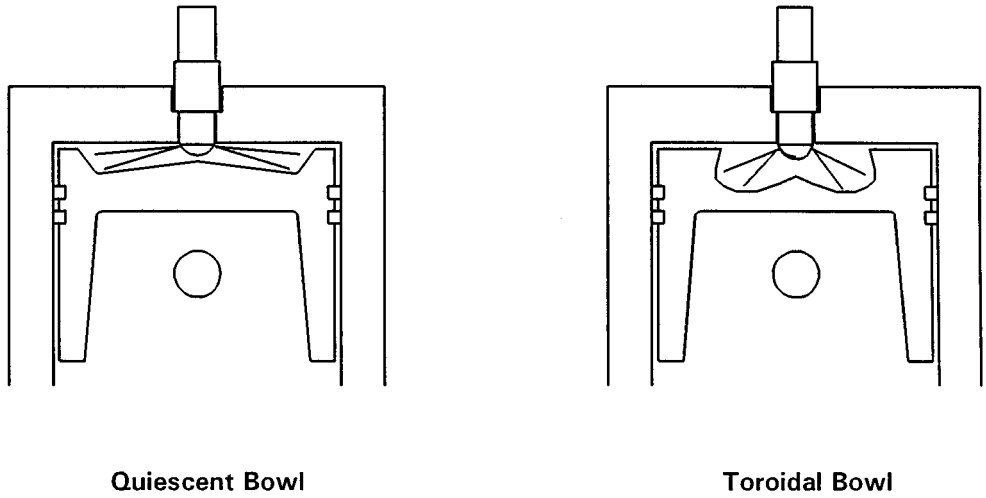

FIGURE 8.3.5 Examples of DI diesel combustion chamber design.

The toroidal bowl combustion chamber is used in conjunction with intake ports and/or valve shrouds designed to produce air swirl to enhance fuel-air mixing. The **swirl ratio** is defined by swirl ratio = swirl speed (rpm)/engine speed (rpm). The swirl velocity component is normal to the fuel spray direction and tends to promote mixing in the regions between the individual spray cones. This system makes better use of the available air and is utilized extensively in moderate-speed engines such as over-the-road truck engines. DI does not lend itself well to high-speed operation, as the time available for proper mixing and combustion is less. Diesel engines for passenger car applications are generally designed for higher-speed operation to produce higher specific output, and typically utilize IDI combustion systems, two of which are illustrated in Figure 8.3.6.

IDI systems make use of small prechambers incorporated in the cylinder head to promote rapid mixing of fuel and air and shorten the ignition delay period. Swirl chambers are designed to produce a strong vortex in the prechamber during compression. The fuel is sprayed into the chamber through a single-hole nozzle and the high vorticity promotes rapid mixing and short ignition delay periods. Precombustion chambers do not attempt to generate an orderly vortex motion within the chamber, but instead rely on a high level of turbulence, created by the rush of air into the chamber during compression, to promote mixing. Both types of prechambers generally include a lining of low-conductivity material (ceramic) to increase the surface temperature to promote further fuel evaporation. Prechambers can be used in small-displacement diesel engines to achieve operating speeds up to 5000 rpm. Disadvantages of the IDI system include poor cold-start characteristics due to high heat-transfer rates from the compressed air to the chamber wall that result from the high velocities and turbulence levels in the chamber. **Glow plugs** are often installed in each prechamber to heat the air to improve cold starting. Higher compression ratios are also used for IDI engines to further improve cold starting. The compression ratios, typically 18 to 24, are higher than the optimum for fuel efficiency (due to decreased mechanical efficiency), and IDI

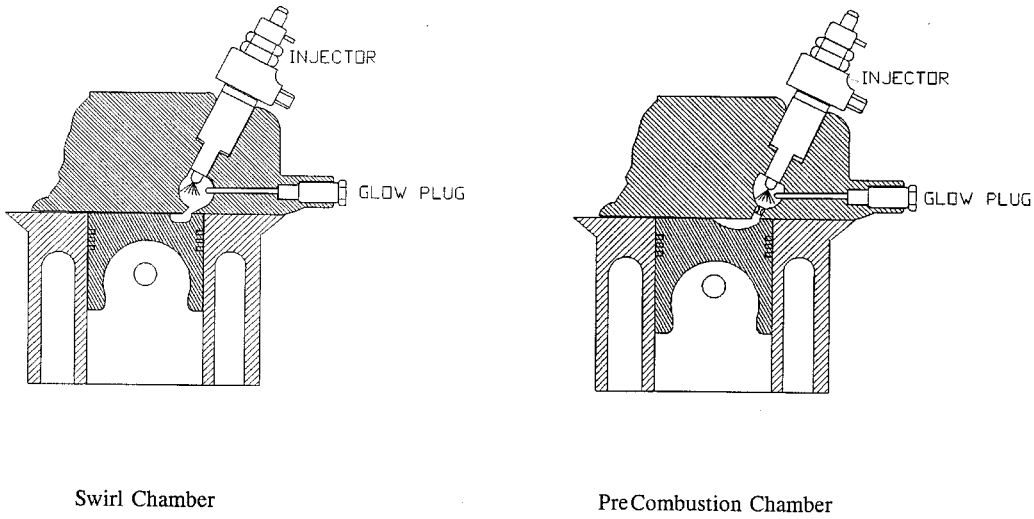

FIGURE 8.3.6 Two examples of IDI combustion chambers.

engines are typically less efficient than larger, slower, DI engines. The use of IDI is generally restricted to high-speed automotive engines, with displacements in the range of 0.3 to 0.8 liter per cylinder, and some degree of fuel economy is sacrificed in the interest of improved driveability.

CI engines are produced in both two-stroke and four-stroke versions. Since the fuel is injected directly into the combustion chamber of CI engines just prior to TDC, two-stroke CI engines do not suffer the same emission and efficiency shortcomings as do two-stroke SI engines. Hence, they are available in much larger displacements for high-power-requirement applications such as locomotive and ship propulsion and electric power generation systems. Two-stroke CI engines are generally of the DI type as the use of IDI in a two-stroke engine would lead to aggravated cold-start problems.

Air Standard Power Cycles

The actual operation of IC engines is idealized at a very basic level by the air standard power cycles (ideal thermodynamic models for converting heat into work on a continuous basis). The following simplifying assumptions are common to the air standard cycles: (1) the working substance is air, (2) the air is assumed to behave as an ideal gas with constant specific heats, (3) heat is added to the cycle from an external source, and (4) expansion and compression processes not involving heat transfer occur isentropically. The air standard cycles, while grossly oversimplified in terms of the complex processes occurring within actual engines, are nevertheless useful in understanding some fundamental principles of SI and CI engines. The simplified models also lend insight into important design parameters, e.g., **compression ratio**, that govern theoretical maximum cycle thermal efficiencies.

Constant-Volume Heat Addition — Ideal Otto Cycle

The theory of operation of the SI engine is idealized by the Otto cycle which assumes that heat is added to the system at constant volume. Constant-volume heat addition is approximated in the SI engine by virtue of the combustion process taking place rapidly when the piston is near TDC. A *P-V* diagram for the Otto cycle is illustrated in Figure 8.3.7. The cycle consists of the following processes: 1 → 2 isentropic compression, 2 → 3 constant-volume heat addition, 3 → 4 isentropic expansion, and 4 → 1 constant-volume heat rejection. The constant-volume heat rejection process is approximated in SI engines by the exhaust valve opening near BDC and the rapid blow down of exhaust gases.

Thermal efficiency for a power cycle is defined as the ratio of work output to heat input per cycle,

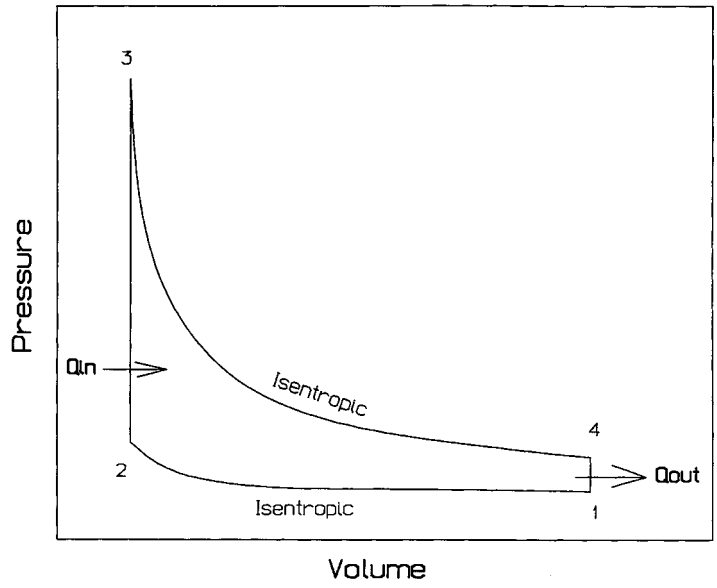

FIGURE 8.3.7 Schematic pressure-volume diagram for the ideal Otto cycle.

$$\eta = \frac{W_{\text{out}}}{Q_{\text{in}}} \tag{8.3.1}$$

For the Otto cycle, the basic efficiency expression can be manipulated into the form

$$\eta = 1 - \frac{1}{r^{\gamma - 1}} \tag{8.3.2}$$

where γ is the ratio of specific heats ($\gamma = C_p/C_v$) and r is the compression ratio, or ratio of the maximum to minimum cycle volumes ($r = V_1/V_2$). In actual IC engines, the minimum cycle volume is referred to as the **clearance volume** and the maximum cycle volume is the **cylinder volume**. The ideal Otto cycle efficiency for air, with $\gamma = 1.4$, is shown plotted in Figure 8.3.8. The theoretical efficiency of the constant volume heat addition cycle increases rapidly with compression ratio, up to about $r = 8$. Further increases in compression ratio bring moderate gains in efficiency. Compression ratios in practical SI engines are limited because of autoignition (knock) and high NO_x emission problems that accompany high compression ratios. Production SI automotive engines typically have compression ratios in the range 8 to 10, whereas high-performance normally aspirated racing engines may have compression ratios as high as 14, but they require the use of special fuels to avoid autoignition.

Constant-Pressure Heat Addition — Ideal Diesel Cycle

The air standard diesel cycle is the idealized cycle underlying the operation of CI or diesel engines. The diesel cycle, illustrated by the *P-V* diagram in Figure 8.3.9, consists of the following processes: 1 → 2 isentropic compression from the maximum to the minimum cycle volume, 2 → 3 constant-pressure heat addition during an accompanying increase in volume to V_3, 3 → 4 isentropic expansion to the maximum cycle volume, and 4 → 1 constant-volume heat rejection.

Actual diesel engines approximate constant-volume heat addition by injecting fuel for a finite duration which continues to burn and release heat at a rate that tends to maintain the pressure in the cylinder over a period of time during the expansion stroke. The efficiency of the ideal diesel cycle is given by

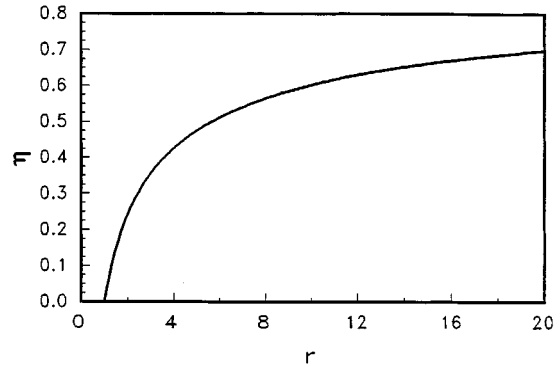

FIGURE 8.3.8 Efficiency of the ideal Otto cycle.

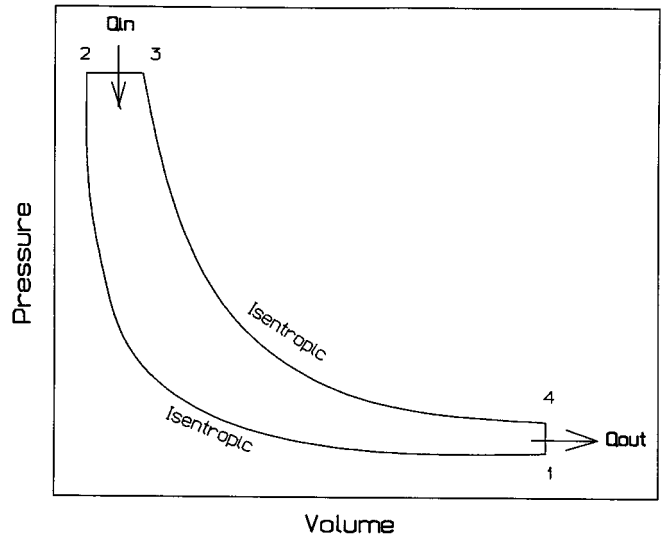

FIGURE 8.3.9 Schematic pressure-volume diagram of ideal diesel cycle.

$$\eta = 1 - \frac{1}{r^{\gamma-1}}\left[\frac{r_c^{\gamma} - 1}{\gamma\left(r_c - 1\right)}\right] \tag{8.3.3}$$

The efficiency of the ideal diesel cycle depends not only on the compression ratio, r, but also on the **cut-off ratio**, $r_c = V_3/V_2$, the ratio of the volume when heat addition ends to the volume when it begins. Equation (8.3.3) is shown plotted in Figure 8.3.10 for several values of r_c and for $\gamma = 1.4$. An r_c value of 1 is equivalent to constant-volume heat addition, i.e., the Otto cycle. The efficiency of the ideal Diesel cycle is less than the efficiency of the ideal Otto cycle for any given compression ratio and any value of the cut-off ratio greater than 1. The fact that CI engines, by design, operate at much higher compression ratios than SI engines (generally between 12 and 24) accounts for their typically higher operating efficiencies relative to SI engines.

Actual Cycles

IC engines do not operate on closed thermodynamic cycles, such as the air standard power cycles, but rather on open mechanical cycles, and heat addition occurs neither at constant volume or constant

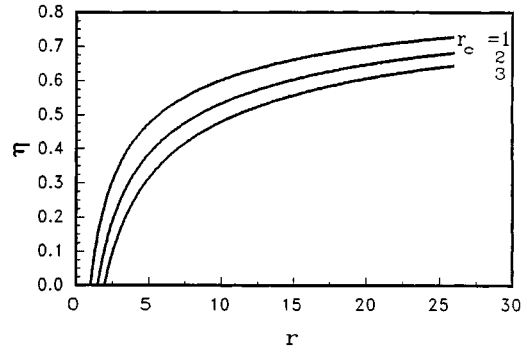

FIGURE 8.3.10 Efficiency of the ideal diesel cycle.

pressure. Figure 8.3.11 is a schematic representation of an **indicator diagram** (pressure-volume history) of a four-stroke IC engine; it could be either SI or CI. The pressure changes during the intake and exhaust strokes are exaggerated in the diagram. The **indicated work** performed per cycle can be calculated by taking the integral of PdV for the complete cycle. The **indicated mean effective pressure**, **imep**, is defined as the ratio of the net indicated work output to the **displacement volume**:

$$\text{imep} = \frac{\text{indicated work output per cycle}}{\text{displacement volume}} \tag{8.3.4}$$

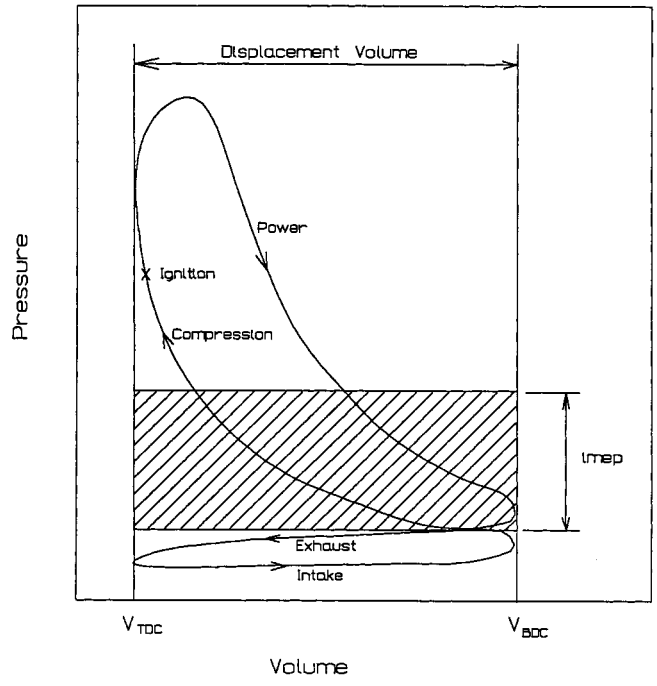

FIGURE 8.3.11 Schematic indicator diagram.

The shaded area in Figure 8.3.11 thus represents the net indicated work output per cycle. During intake and exhaust, the negative work performed represents pumping losses and acts to decrease the net work output of the engine. The magnitude of the pumping losses depends on the flow characteristics of the intake and exhaust systems including the valves, ports, manifolds, piping, mufflers, etc. The more

restrictive these passages, the higher will be the pumping losses. SI engines control power output by throttling the intake air. Thus, under partial-load conditions, the pressure drop resulting from the air throttling represents a significant increase in pumping loss with a corresponding decrease in operating efficiency. SI engines are therefore less efficient at partial-load operation than at full load. The power level of CI engines, on the other hand, is controlled by varying the amount of fuel injected, as opposed to throttling the intake air, making them significantly more efficient than SI engines under partial-load conditions.

Brake work (or power) is the actual work (or power) produced at the output shaft of an engine, as measured by a dynamometer. The brake work will be less than the indicated work due to friction losses and any parasitic power requirements for oil pumps, water pumps, etc. The **brake mean effective pressure**, **bmep**, is defined as

$$\text{bmep} = \frac{\text{brake work output per cycle}}{\text{displacement volume}} \tag{8.3.5}$$

The mechanical efficiency can then be defined as

$$\eta_m = \frac{\text{brake work (power)}}{\text{indicated work (power)}} = \frac{\text{bmep}}{\text{imep}} \tag{8.3.6}$$

Engine thermal efficiency can be determined from the ratio of power output to rate of fuel energy input, or

$$\eta_t = \frac{\text{Power}}{m_f Q_c} \tag{8.3.7}$$

where m_f is the rate of fuel consumption per unit time and Q_c is the heat of combustion per unit mass of fuel. The thermal efficiency in Equation (8.3.7) could be either indicated or brake depending on the nature of the power used in the calculation. Uncertainty associated with variations of energy content of fuels may present a practical difficulty with determining engine thermal efficiency. In lieu of thermal efficiency, **brake specific fuel consumption** (**bsfc**), is often used as an efficiency index.

$$\text{bsfc} = \frac{\text{fuel consumption rate (kg/hr)}}{\text{brake power (kW)}} \tag{8.3.8}$$

The efficiency of engines operating on the same fuel may be directly compared by their bsfc.

Volumetric efficiency, η_v, is an important performance parameter for four-stroke engines defined as

$$\eta_v = \frac{m_{\text{actual}}}{m_d} \tag{8.3.9}$$

where m_{actual} is the mass of intake mixture per cycle at inlet conditions (pressure and temperature near the inlet port) and m_d is the mass of mixture contained in the displacement volume at inlet conditions. For SI engines the mixture mass includes both air and fuel; for CI engines only air is present during intake. With the intake mixture density determined at inlet conditions, η_v accounts for flow losses associated with the intake ports, valves, and cylinder. Sometimes, for convenience, the mixture density is taken at ambient conditions. In this case, η_v is called the overall volumetric efficiency and includes the flow performance of the entire intake system. Since a certain minimum amount of air is required for complete combustion of a given amount of fuel, it follows that the maximum power output of an engine

is directly proportional to its air-flow capacity. Thus, while not affecting in any way the thermal efficiency of the engine, the volumetric efficiency directly affects the maximum power output for a given displacement, and thus can affect the efficiency of the overall system in which the engine is installed because of the effect on system size and weight. Volumetric efficiency is affected primarily by intake and exhaust valve geometry, valve lift and timing, intake port and manifold design, mixing of intake charge with residual exhaust gases, engine speed, ratio of inlet pressure to exhaust back pressure, and heat transfer to the intake mixture from warmer flow passages and combustion chamber surfaces. For further information on the fundamentals of IC engine design and operation see Taylor (1985), Ferguson (1986), Heywood (1988), and Stone (1993).

Combustion in IC Engines

Combustion in Spark Ignition Engines

Background. In SI engines, combustion of the fuel-air mixture is initiated by a spark generated between the electrodes of a spark plug. The intake and compression strokes are designed to prepare the mixture for combustion by completely vaporizing the fuel and heating the mixture to just below its autoignition temperature. This is one reason, in addition to controlling emissions, for the current practice of limiting the maximum compression ratio of SI engines to about 10:1. Near the end of compression, the mixture is well conditioned for combustion and the spark is discharged to initiate the combustion process. For best fuel economy, the combustion process must be completed as close as possible to TDC. This requires that the spark timing be controlled for varying operating speed and load conditions of the engine. Fuel metering and control, according to the engine load requirements, and with minimum variation from cylinder to cylinder and cycle to cycle, is essential for good fuel economy, power output, and emission control of the engine.

Both carburetors and fuel injection systems are used for fuel-metering control. Because of the superior control capabilities of fuel injection systems, they are nearly universally used today in production automotive applications. Carburetors are used for applications with less-stringent emission requirements, e.g., small engines for lawn and garden equipment. Figure 8.3.12 illustrates the effect of **fuel-air ratio** on the indicated performance of an SI engine. The **equivalence ratio** (γ) is defined by the ratio Fuel-Air_{actual}/Fuel-$Air_{stoichiometric}$. Rich mixtures have fuel-air ratios greater than stoichiometric ($\gamma > 1$) and lean mixtures have fuel-air ratios less than stoichiometric ($\gamma < 1$). Optimum fuel economy, coinciding with maximum thermal efficiency, is obtained at part throttle with a lean mixture as a result of the fact that the heat release from lean mixtures suffers minimal losses from dissociation and variation of specific heat effects when compared with stoichiometric and rich fuel-air ratios. Maximum power is obtained at full throttle with a slightly rich mixture, an indication of the full utilization of the air inside the cylinders. Idling, with a nearly closed throttle, requires a rich mixture because of the high percentage of exhaust gas residuals that remains in the cylinders. The fuel-air mixture requirement under transient operation, such as acceleration, requires a rich mixture to compensate for the reduced evaporation caused by the sudden opening of the throttle. Cold starting also requires a rich mixture to ensure the vaporization of sufficient amounts of the highly volatile components in the fuel to achieve proper ignition.

Normal Combustion Process. The combustion processes in SI engines can be divided into two categories, normal and abnormal. The normal combustion process occurs in three stages: initiation of combustion, flame propagation, and termination of combustion. Combustion normally starts across the spark plug gap when the spark is discharged. The fuel molecules in and around the spark discharge zone are ignited and a small amount of energy is released. The important criterion for the initial reaction to be self-sustaining is that the rate of heat release from the initial combustion be larger than the rate of heat transfer to the surroundings. The factors that play an important role in making the initial reaction self-sustaining, and thereby establishing a flame kernel, are the ignition energy level, the spark plug gap, the fuel-air ratio, the initial turbulence, and the condition of the spark plug electrodes.

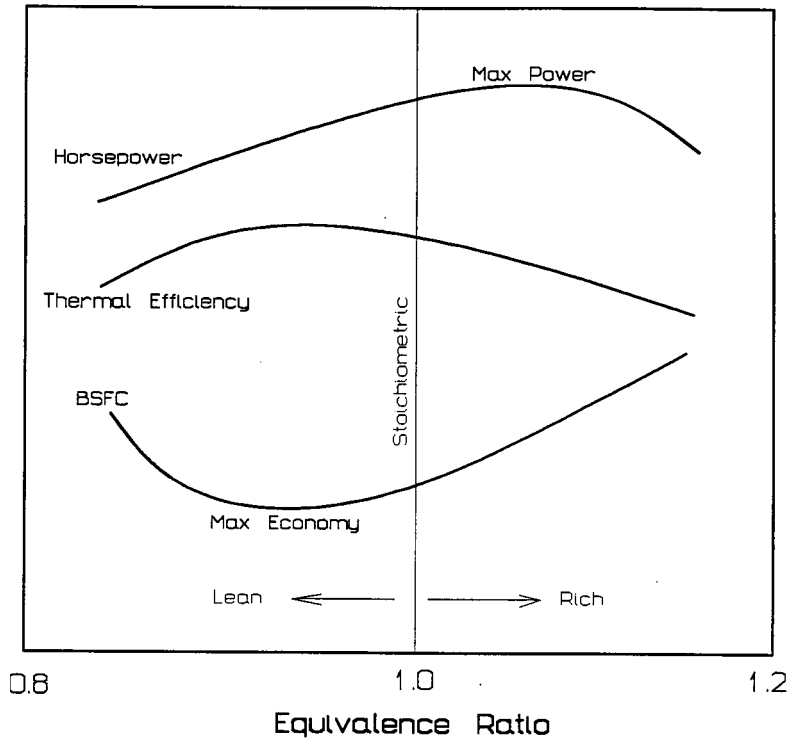

FIGURE 8.3.12 Effect of fuel-air mixture on indicated performance of an SI engine.

After a flame kernel is established, a thin spherical flame front advances from the spark plug region progressively into the unburned mixture zone. Flame propagation is supported and accelerated by two processes. First, the combined effect of the heat transfer from the high-temperature flame region and the bombardment by the active radicals from the flame front into the adjacent unburned zone raises the temperature and accelerates the rate of reactivity of the unburned mixture region directly adjacent to the flame front. This helps condition and prepare this zone for combustion. Second, the increase in the temperature and pressure of the burned gases behind the flame front will cause it to expand and progressively create thermal compression of the remaining unburned mixture ahead of the flame front. It is expected that the flame speed will be low at the start of combustion, reach a maximum at about half the flame travel, and decrease near the end of combustion. Overall, the flame speed is strongly influenced by the degree of turbulence in the combustion chamber, the shape of the combustion chamber, the mixture strength, the type of fuel, and the engine speed.

When the flame front approaches the walls of the combustion chamber, the high rate of heat transfer to the walls slows down the flame propagation and finally the combustion process terminates close to the walls because of surface quenching. This leaves a thin layer of unburned fuel close to the combustion chamber walls which shows up in the exhaust as unburned hydrocarbons.

Abnormal Combustion. Abnormal combustion may occur in SI engines associated with two combustion phenomena: **knock** and **surface ignition**. Knock occurs near the end of the combustion process if the end portion of the unburned mixture, which is being progressively subjected to thermal compression, autoignites prematurely before the flame front reaches it. As a result of the sudden energy release, a violent pressure wave propagates back and forth across the combustion chamber, causing the walls or other parts of the engine to vibrate, producing a sharp metallic noise called knock. If knock persists for a period of time, the high rate of heat transfer caused by the traveling high pressure and temperature wave may overheat the spark plug electrode or ignite carbon deposits that may be present in the

combustion chamber, causing uncontrolled combustion and preignition. As a result, loss of power and serious engine damage may occur.

Knock is sensitive to factors that increase the temperature and pressure of the end portion of the unburned mixture, as well as to fuel composition and other time factors. Factors that increase the probability of knock include (1) increasing the temperature of the mixture by increasing the charge intake temperature, increasing the compression ratio, or turbo/supercharging; (2) Increasing the density of the mixture by turbo/supercharging or increasing the load; (3) advancing the spark timing; (4) increasing the time of exposure of the end portion of the unburned mixture to autoignition conditions by increasing the length of flame travel or decreasing the engine speed and turbulence; and (5) using low-octane fuel and/or maximum power fuel-air ratios. Engine design factors that affect knock in SI engines include the shape of the combustion chamber and the location of the spark plug and inlet and exhaust valves relative to the location of the end portion of the unburned mixture.

Surface ignition is the ignition of the unburned mixture by any source in the combustion chamber other than the normal spark. Such sources could include overheated exhaust valves or spark plug electrodes, glowing carbon deposits, or other hot spots. Surface ignition will create secondary flame fronts which cause high rates of pressure rise resulting in a low-pitched, thudding noise accompanied by engine roughness. Severe surface ignition, especially when it occurs before spark ignition, may cause serious structural and/or component damage to the engine.

Combustion in Compression Ignition Engines

Unlike the SI engine, in which the charge is prepared for combustion as a homogeneous mixture during the intake and compression strokes, fuel preparation for combustion in CI engines occurs in a very short period of time called the ignition delay period. During this period, the fuel injected into the high-temperature air near the end of the compression stroke undergoes two phases of transformation. A physical delay period, during which the fuel is vaporized, mixed with the air, and raised in temperature, is followed by a chemical delay period during which fuel cracking and decomposition occur which leads to autoignition and combustion of the fuel.

The combustion process is **heterogeneous** and involves two modes, usually identified as premixed combustion and diffusion combustion. Premixed combustion occurs early in the process when the fuel which has evaporated and mixed with air during the ignition delay period ignites. This mode is characterized by uncontrolled combustion and is the source of combustion noise since it is accompanied by a high rate of heat release which produces a high rate of pressure rise. When the premixed fuel-air mixture is depleted, diffusion combustion takes over, characterized by a lower rate of heat release and producing controlled combustion during the remainder of the process. Figure 8.3.13 depicts the different stages of the combustion process in CI engines.

The ignition delay period plays a key role in controlling the time duration of the two modes of combustion. Prolonging the ignition delay period, either through engine design factors or variations in operating conditions, will generate a larger portion of premixed fuel-air mixture and will thus tend to increase the premixed combustion mode duration and decrease the diffusion mode duration. This may lead to higher peak cylinder pressure and temperature which may improve thermal efficiency and reduce CO and **unburned hydrocarbon (UHC)** emissions at the expense of increased emissions of oxides of nitrogen ($\mathbf{NO_x}$). Large increases in the ignition delay period will cause high rates of pressure rise during the premixed combustion and may lead to objectionable diesel knock. Reducing the ignition delay period causes the premixed combustion duration to decrease while increasing the diffusion combustion duration. A large reduction in ignition delay may lead to loss of power, decrease in thermal efficiency, and possible deterioration of exhaust emissions. Several factors related to the fuel-air mixture temperature and density, engine speed, combustion chamber turbulence, injection pressure, rate of injection, and fuel composition influence the duration of the ignition delay period.

Knock in CI Engines. As the combustion process in CI engines is triggered by autoignition of the fuel injected during the ignition delay period, factors that prolong the ignition delay period will increase the

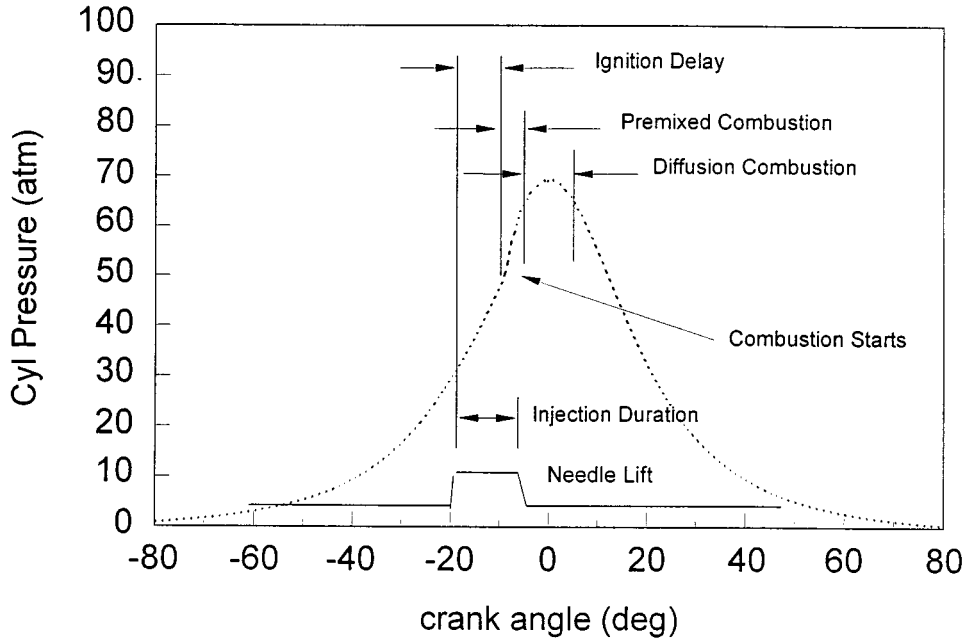

FIGURE 8.3.13 Combustion process in a CI engine.

premixed combustion duration causing very high rates of energy release and thus high rates of pressure rise. As a result, diesel knock may occur. The phenomenon is similar to knock in SI engines except that it occurs at the beginning of the combustion process rather than near the end, as observed in SI combustion. Factors that reduce the ignition delay period will reduce the possibility of knock in diesel engines. Among them are increasing the compression ratio, supercharging, increasing combustion chamber turbulence, increasing injection pressure, and using high-**cetane-number** (**CN**) fuel. For a more detailed discussion of the combustion process in IC engines, see Henein (1972), Lenz (1992), and Keating (1993).

Exhaust Emissions

Harmful Constituents

The products of combustion from IC engines contain several constituents that are considered hazardous to human health, including CO, UHCs NO_x, and **particulates** (from diesel engines). These emission products are discussed briefly below followed by a description of the principal schemes for their reduction.

Carbon Monoxide. CO is a colorless, odorless, and tasteless gas that is highly toxic to humans. Breathing air with a small volumetric concentration (0.3%) of CO in an enclosed space can cause death in a short period of time. CO results from the incomplete combustion of hydrocarbon fuels. One of the main sources of CO production in SI engines is the incomplete combustion of the rich fuel mixture that is present during idling and maximum power steady state conditions and during such transient conditions as cold starting, warm-up, and acceleration. Fuel maldistribution, poor condition of the ignition system, very lean combustion, and slow CO reaction kinetics also contribute to increased CO production in SI engines. CO production is not as significant in CI engines since these engines are always operated with significant excess air.

Unburned Hydrocarbons. When UHCs combine with NO_x (see below) in the presence of sunlight, ozone and photochemical oxidants form that can adversely affect human health. Certain UHCs are also

considered to be carcinogenic. The principal cause of UHC in SI engines is incomplete combustion of the fuel-air charge, resulting in part from flame quenching of the combustion process at the combustion chamber walls, and engine misfiring. Additional sources in four-stroke engines may include fuel mixture trapped in crevices of the top ring land of the piston and outgassed fuel during the expansion (power) stroke that was absorbed into the lubricating oil film during intake. In two-stroke SI engines, the scavenging process often results in a portion of the fresh mixture exiting the exhaust port before it closes, resulting in large UHC emissions.

The presence of UHC in CI engines is related to the heterogeneous nature of the fuel-air mixture. Under certain conditions, fuel-air mixtures that lie outside the flammability limits at both the lean and rich extremes can exist in portions of the combustion chamber and escape combustion, thus contributing significantly to UHC in the exhaust. Fuel injected near the end of the combustion process, and fuel remaining in the nozzle **sac volume** at the end of injection, both contribute to UHC emission in CI engines. Engine variables that affect UHC emissions include the fuel-air ratio, intake air temperature, and cooling water temperature.

Oxides of Nitrogen. Nitric oxide (NO) is formed from the combination of nitrogen and oxygen present in the intake air under the high-temperature conditions that result from the combustion process. As the gas temperature drops during the expansion stroke, the reaction is frozen, and levels of NO persist in the exhaust products far in excess of the equilibrium level at the exhaust temperature. In the presence of additional oxygen in the air, some NO transforms to nitrogen dioxide (NO_2), a toxic gas. The NO and NO_2 combined are referred to as oxides of nitrogen or NO_x. The production of NO_x is in general aggravated by conditions that increase the peak combustion temperature. In SI engines the most important variables that affect NO_x production are the air/fuel ratio, spark timing, intake air temperature, and amount of residual combustion products remaining in the cylinder after exhaust. In CI engines, ignition delay, which affects the degree of premixed combustion, plays a key role in NO_x formation. A larger premixed combustion fraction will produce higher combustion temperatures and higher levels of NO_x.

Particulates. Particulates are a troublesome constituent in the exhaust from CI engines. Particulates are defined by the US Environmental Protection Agency (EPA) as any exhaust substance (other than water) that can be trapped on a filter at a temperature of 325 K or below. Particulates trapped on a filter may be classified as soot plus an organic fraction of hydrocarbons and their partial oxidation products. Soot consists of agglomerates of solid uncombusted carbon particles. Particulates are of concern because their small size permits inhalation and entrapment in the lung walls, making them potential lung carcinogens.

Soot is formed in CI engines under conditions of heavy load when the gas temperature is high and the concentration of oxygen is low. Smoke production is affected by such parameters as fuel CN, rate of fuel injection, inlet air temperature, and the presence of secondary injection.

Control of Emissions from IC Engines

Figure 8.3.14 depicts the relative concentrations of CO, NO_x, and UHC in the exhaust products of an SI engine as a function of the fuel-air mixture. Lean mixture combustion, which promotes good thermal efficiency, also results in low UHC and CO production but causes high levels of NO_x emission. Increasing the fuel/air ratio to reduce NO_x results in increased CO and UHC emission. Approaches to reduce total emissions fall under two categories; the first concentrates on engine design and fuel modifications and the second involves treatment of exhaust gases after leaving the engine. In SI engines, the first approach focuses on addressing engine variables and design modifications which improve in-cylinder mixing and combustion in an effort to reduce CO and UHC emissions. To reduce NO_x, attention is focused on factors that reduce peak combustion temperature and reduce the oxygen available in the flame front. Design and operating parameters that have been implemented or modified for decreased emissions include compression ratio reduction, increased coolant temperature, modification of the combustion chamber shape to minimize surface-to-volume ratio and increase turbulence, improvement of intake manifold design for better charge distribution, use of fuel injection instead of carburetors for better mixture control,

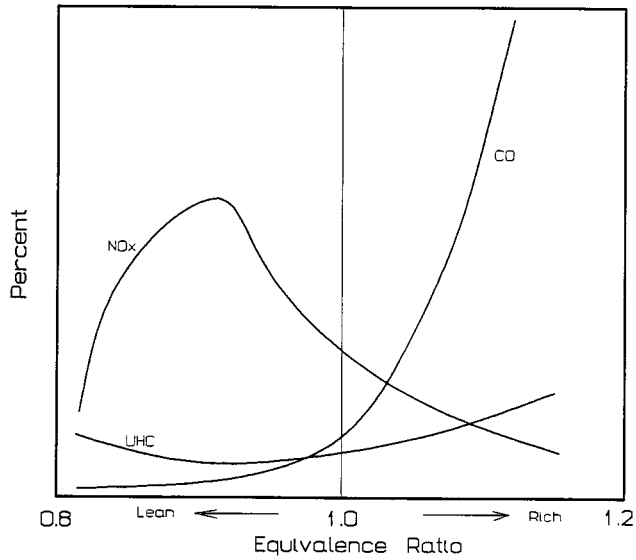

FIGURE 8.3.14 Emission levels from an SI engine vs. fuel-air mixture.

use of exhaust gas recirculation to reduce NO_x by lowering combustion temperatures, positive crankcase ventilation to reduce UHC, and increased aromatic content in gasoline.

Engine modifications that have been implemented to reduce emissions from CI engines include modifications to the combustion chamber shape to match the air swirl pattern and fuel spray pattern for better mixing and complete combustion, use of exhaust gas recirculation to limit NO_x production, use of higher injection pressure for better atomization to reduce soot and UHC, and the use of precise injection timing with electronic control.

In the second approach, several devices have been developed for after treatment of exhaust products. A thermal reactor may be used to oxidize UHC and CO. These typically consist of a well-insulated volume placed close to the exhaust manifold, with internal baffles to increase the gas residence time and an air pump to supply fresh oxygen for the oxidation reactions. Thermal reactors are ineffective for NO_x reduction and thus have limited application.

Catalytic converters utilize a catalyst, typically a noble metal such as platinum, rhodium, or palladium, deposited on a ceramic substrate to promote reactions at lower temperatures. Two types are in use, oxidation converters and reduction converters. Oxidation catalytic converters use the excess air available in lean mixtures (or supplied from an external air pump) to oxidize CO and UHC emissions. Reduction catalytic converters operate with low levels of oxygen to cause reduction of NO_x. Sometimes, dual catalytic converters are employed to treat all three pollutants with a reducing converter, to reduce NOx, placed upstream of an oxidation converter for treating CO and UHC. This arrangement requires that the engine be operated with a rich mixture which decreases fuel economy.

Three-way catalytic converters are a recent development that permits treatment of NO_x, CO, and UHC in a single device, thus reducing size and weight of the exhaust system. Proper operation of a three-way catalyst requires very nearly stoichiometric combustion. If the combustion is too lean, NO_x is not adequately reduced, and if it is too rich, UHC and CO are not adequately oxidized. There is a narrow band for equivalence ratio from about 0.999 to 1.007 within which conversion efficiency is 80% or better for all three pollutants (Kummer, 1980). Maintaining engine operation within this narrow mixture band requires a closed-loop fuel-metering system that utilizes an oxygen sensor placed in the exhaust system to monitor excess oxygen and control the fuel injection to maintain near stoichiometric combustion.

Reduction catalytic converters cannot be used with CI engines to reduce NO_x since they normally run lean with significant amounts of excess oxygen in the exhaust. Thus, engine design factors must be relied on to keep NO_x as low as possible. Soot emission may be reduced by after treatment using a

device called a trap oxidizer. A trap oxidizer filters particulate matter from the exhaust stream and oxidizes it, usually with the aid of a catalyst for reducing the oxidation temperature. They have been used on small, high-speed automotive diesel engines, but their application to larger, slower-speed engines is limited because of the higher level of particulate production and the lower exhaust temperature. For additional information on emissions see Henein (1972), Obert (1973), and *SAE Surface Vehicle Emissions Standards Manual* (1993).

Fuels for SI and CI Engines

Background

The primary distinguishing factor between SI and CI engines is the fundamental difference in the combustion process. SI engines rely on homogeneous, premixed combustion, while CI engines are designed for heterogeneous combustion with a premixed combustion period followed by a diffusion combustion period. The differences in the combustion process call for quite different qualities in the fuels to achieve optimum performance.

By far the most common fuel for SI engines is gasoline, although other fuels can be used in special circumstances including alcohol, natural gas, and propane. Even such low-grade fuels as wood gas and coal gas have been used to fuel SI engines during wartime when conventional fuels were in short supply. Diesel fuel is the predominant fuel for CI engines, but they too can be designed to operate on a variety of other fuels, such as natural gas, bio-gas, and even coal slurries. This discussion is confined to gasoline and diesel fuel, both of which are distilled from crude oil.

Crude oil is composed of several thousand different hydrocarbon compounds, which upon heating are vaporized at different temperatures. In the distillation process, different "fractions" of the original crude are separated according to the temperatures at which they vaporize. The more volatile fraction, naphtha, is followed in order of increasing temperature of vaporization by fractions called distillate, gas oil, reduced crude, and residual oil. These fractions may be further subdivided into light, middle, and heavy classifications. Light virgin naphtha can be used directly as gasoline, although it has relatively poor antiknock quality. The heavier fractions can be chemically processed through coking and catalytic cracking to produce additional gasoline. Diesel fuel is derived from the light to heavy virgin gas oil fraction and from further chemical processing of reduced crude.

Gasoline

Gasoline fuels are mixtures of hydrocarbon compounds with boiling points in the range of 32 to 215°C. The two most important properties of gasoline for SI engine performance are volatility and octane rating. Adequate volatility is required to ensure complete vaporization, as required for homogeneous combustion, and to avoid cold-start problems. If the volatility is too high, however, vapor locking in the fuel delivery system may become a problem. Volatility may be specified by the distillation curve (the distillation temperatures at which various percentages of the original sample have evaporated). Higher-volatility fuels will be characterized by lower temperatures for given fixed percentages of evaporated sample, or conversely, by higher percentages evaporated at or below a given temperature. Producers generally vary the volatility of gasoline to suit the season, increasing the volatility in winter to improve cold-start characteristics and decreasing it in summer to reduce vapor locking.

The octane rating of a fuel is a measure of its resistance to autoignition or knocking; higher-octane fuels are less prone to autoignition. The octane rating system assigns the value of 100 to iso-octane (C_8H_{18}, a fuel that is highly resistant to knock) and the value 0 to *n*-heptane (C_7H_{16}, a fuel that is prone to knock). Two standardized methods are employed to determine the octane rating of fuel test samples, the research method and the motor method; see ASTM Standards Part 47 — Test Methods for Rating Motor, Diesel and Aviation Fuels (ASTM, 1995). Both methods involve testing the fuel in a special variable-compression-ratio engine (cooperative fuels research or CFR engine). The test engine is operated on the fuel sample and the compression ratio is gradually increased to obtain a standard knock intensity reading from a knock meter. The octane rating is obtained from the volumetric percentage of iso-octane

in a blend of iso-octane and *n*-heptane that produces the same knock intensity at the same compression ratio. The principal differences between the research method and the motor method are the higher operating speed, higher mixture temperature, and greater spark advance employed in the motor method. Ratings obtained by the research method are referred to as the **research octane number** (RON), while those obtained with the motor method are called the motor octane number (MON). MON ratings are lower than RON ratings because of the more stringent conditions, i.e., higher thermal loading of the fuel. The octane rating commonly advertised on gasoline pumps is the **antiknock index**, $(R + M)/2$, which is the average of the values obtained by the two methods. The typical range of antiknock index for automotive gasolines currently available at the pump is 87 to 93. In general, higher compression SI engines require higher-octane fuels to avoid autoignition and to realize full engine performance potential from engines equipped with electronic control systems incorporating a knock sensor.

Straight-run gasoline (naphtha) has a poor octane rating on the order of 40 to 50 RON. Higher-octane fuels are created at the refinery by blending with higher-octane components produced through alkylation wherein light olefin gases are reacted with isobutane in the presence of a catalyst. Iso-octane, for example, is formed by reacting isobutane with butene. Aromatics with double carbon bonds shared between more than one ring, such as naphthalene and anthracene, serve to increase octane rating because the molecules are particularly difficult to break.

Additives are also used to increase octane ratings. In the past, a common octane booster added to automotive fuels was lead alkyls, either tetraethyl or tetramethyl lead. For environmental reasons, lead has been removed from automotive fuels in most countries. It is, however, still used in aviation fuel. Low-lead fuel has a concentration of about 0.5 g/L which boosts octane rating by about five points. The use of leaded fuel in an engine equipped with a catalytic converter to reduce exhaust emissions will rapidly deactivate the catalyst (typically a noble metal such as platinum or rhodium), quickly destroying the utility of the catalytic converter. Octane-boosting additives that are in current use include the oxygenators methanol, ethanol, and methyl tertiary butyl ether (MTBE).

RON values of special-purpose high-octane fuels for racing and aviation purposes can exceed 100 and are arrived at through an extrapolation procedure based on the knock-limited indicated mean effective pressure (klimep). The klimep is determined by increasing the engine intake pressure until knock occurs. The ratio of the klimep of the test fuel to that for iso-octane is used to extrapolate the octane rating above 100.

Diesel Fuels

Diesel fuels are blends of hydrocarbon compounds with boiling points in the range of 180 to 360°C. Properties that are of primary importance for CI fuels include the density, viscosity, cloud point, and ignition quality (CN). Diesel fuel exhibits a much wider range of variation in properties than does gasoline. The density of diesel fuels tends to vary according to the percentages of various fractions used in the blend. Fractions with higher distillation temperatures tend to increase the density. Variations in density result in variations in volumetric energy content and hence fuel economy, since fuel is sold by volume measure. Higher-density fuel will also result in increased soot emission. Viscosity is important to proper fuel pump lubrication. Low-viscosity fuel will tend to cause premature wear in injection pumps. Too high viscosity, on the other hand, may create flow problems in the fuel delivery system. Cloud point is the temperature at which a cloud of wax crystals begins to form in the fuel. This property is critical for cold-temperature operation since wax crystals will clog the filtration system. ASTM does not specify maximum cloud point temperatures, but rather recommends that cloud points be no more than 6°C above the tenth percentile minimum ambient temperature for the region for which the fuel is intended; see ASTM D 975 (ASTM 1995).

CN provides a measure of the autoignition quality of the fuel and is the most important property for CI engine fuels. The CN of a fuel sample is obtained through the use of a CI CFR engine in a manner analogous to the determination of octane rating. The test method for CN determination is specified in standard ASTM D 613. *n*-Cetane (same as hexadecane, $C_{16}H_{34}$) has good autoignition characteristics and is assigned the cetane value of 100. The bottom of the cetane scale was originally defined in terms

of α-methyl naphthalene ($C_{11}H_{10}$) which has poor autoignition characteristics and was assigned the value 0. In 1962, for reasons of availability and storability, the poor-ignition-quality standard fuel used to establish the low end of the cetane scale was changed to heptamethylnonane (HMN), with an assigned CN of 15. The CN of a fuel sample is determined from the relative volumetric percentages of cetane and HMN in a mixture that exhibits the same ignition delay characteristics as the test sample using the relation

$$\text{CN} = \%\ n\text{-cetane} + 0.15\,(\%\ \text{HMN}) \tag{8.3.10}$$

ASTM standard D 976 (ASTM, 1995) provides the following empirical correlation for calculating the **cetane index** of straight petroleum distillate fuels (no additives) as an approximation to the measured CN:

$$\text{Cetane Index} = 454.74 - 1641.416D + 774.74D^2 - 0.554B + 97.803\,(\log B)^2 \tag{8.3.11}$$

where D = density at 15°C (g/mL) and B = mid-boiling temperature (°C).

ASTM standard D 975 (ASTM, 1995) establishes three classification grades for diesel fuels (No. 1-D, No. 2-D, and No. 4-D) and specifies minimum property standards for these grades. No. 1-D is a volatile distillate fuel for engines that must operate with frequent changes in speed and load. No. 2-D is a lower-volatility distillate fuel for industrial and heavy mobile service engines. No. 4-D is a heavy fuel oil for low- and medium-speed engines. Nos. 1-D and 2-D are principally transportation fuels, while No. 4-D is for stationary applications. The ASTM minimum CN for No. 1-D and No. 2-D is 40, and for No. 4-D the minimum is 30. Typical CNs for transportation fuels lie in the range 40 to 55. Use of a low-cetane fuel aggravates diesel knock because of the longer ignition delay period which creates a higher fraction of premixed combustion.

Antiknock quality (octane number) and ignition quality (CN) are opposing properties of distillate fuels. The CN increases with decreasing octane rating of various fuels. Gasoline, with good antiknock quality, has a CN of approximately 10, while a diesel fuel with a CN of 50 will have an octane number of about 20. Thus, gasoline is not a suitable fuel for CI engines because of its poor autoignition quality, and diesel fuel is inappropriate for use in SI engines as a result of its poor antiknock quality. For additional information on fuels for IC engines see Owen and Coley (1995) and the *SAE Fuels and Lubricants Standards Manual* (1993).

Intake Pressurization — Supercharging and Turbocharging

Backround

Pressurizing the intake air (or mixture) by means of a compressor may be used to boost the specific power output of both SI and CI engines. Supercharging generally refers to the use of compressors that are mechanically driven from the engine crankshaft, while turbocharging refers to compressors powered by a turbine which extracts energy from the exhaust stream. Increasing the intake pressure increases the density and hence the mass flow rate of the intake mixture, allowing an increase in the fueling rate, thereby producing additional power. The mere process of increasing the cylinder pressure results in increased work output per cycle, as illustrated in the *P-V* diagram in Figure 8.3.15 which compares supercharged and naturally aspirated, air standard Otto cycles having the same compression ratio. The work done for the compressed intake cycle (Area 1,2,3,4,1 and Area 5,6,7,1,5) is greater than that for the naturally aspirated cycle (Area 1′,2′,3′,4′,1′) due to the boost of the intake pressure. Positive-displacement superchargers are capable of producing higher boost pressures than turbochargers, which are nearly always centrifugal-type fans. From a practical standpoint, the maximum useful boost pressure from either system is limited by the onset of autoignition in SI engines, and by the permissible mechanical and thermal stresses in CI engines.

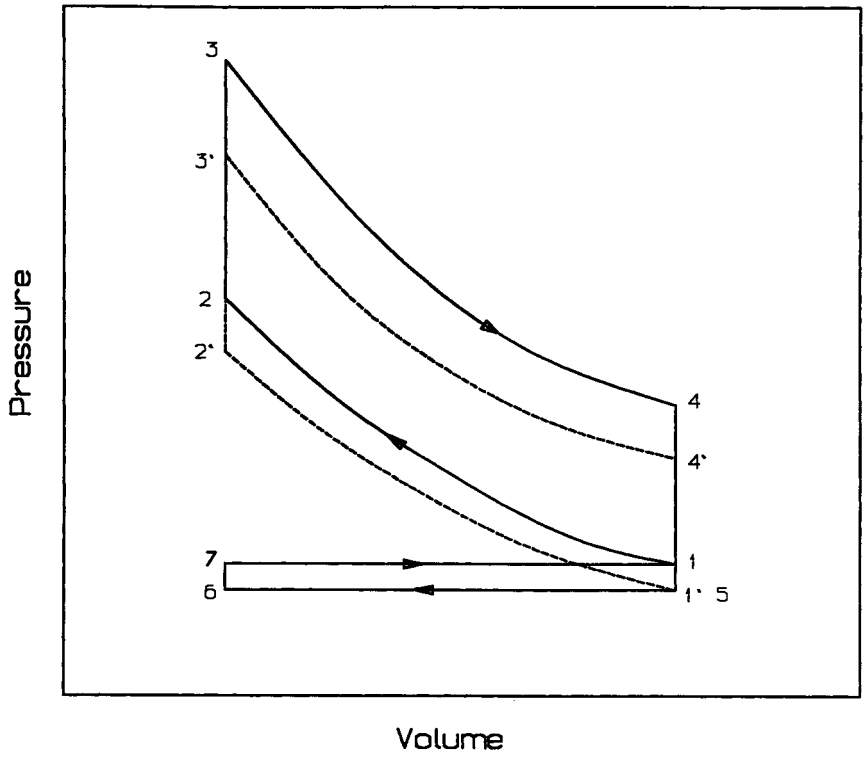

FIGURE 8.3.15 Comparison of supercharged and naturally aspirated Otto cycle.

Supercharging

The principal applications of supercharging of SI engines are in high-output drag-racing engines and in large aircraft piston engines to provide high specific output at takeoff and to improve power output at high altitudes. For diesel applications, supercharging is used mainly in marine and land-transportation applications. It is common to use either supercharging or turbocharging to improve the scavenging process in two-stroke diesel engines. Figure 8.3.16 is a schematic of an engine with a mechanically driven supercharger. Superchargers may be belt, chain, or gear driven from the engine crankshaft.

Two types of superchargers are in use: the positive displacement type (Roots blower) and the centrifugal type. Roots blowers may be classified as: (1) straight double lobe, (2) straight triple lobe, and (3) helix triple lobe (twisted 60%). The helix-triple-lobe-type runs quieter than the others and is generally recommended, especially for diesel engines operating under high torque at various speed conditions. The centrifugal-type, because of its high capacity and small weight and size, is best suited for applications where power and volumetric efficiency improvement are required at high engine speed, e.g., with aircraft engines. A centrifugal blower will also survive a backfire more readily than a Roots blower in SI applications. Since superchargers are directly driven from the engine output shaft, there is no inherent lag in the rate of pressure increase with engine speed, as is typically the case with turbochargers.

Turbocharging

Turbochargers utilize a centrifugal compressor that is directly connected to a turbine which extracts energy from the exhaust gases of the engine and converts it to the shaft work necessary to drive the compressor. Turbocharging is widely used to increase power output in automotive and truck applications of four-stroke SI and CI engines and to improve scavenging of two-stroke CI engines.

There are three methods of turbocharging: the constant-pressure, the pulse, and the pulse converter methods. In the constant-pressure method, as illustrated in Figure 8.3.17, the exhaust pressure is main-

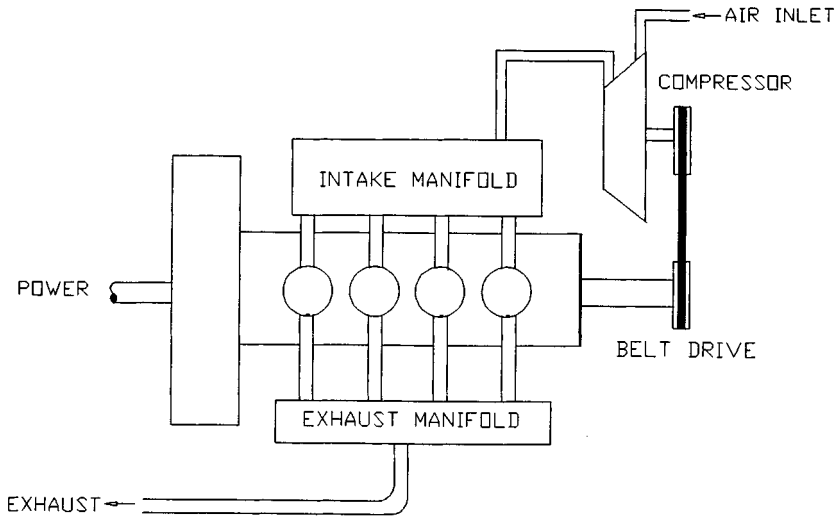

FIGURE 8.3.16 Schematic diagram of supercharged engine.

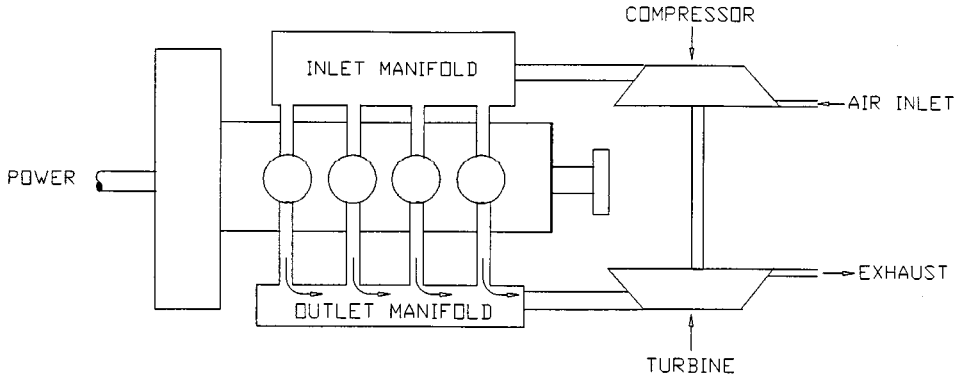

FIGURE 8.3.17 Schematic diagram of a constant-pressure turbocharger.

tained at a nearly constant level above atmospheric. To accomplish this, the exhaust manifold must be large enough to damp out the pressure fluctuations caused by the unsteady flow characteristic of the engine exhaust process. In this method, the turbine operates efficiently under steady-flow conditions; however, some engine power is lost because of the increased backpressure in the exhaust manifold.

The pulse turbocharger, as illustrated in Figure 8.3.18, utilizes the kinetic energy generated by the exhaust blow-down process in each cylinder. This is accomplished by using small exhaust lines grouped together in a common manifold to receive the exhaust from the cylinders which are blowing down sequentially. In this method, the pressure at the turbine inlet tends to fluctuate, which is not conducive to good turbine efficiency. This is offset to a large degree, however, by improved engine performance as a result of the lower exhaust backpressure relative to the constant-pressure method. The pulse converter method represents a compromise between the previous two techniques. In principle, this is accomplished by converting the kinetic energy in the blow-down process into a pressure rise at the turbine by utilizing one or more diffusers. Details of the different methods of turbocharging may be found in Watson and Janota (1982).

Recent advances in turbocharging technology have focused mainly on (1) improvement of the turbine transient response (turbo-lag), (2) improvement of the torque-speed characteristics of the engine, and (3) increasing the power output by increasing the boost pressure and using charge cooling (intercooling).

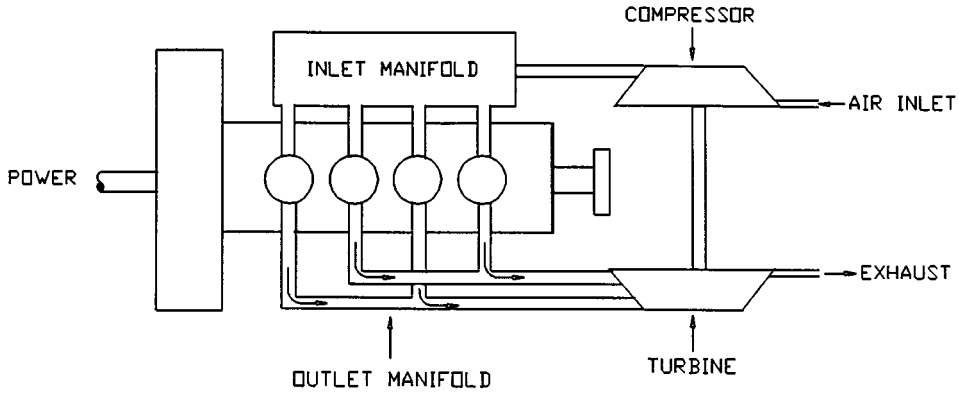

FIGURE 8.3.18 Schematic diagram of a pulse turbocharger.

The use of ceramic materials in fabricating turbine rotors improves the turbine transient response since they are lighter in weight and have less rotational inertia. Ceramic rotors also have greater thermal operating range because of their lower thermal expansion. The use of variable-geometry turbochargers can improve the low-speed torque characteristics of the engine and help reduce the transient response time. This is due to the ability of the variable-geometry turbocharger to change its internal geometry to accommodate low flow rates at low engine speeds and higher-volume flow rates at high engine speeds. However, since the geometry of the turbine rotor remains unchanged while the internal geometry varies, the turbine efficiency will be reduced for all internal geometries other than the optimum design geometry. In response to increased demand for diesel engines with high boost pressure and with size constraints, advances in the aerothermodynamics of axial/radial flow and of two-stage turbochargers, and also in the design of compressor and turbine blades, have allowed high boost pressure at improved overall turbocharger efficiency.

Charge cooling by means of a heat exchanger (intercooler) between the compressor and the intake ports is effective in reducing NO_x emissions and improving the power output of turbocharged diesel engines and in reducing the probability of knock in SI engines. There are two types of charge cooling in use, air-to-air and air-to-water. Air-to-water cooling is used in marine applications, where a source of cool water is available, while air-to-air intercoolers are used for automotive and truck applications.

Defining Terms

Antiknock index: The average of the two octane numbers obtained by the research method and the motor method.

Autoignition: The ability of a fuel-air mixture to spontaneously ignite under conditions of high temperature and pressure.

Bottom dead center (BDC): Piston located at its lowest position in the cylinder. Cylinder volume is maximum at BDC.

Brake mean effective pressure (bmep): Ratio of brake work output per cycle to the displacement volume.

Brake specific fuel consumption (bsfc): The ratio of fuel consumption rate in kg/hr to the engine output in kw.

Brake work: Work produced at the output shaft of an IC engine as measured by a dynamometer.

Cetane index: An approximation to the measured cetane number determined from an empirical relationship specified in ASTM D 976.

Cetane number: A measure of the autoignition quality of a fuel important for proper performance of CI engines determined experimentally through use of a CI CFR test engine.

Clearance volume: Combustion chamber volume remaining above the piston at TDC.

Compression ignition (CI) engine: Air alone is compressed in the cylinder and fuel is injected near TDC. Combustion results from autoignition of the fuel-air mixture due to the high temperature of the air.

Compression ratio: The ratio of the cylinder volume at BDC to the volume at TDC.

Cut-off ratio: Ratio of cylinder volume at the end of heat addition to the volume at the start of heat addition in the ideal diesel cycle.

Cylinder volume: Volume above piston at BDC. Equals displacement volume plus clearance volume.

Direct injection (DI): Method of fuel injection in low- and medium-speed CI engines wherein fuel is injected into the main combustion chamber which is formed by a bowl in the top of the piston.

Displacement volume: Difference in cylinder volume between TDC and BDC.

Equivalence ratio: Actual fuel-air ratio divided by stoichiometric fuel-air ratio.

Four-stroke engine: Entire cycle completed in two revolutions of the crankshaft and four strokes of the piston.

Fuel-air ratio: Ratio of mass of fuel to mass of air in the cylinder prior to combustion.

Glow plug: Electric heater installed in prechamber of an IDI diesel engine to aid cold starting.

Heterogeneous combustion: Refers to the mixture of liquid fuel droplets and evaporated fuel vapor and air mixture that is present in CI engine combustion chambers prior to ignition.

Ignition delay period: Period between start of injection and onset of autoignition in a CI engine.

Indicated mean effective pressure (imep): Ratio of net indicated work output of an IC engine to the displacement volume.

Indicated work: Work output of an IC engine cycle determined by an area calculation from an indicator diagram.

Indicator diagram: Pressure-volume trace for an IC engine cycle. Area enclosed by diagram represents work.

Indirect injection (IDI): Method of fuel injection used in high-speed CI engines wherein the fuel is injected into a precombustion chamber to promote fuel-air mixing and reduce ignition delay.

Knock: In SI engines: the noise that accompanies autoignition of the end portion of the uncombusted mixture prior to the arrival of the flame front. In CI engines: The noise that accompanies autoignition of large premixed fractions that are generated during prolonged ignition delay periods. Knock is detrimental to either type of engine.

NO_x: Harmful oxides of nitrogen (NO and NO_2) appearing in the exhaust products of IC engines.

Octane number: Antiknock rating for fuels important for prevention of autoignition in SI engines.

Particulates: Any exhaust substance, other than water, that can be collected on a filter. Harmful exhaust product from CI engines.

Power density: Power produced per unit of engine mass.

Premixed homogeneous combustion: Fuel and air are mixed in an appropriate combustible ratio prior to ignition process. This is the combustion mode for SI engines and for the initial combustion phase in CI engines.

Sac volume: Volume of nozzles below the needle of a diesel fuel injector that provides a source of UHC emissions in CI engines.

Scavenging: The process of expelling exhaust gases and filling the cylinder with fresh charge in two-stroke engines. This is often accomplished in SI engines by pressurizing the fresh mixture in the crankcase volume beneath the piston and in CI engines by using a supercharger or turbocharger.

Spark ignition (SI) engine: Homogeneous charge of air-fuel mixture is compressed and ignited by a spark.

Stroke: Length of piston movement from TDC to BDC, equal to twice the crankshaft throw.

Supercharging: Pressurizing the intake of an IC engine using a compressor that is mechanically driven from the crankshaft.

Surface ignition: A source of autoignition in SI engines caused by surface hot spots.

Swirl: Circular in-cylinder air motion designed into CI engines to promote fuel-air mixing.

Swirl ratio: Ratio of rotational speed of in-cylinder air (rpm) to engine speed (rpm).

Top dead center (TDC): Piston located at its uppermost position in the cylinder. Cylinder volume (above the piston) is minimum at TDC.

Turbocharging: Pressurizing the intake of an IC engine with a compressor that is driven by a turbine which extracts energy from the exhaust gas stream.

Two-stroke engine: Entire cycle completed in one revolution of the crankshaft and two strokes of the piston.

Unburned hydrocarbons (UHC): Harmful emission product from IC engines consisting of hydrocarbon compounds that remain uncombusted.

Volumetric efficiency: Ratio of the actual mass of air intake per cycle to the displacement volume mass determined at inlet temperature and pressure.

References

ASTM, 1995. *Annual Book of ASTM Standards*. American Society for Testing and Materials, Philadelphia.

Blair, G.P. Ed. 1988. *Advances in Two Stroke Cycle Engine Technology.* Society of Automotive Engineers, Inc., Warrendale, PA.

Ferguson, C.R. 1986. *Internal Combustion Engines, Applied Thermosciences*. John Wiley & Sons, New York.

Henein, N.A. 1972. *Emissions from Combustion Engines and Their Control*. Ann Arbor Science Publishers, Ann Arbor, MI.

Heywood, J.B. 1988. *Internal Combustion Engine Fundamentals*. McGraw-Hill, New York.

Keating, E.L. 1993. *Applied Combustion*. Marcel Dekker, New York.

Kummer, J.T. 1980. Catalysts for automobile emission control. *Prog. Energy Combust. Sci.* 6:177–199.

Lenz, H.P. 1992. *Mixture Formation in Spark-lgnition Engines*. Springer-Verlag, New York.

Norbye, J.P. 1971. *The Wankel Engine*. Chilton Press, Philadelphia.

Obert, E.F. 1973. *Internal Combustion Engines and Air Pollution,* 3rd ed. Harper & Row, New York.

Owen, K. and Coley, T. 1995. *Automotive Fuels Reference Book,* 2nd ed. Society of Automotive Engineers, Inc., Warrendale, PA.

SAE Fuels and Lubricants Standards Manual. 1993. Society of Automotive Engineers, Inc., Warrendale, PA.

SAE Surface Vehicle Emissions Standards Manual. 1993. Society of Automotive Engineers, Inc., Warrendale, PA.

Stone, R. 1993. *Introduction to Internal Combustion Engines,* 2nd ed. Society of Automotive Engineers, Inc., Warrendale, PA.

Taylor, C.F. 1985. *The Internal Combustion Engine in Theory and Practice,* 2nd ed. Vol. I and II. MIT Press, Cambridge, MA.

Watson, N. and Janota, M.S. 1982. *Turbocharging the Internal Combustion Engine,* John Wiley & Sons, New York.

Further Information

The textbooks on IC engines by Ferguson (1986), Heywood (1988), Obert (1973), Stone (1993), and Taylor (1985) listed under the references all provide excellent treatments of this subject. The book by Stone, in particular, is up-to-date and informative. The *Handbook of Engineering* (1966) by CRC Press, Boca Raton, FL, contains a chapter on IC Engines by A. Kornhauser. The Society of Automotive Engineers (SAE) publishes transactions, proceedings, and books related to all aspects of automotive engineering, including IC engines. Two very comprehensive handbooks distributed by SAE are the *Bosch Automotive Handbook,* and the *SAE Automotive Handbook*. For more information contact: SAE Publications, 400 Commonwealth Drive, Warrendale, PA, 15096–0001. (412)776-4970.

8.4 Hydraulic Turbines

Roger E. A. Arndt

Introduction

A hydraulic turbine is a mechanical device that converts the potential energy associated with a difference in water elevation **(head)** into useful work. Modern hydraulic turbines are the result of many years of gradual development. Economic incentives have resulted in the development of very large units (exceeding 800 mW in capacity) with efficiencies that are sometimes in excess of 95%.

The emphasis on the design and manufacture of very large turbines is shifting to the production of smaller units, especially in developed nations, where much of the potential for developing large-baseload plants has been realized. At the same time, the escalation in the cost of energy has made many smaller sites economically feasible and has greatly expanded the market for smaller turbines. The increased value of energy also justifies the cost of refurbishment and increasing the capacity of older facilities. Thus, a new market area is developing for updating older turbines with modern replacement **runners** having higher efficiency and greater capacity.

General Description

Typical Hydropower Installation

As shown schematically in Figure 8.4.1, the hydraulic components of a hydropower installation consist of an intake, penstock, guide vanes or distributor, turbine, and **draft tube**. Trash racks are commonly provided to prevent ingestion of debris into the turbine. Intakes usually require some type of shape transition to match the passageway to the turbine and also incorporate a gate or some other means of stopping the flow in case of an emergency or for turbine maintenance. Some types of turbines are set in an open flume; others are attached to a closed-conduit penstock.

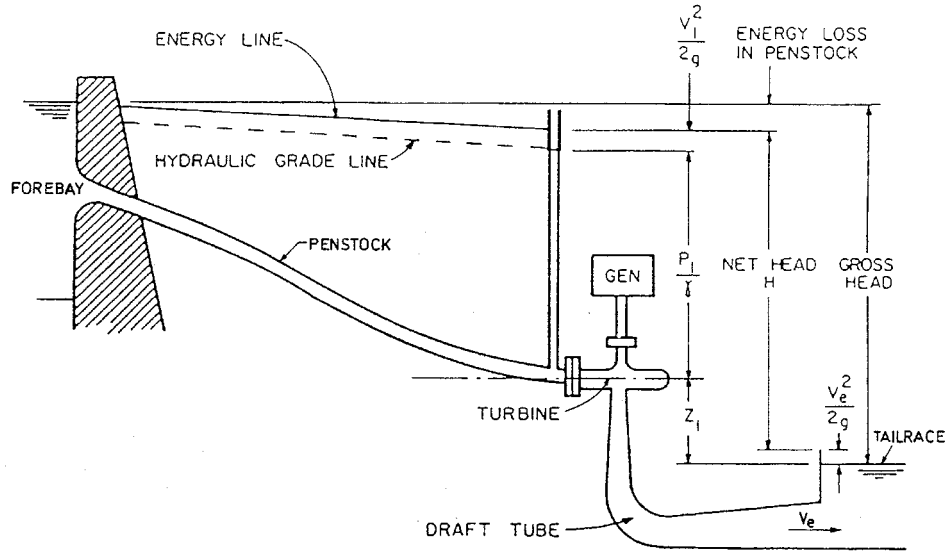

FIGURE 8.4.1 Schematic of a hydropower installation.

Turbine Classification

There are two types of turbines, denoted as impulse and reaction. In an impulse turbine, the available head is converted to kinetic energy before entering the **runner**; the power available is extracted from the flow at approximately atmospheric pressure. In a reaction turbine, the runner is completely submerged and both the pressure and the velocity decrease from inlet to outlet. The velocity head in the inlet to the turbine runner is typically less than 50% of the total head available.

Impulse Turbines. Modern impulse units are generally of the Pelton type and are restricted to relatively high-head applications (Figure 8.4.2). One or more jets of water impinge on a wheel containing many curved buckets. The jet stream is directed inward, sideways, and outward, thereby producing a force on the bucket, which in turn results in a torque on the shaft. All kinetic energy leaving the runner is "lost." A draft tube is generally not used since the runner operates under approximately atmospheric pressure and the head represented by the elevation of the unit above tailwater cannot be utilized.* Since this is a high-head device, this loss in available head is relatively unimportant. As will be shown later, the Pelton wheel is a low-**specific-speed** device. Specific speed can be increased by the addition of extra nozzles, the specific speed increasing by the square root of the number of nozzles. Specific speed can also be increased by a change in the manner of inflow and outflow. Special designs such as the Turgo or cross-flow turbines are examples of relatively high specific speed impulse units (Arndt, 1991).

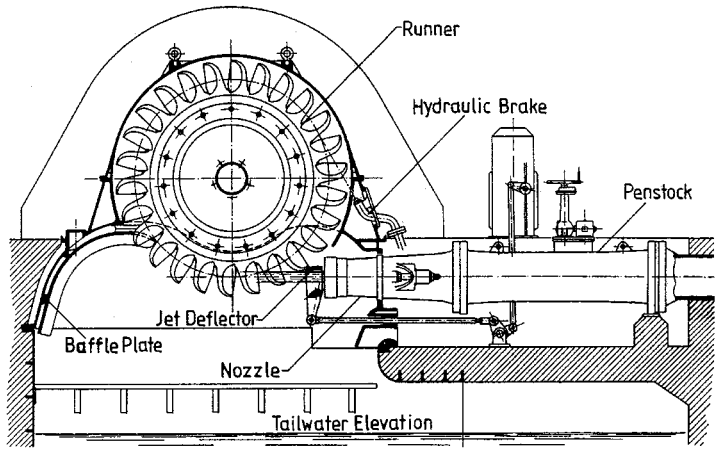

FIGURE 8.4.2 Cross section of a single wheel, single jet Pelton turbine. This is the third-highest-head pelton turbine in the world, H = 1447 m, n = 500 rpm, P = 35.2 MW, $N_s \sim 0.038$. (Courtesy of Vevey Charmilles Engineering Works, Adapted from J. Raabe, *Hydro Power: The Design, Use, and Function of Hydromechanical, Hydraulic, and Electrical Equipment*, VDI Verlag, Dusseldorf, Germany.)

Most Pelton wheels are mounted on a horizontal axis, although newer vertical-axis units have been developed. Because of physical constraints on orderly outflow from the unit, the maximum number of nozzles is generally limited to six or fewer. While the power of a reaction turbine is controlled by the **wicket gates**, the power of the Pelton wheel is controlled by varying the nozzle discharge by means of an automatically adjusted needle, as illustrated in Figure 8.4.2. Jet deflectors, or auxiliary nozzles are provided for emergency unloading of the wheel. Additional power can be obtained by connecting two wheels to a single generator or by using multiple nozzles. Since the needle valve can throttle the flow while maintaining essentially constant jet velocity, the relative velocities at entrance and exit remain unchanged, producing nearly constant efficiency over a wide range of power output.

* In principle, a draft tube could be used, which requires the runner to operate in air under reduced pressure. Attempts at operating an impulse turbine with a draft tube have not met with much success.

Reaction Turbines. Reaction turbines are classified according to the variation in flow direction through the runner. In radial- and mixed-flow runners, the flow exits at a radius different than from the radius at the inlet. If the flow enters the runner with only radial and tangential components, it is a radial-flow machine. The flow enters a mixed-flow runner with both radial and axial components. Francis turbines are of the radial- and mixed-flow types, depending on the design specific speed. A Francis turbine is illustrated in Figure 8.4.3.

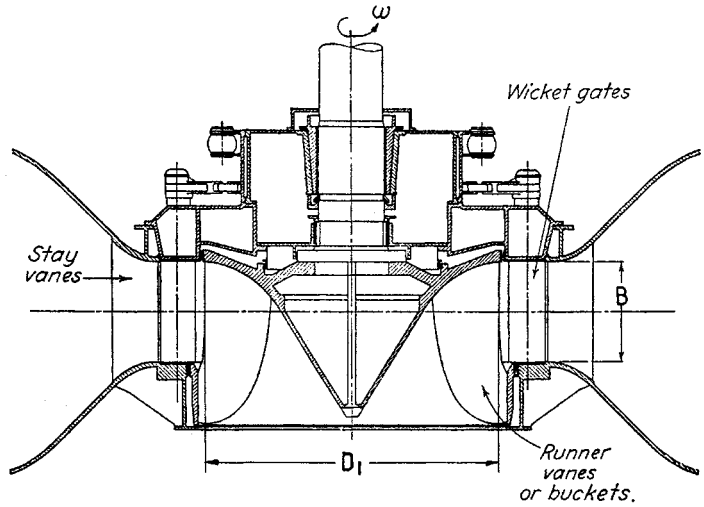

FIGURE 8.4.3 Francis turbine, $N_s \sim 0.66$. (Adapted from J.W. Daily, in *Engineering Hydraulics*, H. Rouse, Ed., New York, 1950. With permission.)

Axial-flow propeller turbines are generally either of the fixed-blade or Kaplan (adjustable-blade) variety. The "classical" propeller turbine, illustrated in Figure 8.4.4, is a vertical-axis machine with a scroll case and a radial wicket gate configuration that is very similar to the flow inlet for a Francis turbine. The flow enters radially inward and makes a right-angle turn before entering the runner in an axial direction. The Kaplan turbine has both adjustable runner blades and adjustable wicket gates. The control system is designed so that the variation in blade angle is coupled with the wicket gate setting in a manner which achieves best overall efficiency over a wide range of flow rates.

Some modern designs take full advantage of the axial-flow runner; these include the tube, bulb, and Straflo types illustrated in Figure 8.4.5. The flow enters and exits the turbine with minor changes in direction. A wide variation in civil works design is also permissible. The tubular-type can be fixed propeller, semi-Kaplan, or fully adjustable. An externally mounted generator is driven by a shaft which extends through the flow passage either upstream or downstream of the runner. The bulb turbine was originally designed as a high-output, low-head unit. In large units, the generator is housed within the bulb and is driven by a variable-pitch propeller at the trailing end of the bulb. Pit turbines are similar in principle to bulb turbines, except that the generator is not enclosed in a fully submerged compartment (the bulb). Instead, the generator is in a compartment that extends above water level. This improves access to the generator for maintenance.

Principles of Operation

Power Available, Efficiency

The power that can be developed by a turbine is a function of both the head and flow available:

$$P = \eta \rho g Q H \tag{8.4.1}$$

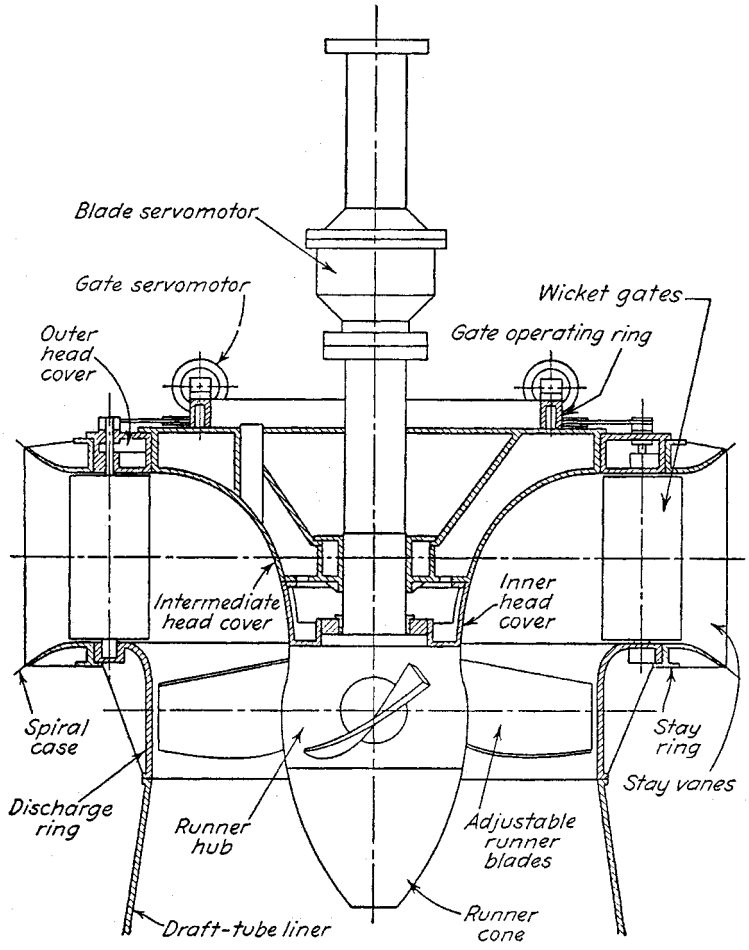

FIGURE 8.4.4 Smith-Kaplan axial flow turbine with adjustable-pitch runner blades $N_s \sim 2.0$. (From J.W. Daily, in *Engineering Hydraulics*, H. Rouse, Ed., New York, 1950. With permission.)

where η is the turbine efficiency, ρ is the density off water (kg/m^3), g is the acceleration due to gravity (m/sec^2), Q is the flow rate (m^3/sec), and H is the *net head* in meters. Net head is defined as the difference between the total head at the inlet to the turbine and the total head at the tailrace as illustrated in Figure 8.4.1. Different definitions of net head are used in practice, which depend on the value of the exit velocity head, $V_e^2/2g$, used in the calculation. The International Electrotechnical Test Code uses the velocity head at the draft tube exit.

The efficiency depends on the actual head and flow utilized by the turbine runner, flow losses in the draft tube, and the frictional resistance of mechanical components.

Similitude and Scaling Formulae

Under a given head, a turbine can operate at various combinations of speed and flow depending on the inlet settings. For reaction turbines, the flow into the turbine is controlled by the wicket gate angle, α. The flow is typically controlled by the nozzle opening in impulse units. Turbine performance can be described in terms of nondimensional variables:

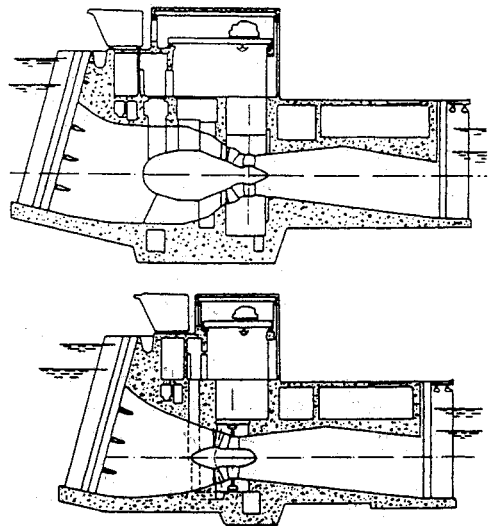

FIGURE 8.4.5 Comparison between bulb (upper) and Straflow (lower) turbines. (Courtesy of U.S. Department of Energy.)

$$\psi = \frac{2gH}{\omega^2 D^2} \tag{8.4.2}$$

$$\phi = \frac{Q}{\sqrt{2gH}D^2} \tag{8.4.3}$$

where ω is the rotational speed of the turbine in radians per second and D is the diameter of the turbine.

The hydraulic efficiency of the runner alone is given by

$$\eta_h = \frac{\phi}{\sqrt{\psi}}\left(C_1 \cos\alpha_1 - C_2 \cos\alpha_2\right) \tag{8.4.4}$$

where C_1 and C_2 are constants that depend on the specific turbine configuration and α_1 and α_2 are the inlet and outlet angles that the absolute velocity vectors make with the tangential direction. The value of $\cos\alpha_2$ is approximately zero at peak efficiency. The terms ϕ, ψ, α_1, and α_2 are interrelated. By using model test data, isocontours of efficiency can be mapped in the ϕ-ψ plane. This is typically referred to as a hill diagram as shown in Figure 8.4.6.

The specific speed is defined as

$$N_s \equiv \frac{\omega\sqrt{Q}}{(2gH)^{3/4}} = \sqrt{\frac{\phi}{\psi}} \tag{8.4.5}$$

A given specific speed describes a specific combination of operating conditions that ensures similar flow patterns and same efficiency in geometrically similar machines regardless of size and rotational speed of the machine. It is customary to define the design specific speed in terms of the value at the design head and flow where peak efficiency occurs. The value of specific speed so defined permits a classification of different turbine types.

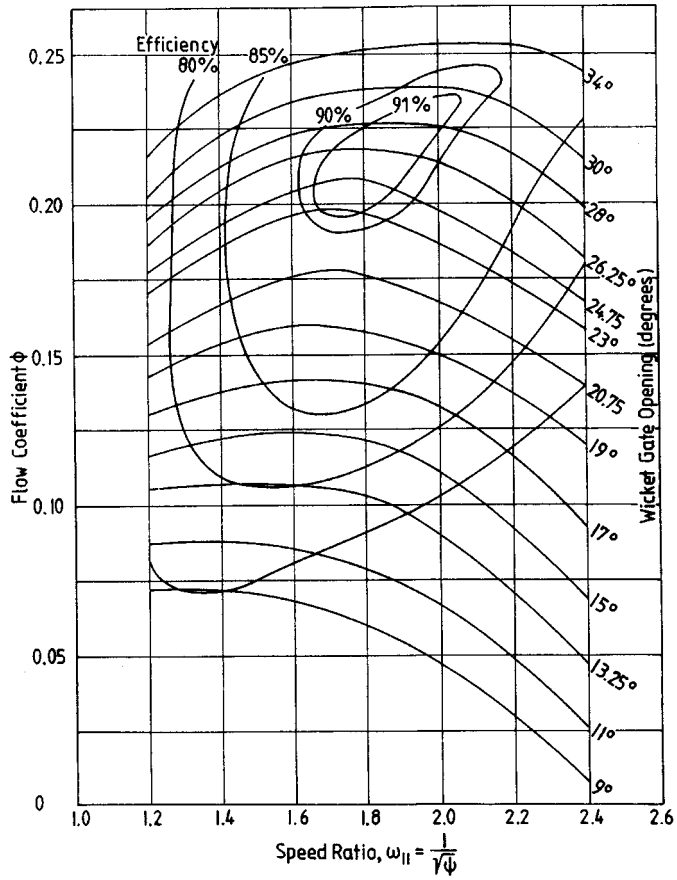

FIGURE 8.4.6 Typical hill diagram. (Adapted from T.L. Wall, Draft tube surging times two: the twin vortex problem, in *Hydro Rev.* 13(1): 60–69, 1994. With permission.)

The specific speed defined herein is dimensionless. Many other forms of specific speed exist which are dimensional and have different numerical values depending on the system of units used (Arndt, 1991).* The similarity arguments used to arrive at the concept of specific speed indicate that a given machine of diameter D operating under a head H will discharge a flow Q and produce a torque T and power P at a rotational speed ω given by

$$Q = \phi D^2 \sqrt{2gH} \tag{8.4.6}$$

$$T = T_{11} \rho D^3 2gH \tag{8.4.7}$$

$$P = P_{11} \rho D^2 (2gH)^{3/2} \tag{8.4.8}$$

$$\omega = \frac{2u_1}{D} = \omega_{11} = \frac{\sqrt{2gH}}{D} \qquad \left[\omega_{11} = \frac{1}{\sqrt{\psi}}\right] \tag{8.4.9}$$

* The literature also contains two other minor variations of the dimensionless form. One differs by a factor of $1/\pi^{1/2}$ and the other by $2^{3/4}$.

with

$$P_{11} = T_{11}\omega_{11} \tag{8.4.10}$$

where T_{11}, P_{11}, and ω_{11} are also nondimensional.* In theory, these coefficients are fixed for a machine operating at a fixed value of specific speed, independent of the size of the machine. Equations 8.4.6 through 8.4.10 can be used to predict the performance of a large machine using the measured characteristics of a smaller machine or model.

Factors Involved in Selecting a Turbine

Performance Characteristics

Impulse and reaction turbines are the two basic types of turbines. They tend to operate at peak efficiency over different ranges of specific speed. This is due to geometric and operational differences.

Impulse Turbines. Of the head available at the nozzle inlet, a small portion is lost to friction in the nozzle and to friction on the buckets. The rest is available to drive the wheel. The actual utilization of this head depends on the velocity head of the flow leaving the turbine and the setting above tailwater. Optimum conditions, corresponding to maximum utilization of the head available, dictate that the flow leaves at essentially zero velocity. Under ideal conditions, this occurs when the peripheral speed of the wheel is one half the jet velocity. In practice, optimum power occurs at a speed coefficient, ω_{11}, somewhat less than 1.0. This is illustrated in Figure 8.4.7. Since the maximum efficiency occurs at fixed speed for fixed H, V_j must remain constant under varying flow conditions. Thus, the flow rate Q is regulated with an adjustable nozzle. However, maximum efficiency occurs at slightly lower values of ω_{11} under partial power settings. Present nozzle technology is such that the discharge can be regulated over a wide range at high efficiency.

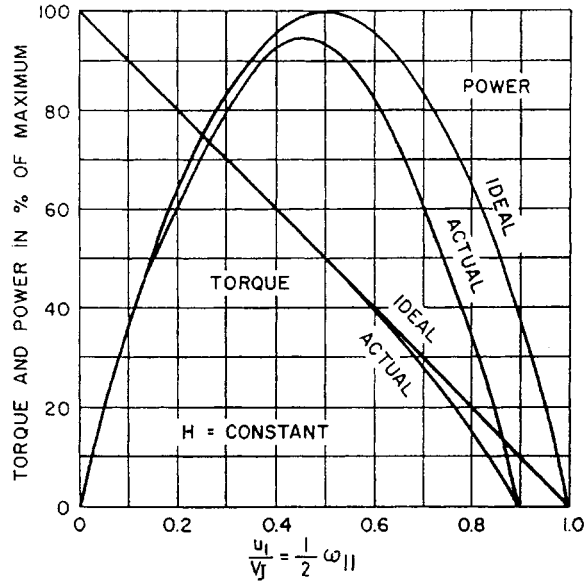

FIGURE 8.4.7 Ideal and actual variable-speed performance for an impulse turbine. (Adapted from J.W. Daily, in *Engineering Hydraulics*, H. Rouse, Ed., New York, 1950. With permission.)

* The reader is cautioned that many texts, especially in the American literature, contain dimensional forms of T_{11}, P_{11}, and ω_{11}.

A given head and penstock configuration establishes the optimum jet velocity and diameter. The size of the wheel determines the speed of the machine. The design specific speed is approximately

$$N_s = 0.77\frac{d_j}{D} \quad \text{(Pelton turbines)} \tag{8.4.11}$$

Practical values of d_j/D for Pelton wheels to ensure good efficiency are in the range 0.04 to 0.1, corresponding to N_s values in the range 0.03 to 0.08. Higher specific speeds are possible with multiple-nozzle designs. The increase is proportional to the square root of the number of nozzles. In considering an impulse unit, one must remember that efficiency is based on net head; the net head for an impulse unit is generally less than the net head for a reaction turbine at the same *gross head* because of the lack of a draft tube.

Reaction Turbines. The main difference between impulse and reaction turbines is the fact that a pressure drop takes place in the rotating passages of the reaction turbine. This implies that the entire flow passage from the turbine inlet to the discharge at the tailwater must be completely filled. A major factor in the overall design of modern reaction turbines is the draft tube. It is usually desirable to reduce the overall equipment and civil construction costs by using high-specific speed runners. Under these circumstances the draft tube is extremely critical both flow-stability and efficiency viewpoints.* At higher specific speed, a substantial percentage of the available total energy is in the form of kinetic energy leaving the runner. To recover this efficiently, considerable emphasis should be placed on the draft tube design.

The practical specific speed range for reaction turbines is much broader than for impulse wheels. This is due to the wider range of variables which control the basic operation of the turbine. The pivoted guide vanes allow for control of the magnitude and direction of the inlet flow. Because there is a fixed relationship among blade angle, inlet velocity, and peripheral speed for shock-free entry, this requirement cannot be completely satisfied at partial flow without the ability to vary blade angle. This is the distinction between the efficiency of fixed-propeller and Francis-types at partial loads and the fully adjustable Kaplan design.

Referring to Equation 8.4.4, optimum hydraulic efficiency of the runner would occur when α_2 is equal to 90°. However, the overall efficiency of the turbine is dependent on the optimum performance of the draft tube as well, which occurs with a little swirl in the flow. Thus, the best overall efficiency occurs with $\alpha_2 \approx 75°$ for high-specific speed turbines.

The determination of optimum specific speed in a reaction turbine is more complicated than for an impulse unit since there are more variables. For a radial-flow machine, an approximate expression is

$$N_s = 1.64\left[C_v \sin\alpha_1 \frac{B}{D_1}\right]^{1/2} \omega_{11} \quad \text{(Francis turbines)} \tag{8.4.12}$$

where C_v is the fraction of net head that is in the form of inlet velocity head and B is the height of the inlet flow passage (Figure 8.4.3). Value of N_s for Francis units is normally found to be in the range 0.3 to 2.5.

Standardized axial-flow machines are available in the smaller sizes. These units are made up of standard components, such as shafts and blades. For such cases,

$$N_s \sim \frac{\sqrt{\tan\beta}}{n_B^{3/4}} \quad \text{(propeller turbines)} \tag{8.4.13}$$

* This should be kept in mind when retrofitting an older, low-specific-speed turbine with a new runner of higher capacity.

where β is the blade pitch angle and n_B is the number of blades. The advantage of controllable pitch is also obvious from this formula, the best specific speed simply being a function of pitch angle.

It should be further noted that ω_{11} is approximately constant for Francis units and N_s is proportional to $(B/D_1)^{1/2}$. It can be also shown that velocity component based on the peripheral speed at the throat, ω_{11e}, is proportional to N_s. In the case of axial-flow machinery, ω_{11} is also proportional to N_s. For minimum cost, peripheral speed should be as high as possible, consistent with cavitation-free performance. Under these circumstances, N_s would vary inversely with the square root of head:

$$N_s = \frac{C}{\sqrt{H}} \quad (H \text{ is in meters}) \tag{8.4.14}$$

where the range of C is 21 to 30 for fixed propeller units, 21 to 32 for Kaplan units, and 16 to 25 for Francis units.

Performance Comparison. The physical characteristics of various runner configurations are summarized in Figure 8.4.8. It is obvious that the configuration changes with speed and head. Impulse turbines are efficient over a relatively narrow range of specific speed, whereas Francis and propeller turbines have a wider useful range. An important consideration is whether or not a turbine is required to operate over a wide range of load. Pelton wheels tend to operate efficiently over a wide range of power loading because of their nozzle design. In the case of reaction machines that have fixed geometry, such as Francis and propeller turbines, efficiency can vary widely with load. However, Kaplan and Deriaz* turbines can maintain high efficiency over a wide range of operating conditions. The decision of whether to select a simple configuration with a relatively "peaky" efficiency curve or go to the added expense of installing a more complex machine with a broad efficiency curve will depend on the expected operation of the plant and other economic factors.

Note in Figure 8.4.8 that there is an overlap in the range of application of various types of equipment. This means that either type of unit can be designed for good efficiency in this range, but other factors, such as generator speed and cavitation, may dictate the final selection.

Speed Regulation

The speed regulation of a turbine is an important and complicated problem. The magnitude of the problem varies with size, type of machine and installation, type of electrical load, and whether or not the plant is tied into an electrical grid. Note that runaway or no-load speed can be higher than design speed by factors as high as 2.6. This is an important design consideration for all rotating parts, including the generator.

The speed of a turbine has to be controlled to a value that matches the generator characteristics and the grid frequency:

$$n = \frac{120 f}{N_p} \tag{8.4.15}$$

where n is turbine speed in rpm, f is the required grid frequency in Hz, and N_p is the number of poles in the generator. Typically, N_p is in multiples of 4. There is a tendency to select higher speed generators to minimize weight and cost. However, consideration has to be given to speed regulation.

It is beyond the scope of this section to discuss the question of speed regulation in detail. Regulation of speed is normally accomplished through flow control. Adequate control requires sufficient rotational inertia of the rotating parts. When load is rejected, power is absorbed, accelerating the flywheel; and when load is applied, some additional power is available from deceleration of the flywheel. Response

* An adjustable blade mixed-flow turbine (Arndt, 1991).

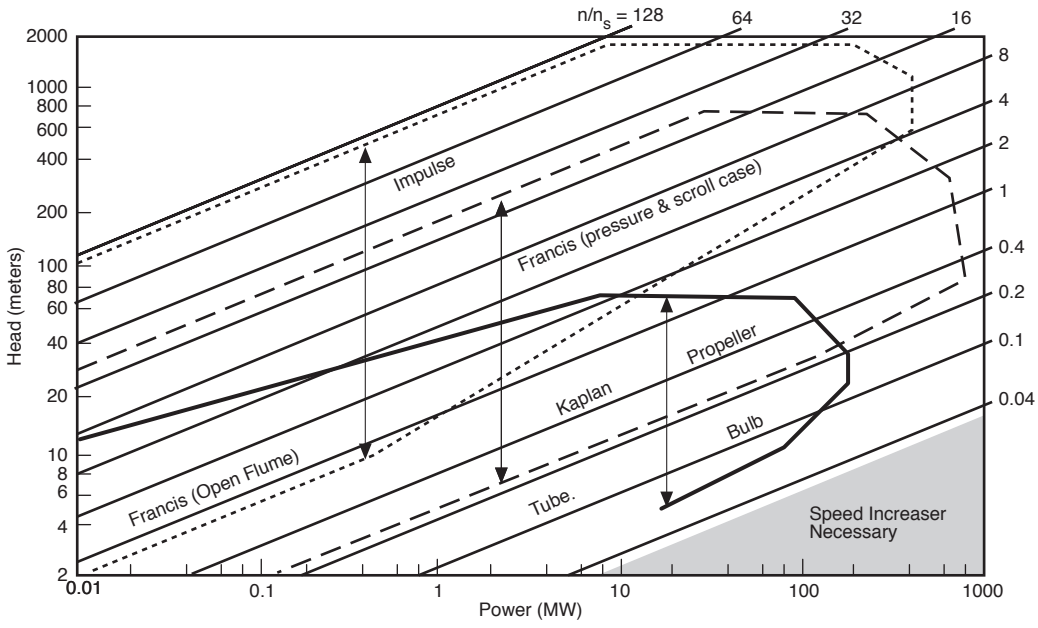

FIGURE 8.4.8 Application chart for various turbine types (n/n_S is the ratio of turbine speed in rpm, n, to specific speed defined in the metric system, $n_S = nP^{1/2}/H^{3/4}$ with P in kilowatts). (From Arndt, R.E.A., in *Hydropower Engineering Handbook*, J.S. Gulliver and R.E.A. Arndt, Eds., McGraw-Hill, New York, 1991, 4.1–4.67. With permission.)

time of the governor must be carefully selected, since rapid closing can lead to excessive pressures in the penstock.

A Francis turbine is controlled by opening and closing the wicket gates, which vary the flow of water according to the load. The actuator components of a governor are required to overcome the hydraulic and frictional forces and to maintain the wicket gates in fixed position under steady load. For this reason, most governors have hydraulic actuators. On the other hand, impulse turbines are more easily controlled, because the jet can be deflected or an auxiliary jet can by bypass flow from the power-producing jet without changing the flow rate in the penstock. This permits long delay times for adjusting the flow rate to the new flywheel; and when load is applied power conditions. The spear or needle valve controlling the flow rate can close quite slowly, say, in 30 to 60 sec, thereby minimizing pressure rise in the penstock.

Several types of governors are available, which vary with the work capacity desired and/or the degree of sophistication of control. These vary from pure mechanical to mechanical-hydraulic and electrohydraulic. Electrohydraulic units are sophisticated pieces of equipment and would not be suitable for remote regions. The precision of governing necessary will depend on whether the electrical generator is synchronous or asynchronous (induction type). There are advantages to the induction type of generator. It is less complex and therefore less expensive, but has typically slightly lower efficiency. Its frequency is controlled by the frequency of the grid it is feeding into, thereby eliminating need of an expensive the conventional governor. It cannot operate independently but can only feed into a network and does so with lagging power factor which may or may not be a disadvantage, depending on the nature of the load. Long transmission lines, for example, have a high capacitance and in this case the lagging power factor may be an advantage.

Speed regulation is a function of the flywheel effect of the rotating components and the inertia of the water column of the system. The start-up time of the rotating system is given by

$$t_s = \frac{I\omega^2}{P} \tag{8.4.16}$$

where I = moment of inertia of the generator and turbine, kg · m^2 (Bureau of Reclamation, 1966).

The start-up time of the water column is given by

$$t_p = \frac{\sum LV}{gH} \tag{8.4.17}$$

where L = length of water column
V = velocity in each component of the water column

For good speed regulation, it is desirable to keep $t_s/t_p > 4$. Lower values can also be used, although special precautions are necessary in the control equipment. Higher ratios of t_s/t_p can be obtained by increasing I or decreasing t_p. Increasing I implies a larger generator, which also results in higher costs. The start-up time of the water column can be reduced by reducing the length of the flow system, by using lower velocities, or by adding **surge tanks**, which essentially reduce the effective length of the conduit. A detailed analysis should be made for each installation, since for a given length, head, and discharge the flow area must be increased to reduce t_p, which leads to associated higher construction costs.

Cavitation and Turbine Setting

Another factor that must be considered prior to equipment selection is the evaluation of the turbine with respect to tailwater elevations. Hydraulic turbines are subject to pitting due to cavitation (Arndt, 1981, 1991). For a given head, smaller, lower-cost, high-speed runner must be set lower (i.e, closer to tailwater or even below tailwater) than a larger, higher-cost, low-speed turbine runner. Also, atmospheric pressure or elevation above sea level is a factor, as are tailwater elevation ion variations and operating requirements. This is a complex concept which can only be accurately resolved by model tests. The runner design will have different cavitation characteristics. Therefore, the anticipated turbine location or setting with respect to tailwater elevations is an important consideration in turbine selection.

Cavitation is not normally a problem with impulse wheels. However, by the very nature of their operation, cavitation is an important factor in reaction turbine installations. The susceptibility for cavitation to occur is a function of the installation and the turbine design. This can be expressed conveniently in terms of Thoma's sigma defined as

$$\sigma_T = \frac{H_a - H_v - z}{H} \tag{8.4.18}$$

where H_a is the atmospheric pressure head, H_V is the vapor pressure need (generally negligible), and z is the elevation of a turbine reference plane above the tailwater (see Figure 8.4.1). Draft tube losses and the exit velocity head have been neglected.

σ_T must be above a certain value to avoid cavitation problems. The critical value of σ_T is a function of specific speed (Arndt, 1991). The Bureau of Reclamation (1966) suggests that cavitation problems can be avoided when

$$\sigma_T > 0.26 N_s^{1.64} \tag{8.4.19}$$

Equation 8.4.19 does not guarantee total elimination of cavitation, only that cavitation is within acceptable limits. Cavitation can be totally avoided only if the value σ_T at an installation is much greater than the limiting value given in Equation 8.4.19. The value of σ_T for a given installation is known as

the plant sigmas, σ_p. Equation 8.4.19 should only be considered as a guide in selecting σ_p, which is normally determined by a model test in the manufacturer's laboratory. For a turbine operating under a given head, the only variable controlling σ_p is the turbine setting z. The required value of σ_p then controls the allowable setting above tailwater:

$$z_{\text{allow}} = H_a - H_v - \sigma_p H \tag{8.4.20}$$

It must be borne in mind that H_a varies with elevation. As a rule of thumb, H_a decreases from the sea-level value of 10.3 m by 1.1 m for every 1000 m above sea level.

Defining Terms

Draft tube: The outlet conduit from a turbine which normally acts as a diffuser. This is normally considered to be an integral part of the unit.

Forebay: The hydraulic structure used to withdraw water from a reservoir or river. This can be positioned a considerable distance upstream from the turbine inlet.

Head: The specific energy per unit weight of water. *Gross head* is the difference in water surface elevation between the forebay and tailrace. *Net head* is the difference between *total head* (the sum of velocity head $V^2/2g$, pressure head $p/\rho g$, and elevation head z at the inlet and outlet of a turbine. Some European texts use specific energy per unit mass, e.g., specific kinetic energy is $V^2/2$.

Runner: The rotating component of a turbine in which energy conversion takes place.

Specific speed: A universal number for a given machine design.

Spiral case: The inlet to a reaction turbine.

Surge tank: A hydraulic structure used to diminish overpressures in high-head facilities due to water hammer resulting from the sudden stoppage of a turbine

Wicket gates: Pivoted, streamlined guide vanes that control the flow of water to the turbine.

References

Arndt, R.E.A. 1981. Cavitation in fluid machinery and hydraulic structures. *Ann. Rev. Fluid Mech.* 13:273–328.

Arndt, R.E.A. 1991. Hydraulic turbines, in *Hydropower Engineering Handbook,* J.S. Gulliver and R.E.A. Arndt, Eds., pp. 4.1–4.67 McGraw-Hill, New York.

Bureau of Reclamation. 1966. Selecting Hydraulic Reaction Turbines, Engineering Monograph No. 20.

Daily, J.W. 1950. Hydraulic machinery, in H. Rouse, Ed., Engineering Hydraulics, New York.

International Code for the Field Acceptance Tests of Hydraulic Turbines, 1963. International Electrotechnical Commission, Publication 41.

Raabe, J. 1985. *Hydro Power: The Design, Use, and Function of Hydromechanical, Hydraulic, and Electrical Equipment*. VDI Verlag, Dusseldorf, Germany.

Wahl, T.L. 1994. Draft tube surging times two: The twin vortex problem. *Hydro Rev.* 13(1):60–69.

Further Information

J. Fluids Eng, published quarterly by the ASME.

ASME Symposia Proc. on Fluid Machinery and Cavitation, published by the Fluids Eng. Div.

Hydro Review, published eight times per year by HCI Publications, Inc., Kansas City, MO.

L.F. Moody and T. Zowski, Hydraulic machinery, in *Handbook of Applied Hydraulics,* C.V. Davis and K.E. Sorenson, Eds., McGraw-Hill, New York, 1992.

Waterpower and Dam Construction, published monthly by Reed Business Publishing, Surrey, U.K.

8.5 Stirling Engines

William B. Stine

Introduction

The Stirling engine was patented in 1816 by Rev. Robert Stirling, a Scottish minister (Figure 8.5.1). Early Stirling engines were coal-burning, low-pressure air engines built to compete with saturated steam engines for providing auxiliary power for manufacturing and mining. In 1987, John Ericsson built an enormous marine Stirling engine with four 4.2-m-diameter pistons. Beginning in the 1930s, the Stirling engine was brought to a high state of technology development by Philips Research Laboratory in Eindhoven, The Netherlands with the goal of producing small, quiet electrical generator sets to be used with high-power-consuming vacuum tube electronic devices. Recently, interest in Stirling engines has resurfaced, with solar electric power generation (Stine and Diver, 1994) and hybrid automotive applications in the forefront.

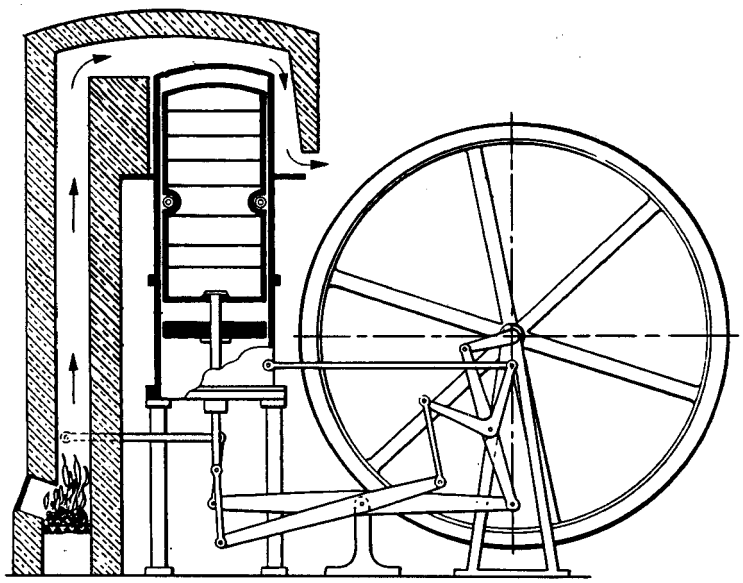

FIGURE 8.5.1 The original patent Stirling engine of Rev. Robert Stirling.

In theory, the **Stirling cycle** engine can be the most efficient device for converting heat into mechanical work with high efficiencies requiring high-temperatures. In fact, with regeneration, the efficiency of the Stirling cycle equals that of the Carnot cycle, the most efficient of all ideal thermodynamic cycles. (See West, 1986 for further discussion of the thermodynamics of Stirling cycle machines.)

Since their invention, prototype Stirling engines have been developed for automotive purposes; they have also been designed and tested for service in trucks, buses, and boats (Walker, 1973). The Stirling engine has been proposed as a propulsion engine in yachts, passenger ships, and road vehicles such as city buses (Meijer, 1992). The Stirling engine has also been developed as an underwater power unit for submarines, and the feasibility of using the Stirling for high-power space-borne systems has been explored by NASA (West, 1986). The Stirling engine is considered ideal for solar heating, and the first solar application of record was by John Ericsson, the famous British-American inventor, in 1872 (Stine and Diver, 1994).

Stirling engines are generally externally heated engines. Therefore, most sources of heat can be used to drive them, including combustion of just about anything, radioisotopes, solar energy, and exothermic

chemical reactions. High-performance Stirling engines operate at the thermal limits of the materials used for their construction. Typical temperatures range fiom 650 to 800°C (1200 to 1470°F), resulting in engine conversion efficiencies of around 30 to 40%. Engine speeds of 2000 to 4000 rpm are common

Thermodynamic Implementation of the Stirling Cycle

In the ideal Stirling cycle, a **working gas** is alternately heated and cooled as it is compressed and expanded. Gases such as helium and hydrogen, which permit rapid heat transfer and do not change phase, are typically used in the high-performance Stirling engines. The ideal Stirling cycle combines four processes, two constant-temperature heat-exchange processes and two constant-volume heat-exchange processes. Because more work is done by expanding high-temperature, high-pressure gas than is required to compress low-temperature, low-pressure gas, the Stirling cycle produces net work, which can drive an electric alternator or other mechanical devices.

Working Gases

In the Stirling cycle, the working gas is alternately heated and cooled in constant-temperature and constant-volume processes. The traditional gas for Stirling engines has been air at atmospheric pressure. At this pressure, air has a reasonably high density and therefore can be used directly in the cycle with loss of working gas through seals a minor problem. However, internal component temperatures are limited because of the oxygen in air which can degrade materials rapidly.

Because of their high heat-transfer capabilities, hydrogen and helium are used for high-speed, high-performance Stirling engines. To compensate for the low density of these gases, the mean pressure of the working gas is raised by charging the gas spaces in the engine to high pressures. Compression and expansion vary above and below this **charge pressure**. Hydrogen, thermodynamically a better choice, generally results in more-efficient engines than does helium (Walker, 1980). Helium, on the other hand, has fewer material-compatibility problems and is safer to work with. To maximize power, high-performance engines typically operate at high pressure, in the range of 5 to 20 MPa (725 to 2900 psi). Operation at these high gas pressures makes sealing difficult, and seals between the high-pressure region of the engine and those parts at ambient pressure have been problematic in some engines. New designs to reduce or eliminate this problem are currently being developed.

Heat Exchange

The working gas is heated and cooled by heat exchangers that add heat from an external source, or reject heat to the surroundings. Further, in most engines, an internal heat storage unit stores and rejects heat during each cycle.

The **heater** of a Stirling engine is usually made of many small-bore tubes that are heated externally with the working gas passing through the inside. External heat transfer by direct impingement of combustion products or direct adsorption of solar irradiation is common. A trade-off between high heat-transfer rate using many small-bore tubes with resulting pumping losses, and fewer large-bore tubes and lower pumping losses drives the design. A third criterion is that the volume of gas trapped within these heat exchangers should be minimal to enhance engine performance. In an attempt to provide more uniform and constant-temperature heat transfer to the heater tubes, **reflux** heaters are being developed (Stine and Diver, 1994). Typically, by using sodium as the heat-transfer medium, liquid is evaporated at the heat source and is then condensed on the outside surfaces of the engine heater tubes.

The **cooler** is usually a tube-and-shell heat exchanger. Working gas is passed through the tubes, and cooling water is circulated around the outside. The cooling water is then cooled in an external heat exchanger. Because all of the heat rejected from the power cycle comes from the cooler, the Stirling engine is considered ideal for cogeneration applications.

Most Stirling engines incorporate an efficiency-enhancing **regenerator** that captures heat from the working gas during constant-volume cooling and replaces it when the gas is heated at constant volume. Heating and cooling of the regenerator occurs at over 60 times a second during high-speed engine operation. In the ideal cycle, all of the heat-transferred during the constant volume heating and cooling

processes occurs in the regenerator, permitting the external heat addition and rejection to be efficient constant-temperature heat-transfer processes. Regenerators are typically chambers packed with fine-mesh screen wire or porous metal structures. There is enough thermal mass in the packing material to store all of the heat necessary to raise the temperature of the working gas from its low to its high temperature. The amount of heat stored by the regenerator is generally many times greater than the amount added by the heater.

Power Control

Rapid control of the output power of a Stirling engine is highly desirable for some applications such as automotive and solar electric applications. In most Stirling engine designs, rapid power control is implemented by varying the density (i.e., the mean pressure) of the working gas by bleeding gas from the cycle when less power is desired. To return to a higher power level, high-pressure gas must be reintroduced into the cycle. To accomplish this quickly and without loss of working gas, a complex system of valves, a temporary storage tank, and a compressor are used.

A novel method of controlling the power output is to change the length of stroke of the power piston. This can be accomplished using a variable-angle swash plate drive as described below. Stirling Thermal Motors, Inc., uses this method on their STM 4-120 Stirling engine (Figure 8.5.2).

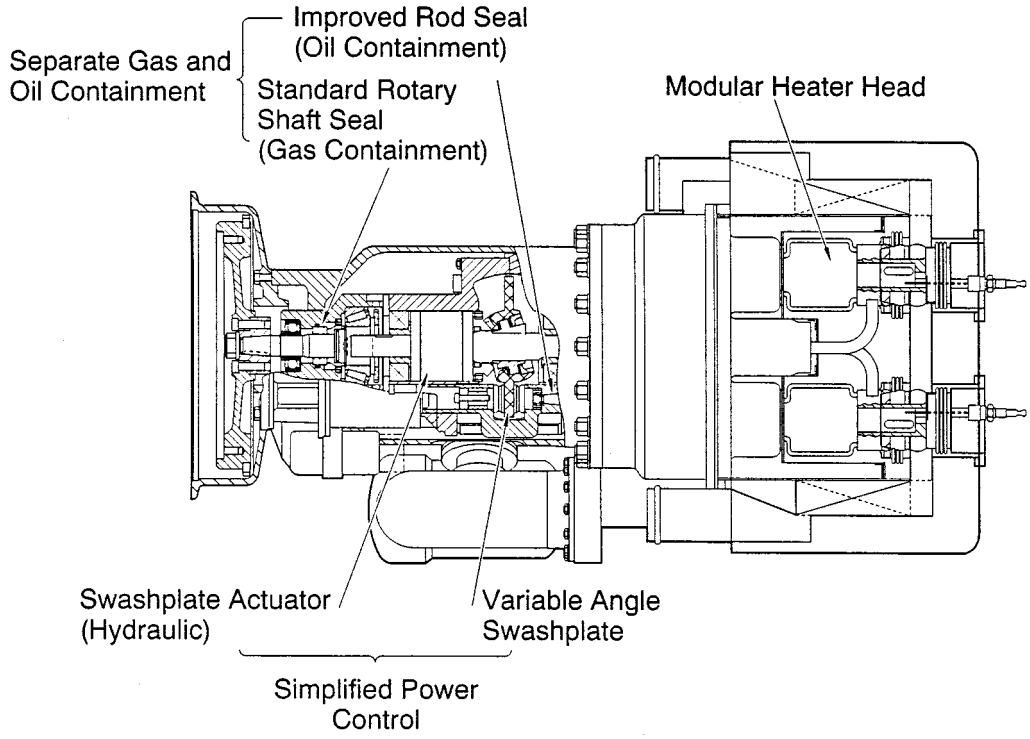

FIGURE 8.5.2 Stirling Thermal Motors 4-120 variable swash plate Rinia configuration engine. (Courtesy Stirling Thermal Motors, Ann Arbor, Michigan.)

Mechanical Implementation of the Stirling Cycle

Piston/Displacer Configurations

To implement the Stirling cycle, different combinations of machine components have been designed to provide for the constant-volume movement of the working gas between the high- and low-temperature regions of the engine, and compression and expansion during the constant-temperature heating and

cooling. The compression and expansion part of the cycle generally take place in a cylinder with a piston. Movement of the working gas back and forth through the heater, regenerator, and cooler at constant volume is often implemented by a **displacer**. A displacer in this sense is a hollow plug that, when moved to the cold region, displaces the working gas from the cold region causing it to flow to the hot region and vice versa. Only a small pressure difference exists between either end of the displacer, and, therefore, sealing requirements and the force required to move it are minimal.

Three different design configurations are generally used (Figure 8.5.3). Called the alpha-, beta-, and gamma-configurations. Each has its distinct mechanical design characteristics, but the thermodynamic cycle is the same. The **alpha-configuration** uses two pistons on either side of the heater, regenerator, and the cooler. These pistons first move uniformly in the same direction to provide constant-volume processes to heat or cool the gas. When all of the gas has been moved into one cylinder, one piston remains fixed and the other moves to compress or expand the gas. Compression work is done by the **cold piston** and expansion work done on the **hot piston** The alpha-configuration does not use a displacer. The Stirling Power Systems V-160 engine (Figure 8.5.4) is an example of this configuration.

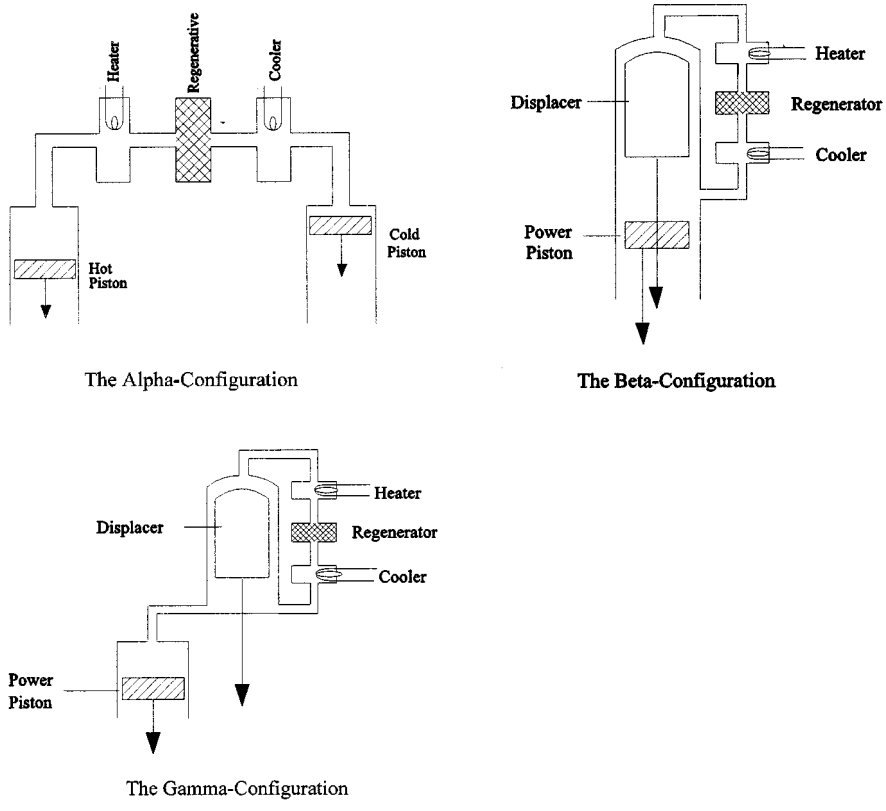

FIGURE 8.5.3 Three fundamental mechanical configurations for Stirling Engines.

A variation on using two separate pistons to implement the alpha-configuration is to use the front and back side of a single piston called a **double-acting piston**. The volume at the front side of one piston is connected, through the heater, regenerator, and cooler, to the volume at the back side of another piston. With four such double-acting pistons, each 90° out of phase with the next, the result is a four-cylinder alpha-configuration engine. This design is called the *Rinia* or *Siemens configuration* and the United Stirling 4-95 (Figure 8.5.5) and the Stirling Thermal Motors STM 4-120 (Figure 8.5.2) are current examples.

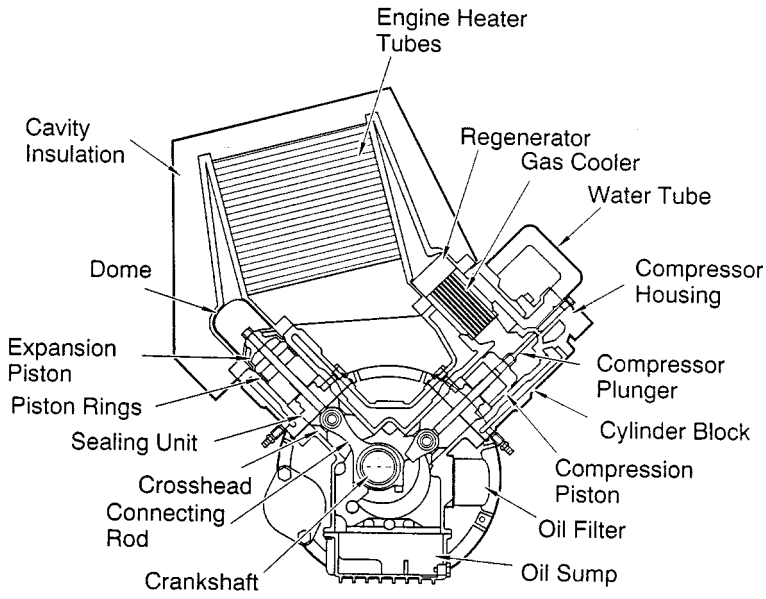

FIGURE 8.5.4 Stirling Power Systems/Solo Kleinmotoren V-160 alpha-configuration Stirling engine.

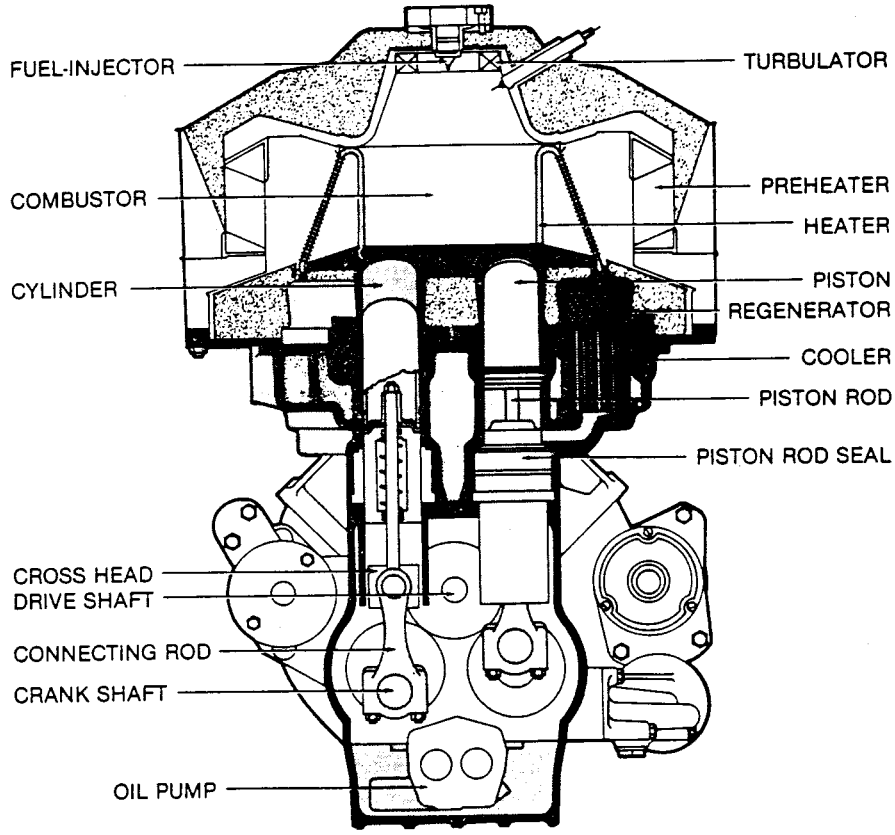

FIGURE 8.5.5 The 4-95 high-performance Siemens configuration Rinia engine by United Stirling (Malmo, Sweden).

The **beta-configuration** is a design incorporating a displacer and a power piston in the same cylinder. The displacer shuttles gas between the hot end and the cold end of the cylinder through the heater, regenerator, and cooler. The power piston, usually located at the cool end of the cylinder, compresses the working gas when the gas is in the cool end and expands the working gas when the gas has been moved to the hot end. The original patent engine by Robert Stirling and most free-piston Stirling engines discussed below are of the beta-configuration.

The third configuration, using separate cylinders for the displacer and the power piston, is called the **gamma-configuration**. Here, the displacer shuttles gas between the hot end and the cold end of a cylinder through the heater, regenerator, and cooler, just as with the beta-configuration. However, the power piston is in a separate cylinder, pneumatically connected to the displacer cylinder.

Piston/Displacer Drives

Most Stirling engine designs dynamically approximate the Stirling cycle by moving the piston and displacer with **simple harmonic motion**, either through a crankshaft, or bouncing as a spring/mass second-order mechanical system. For both, a performance penalty comes from the inability of simple harmonic motion to perfectly follow the desired thermodynamic processes. A more desirable dynamic from the cycle point of view, called overdriven or **bang-bang motion**, has been implemented in some designs, most notably the **Ringbom configuration** and engines designed by Ivo Kolin (West, 1986).

Kinematic Engines. Stirling engine designs are usually categorized as either kinematic or free-piston. The power piston of a **kinematic Stirling engine** is mechanically connected to a rotating output shaft. In typical configurations, the power piston is connected to the crankshaft with a connecting rod. In order to eliminate side forces against the cylinder wall, a **cross-head** is often incorporated, where the connecting rod connects to the cross-head, which is laterally restrained so that it can only move linearly in the same direction as the piston. The power piston is connected to the cross-head and therefore experiences no lateral forces. The critical sealing between the high-pressure and low-pressure regions of the engine can now be created using a simple **linear seal** on the shaft between the cross-head and the piston. This design also keeps lubricated bearing surfaces in the low-pressure region of the engine, reducing the possibility of fouling heat-exchange surfaces in the high-pressure region of the engine. If there is a separate displacer piston as in the beta- and gamma configurations, it is also mechanically connected to the output shaft.

A variation on crankshaft/cross-head drives is the **swash plate** or **wobble-plate drive**, used with success in some Stirling engine designs. Here, a drive surface affixed to the drive shaft at an angle, pushes fixed piston **push rods** up and down as the slanted surface rotates beneath. The length of stroke for the piston depends on the angle of the plate relative to the axis of rotation. The STM 4-120 engine (Figure 8.5.2) currently being commercialized by Stirling Thermal Motors incorporates a **variable-angle swash plate drive** that permits variation in the length of stroke of the pistons.

Free-Piston Engine/Converters. An innovative way of accomplishing the Stirling cycle is employed in the free-piston engine. In this configuration, the power piston is not mechanically connected to an output shaft. It bounces alternately between the space containing the working gas and a spring (usually a gas spring). In many designs, the displacer is also free to bounce on **gas springs** or mechanical springs (Figure 8.5.6). This configuration is called the Beale free-piston Stirling engine after its inventor, William Beale. Piston stroke, frequency, and the timing between the two pistons are established by the dynamics of the spring/mass system coupled with the variations in cycle pressure. To extract power, a magnet can be attached to the power piston and electric power generated as it moves past stationary coils. These Stirling engine/alternator units are called **free-piston Stirling converters**. Other schemes for extracting power from free-piston engines, such as driving a hydraulic pump, have also been considered.

Free-piston Stirling engines have only two moving parts, and therefore the potential advantages of simplicity, low cost, and ultra-reliability. Because electricity is generated internally, there are no dynamic seals between the high-pressure region of the engine and ambient, and no oil lubrication is required. This design promises long lifetimes with minimal maintenance. A number of companies are currently

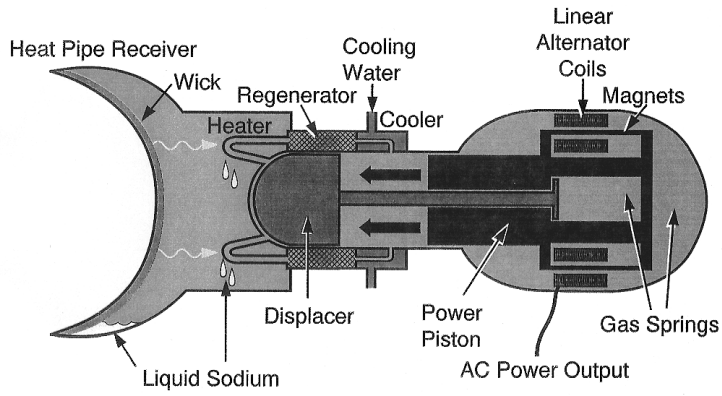

FIGURE 8.5.6 Basic components of a Beale free-piston Stirling converter incorporating a sodium heat pipe receiver for heating with concentrated solar energy.

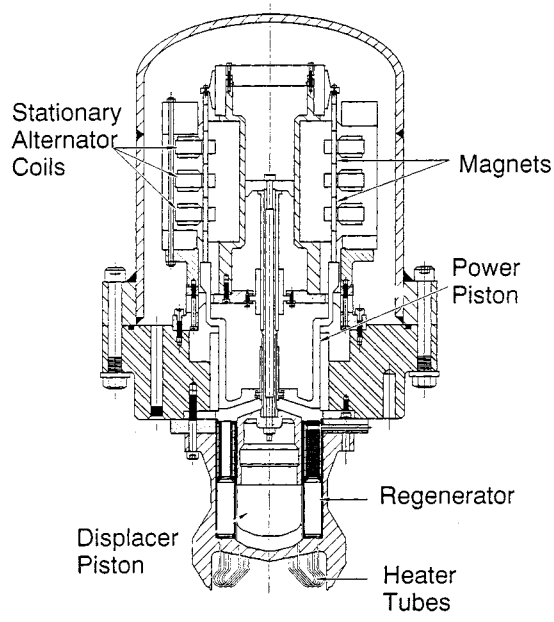

FIGURE 8.5.7 The Sunpower 9-kWe free-piston beta-configuration Stirling engine.

developing free-piston engines including Sunpower, Inc. (Figure 8.5.7), and Stirling Technology Company.

Seals and Bearings

Many proposed applications for Stirling engine systems require long-life designs. To make systems economical, a system lifetime of at least 20 years with minimum maintenance is generally required. Desired engine lifetimes for electric power production are 40,000 to 60,000 hr — approximately ten times longer than that of a typical automotive internal combustion engine. Major overhaul of engines, including replacement of seals and bearings, may be necessary within the 40,000- to 60,000-hr lifetime, which adds to the operating cost. A major challenge, therefore, in the design of Stirling engines is to reduce the potential for wear in critical components or to create novel ways for them to perform their tasks.

Piston seals differ from those used in internal combustion engines in a number of ways. Sealing of the power piston is critical since **blow-by loss** of the hydrogen or helium working gas must be captured and recompressed, or replaced from a high-pressure cylinder. Displacer sealing is less critical and only necessary to force most of the working gas through the heater, regenerator, and cooler. Oil for friction reduction or sealing cannot be used because of the danger of it getting into the working gas and fouling the heat-exchange surfaces. This leads to two choices for sealing of pistons, using **polymer sealing rings** or **gas bearings** (simply close tolerance fitting between piston and wall).

Free-piston engines with gas springs have special internal sealing problems. Small leakage can change the force-position characteristics of the "spring" and rapidly upset the phase and displacement dynamics designed into the engine. In order to prevent this, *centering ports* are used to ensure that the piston stays at a certain location; however, these represent a loss of potential work from the engine.

Materials

Materials used in Stirling engines are generally normal steels with a few exceptions. Materials that can withstand continuous operation at the cycle high temperature are required for the heater, regenerator, and the hot side of the displacement volume. Because most engines operate at high pressure, thick walls are often required. In the hot regions of the engine, this can lead to *thermal creep* due to successive heating and cooling. In the cool regions, large spaces for mechanical linkages can require heavy, thick walls to contain the gas pressure. Use of composite structure technology or reducing the size of the pressurized space can eliminate these problems.

Future of the Stirling Engine

The principal advantages of the Stirling engine, external heating and high efficiency, make this the engine of the future, replacing many applications currently using internal combustion engines and providing access to the sun as an inexpensive source of energy (Figure 8.5.6). For hybrid-electric automotive applications, the Stirling engine is not only almost twice as efficient as modern spark-ignition engines, but because of the continuous combustion process, it burns fuel more cleanly and is not sensitive to the quality or type of fuel. Because of the simplicity of its design, the Stirling engine can be manufactured as an inexpensive power source for electricity generation using biomass and other fuels available in developing nations.

Most importantly, the Stirling engine will provide access to inexpensive solar energy. Because it can receive its heat from a resource 93 million miles away using concentrating solar collectors, and because its manufacture is quite similar to the gasoline or diesel engine, and because economies of scale are certain when producing thousands of units per year, the Stirling engine is considered to be the least expensive alternative for solar energy electric generation applications in the range from 1 kWe to 100 MWe.

Defining Terms

Alpha-configuration: Design of a Stirling engine where two pistons moving out of phase, and cause the working gas between them to go through the four processes of the Stirling cycle.

Beale free-piston Stirling engine: Stirling engine configuration where the power piston and displacer in a single cylinder are free to bounce back and forth along a single axis, causing the enclosed working gas to go through the four processes of the Stirling cycle. Restoration forces are provided by the varying pressure of the working gas, springs (gas or mechanical), and the external load which can be a linear alternator or a fluid pump.

Beta-configuration: Design of a Stirling engine where the displacer and power piston are located in the same cylinder and cause the enclosed working gas to go through the four processes of the Stirling cycle.

Blow-by: The gas that leaks past a seal, especially a piston-to-cylinder seal.

Charge pressure: Initial pressure of the working gas.

Cooler: Heat exchanger that removes heat from the working fluid and transfers it out of the cycle.

Cross-head: A linear sliding bearing surface connected to a crankshaft by a connecting rod. It is purpose is to provide linear reciprocating motion along a single line of action.

Displacer: Closed volume 'plug' that forces the working fluid to move from one region of the engine to another by displacing it.

Double-acting piston: A piston in an enclosed cylinder where pressure can be varied on both sides of the piston, resulting a total amount of work being the sum of that done on or by both sides.

Dynamic seals: Seals that permit transfer of motion without permitting gas or oil leakage. These can be either *linear seals* permitting a shaft to move between two regions (i.e., the piston rod seals in a Stirling engine), or *rotating seals* that permit rotating motion to be transmitted from one region to another (i.e., the output shaft of a Stirling engine).

Free-piston Stirling converters: A name given to a hermetically sealed free-piston Stirling engine incorporating an internal alternator or pump.

Gamma-configuration: A design of a Stirling engine where the displacer and power piston are located in separate, connected cylinders and cause the enclosed working gas to go through the four processes of the Stirling cycle.

Gas bearing: A method of implementing the sliding seal between a piston and cylinder as opposed to using piston rings. Uses a precision-fitting piston that depends on the small clearance and long path for sealing and on the viscosity of the gas for lubrication.

Gas spring: A piston that compresses gas in a closed cylinder where the restoration force is linearly proportional to the piston displacement. This is a concept used in the design of free-piston Stirling engines.

Heater: A heat exchanger which adds heat to the working fluid from an external source.

Kinematic stirling engine: Stirling engine design that employ physical connections between the power piston, displacer, and a mechanical output shaft.

Linear seal: see **dynamic seals**.

Overdriven (bang-bang) motion: Linear motion varying with time as a square-wave function. An alternative to simple harmonic motion and considered a better motion for the displacer of a Stirling engine but difficult to implement.

Phase angle: The angle difference between displacer and power piston harmonic motion with a complete cycle representing 360°. In most Stirling engines, the harmonic motion of the power piston follows (lags) the motion of the displacer by approximately 90°.

Push rod: A thin rod connected to the back of the piston that transfers linear motion through a dynamic linear seal, between the low- and high-pressure regions of an engine.

Reflux: A constant-temperature heat-exchange process where a liquid is evaporated by heat addition and then condensed as a result of cooling.

Regenerator: A heat-transfer device that stores heat from the working gas during part of a thermodynamic cycle and returns it during another part of the cycle. In the Stirling cycle the regenerator stores heat from one constant-volume process and returns it in the other constant-volume process.

Ringbom configuration: A Stirling engine configuration where the power piston is kinematically connected to a power shaft, and the displacer is a free piston that is powered by the difference in pressure between the internal gas and atmospheric pressure.

Simple harmonic motion: Linear motion varying with time as a sine function. Approximated by a piston connected to a crankshaft or a bouncing of a spring mass system.

Stirling cycle: A thermodynamic power cycle with two constant-volume heat addition and rejection processes and two constant-temperature heat-addition and rejection processes.

Swash plate drive: A disk on a shaft, where the plane of the disk is tilted away from the axis of rotation of the shaft. Piston push rods that move parallel to the axis of rotation but are displaced from the axis of rotation, slide on the surface of the rotating swash plate and therefore move up and down.

Variable-angle swash plate drive: A swash plate drive where the tilt angle between the drive shaft and the plate can be varied, resulting in a change in the displacement of the push rods.

Wobble plate drive: Another name for a swash plate drive.

Working gas: Gas within the engine that exhibits pressure and temperature change as it is heated or cooled and/or compressed or expanded.

References

Meijer, R.F. 1992. Stirling engine, in *McGraw-Hill Encyclopedia of Science and Technology*, 7th ed., pp. 440–445, McGraw-Hill, New York.

Stine, W.B. and Diver, R.E. 1994. A *Compendium of Solar Dish Stirling Technology,* Report SAND94-7026, Sandia National Laboratories, Albuquerque, NM 87185.

Walker, G. 1973. The Stirling engine, *Sci. Am.,* 229(2):80–87.

Walker, G. 1980. *Stirling Engines,* Clarendon Press, Oxford.

West, C.D. 1986. *Principles and Applications of Stirling Engines,* Van Nostrand Reinhold, New York.

Further Information

Books

Hargraves, C.M. *The Philips Stirling Engine,* Elsevier Press, London, 1991.

Organ, A.J. *Thermodynamics and Gas Dynamics of the Stirling Cycle Machine,* Cambridge University Press, Cambridge, 1992.

Senft, J.R. *Ringbom Stirling Engines,* Oxford University Press, Oxford, 1993.

Stine, W.B. and R.E. Diver, A *Compendium of Solar Dish/Stirling Technology,* SAND93-7026, Sandia National Laboratory, Albuquerque, 1994.

Urieli, I. and D.M. Berchowitz, *Stirling Cycle Engine Analysis,* Adam Hilger, Bristol, 1984

Walker, G. *Stirling Engines,* Clarendon Press, Oxford, 1980.

Walker, G. and J.R. Senft, *Free-Piston Stirling Engines,* Springer-Verlag, New York, 1985.

Walker, G., G. Reader, O.R. Fauvel, E.R. Bingham, *The Stirling Alternative,* Bordon & Breach, New York, 1994.

West, C.D. *Principles and Applications of Stirling Engines,* Van Nostrand Reinhold, New York, 1986.

Periodicals

Proceedings of the Intersociety Energy Conversion Engineering Conference (IECEC), published annually.

Stirling Machine World, a quarterly newsletter devoted to advancements in Stirling engines, edited by Brad Ross, 1823 Hummingbird Court, West Richland, WA 99353-9542.

Stirling Engine Developers

Stirling Technology Company, 4208B W. Clearwater Ave., Kennewick, WA 99336.
Stirling Thermal Motors, 275 Metty Drive, Ann Arbor, MI 48103.
Sunpower Incorporated, 6 Byard Street, Athens, OH 45701.
Clever Fellows Innovation Consortium, 302 Tenth St., Troy, NY 12180.
Mechanical Technologies Inc., 968 Albany-Shaker Rd., Latham, NY 12110.
Solo Kleinmotoren GmbH, Postfach 60 0152; D-71050 Sindelfingen; Germany.
Aisin-Seiki Ltd., 1, Asahi-Mach: 2-chome; Kariya City Aich: Pref 448; Japan.

8.6 Advanced Fossil Fuel Power Systems

Anthony F. Armor

Introduction

The generation of electric power from fossil fuels has undergone significant and, in some cases, dramatic changes over the last 20 years or so. Technology improvements in fossil fuel combustion have been largely driven by environmental issues, by the need to conserve fossil fuel resources, and by the economics of the competitive marketplace. The importance of fossil fuel-fired electric generation to the world is undeniable — more than 70% of all power in the U.S. is fossil fuel based, and worldwide the percentage is higher and growing. Today, most power plants worldwide burn coal, but increasingly generating companies are turning to natural gas, as the cost of gas-fired generation and the long-term supply of gas appear favorable. This section reviews the current status and likely future deployment of competing generation technologies based on fossil fuels.

It is likely, particularly in the developed world, that gas turbine-based plants will dominate the new generation market in the immediate future. The most advanced combustion turbines (CTs) now achieve more than 40% **lower heating value** (LHV) efficiency in simple cycle mode and greater than 50% efficiency in **combined cycle** (CC) mode. In addition, combustion turbine/combined cycle (CT/CC) plants offer siting flexibility, swift construction schedules, and capital costs between $400/kW and $800/kW. These advantages, coupled with adequate natural gas supplies and the assurance, in the longer term, of **coal gasification** backup, make this technology currently the prime choice for green field and repowered plants in the United States and in Europe.

But for the developing world, particularly China and India, there is good reason why the direct coal-fired power plant may still be the primary choice for many generation companies. Fuel is plentiful and inexpensive, and sulfur dioxide scrubbers have proved to be more reliable and effective than early plants indicated. In fact, as high as 99% SO_2 removal efficiency is now possible.

Combustion of coal can occur in three basic forms, direct combustion of pulverized coals (PC), combustion of coal in a suspended bed of coal and inert matter, and coal gasification. The pulverized coal (PC) plant, the most common form of coal combustion, has the capability for much improved efficiency even with full **flue gas desulfurization** (FGD), because materials technology has now advanced to the point where higher steam pressures and temperatures are possible. In the United States, Europe, Japan, and Russia, the advanced superficial PC plant is moving ahead commercially.

Worldwide, the application of atmospheric and pressurized fluidized bed combustion (FBC) plants has increased, and such plants offer reductions in both SO_2 and NO_x while permitting the efficient combustion of vast deposits of low-rank fuels such as lignites. In the United States, there are now over 150 large operating units for power generation, and throughout Europe, China, and the former Soviet Union countries small FBC units have been extensively deployed.

Coal gasification power plants exist at the 100 and 160 MW levels and are planned up to 450 MW. Much of the impetus is now coming from the U.S. Department of Energy (DOE) clean coal program where three gasification projects are in progress and four more are planned, and gasification plants are under construction in Europe and Japan. Gasification not only leads to minimum atmospheric and solid emissions, but also provides an opportunity to take advantage of gas turbine advances. With the rapid a, advances now being introduced in CT technology, the coal gasification option is a leading turn-of-the-century candidate for new plant construction.

Clean Coal Technology Development

At an increasing rate in the last few years, innovations have been developed and tested that are aimed at reducing emissions through improved combustion and environmental control, in the near term, and, in the longer term, through fundamental changes in the way coal is preprocessed before converting its

chemical energy to electricity. Such technologies are referred to as "clean coal technologies" described as a family of precombustion, combustion/conversion, and postcombustion technologies (Torrens, 1990). They are designed to provide the coal user with added technical capabilities and flexibility and the world with an opportunity to exploit our most abundant fossil source. They can be categorized as

- *Precombustion*, where sulfur and other impurities are removed from the fuel before it is burned;
- *Combustion*, where techniques to prevent pollutant emissions are applied in the boiler while the coal burns;
- *Postcombustion*, where the flue gas released from the boiler is treated to reduce its content of pollutants;
- *Conversion*, where coal, rather than being burned, is changed into a gas or liquid that can be cleaned and used as a fuel.

Coal Cleaning

Cleaning of coal to remove sulfur and ash is well established in the United States with more than 400 operating plants, mostly at the mine. Coal cleaning removes primarily pyritic sulfur (up to 70% SO_2 reduction is possible) and in the process increases the heating value of the coal, typically about 10% but occasionally 30% or higher. Additionally, if slagging is a limiting item, increased megawatts may be possible, as occurred at one station which increased generation from 730 to 779 MW. The removal of organic sulfur, chemically part of the coal matrix, is more difficult, but may be possible using microorganisms or through chemical methods; research is underway (Couch, 1991). Finally, heavy metal trace elements can be removed also, conventional cleaning removing (typically) 30 to 80% of arsenic, mercury, lead, nickel, antimony, selenium, and chromium.

Cleaning of Low-Rank Coal

With large deposits of high-moisture, and sometimes high-ash, low-rank coals and lignites, there is interest, but as yet no large-scale activity, in cleaning these coals. Improvement in heating value and reduction of boiler **slagging and fouling** problems are outcomes. Economics will decide whether precleaning or direct combustion (perhaps in a fluidized bed) will be the future choice. Large subbituminous and lignite fields exist in the United States, the former U.S.S.R., Germany, and Eastern Europe, as Table 8.6.1 indicates.

TABLE 8.6.1 World Coal Production

Country	Total Coal Production, Mt	Bituminous, Mt	Subbituminous and Lignite, Mt	Approximate Amount Bituminous Cleaned, %
China	1018	985	33	20
United States	833	581	252	55
Former U.S.S.R.	760	550	210	60
Germany	487	77	410	95
Poland	266	193	73	40
Australia	224	179	45	75
South Africa	214	214	0	—
India	191	180	11	20
Czechoslovakia	126	26	100	—
U.K.	100	100	0	75
Canada	61	33	28	—

Source: World Energy Conference, 1989.

Pulverized Coal Plants

There has been a perception that the PC power plant has come to the end of the road, that advanced coal technologies will quite soon make obsolete the PC plant with a scrubber, whose efficiency hovers around 35%. This perception may be premature. In fact, the PC plant has the capability for much improved heat rate (about 8500 Btu/kWh) even with full FGD. Beyond these units, the PC-fired CC with topping turbine (Figure 8.6.1) has a projected heat rate of 7200 Btu/kWhr, which includes full scrubbing capability. The PC plant is a proven, reliable power source with unit capabilities demonstrated at more than to 1000 MW using a single-shaft steam turbine. One plant, commercially available now, uses steam at 4500 psig and 1100°F, all ferritic materials for major boiler and turbine components, leading-edge technology in environmental controls, and the latest techniques in waste heat utilization (Poe et al., 1991). It is modular, fuel flexible, and designed for **on/off cycling capability**.

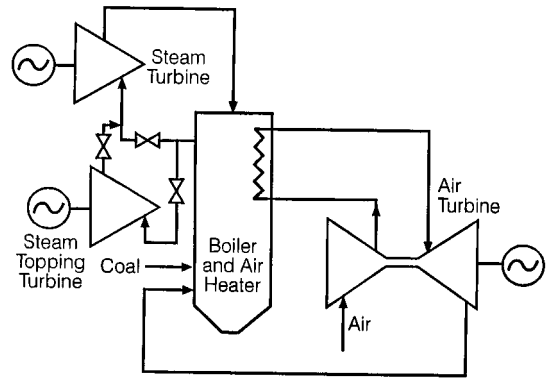

FIGURE 8.6.1 A PC CC with topping steam turbine has a projected heat rate of 7200 Btu/kWhr. The air turbine uses 1800°F air, or 2300°F air with supplemental firing. The topping turbine uses steam at 1300°F.

Higher steam temperatures (to 1150°F) and **supercritical steam pressures** are an important aspect of the modern advanced PC plant. They are possible now because of advances in ferritic materials technology that will extend life, provide greater creep and fatigue strength, and be resistant to **temper embrittlement** and, in the boiler, to coal ash corrosion (Armor et al., 1988).

Of particular note are

- **Coextruded tubing** or monotubing for superheaters and reheaters, resistant to coal ash corrosion.
- Super-9-chrome steel (P91), for steam piping, valves, headers, casings.
- Improved creep-resistant 12-chrome forgings for high-pressure/intermediate-pressure (HP/IP) turbines.
- "Superclean" 3.5 NiCrMoV rotors for low-pressure (LP) turbines, resistant to temper embrittlement.

Built in 1959, Eddystone 1 at PECO Energy was, and still is, the supercritical power unit with the highest steam conditions in the world. When constructed in the early 1960s, Eddystone 1 had a main steam pressure of 5000 psi, and main steam temperature of 1200°F. **Double reheat** of the steam was employed. PECO Energy continues to operate Eddystone 1, an impressive achievement for a prototype unit. More-recent advanced plants include the Chuba Electric Kawagoe unit in Japan, a 700-MW double-reheat supercritical with steam conditions of 4750 psi, 1050°F, and the Esbjerg unit of Elsam in Denmark, a 400-MW supercritical with steam conditions of 3700 psi, 1040°F. Both plants use advanced ferritic steels for turbine and boiler thick wall components. There are over 170 supercritical units in the United States, more than 220 in Russia (Oliker and Armor 1992), and over 60 in Japan. A number are installed in Germany, Denmark, Holland, and other European countries, and increasingly in the Far East.

Emissions Controls for Pulverized Coal Plants

Today, worldwide, about 40% of electricity is generated from coal and the total installed coal-fired generating capacity is more than 1000 GW, largely made up of 340 GW in North America; 220 GW in Western Europe, Japan, and Australia; 250 GW in Eastern Europe and the former U.S.S.R., and 200 GW in China and India. In the decade 1990 to 2000, 190 GW of new coal-fired capacity will likely be added. So the control of particulates, sulfur dioxides, and nitrogen oxides from those plants is one of the most pressing needs of today and of the future, together with the potential impact of carbon dioxide emissions, with their contribution to global warming. To combat these concerns, a worldwide move toward environmental retrofitting of older fossil-fired power plants is underway, focused largely on sulfur dioxide scrubbers and combustion or postcombustion optimization for nitrogen oxides.

Conventional Lime/Limestone Wet Scrubber

The dominant SO_2 scrubbing system is the wet limestone design, limestone being one quarter the cost of lime as a reagent. In this system (Figure 8.6.2) the limestone is ground and mixed with water in a reagent preparation area. It is then conveyed to a spray tower called an absorber, as a slurry of 90% water and 10% solids, and sprayed into the flue gas stream. The SO_2 in the flue gas is absorbed in the slurry and collected in a reaction tank where it combines with the limestone to produce water and calcium sulfate or calcium sulfate crystals. A portion of the slurry is then pumped to a thickener where these solids/crystals settle out before going to a filter for final dewatering. Mist eliminators installed in the system ductwork at the spray tower outlet collect slurry/moisture entrained in the flue gas stream. Calcium sulfate is typically mixed with fly ash (1:1) and lime (5%) and disposed of in a landfill.

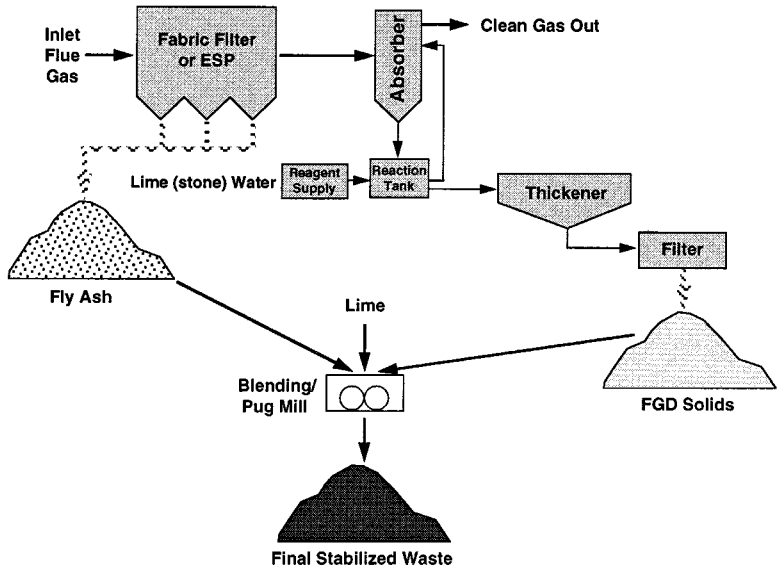

FIGURE 8.6.2 The conventional lime/limestone wet scrubber is the dominant system in operation in the United States. With recent refinements this system can be 98 to 99% effective in removing SO_2.

Various improvements can be made to this basic process, including the use of additives for performance enhancement and the use of a hydrocyclone for dewatering, replacing the thickener, and leading to a salable gypsum by-product. The Chiyoda-121 process (Figure 8.6.3) reverses the classic spray scrubber and bubbles the gas through the liquid. This eliminates the need for spray pumps, nozzle headers, separate oxidation towers, and thickeners. The Chiyoda process is being demonstrated in a DOE Clean Coal Technology (CCT) project on a 100-MW unit at the Yates plant of the Georgia Power Company.

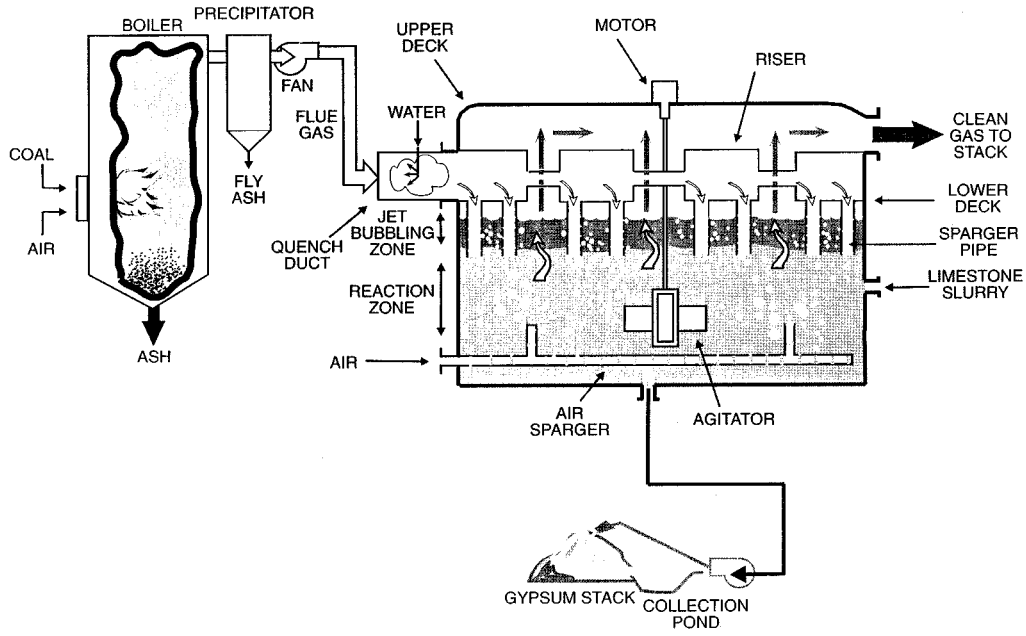

FIGURE 8.6.3 The Chioda-121 scrubber simplifies the process by bubbling the flue gas through the liquid, eliminating some equipment needs.

Spray Drying

Spray drying (Figure 8.6.4) is the most advanced form of dry SO_2 control technology. Such systems tend to be less expensive than wet FGD but remove typically a smaller percentage of the sulfur (90% compared with 98%). They are usually used when burning low-sulfur coals, and utilize fabric filters for particle collection, although recent tests have shown applicability to high-sulfur coals also.

Spray driers use a calcium oxide reagent (quicklime) which when mixed with water produces a calcium hydroxide slurry. This slurry is injected into the spray drier where it is dried by the hot flue gas. As the drying occurs, the slurry reacts to collect SO_2. The dry product is collected at the bottom of the spray tower and in the downstream particulate removal device where further SO_2 removal may take place. It may then be recycled to the spray drier to improve SO_2 removal and alkali utilization.

For small, older power plants with existing **electrostatic precipitators** (ESPs), the most cost-effective retrofit spray-dry configuration locates the spray drier and fabric filter downstream of the ESP, separating in this manner the spray drier and fly ash waste streams. The fly ash can then be sold commercially.

Control of Nitrogen Oxides

Nitrogen oxides can be removed either during or after coal combustion. The least-expensive option and the one generating the most attention in the United States is combustion control, first through adjustment of the fuel/air mixture and second through combustion hardware modifications. Postcombustion processes seek to convert NO_x to nitrogen and water vapor through reactions with amines such as ammonia and urea. Selective catalytic reduction (SCR) injects ammonia in the presence of a catalyst for greater effectiveness. So the options (Figure 8.6.5) can be summarized as

Operational changes. Reduced excess air and biased firing, including taking burners out of service;
Hardware combustion modifications. Low-NO_x burners, air staging, and fuel staging (reburning);
Postcombustion modifications. Injection of ammonia or urea into the convection pass, SCR, and wet or dry NO_x scrubbing (usually together with SO_2 scrubbing).

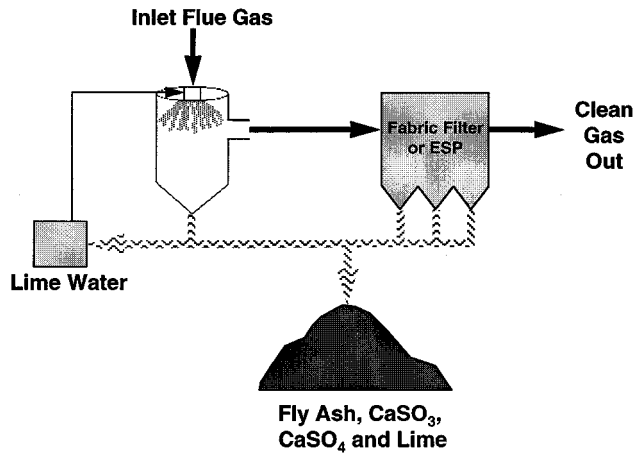

FIGURE 8.6.4 Spray driers use a calcium oxide reagent mixed with water, which is dried by the flue gas. A dry product is collected in a fabric filter.

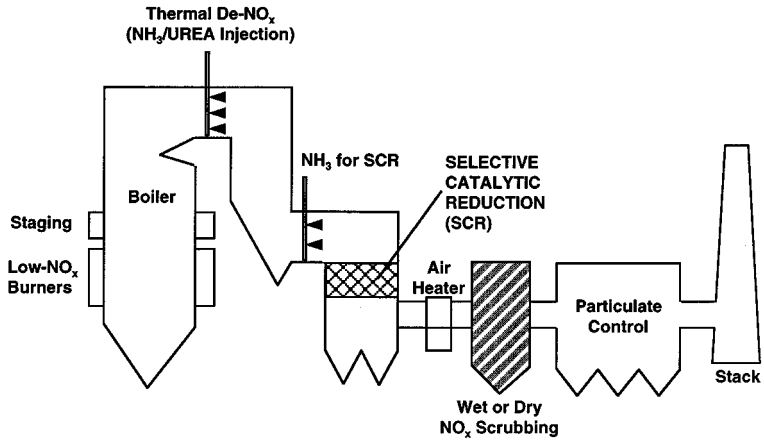

FIGURE 8.6.5 Control options for NO_x include operational, hardware, and postcombustion modifications.

Low-NO_x burners can reduce NO_x by 50% and SCR by 80%, but the low-NO_x burner option is much more cost-effective in terms of cost per ton of NO_x removed. Reburning is intermediate in cost per removed ton and can reduce NO_x 50 or 75% in conjunction with low-NO_x burners.

Fluidized Bed Plants

Introduced nearly 30 years ago, the **fluidized bed** combustion boiler has found growing application for power generation. From the first FBC boiler, generating 5000 lb/hr of steam in 1967, the technology has matured to the 250-MW-size units available today. In North America more than 170 units now

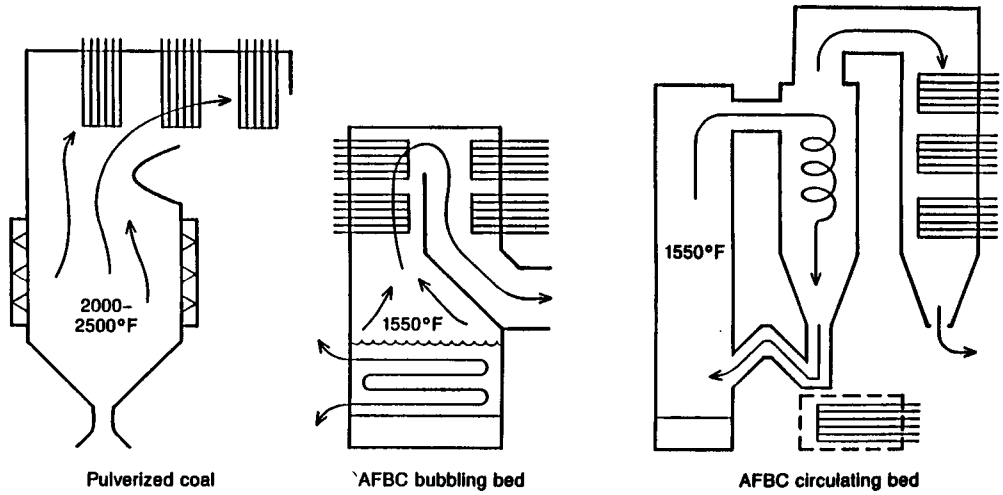

FIGURE 8.6.6 An illustration of the distinguishing features of PC and fluidized bed boilers. Noticeable in this diagram are the in-bed tubes characteristic of bubbling beds and the cyclone separator of the circulating bed.

generate in excess of 6000 MW. Burning coal in a suspended bed with limestone or dolomite permits effective capture of sulfur, and fuel flexibility allows a broad range of opportunity fuels. These fuels might include coal wastes (culm from anthracite, gob from bituminous coal), peat, petroleum coke, and a wide range of coals from bituminous to lignite. A low (1500°F) combustion temperature leads to low NO_x formation. The salient features of atmospheric fluidized bed boilers, compared with a PC boiler, are shown in Figure 8.6.6.

Utility-size demonstration projects at the Tennessee Valley Authority in 1989 (Shawnee, 160 MW) (Manaker, 1992) and Northern States Power in 1986 (Black Dog, 133 MW) (Hinrichsen, 1989) are examples of successful atmospheric bubbling bed units. The Black Dog unit has been dispatched in a daily cycling mode and has successfully fired a blend of coal and petroleum coke. But the focus of atmospheric FBC (AFBC) in the United States is now on the circulating fluid bed (CFB). In fact, more than 70% of operating fluid bed boilers in the United States are of the circulating type. The CFB unit at Nucla (Tri-State G&T Association) (Blunder, 1989) has been successful in demonstrating the technology at the 110-MW level, and commercial CFB plants have now reached 250 MW in size. Most fluidized bed units for electricity generation are being installed by independent power producers in the 50- to 100-MW-size range, where the inherent SO_2 and NO_x advantages over the unscrubbed PC plant have encouraged installations even in such traditional non-coal arenas as California (Melvin and Friedman, 1994). Worldwide, the AFBC boiler is employed largely for steam heat, with hundreds of them in operation in Russia and India, and thousands in China. The extension of the concept of fluidized beds to units where the fuel mixture is burned under several atmospheres pressure (PFBC) has now opened the way to smaller modular units with opportunities to move to efficient PFBC CCs.

Atmospheric Fluidized Bed Combustion

In the bubbling bed version of the AFBC, the fuel and inert matter, together with limestone or dolomite for SO_2 capture, is suspended through the action of fluidizing air, which flows at a velocity of 3 to 8 ft/sec in essentially a one-pass system. CFBs differ from bubbling beds in that much of the bed material passes through a cyclone separator before being circulated back to the boiler (Figure 8.6.7). In-bed tubes are generally not used for CFB units, permitting a much higher fluidizing velocity of 16 to 26 ft/sec. Since the early AFBC designs, attention has been directed toward increasing unit efficiency, and reheat designs are now usual in large units. When SO_2 capture is important, a key parameter is the ratio of calcium in the limestone to sulfur in coal. Typical calcium-to-sulfur ratios for 90% SO_2 reduction are

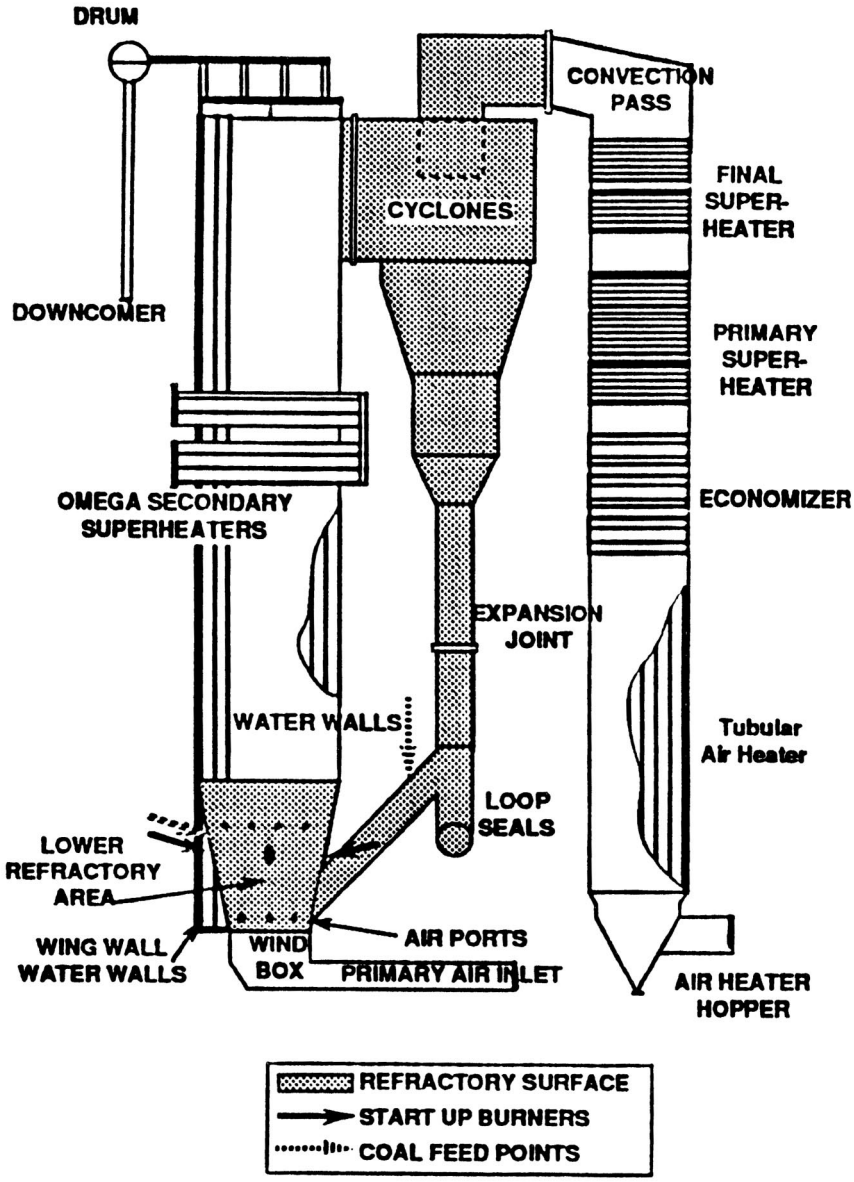

FIGURE 8.6.7 A Pyropower circulating fluid bed boiler installed at the ACE Cogeneration Company at Trona, California. This 108-MW unit burns low sulfur, western bituminous coal with limestone in a bed which circulates back to the boiler after passing through a cyclone separator.

in the range of 3.0 to 3.5 for bubbling beds and 2.0 to 2.5 for circulating beds. This depends on the fuel, however, and the 200-MW CFB units at the Conoco/Entergy plant in Lake Charles, Louisiana burning 100% **petroleum coke** (4.5% S), have a Ca/S ratio of below 1.7 for more than 90% sulfur capture. NO_x levels in AFBCs are inherently low and nominally less than 0.2 lb/MM Btu.

It is important to note that for CFBs, boiler efficiencies can be as high as a PC unit (Table 8.6.2). In fact, designs now exist for AFBCs with supercritical steam conditions, with prospects for cycles up to 4500 psia, 1100°F with **double reheat** (Skowyra et al., 1995).

TABLE 8.6.2 Typical Boiler Efficiencies, PC and Fluidized Beds

		Calculated Heat Loss %		
Loss/Gain Parameter	**PC**	**Highest-Efficiency CFB**	**Lowest-Efficiency CFB**	**Bubbling Bed**
Moisture in limestone	NA	0.06	0.10	0.10
Calcination	NA	1.02	1.69	2.70
Sulfation credit	NA	–1.60	–1.60	–1.60
Unburned carbon	0.25	0.50	2.0	4.0
Heat in dry flue gas	5.28	5.57	5.60	5.75
Moisture in fuel	1.03	1.03	1.03	1.03
Moisture from burning H_2	41.9	4.19	4.19	4.19
Radiation and convection	0.30	0.30	0.80	0.30
Moisture in air	0.13	0.14	0.14	0.14
Sensible heat in boiler ash	0.03	0.09	0.76	0.50
Bottom ash	0.05	NA	NA	NA
Fan-power credit	–0.25	–0.75	–0.40	–0.50
Pulverizer/crusher power gain	–0.20	NA	NA	NA
Total losses/gains	10.81	10.55	14.31	16.51
Overall boiler efficiency, %	89.19	89.45	85.69	83.49

Source: POWER, January 1987.

Pressurized Fluidized Bed Combustion

In a PFBC CC unit (Figure 8.6.8), coal in a fluid bed is burned with dolomite or limestone in a pressurized steel chamber, raising steam for a steam turbine generator. The pressurized flue gases are expanded through a gas turbine. Commercial plants at about the 80-MW level in Sweden, the United States, and Spain have demonstrated that bubbling bed PFBC plants with a calcium-to-sulfur molar ratio of about 1.5 offer sulfur capture up to 95%, together with inherently low NO_x emissions due to low combustion temperatures. Cleanup of the flue gas before entry to the gas turbines is a key technical objective, and first-generation units have used cyclones together with gas turbines ruggedized with special blade coatings. For more-advanced, higher-efficiency PFBC systems, hot-gas cleanup technology, where the gas is directed through large ceramic filter units, will likely be needed.

To date, the 80-MW units at Vaertan (Sweden) and Escatron (Spain) and the 70-MW unit at Tidd (AEP) have operated satisfactorily, and larger units up to 350 MW are now under development. The modular aspect of the PFBC unit is a particularly attractive feature leading to short construction cycles and low-cost power. This was particularly evident in the construction of the Tidd plant, which first generated power from the CC on November 29, 1990. The heat rate and capital cost of the PFBC plant are forecast to reach very competitive levels which, when combined with shortened construction schedules, will position the technology for a role in future generation plans, particularly where modular additions have advantages.

One promising use for PFBC units is for small in-city cogeneration plants where the inherent size advantages, high efficiencies, and effective coal gas cleanup approach permit compact plants to be retrofitted in place of heating boilers, while the small steam turbines can be easily adapted to both electricity and hot water supply (Olesen, 1985).

Advanced PFBCs

In conventional PFBC plants, the overall cycle efficiency is limited to less than 42%. That is because the operating temperature of the combustor — which must be held to 1650°F (900°C) or less to avoid sintering the ash and releasing alkali metals that could foul or corrode the gas turbine — in effect sets the gas turbine inlet temperature far below the 2350°F (1290°C) or so featured in the most-efficient heavy-frame machines currently in use firing natural gas or oil.

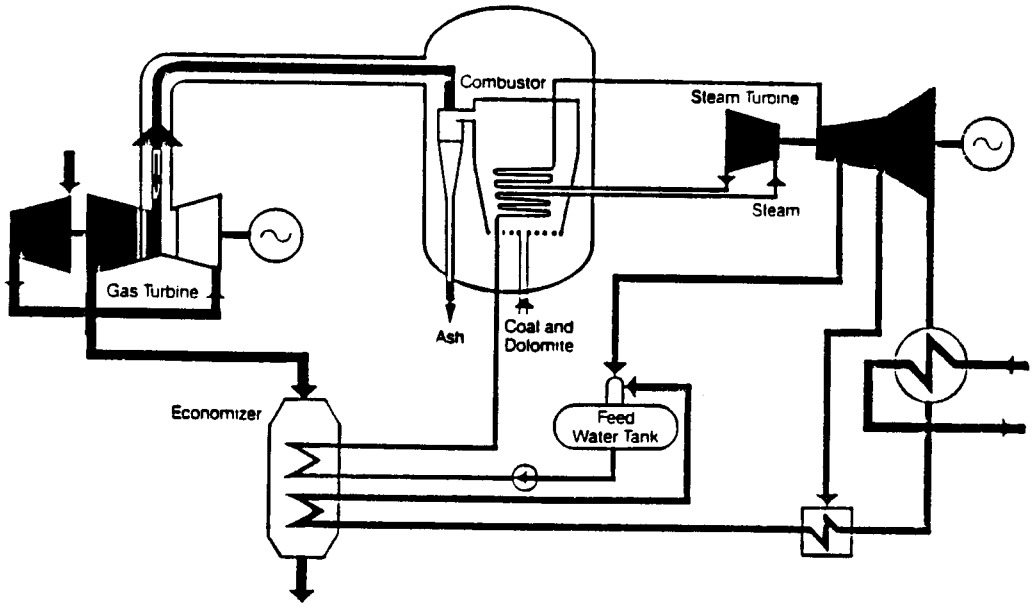

FIGURE 8.6.8 Pressurized fluidized bed with combined cycle. This 70-MW system has operated at the Tidd plant of American Electric Power.

Increasing the inlet temperature of the gas turbine, which typically provides 20 to 25% of the power in a PFBC plant, could raise the overall cycle efficiency to more than 45%. A simple means of boosting the flue gas temperature would be to fire a topping fuel, such as natural gas, ahead of the gas turbine. But 2350°F would be well above the **ash-softening temperature**, so high temperature, HP filtration systems would be essential to remove all particulate matter before firing the natural gas.

A further advance would be to use gas from coal rather than natural gas as the topping fuel. The coal would be pyrolyzed in a low-oxygen environment under pressure to produce both a low-Btu fuel gas and a residual char. The fuel gas would be passed through its own hot-gas cleanup filters before being fired in a topping combustor ahead of the gas turbine; the char would be burned in a circulating bed PFBC, from which the flue gas would also be filtered and then combined with the topping cycle gas stream. (Or the char could be simply fired in an AFBC.) With net heat rates below 7600 Btu/kWhr (45% efficiency), carbon dioxide emissions would be correspondingly low.

A U.S. DOE CCT project known as the Four Rivers Energy Modernization Project, involves building a Foster-Wheeler 95-MW advanced circulating-type PFBC unit at the Air Products chemical manufacturing facility in Calvert City, Kentucky. Steam from the unit, which will feature a coal-gas-fired topping combustor and a hot-gas cleanup system, will be used in chemical production, and the power will be sold to the Tennessee Valley Authority. The project is scheduled to begin commercial operation in October, 1998 (Carpenter and Dellefield, 1994).

Gasification Plants

One option of growing interest to coal-burning utilities is that of coal gasification. After the EPRI Cool Water demonstration in 1984 at the 100-MW level, the technology has moved ahead in the United States largely through demonstrations under the CCT program (U.S. DOE, 1994). Overseas, the 250-MW Buggenham plant in Holland is now operational, and the PSI/Destec 262-MW and TECO Energy 250-MW gasification plant demonstrations are also on-line. Beyond this, there is a 300-MW gasification unit scheduled for Endesa, Spain and a 330-MW unit for RWE in Germany (Figure 8.6.9).

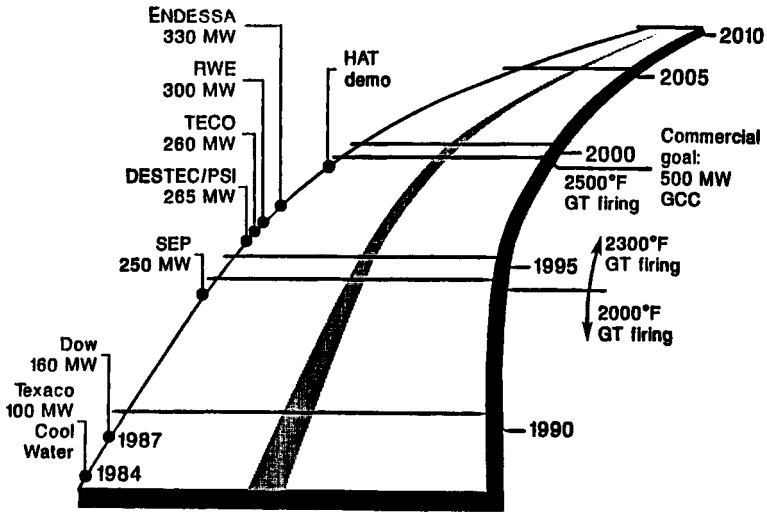

FIGURE 8.6.9 By building on the early success of the 100-MW Cool Water gasification-CC plant in California, demonstrations in the 250 to 350 MW range will be carried out in the 1995 to 2000 time frame.

Gasification-based plants have among the lowest emissions of pollutants of any central station fossil technology. Through use of the efficiency advantages of CCs, CO_2 emissions are also low. Fuel flexibility is an additional benefit since the gasifier can accommodate a wide range of coals, plus petroleum coke. Integrated gasification CC (IGCC) plants permit a hedge against long-term increases in natural gas prices since natural gas-fired CTs can be installed initially, and gasifiers at a later time when a switch to coal becomes prudent (Douglas, 1986).

The pioneering Cool Water plant, the first of its kind in the world, operated for more than 4 years, gasifying 1.1 million tons of coal and producing 2.8 million MWhr of electricity. The project was a collaborative effort of the industry involving the utility (Southern California Edison), equipment manufacturers (Texaco, General Electric), and consultants/research consortia (Bechtel, EPRI, and others). Particularly notable was the achievement of exceptionally low levels of emissions of SO_2, NO_x, and particulates, as shown in Figure 8.6.10.

Basically, IGCC plants replace the traditional coal combustor with a gasifier and gas turbine. Ultra-low emissions are realized, over 99% of the sulfur in the coal being removed before the gas is burned in the gas turbine. A gasification cycle can take advantage of all the technology advances being made in CTs and steam turbines, so as to enhance overall cycle efficiency. Net system efficiencies of 45% are expected to be demonstrated by the turn of the century, and when, in the next decade, the **fuel cell** begins to replace the gas turbine, plant efficiencies will climb to the 60% level. Major demonstrations are underway, as part of the CCT program, at Sierra Pacific Power, Pinon Pine (a KRW 99-MW air-blown, pressurized, fluidized bed coal gasifier); Tampa Electric, Polk County (a Texaco, 250-MW oxygen-blown, entrained-flow gasifier); at Tamco Power, Toms Creek (a 190-MVV joint gasification/PC plant with a Tampella Power fluidized bed gasifier); and at PSI Energy/Destec Energy, Wabash River (a 262-MW plant based on the Destec two-stage, entrained-flow, oxygen-blown gasifier). More-detailed descriptions of the Pinon Pine and Polk County gasification systems follow.

Pinon Pine IGCC

At the Sierra Pacific Power Pinon Pine plant (Figure 8.6.11), dried and crushed coal is introduced into a pressurized, air-blown, fluidized bed gasifier. Crushed limestone is added to the gasifier to capture a portion of the sulfur and to inhibit conversion of fuel nitrogen to ammonia. The sulfur reacts with the limestone to form calcium sulfide, which, after oxidation, exits along with the coal ash in the form of agglomerated particles suitable for landfill.

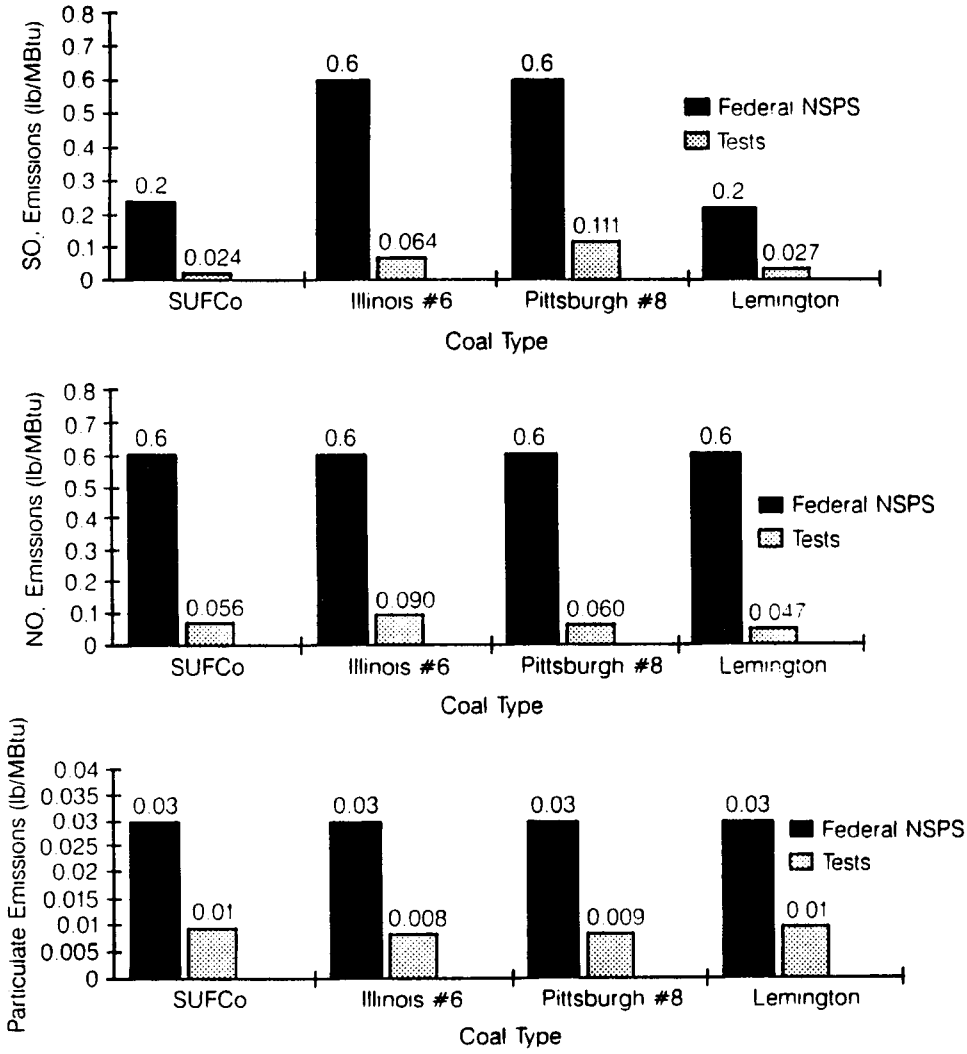

FIGURE 8.6.10 Tests at Cool Water on four coals show emissions of SO_2, NO_x, and particulates substantially below the Federal New Source Performance Standards.

Hot, low-Btu coal gas leaving the gasifier passes through cyclones, which return most of the entrained particulate matter to the gasifier. The gas, which leaves the gasifier at about 1700°F, is cooled to about 1100°F before entering the hot-gas cleanup system. During cleanup, virtually all of the remaining particulates are removed by ceramic candle filters, and final traces of sulfur are removed by reaction with metal oxide sorbent.

The hot, cleaned gas then enters the CT, which is coupled to a generator designed to produce 61 MW. Exhaust gas is used to produce steam in a heat-recovery steam generator. Superheated HP steam drives a condensing steam turbine/generator designed to produce about 46 MW.

Owing to the relatively low operating temperature of the gasifier and the injection of steam into the combustion fuel stream, the NO_x emissions are likely to be below 0.053 lb/M Btu. Because of the combination of in-bed sulfur capture and **hot-gas cleanup**, SO_2 emissions will be below 0.045 lb/M Btu (98% reduction).

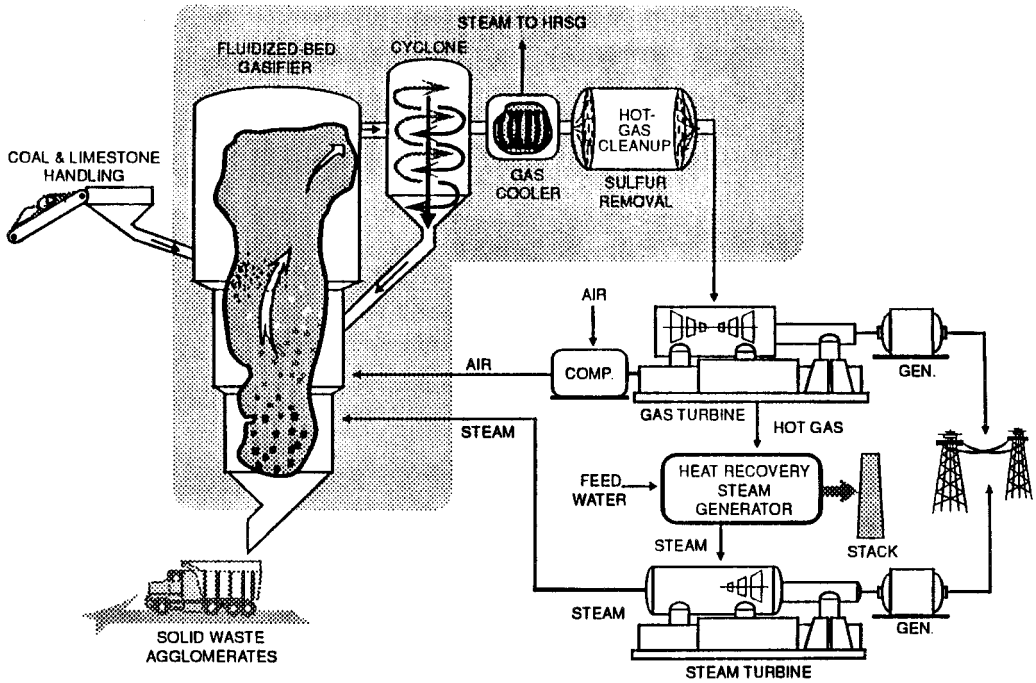

FIGURE 8.6.11 Integrated gasification CC at Sierra Pacific Power, Pinon Pine plant. This uses a KRW air-blown, pressurized fluidized bed coal gasifier, and produces 99 MW (net).

At Pinon Pine, 880 ton/day of coal are converted into 107 MW (gross), or 99 MW (net), for export to the grid. Western bituminous coal (0.5 to 0.9% sulfur) from Utah is the design coal although tests will be done using West Virginia or Pennsylvania bituminous coal containing 2 to 3% sulfur.

Polk County IGCC

The Texaco pressurized, oxygen-blown, entrained-flow gasifier will be used at the Tampa Electric Polk County plant to produce a medium-Btu fuel gas (Figure 8.6.12). Coal/water slurry and oxygen are combined at high temperature and pressure to produce a high-temperature syngas. Molten coal ash flows out of the bottom of the vessel and into a water-filled quench tank, where it is turned into a solid slag. The syngas from the gasifier moves to a high-temperature heat-recovery unit which cools the gases.

The cooled gases flow to a particulate-removal section before entering gas cleanup trains. A portion of the syngas is passed through a moving bed of metal oxide absorbent to remove sulfur. The remaining syngas is further cooled through a series of heat exchangers before entering a conventional gas cleanup train where sulfur is removed by an acid-gas removal system. These cleanup systems combined are expected to maintain sulfur levels below 0.21 lb/M Btu (96% capture). The cleaned gases are then routed to a CC system for power generation. A gas turbine generates about 192 MW. Thermally generated NO_x is controlled to below 0.27 lb/M Btu by injecting nitrogen as a diluent in the combustion section of the turbine. A heat-recovery steam generator uses heat from the gas turbine exhaust to reduce HP steam. This steam, along with the steam generated in the gasification process, is routed to the steam turbine to generate an additional 120 MW. The IGCC heat rate for this demonstration is expected to be approximately 8600 Btu/kWhr (40% efficient).

The demonstration project involves only the first 250-MW portion of the planned 1150-MW Polk County power station. Coals being used in the demonstration are Illinois 6 and Pittsburgh 8 bituminous coals having sulfur contents ranging from 2.5 to 3.5%.

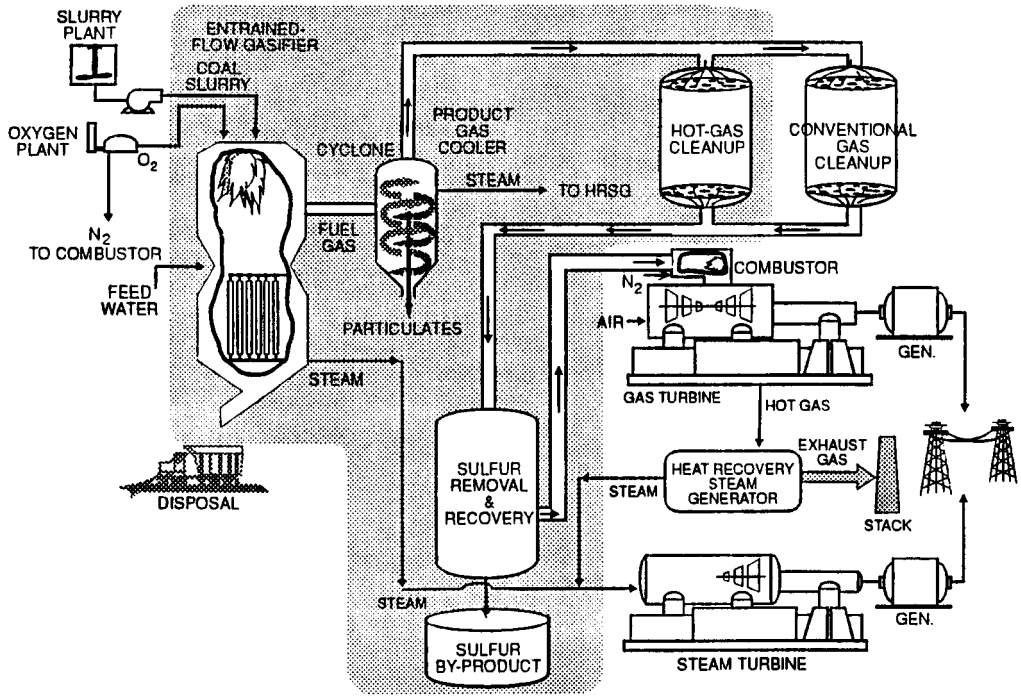

FIGURE 8.6.12 Integrated gasification CC at Tampa Electric, Polk County plant. A Texaco oxygen-blown gasifier is used. Total net generation is 250 MW.

By-products from the process — sulfuric acid and slag — can be sold commercially, sulfuric acid by-products as a raw material to make agricultural fertilizer and the nonleachable slag for use in roofing shingles and asphalt roads and as a structural fill in construction projects.

Buggenum IGCC

Meanwhile, tests are in progress on the 250-MW IGCC plant in Buggenum, Netherlands. After successful operations running on natural gas, a switch was made to coal gas using Columbia coals. Buggenum comprises a 2000-ton/day single reactor coal gasification unit and an air separation plant able to produce 1700 ton/day of 95% pure oxygen. Syngas drives a Siemens CC power unit, including a 156-MW V94.2 gas turbine and a 128-MW steam turbine. The gasifier, operating at 28 bar pressure and 2700°F is designed to produce syngas containing 42% nitrogen, 25% carbon monoxide, and 12% hydrogen, with a combustion value of 4.3 MJ/kg.

The environmental constraints are defined by permit requirements fixing upper limits of SO_2 at 0.22 g/kWhr, NO_x at 0.62g/kWhr, and particulates at 0.007 g/kWhr.

Key steps for limiting emissions include

- Removing fly ash with cyclone and candle filters after gas cooling;
- Removing halogens and other soluble pollutants with water scrubbing;
- Desulfurizing gas by catalytic and chemical processes. Sulfur is fixed in sulfinol-M solvent, which is further treated to produce elemental sulfur; and
- Desulfurized gas is mixed with nitrogen from the air separation units and saturated with water vapor to reduce its lower heating value from about 11,000 to 4300 kJ/kg greatly reducing NO_x production.

Combustion Turbine Plants

CT-based plants are the fastest growing technology in power generation. Through the turn of the century natural gas-fired CTs and CCs burning gas will account for 50 to 70% of the 900 to 1000 GW of new generation to be ordered worldwide. Almost all of these CT and CC plants will be gas fired, leading to a major expansion of gas for electricity generation (Armor et al., 1992).

It is likely that CTs and CCs will grow steadily more important in all generation regimes, peaking, midrange, and base load. If the present 2300°F firing temperature machines operate reliably and durably, CT and CC plants will begin to replace older steam plants and uneconomic nuclear plants. So until the emergence of large-scale fuel cells, CT plants will be a competitive choice for new fossil generation, and advanced CT cycles, with intercooling, reheat, possibly chemical recuperation, and most likely with humidification, will spearhead the drive to higher efficiencies and lower capital costs. Gasification, which guarantees a secure bridge to coal in the near term, will come into its own if natural gas prices rise under demand pressure, and by 2015 coal through gasification may be the economic fuel for a significant fraction of new base-load generation. The rate at which these trends develop depends in large measure on the speed of deregulation and advent of competition in the electricity industry.

Modern gas turbines for power generation are mostly heavy-frame machines, with ratings in a simple cycle configuration around 150 to 170 MW for the high firing temperatures (~2300°F) of the **"F-class" machines**. Efficiencies (LHV) are 36 to 38% in simple cycles. In CCs, the units are 220 to 350 MW in size and 53 to 55% efficient. The next generation of CTs, with efficiencies from 57 to 60% has recently been announced (Table 8.6.3). Smaller-scale aeroderivative machines have benefited from turbofan engines designed for wide-body aircraft and today are available in ratings of 35 to 65 MW and with efficiencies of 40% or more for turbine inlet temperatures around 2250°F. Beyond this, work is underway to design and build an advanced **aeroderivative turbine**, and three teams are involved: United Technologies/Fluor Daniel is looking at a humid air turbine at 200 MW and 55% efficiency; Rolls-Royce/Bechtel is studying an intercooled, regenerative design based on the Aero-Trent machine; and General Electric/Bechtel is melding the GE LM 6000 and the GE heavy-frame designs to achieve close to 60% efficiency in a 100-MW combined cycle.

TABLE 8.6.3 Modern Gas Turbine Specifications

		Large Heavy-Frame Machines			
		Simple Cycle		Combined Cycle	
Turbine		MW	Efficiency % (LHV)	MW	Efficiency % (LHV)
		Current			
GE	GE7FA/9FA	168/227	36.0	253/351	55.0
W/MHI	*W*501F/701F	164/237	38.1	236/337	53.7
Siemens	V84.3/94.3	154/222	36.2	227/328	54.5
		New			
ABB	GT24/26	165/240	37.6	250/365	57.2
Siemens	V84.3A/94.3A	170/240	38.0	254/359	57.0
W/MHI	*W*501G/701G	230/255	38.5	345/380	58.0
GE	GE7G/9G	240/282	39.5	350/420	58.0
GE	GE7H/9H	—	—	400/480	60.0

Recently, General Electric announced a new concept which uses steam from the steam turbine to cool the gas turbine blades permitting a firing temperature of 2600°F. This avoids the losses due to the normal method of diverting compressor air for cooling. This "H" class turbine, it is said, will break the 60% barrier for a 400-MW CC. Comparison of the F- and H-class machines for General Electric is shown in Table 8.6.4.

TABLE 8.6.4 Comparison of F- and H-Class Machines

	General Electric Advanced Machines			
	7FA	**7H**	**9FA**	**9H**
Characteristics				
Firing temperature °F(°C)	2350 (1300)	2600/1430	2350 (1300)	2600 (1430)
Air flow, lb/sec (kg/sec)	974 (442)	1230/558	1327 (602)	1510 (685)
Pressure ratio	15	23	15	23
Specific work, MW/lb/sec (MW/kg/sec)	0.26 (0.57)	0.33 (0.72)	0.26 (58)	0.32 (70)
Performance				
Simple cycle output, MW	168	—	227	—
Simple cycle efficiency, %	36	—	36	—
CC net output, MW	253	400	349	480
CC net efficiency, %	55	60	55	60
NOX (ppmvd at 15% O_2)	9	9	25	25

Source: GE Power Systems, *Power System for the 21st Century: H Gas Turbine Combined Cycle*, 1995. With permission.

Humidified Air Power Plants (Cohn, 1994)

A new class of CTs has been designed based on humidifying the combustion air. In these combustion turbine cycles the compressor exit air is highly humidified prior to combustion. This reduces the mass of dry air needed and the energy required to compress it, raising plant efficiency.

The continuous plant cycle for this concept is termed the **humid air turbine** (HAT). This cycle has been calculated to have a heat rate for natural gas about 5% better than current high-technology CCs. The HAT cycle is adaptable to coal gasification leading to the low emissions and high-efficiency characteristics of gasification CC plants but at a low capital cost since the steam turbine bottoming cycle is eliminated. A simple humidified air turbine cycle is shown in Figure 8.6.13. The addition of moisture means that perhaps 25% more mass flow goes through the turbine, than through the compressor. This suggests the use of separate spools for the turbine and compressor. By using present-day 2350°F firing temperatures it is reasonable to expect a HAT heat rate of about 6100 Btu/kWhr from this cycle.

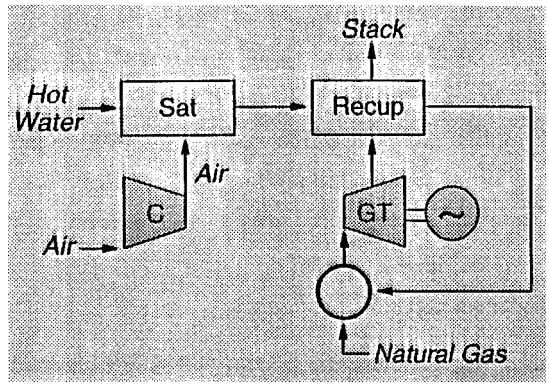

FIGURE 8.6.13 The HAT cycle adds moisture to the compressor exit air, reducing the air mass flow needed and increasing cycle efficiency.

As noted above, the ideal natural gas-fired HAT plant has been calculated to have higher efficiency (about 2 points higher) than a CC for the same turbine cooling technology. Thus, it would provide the lowest heat rate for a natural gas-fired thermal plant and would be utilized in base-load or long intermediate dispatch. The capital cost of this power plant has been calculated to be only slightly higher

than that of a CC. However, the anticipated development cost for the ideal turbomachinery has been estimated to be very high, in excess of $250 million.

In contrast, the CHAT (cascaded humid air turbine) plant utilizes turbine components, which are now available, with few exceptions, in a cascade arrangement that allows them to match together. The development cost of the CHAT equipment is currently estimated to be only in the $5 to 10 million range, making its development much more practical.

The HAT and CHAT cycles can be integrated with gasification. Because these cycles directly incorporate humidification, they can make direct use of hot water generated in the gasification plant, but cannot readily utilize steam. Thus, they match well with the lower-capital-cost, but lower-efficiency, quench types of gasifier. This provides an overall power plant with efficiency about the same as an IGCC. Moreover, the capital cost of the IGHAT plant has been calculated to be about $150/kW less than an IGCC plant. These humidification cycles have yet to be offered commercially. The main obstacle is the need to demonstrate experimentally low-emission, high-efficiency, full-scale combustors utilizing very humid air.

Other Combustion Turbine Cycle Enhancements

There are several variants of the CT-based Brayton cycle which increase plant efficiency and capacity (Lukas, 1986). **Regenerative cycles** use storage-type heat exchangers, where porous or honeycomb wall structures store energy from the hot gases. This is released later to the cold gases. A **recuperative cycle** uses a heat exchanger where the hot and cold streams are separated by walls through which heat transfer occurs. This is the approach commonly used in CTs allowing gains in efficiency and reduced fuel consumption, but no specific output increase.

Intercooling between compressor stages increases useful output by about 30% for a given air mass flow, by reducing the volume flow and increasing available energy to the power turbine. It has minimal effect on efficiency, since heat removed must be added back in the combustion chamber, but is commonly used in conjunction with recuperation.

In a reheat cycle the fuel is introduced at two locations, increasing the total energy available to produce work. A combination of intercooling, reheat, and recuperation is shown in Figure 8.6.14.

Steam injection, where the steam is injected directly into the combustion chamber, increases the mass flow through the turbine and results in increased output power. Steam-injected gas turbine (SIGT) cycles have been compared from the viewpoints of efficiency, power generation, capital and operating costs, and environmental impacts with CC systems (Esposito, 1989). Above 50-MW size, it was found that CC plants were more economical and achieved significantly better heat rates, although cooling tower fog, visible plumes, and drift deposition favored SIGT plants for a flat site.

Capital and Operating Costs of Power Plants

Table 8.6.5 lists typical costs for constructing and operating fossil fuel plants as of 1993. These costs are variable depending on plant design and location; the table assumes a plant in the Northeast United States burning Pittsburgh bituminous coal. Fuel costs, not listed explicitly, will be affected by the plant efficiency, listed in the table.

Costs will vary according to type of coal burned, the size of the unit, the plant location in the United States, and the extent of environmental control employed. In this table, Pittsburgh bituminous coal is assumed, which has 7% ash, 2% sulfur, 5% moisture, and a higher heating value of 13,395 Btu/lb. Wet scrubbers for PC plants use limestone-forced oxidation. Fixed O&M costs include labor, maintenance, and overhead. Variable O&M costs are largely consumables: water, chemicals, other materials.

Summary

The preceding section has described how the future for electric power generation will increasingly be dominated by environmental control needs, putting an emphasis on the base efficiency of new generation and on heat rate recovery for existing units. The PC-fired power plant with FGD will remain a focus of

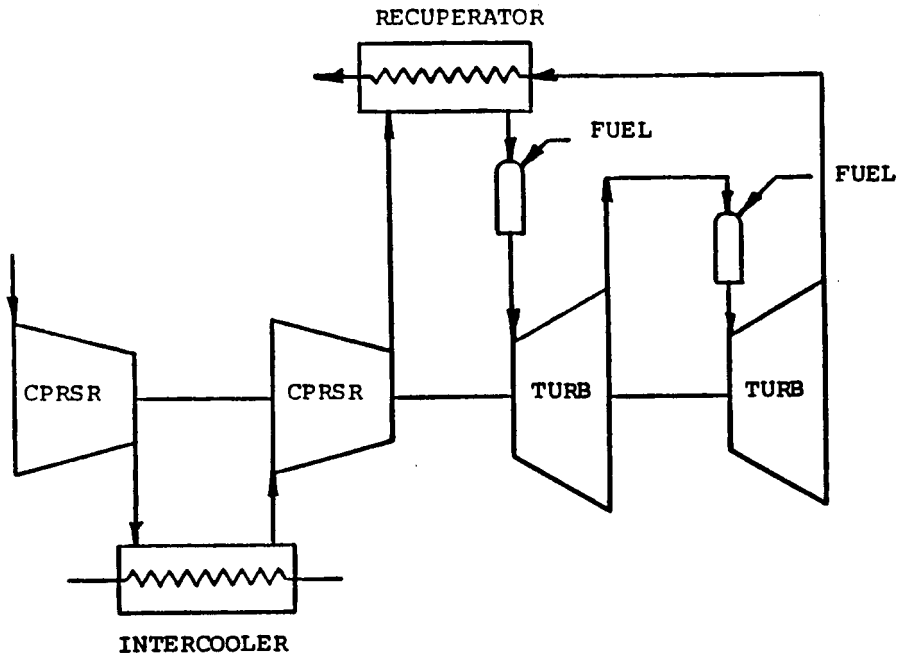

FIGURE 8.6.14 Improvement in CT performance is illustrated in this schematic, which combines an intercooler for the compressor, with a recuperator using CT exhaust heat, and a reheat cycle for the turbine to improve efficiency.

TABLE 8.6.5 Cost Projections for Representative Generation Technologies for a Plant in the Northeast U.S.

	PC Plants			
Plants	**Subcritical Wet Scrubber, 300 MW**	**Supercritical Wet Scrubber, 400 MW**	**AFBC Circulating Bed, 200 MW**	**PFBC CC, 340 MW**
Capital cost (1993),[a] $/kW	1607	1600	1805	1318
Nonfuel O&M costs				
Variable, MILLS/kWhr	3.0	2.8	5.4	1.8
Fixed, $/kW·year	46.6	43.1	37.0	37.6
Efficiency, % (HHV)	36	39	35	41

	Coal Gasification CC, 500 MW	**Coal Gasification Humid Air Turbine, 500 MW**	**Coal Gasification Molten Carbonate Fuel Cell, 400 MW**	**Gas-Fired CC, 225 MW**
Capital cost (1993),[a] $/kW	1648	1447	2082	595
Nonfuel O&M costs				
Variable, MILLS/kWhr	0.5	1.3	1.1	0.4
Fixed, $/kW·year	49.9	40.4	57.2	26.5
Efficiency, % (HHV)	42	42	50	46

[a] Costs of new plants are likely to reduce, in real terms, over the next 10 years due to technology developments and increased worldwide competition for markets in the developing countries. New technologies (PFBC, IGCC, fuel cells) will lower capital costs as production capacity grows.

Source: Technical Assessment Guide, EPRI TR-102275-V1R7, Electrical Power Research Institute, Palo Alto, CA, June, 1993. With permission.

most near-term activity related to upgrades and retrofits. But new technology, based on coal gasification, is under development and being tested in a growing number of demonstration plants which promise extremely low emissions.

The future for many nations will be based on exploiting the opportunities offered by clean and efficient use of coal. This implies access to the range of new technologies now being tested at large scale in the United States and other developed nations. This strategy is both timely and prudent on a global basis, as the world increasingly voices concerns related to carbon combustion.

Base-load, central generation plants will largely be focused in the immediate future on the rapidly developing areas of the world — Asia (particularly China and India) and Latin America. In these areas the fuel of choice will likely be coal, particularly in Asia, and the generating unit most often will be a conventional PC unit, but also could be an atmospheric or pressurized fluidized bed unit. In North America, Europe, and Japan, gas-fired central plants using CTs, often in a CC, will dominate through the next decade. As the cost of natural gas, relative to coal, increases, this will then encourage the installation of gasification units enabling the enormous world coal reserves to be utilized. Then, sometime after the turn of the century, smaller distributed generating sources will begin to emerge, based on gas-fired fuel cells, small CTs, or possibly photovoltaics. As the economics for the distributed option become favorable, these smaller generating units could encourage broad electrification of the developing countries of the world.

Defining Terms

Aeroderivative turbine: In the 1960s gas turbines derived from military jet engines formed a source of utility peaking capacity. Now, modern airline fan-jets are being converted to utility service. These lighter CTs are highly efficient and can have low NO_x emissions, high pressure ratios, and low capital cost.

Ash-softening temperature: The tendency for fly ash to adhere to tube banks is increased as the ash softens and melts. The point at which the ash begins to soften is dependent on the type of coal and is difficult to predict, depending on the many coal constituents. Slagging and fouling of tubes can lead to severe tube corrosion.

Coal gasification: Coal can be converted into a mixture of carbon monoxide and hydrogen by burning it with a controlled deficiency of oxygen. Use of pure oxygen produces a medium-calorific-value gas, and air a low calorific value gas. This "syngas" can then be used to power a CT.

Coextruded tubing: Tubing for superheaters and reheaters must be strong enough to withstand the pressures and temperatures expected, and also corrosion resistant to depositions of fly ash. By making tubing with a strong inner layer and corrosion-resistant outer layer through an extrusion process, both concerns can be dealt with.

Cogeneration: Cogeneration refers to the production of multiple products from a power plant. Typically, process steam, or hot water for heating, is produced in addition to electricity. This approach leads to high plant utilization, the "effective" heat rate being 70% or more.

Combined cycle: Power stations which employ both CTs (Brayton cycle) and condensing steam turbines (Rankine cycle) where the waste heat from the CTs generates steam for the steam turbines, are called *combined* cycle plants. Overall plant efficiency improves.

Electrostatic precipitators: Flue gas particles, when electrically charged in an ionized gas flow, collect on electrodes in the presence of a strong electrostatic field. Collected dust is discharged by rapping into hoppers. A collection efficiency above 99% is possible.

Double reheat: Modern designs of fossil steam-generating units remove a portion of the steam before full expansion through the turbine and reheat it in the boiler before returning it to the turbine. This enhances the thermal efficiency of the cycle by up to 5%. For supercritical cycles two stages of reheat can be justified — double reheat.

F-class machines: Recent designs of CTs have increased efficiencies resulting from increased firing temperatures. The first generation of these machines has firing temperatures of about 2300°F. They have been termed F-class machines (for example the GE 7F). Even higher temperatures have now been incorporated into "G-class" turbines.

Flue gas desulfurization: Removal of sulfur dioxide, SO_2, from combustion gases is accomplished in a number of FGD methods. Most of these involve wet "scrubbing" of the gas using lime or limestone and result in a calcium sulfate waste product. A 95% removal efficiency, or higher, is possible.

Fluidized bed: A process of burning solid fuels, particularly coal, by suspending the fuel within a column of air supplied from below the furnace. This method permits effective combustion of poor-quality fuels, lowers NO_x emissions due to low combustion temperatures, and captures sulfur in the bed by mixing limestone or dolomite in with the fuel.

Fuel cell: Fuel cells convert gaseous or liquid fuels directly to electricity without any combustion process. Like a continuous battery, the fuel cell has electrodes in an electrolyte medium. Typically, hydrogen and air are supplied and DC electricity, water, and carbon dioxide are produced. They are currently high-cost, low-size devices, but with minimum environmental emissions.

Hot-gas cleanup: Cycles which use gas from the combustion of coal, typically pressurized fluidized bed or gasification cycles, need to clean up the ash particles before passing them through a gas turbine. This prevents severe erosion of the turbine blades and other components. Hot-gas cleanup can involve the application of hanging particulate traps, using ceramic filters.

Humid air turbine: A new type of CT uses humidified compressor exit air for the combustor. The mass of dry air needed is thus lessened for a given mass flow, and turbine efficiency increases. Several applications of this HAT appear attractive in gasification and compressed air storage cycles.

Intercooling: Increased output from a CT can be obtained by cooling the air between compressor stages. This reduces volume flow and increases energy to the power turbine.

Lower heating value: Fuels containing hydrogen produce water vapor as a product of combustion. The fuel heating value is said to be "lower" if the combustion process leaves all products in the gaseous state, but "higher" if the fuel heating value includes the latent heat of vaporization. Practice in the United States is to use the higher value.

On/off cycling capability: Generating units are often not required on a 24-hr basis. Some are shut down during low-demand times and started up perhaps hours later. This form of on/off cycling imposes thermal stresses on the equipment, leading to premature equipment failure unless special measures are taken to deal with this.

Petroleum coke: Petroleum coke is a residual product of the oil-refining process, and in its fuel-grade form is an almost pure carbon by-product. About 19 million tons of fuel-grade pet coke is produced each year in the United States. It is inexpensive although it may have high sulfur and vanadium content.

Recuperative cycle: Recuperative cycles for CTs use walls between the hot and cold streams through which heat is transferred. This improves efficiency and reduces fuel consumption.

Regenerative cycles: Combustion turbine cycles using heat exchangers to store and transfer heat from the hot gases to the cold gases are termed regenerative cycles.

Slagging and fouling: The mineral matter in coal can attach itself following combustion to the boiler walls and heat-exchanger surfaces. Oxides of silicon, aluminum, iron, calcium, and magnesium can foul all boiler surfaces, requiring soot blowers for cleaning. Hot ash can melt, becoming sticky and sometimes coalescing in the furnace to cause slagging problems.

Spray drying: Spray driers, for desulfurization, used typically when burning lower-sulfur coals, use a spray of quicklime which is dried by the hot flue gas and results in a dry solid product. A 90% removal efficiency is typical.

Steam injection: Injecting stream directly into the combustion chamber of a CT increases turbine mass flow and thus increases the output power.

Temper embrittlement: Tempering of steel in the manufacturing process removes some of the brittleness and is carried out by a heating and cooling process. During operation, though, it is possible that ductility can worsen close to specific tempering temperatures. The material is then said to be temper embrittled, and premature cracking may follow.

References

Armor, A.F., Generation technologies through the year 2005, in *The Electric Industry in Transition*, Public Utilities Reports, Inc., December 1994.

Armor, A.F. et al., Improved materials for life extension of coal-fired power plants, in *Proceedings, International Conference on Life Extension and Assessment*, Nederlands Instituut Voor Lastechniek, The Hague, Holland, June 13–15, 1988.

Armor, A.F., Touchton, G.L., and Cohn, A., Powering the future: advanced combustion turbines and EPRI's program, paper presented at EPRI Coal Gasification Conference, San Francisco, October 1992.

Blunden, W.E., Colorado-UTE's Nucla Circulating AFBC Demonstration Project, EPRI Report CS-5831, February 1989.

Carpenter, L.K. and Dellefield, R.J., The U.S. Department of Energy PFBC perspective, paper presented at EPRI Fluidized Bed Combustion for Power Generation Conference, Atlanta, Georgia, May 17–19, 1994.

Cohn, A., Humidified power plant options, in *AFPS Developments*, Electric Power Research Institute, Spring 1994.

Couch, G., Advanced coal cleaning technology, IEACR/44, London, IEA Coal Research, December 1991.

Douglas, J., IGCC: Phased construction for flexible growth," *EPRI Journal,* September 1986.

Esposito, N.T., A Comparison of Steam-lnjected Gas Turbine and Combined Cycle Power Plants, EPRI Report GS-6415, June 1989.

Hinrichsen, D., AFBC Conversion at Northern States Power Company, EPRI Report CS-5501, April, 1989.

Lucas, H., Survey of Alternative Gas Turbine and Cycle Designs, EPRI Report AP-4450, February 1986.

Manaker, A.M., TVA 160-MWe Atmospheric Fluidized-Bed Combustion Demonstration Project, EPRI Report TR-100544, December 1992.

Melvin, R.H. and Friedman, M.A., Successful Coal-Fired AFBC Cogeneration in California: 108 MW ACE Cogeneration Facility, paper presented at EPRI Fluidized Bed Combustion Conference, Atlanta, May 17–19, 1994.

Olesen, C., Pressurized fluidized bed combustion for power generation, in EPRI CS-4028, *Proceedings: Pressurized Fluidized-Bed Combustion Power Plants,* May 1985.

Oliker, I. and Armor, A.F., *Supercritical Power Plants in the U.S.S.R.,* EPRI Report TR-100364, February 1992.

Poe, G.G. et al., EPRI's state-of-the-art power plant, in *Proceedings, Third International Conference on Improved Coal-Fired Power Plants,* San Francisco, April 2–4, 1991.

Skowyra, et al., Design of a supercritical sliding pressure circulating fluidized bed boiler with vertical waterwalls, in *Proceedings of 13th International Conference on Fluidized Bed Combustion,* ASME, New York, 1995.

Torrens, I.M., Developing clean coal technologies, *Environment*, 32(6):11–33, July/August 1990.

U.S. Department of Energy, Clean Coal Technology Demonstration Program, DOE/FE-0299P, March 1994.

Further Information

Steam, Its Generation and Use, Babcock and Wilcox, New York.

Combustion: Fossil Power Systems, Combustion Engineering, Inc., Windsor, CT.

Tapping global expertise in coal technology, *EPRI J.*, Jan/Feb., 1986.

IGCC: new fuels, new players, *EPRI J.*, July/Aug., 1994.

A brighter future for PFBC, *EPRI J.*, Dec. 1993.

Fuel cells for urban power, *EPRI J.*, Sept. 1991.

Distributed generation, *EPRI J.*, April/May, 1993.

8.7 Energy Storage

Chand K. Jotshi and D. Yogi Goswami

Introduction

Energy storage is very important for utility load leveling, electrical vehicles, solar energy systems, uninterrupted power supply, and energy systems at remote locations. Two important parameters for energy storage are duration of storage and **specific energy** or **energy density**. Duration of energy storage may vary from many years to a fraction of a second. In a nuclear power plant, nuclear fuel is stored within a reactor for a year. Coal piles, gas and oil storage tanks, or pumped hydro are kept by power utilities for several days use, depending upon the need. Similarly for a solar energy system, requirement of energy storage may be on an hourly, daily, or weekly basis. Specific energy or energy density is a critical factor for the size of a storage system.

Energy can be stored as mechanical, thermal, chemical, electrical, or magnetic energy. In this section, storage of thermal, mechanical, and electrical energy are described.

Thermal Energy Storage (TES)

Thermal energy can be stored as sensible heat, latent heat, or as the heat of chemical reaction (thermochemical).

Sensible heat, Q, is stored in a material of mass m and specific heat C_p by raising the temperature of the storage material and is expressed by Equation (8.7.1):

$$Q = mc_p\Delta T \tag{8.7.1}$$

Most common sensible heat storage materials are water, organic oils, rocks, ceramics, and molten salts. Some of these materials along with their physical properties are listed in Table 8.7.1. Water has the highest specific heat value of 4190 J/kg · C.

TABLE 8.7.1 Physical Properties of Some Sensible Heat Storage Materials

Storage Medium	Temperature Range, °C	Density (ρ), kg/m³	Specific Heat (C), J/kg K	Energy Density(ρC) kWhr/m³ K	Thermal Conductivity (W/m K)
Water	0–100	1000	4190	1.16	0.63 at 38°C
Water (10 bar)	0–180	881	4190	1.03	—
50-ethylene glycol–50 water	0–100	1075	3480	0.98	—
Dowtherm A® (Dow Chemical, Co.)	12–260	867	2200	0.53	0.112 at 260°C
Therminol 66® (Monsanto Co.)	–9–343	750	2100	0.44	0.106 at 343°C
Draw salt ($50NaNO_3$-$50KNO_3$)[a]	220–540	1733	1550	0.75	0.57
Molten Salt ($53KNO_3/40NaNO_2/7NaNO_3$)[a]	142–540	1680	1560	0.72	0.61
Liquid sodium	100–760	750	1260	0.26	67.5
Cast iron	m.p. (1150–1300)	7200	540	1.08	42.0
Taconite	—	3200	800	0.71	—
Aluminum	m.p. 660	2700	920	0.69	200
Fireclay	—	2100–2600	1000	0.65	1.0–1.5

[a] Composition in percent by weight.
Note: m.p. = melting point.

Thermal energy, Q, can be stored as latent heat in a material of mass, *m*, that undergoes phase transformation as given by Equation (8.7.2):

$$Q = m\lambda \tag{8.7.2}$$

where λ = heat of phase transformation.

Four types of phase transformations useful for latent heat storage are: solid $\rightleftarrows$ liquid, liquid $\rightleftarrows$ vapor, solid $\rightleftarrows$ vapor, and solid $\rightleftarrows$ solid. Since phase transformation is an isothermal process, thermal energy is stored and retrieved at a fixed temperature known as the transition temperature. Some common phase change materials (PCMs) used for thermal storage are paraffin waxes, nonparaffins, inorganic salts (both anhydrous and hydrated), and eutectics of organic and/or inorganic compounds. Table 8.7.2 lists some PCMs with their physical properties.

TABLE 8.7.2 Physical Properties of Latent Heat Storage Materials or PCMs

Storage Medium	Melting Point °C	Latent Heat, kJ/kg	Specific Heat (kJ/kg °C)		Density (kg/m³)		Energy Density (kWhr/m³ K)	Thermal Conductivity (W/m K)
			Solid	Liquid	Solid	Liquid		
$LiClO_3 \cdot 3H_2O$	8.1	253	—	—	1720	1530	108	—
$Na_2SO_4 \cdot 10H_2O$	32.4	251	1.76	3.32	1460	1330	92.7	2.25
$Na_2S_2O_3 \cdot 5H_2O$	48	200	1.47	2.39	1730	1665	92.5	0.57
$NaCH_3COO \cdot 3H_2O$	58	180	1.90	2.50	1450	1280	64	0.5
$Ba(OH)_2 \cdot 8H_2O$	78	301	0.67	1.26	2070	1937	162	0.653ℓ
$Mg(NO_3) \cdot 6H_2O$	90	163	1.56	3.68	1636	1550	70	0.611
$LiNO_3$	252	530	2.02	2.041	2310	1776	261	1.35
$LiCO_3/K_2CO_3$, (35:65)[a]	505	345	1.34	1.76	2265	1960	188	—
$LiCO_3/K_2CO_3/Na_2CO_3$ (32:35:33)[a]	397	277	1.68	1 63	2300	2140	165	—
n-Tetradecane	5.5	228	—	—	825	771	48	0.150
n-Octadecane	28	244	2.16	—	814	774	52.5	0.150
HDPE (cross-linked)	126	180	2.88	2.51	960	900	45	0.361
Steric acid	70	203	—	2.35	941	847	48	0.172ℓ

[a] Composition in percent by weight.

Note: ℓ = liquid.

Thermochemical energy can be stored as heat of reaction in reversible chemical reactions. In this mode of storage, the reaction in the forward direction is endothermic (storage of heat), while the reverse reaction is exothermic (release of heat). For example,

$$A + \Delta H \rightleftarrows B + C \tag{8.7.3}$$

The amount of heat *Q* stored in a chemical reaction depends on the heat of reaction and the extent of conversion as given by Equation (8.7.4):

$$Q = a_r m \Delta H \tag{8.7.4}$$

where a_r = fraction reacted, ΔH = heat of reaction per unit mass, and *m* = mass.

Chemical reaction is generally a highly energetic process. Therefore, a large amount of heat can be stored in a small quantity of a material. Another advantage of thermochemical storage is that the products of reaction can be stored at room temperature and need not be insulated. For sensible and latent heat storage materials, insulation is very important. Examples of reactions include decomposition of metal hydrides, oxides, peroxides, ammoniated salts, carbonates, sulfur trioxide, etc. Some useful chemical reactions are reported in Table 8.7.3.

TABLE 8.7.3 Properties of thermochemical storage media

Reaction	Condition of Reaction: Pressure, kPa	Condition of Reaction: Temperature, °C	Component (Phase)	Pressure, kPa	Temperature, °C	Density, kg/m³	Volumetric Storage Density, kWhr/m³
$MgCO_3$ (s) + 1200 kJ/kg =	100	427–327	$MgCO_3$(s)	100	20	1500	
MgO (s) + CO_2(g)			$CO_2(\ell)$	7400	31	465	
							187
$Ca(OH)_2$(s) + 1415 kJ/kg =	100	572–402	$Ca(OH)_2$(s)	100	20	1115	
CaO(s) + H_2O(g)			$H_2O(\ell)$	100	20	1000	345
SO_3(g) + 1235 kJ/kg =	100	520–960	$SO_3(\ell)$	100	45	1900	
SO_2(g) + $^1/_2O_2$(g)			$SO_2(\ell)$	630	40	1320	
			O_2(g)	10000	20	130	280

Note: s = solid, ℓ = liquid, g =gas.

Applications and Examples

Cool Storage has major applications in space cooling of buildings, food and medicine preservation, and transportation of items that need to be stored at low temperatures. A major application of cool storage is in the use of off-peak electricity for air-conditioning during peak hours. During off-peak hours electricity can be used to make ice or chilled water, which can be used later for air-conditioning of buildings during the peak hours. The advantage of using ice as a storage medium over chilled water is that a much larger amount of coolness can be stored in ice; 1 kg of ice stores 335 kJ, whereas 1 kg of water stores only 42 kJ for a temperature swing of 10°C. The disadvantage of ice is its lower thermal conductivity, which is responsible for lower heat-transfer rates.

Cool storage systems have been used in several buildings in the United States and Canada. The Merchandise Mart of Chicago boasts the largest ice storage system in the world: each day more than 2 million lb of ice are made and melted. For long-term cool storage, aquifers have been used for chilled water storage. Examples include cooling of buildings at the University of Alabama and the United States Postal Service in Long Island, NY, using chilled water stored in aquifers (Tomlinson and Kannberg, 1990). Other materials which have been found to have cool storage potential are PCMs like $LiClO_3 \cdot 3H_2O$, a eutectic of Glauber's salt, paraffins and their mixtures, and some gas hydrates or clatherates.

Heat Storage has major applications in space heating, crop drying, cooking, electric power generation, industrial process heat (air and steam), waste heat utilization, and solar energy utilization, etc. Heat storage in water is the most economical and well-developed technology. Epoxy-lined steel, fiberglass-reinforced polymer, concrete with plastic liner, and wood tanks are suitable containment materials for systems using water as the storage material. The storage tanks may be located above or below ground. In North America and China, aquifers have been used for long-term storage of hot water and chilled water. Pressurized water tanks are used to store heat from off-peak electricity (ASHRAE, 1995). For example, water is heated to maximum temperatures of about 138°C in a tank at a pressure of 50 psig.

Molten nitrate salt (50 wt% $NaNO_3$/50 wt% KNO_3) also known as Draw salt, which has a melting point of 222°C, has been used as a storage and a heat-transfer fluid in an experiment in Albuquerque, NM. It was the first commercial demonstration of generating power from storage (Delameter and Bergen, 1986). Solar Two, a 10-MW solar thermal power demonstration project in Barstow, CA, is also designed to use this molten salt to store solar energy (Chavez et al., 1995). Another molten nitrate salt is 40 wt% $NaNO_2$/7 wt% $NaNO_3$/53 wt% KNO_3, known as HTS (heat-transfer salt) with a melting point of 142°C. This salt has been widely used in the chemical industry.

For applications in heating and cooling of buildings the containment of PCM can become an integral part of the building. It may be part of the ceiling, wall, or floor of the building and may serve a structural or a nonstructural function. Tubes, trays, rods, panels, balls, canisters, and tiles containing PCMs have been studied in the 1970s and 1980s for space-heating applications (Moses and Lane, 1983). The PCMs used were mostly salt hydrates such as Glauber's salt ($Na_2SO_4 \cdot 10H_2O$), Hypo ($Na_2S_2O_3 \cdot 5H_2O$),

$NaCH_3COO \cdot 3H_2O$, $Na_2HPO_4 \cdot 12H_2O$, $Ba(OH)_2 \cdot 8H_2O$, $MgCl_2 \cdot 6H_2O$, and $Mg(NO_3)_2 \cdot 6H_2O$. Paraffin mixtures have been used for thermal storage in wall boards. Some PCMs, such as salt hydrates, exhibit supercooling and phase segregation problems during heat removal. Low thermal conductivity and complex mechanism of heat transfer during melting and freezing introduce complexities in the design of their containment systems.

Mechanical Energy Storage

Mechanical energy may be stored as potential or kinetic energy.

Kinetic Energy

Kinetic energy can be stored in the rotating mass of a wheel, commonly known as a flywheel. Kinetic energy of a rotating body is given by Equation (8.7.5):

$$KE = \frac{1}{2} I\omega^2 \tag{8.7.5}$$

where I = moment of inertia, and ω = angular velocity.

The maximum specific energy of a flywheel is expressed by the following equation (Jenser, 1980):

$$\frac{KE_{max}}{m} = A\frac{\rho_{max}}{\rho} \tag{8.7.6}$$

where A = shape factor, and its value depends on the geometry of flywheel; $A = 1.0$ for a constant stress disk and 0.5 for a thin-rimmed flywheel. This equation shows that high tensile strength and low density are the key parameters to store maximum energy. Tensile strength, density, and specific energy of some materials are given in Table 8.7.4.

TABLE 8.7.4 Flywheel Rotor Materials

Material	Design Stress, MN/m²	Density, kg/m³	Specific Energy, Whr/kg
Composite fiber[a]/epoxy	750	1550	51.5
E-glass fiber[a]/epoxy	250	1990	14.0
S-glass fiber[a]/epoxy	350	1900	19.6
Kevlar fiber[a]/epoxy	1000	1400	76.2
Maraging steel	900	8000	24.2
Titanium alloy	650	4500	30.8

[a] 60% fiber.

Storing energy in a flywheel is one of the oldest techniques used in ancient potteries. Present-day flywheels are much more advanced as a result of superstrong/ultralight composite materials and frictionless high-performance magnetic bearings.

Potential Energy

If a body of mass m is elevated against the gravitational force g to a height Δh, the potential energy stored is given by

$$PE = mg\Delta h \tag{8.7.7}$$

From Equation (8.7.7), 1 Wh of energy can be stored in 1 kg mass of a body by raising it to a height of 367 m.

Potential energy is also stored in a spring, either by compressing or expanding. Here, energy stored is given by

$$\text{PE} = (1/2)kx^2 \tag{8.7.8}$$

where k = spring constant and x is the distance to which the spring is compressed or expanded. Springs have been widely used to power toys and watches mainly because of very low values of energy density.

Pumped Hydro

Water may be pumped from a lower reservoir to a higher reservoir using electricity during off-peak hours, which may be used to generate electricity using hydraulic turbines during peak hours. Figure 8.7.1a shows a schematic diagram of an above-ground pumped hydro system. Advantages of pumped hydro units include simple operation, high reliability, low maintenance, long life, quick start from standstill, and economic generation of peaking electrical energy. In the United States a large number of such systems are in operation. Power-generating capacities of these systems vary between 5 and 2000 MW (Makansi, 1994). The overall efficiencies of these power plants vary between 65 and 90%, which includes the efficiencies of pumps, hydraulic turbines, generators, and losses from the upper reservoir. In spite of the technical and economic viability of pumped hydro, the requirement of a specific type of topography and some environmental concerns limit its application. To overcome these problems, a concept of underground pumped hydro storage as shown in Figure 8.7.1b can be used. In this case, large caverns or aquifers can be used as the lower reservoir.

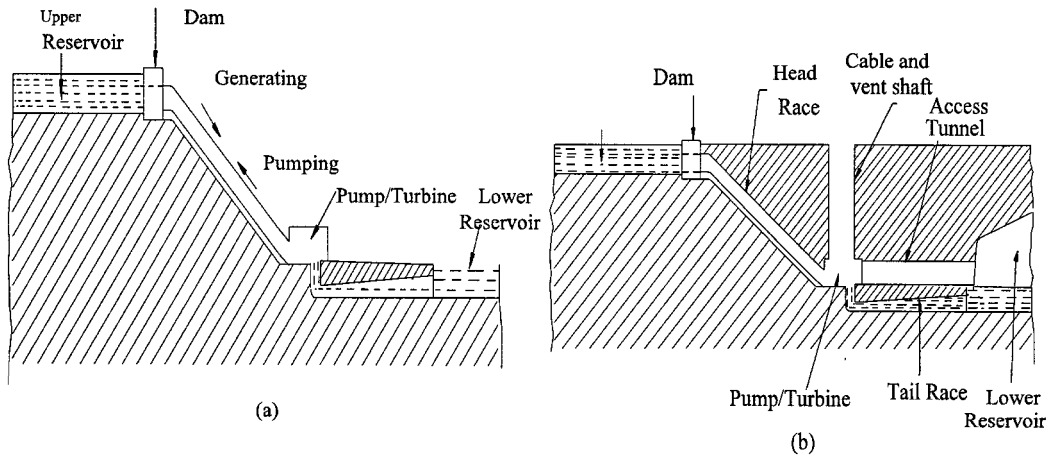

FIGURE 8.7.1 Pumped hydrostorage: (a) above ground; (b) underground.

Compressed Air Storage

In a fossil fuel power plant, approximately half of the output of a conventional gas turbine is used to drive the compressors. If the air is compressed during off-peak hours and stored, it can be used later during peak hours. Compressed air can be stored underground in abandoned mines, oil or gas fields, sealed aquifers, or natural caverns. A compressed air storage plant in Huntorf, Germany that has been in operation since 1978 is the oldest unit. A 110-MW demonstration facility at the Alabama Electric Cooperative (AEC), Inc., McIntosh, Alabama , site has been in operation since 1991. The Hunterof unit is a 4-hr facility and the AEC site is a 26-hr facility (Makansi, 1994).

Electrical Energy Storage

Electrochemical energy storage, more commonly known as battery storage, stores electrical energy as chemical energy. Batteries are classified as primary and secondary batteries. Only secondary batteries are rechargeable and are therefore suitable for energy storage applications. Lead-acid and nickel-cadmium are well-known rechargeable batteries that are most commonly used. Lead-acid batteries have been used for over a century and are still the most popular batteries.

Electrochemical operation of a cell during discharge and charge is shown in Figures 8.7.2a and b. During discharge when a cell is connected to a load, electrons flow from the anode to the cathode. In this operation oxidation, or loss of electrons, takes place at the anode, and reduction, or gain of electrons, occurs at the cathode. The cell chemistry of a lead-acid battery is as follows: the anode is lead (Pb) and the cathode is lead oxide (PbO_2); the electrolyte is H_2SO_4. The cell reaction is

$$2H_2SO_4 \rightarrow 4H^+ + 2SO_4^-$$

$$\text{Anodic reaction:} \quad Pb + SO_4^{2-} = PbSO_4 + 2e^- \tag{8.7.9}$$

$$\text{Cathodic reaction:} \quad PbO_2 + SO_4^{2-} + 4H^+ + 2e^- = PbSO_4 + 2H_2O \tag{8.7.10}$$

Theoretical voltages and capacities of some known batteries are reported in Table 8.7.5.

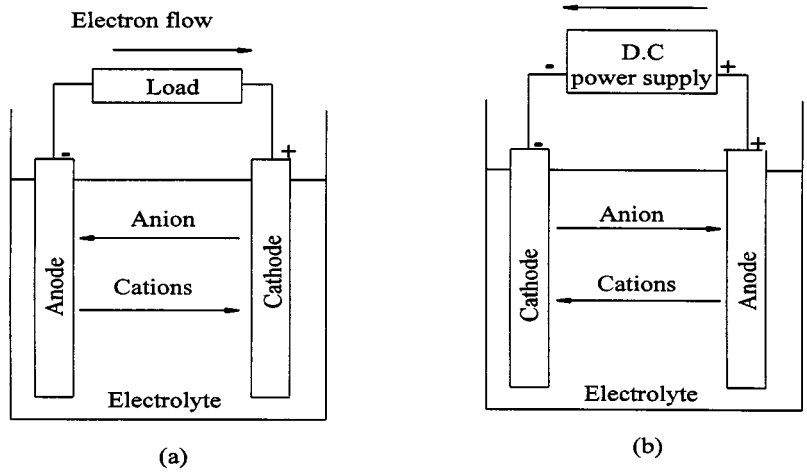

FIGURE 8.7.2 Electrochemical operation of a cell: (a) discharge; (b) charge.

TABLE 8.7.5 Properties of Some Rechargeable Batteries

No.	System	Electrolyte	Temp. °C	O.C.V. (V)	Energy Density (Theoretical), Whr/kg	Energy Density (Achievable), Whr/kg	In/Out Electrical Effciency	Cycle Life
1	Lead-Acid	H_2SO_4	20–30	2.05	171	50	75	1000
2	Nickel-Iron	KOH	20–30	1.37	267	60	55	2000
3	Zinc-Iron	KOH	50–60	1.65	1084	90	45	600
4	Sodium-Sulfur	β-Al_2O_3	300–375	1.76–2.08	664	120	75	2000
5	Lithium-Iron Sulfide	LiCl-KCl (eutectic)	400–450	1.6	869	150	75	1000

Note: O.C.V. = open cell voltage.

Applications

Battery storage is used in a wide range of applications. Currently, the main emphasis of research is on applications in vehicles and load leveling.

Electric Vehicles. For electric vehicles, the specific energy and specific power are two important parameters. The greater the specific energy, the farther a vehicle can travel. If specific power is high, a vehicle can accelerate more quickly and have a higher top speed. Other important requirements are the ability to charge and discharge a large number of times, to retain charge over an extended period of time, and to charge and discharge over a wide range of temperatures. Table 8.7.5 provides information about some rechargeable batteries.

Power Plants. Recent start-up of a commercial unit for the Puerto Rico Electric Power Authority (PREPA) is the latest development in large-scale application of lead-acid batteries. The facility stores 20 MW for 20 min, both for peaking requirement and voltage and frequency control. Maximum discharge is limited to 10 MW (Makanasi, 1994).

Defining Terms

Cool storage: The storage of thermal energy at temperatures below the nominal temperature required by the space or process.

Heat storage: The storage of thermal energy at temperatures above the nominal temperature required by the space or process.

Energy density: Amount of energy stored per unit volume, kJ/m^3 or kWhr/m^3.

Specific energy: Amount of energy stored per unit mass, kJ/kg or kWhr/kg.

References

ASHRAE, 1995. Thermal storage, in *ASHRAE Handbook, HVAC Application*, p. 40.15. American Society of Heating, Refrigerating and Air-Conditioning Engineers, 1791 Tullie Circle, N.E., Atlanta.

Beckman, G. and Gilli, P.V. 1984. *Topics in Energy — Thermal Energy Storage*. Springer-Verlag, New York.

Chavez, J.M. et al. 1995. The Solar Two Power Tower Project: a 10MWe power plant, in *Proceedings of the 1995 IECEC*, Vol. 2, pp. 469–475, ASME, New York.

Delameter, W.R. and Bergen, N.E. 1986. Review of Molten Salt Electric Experiment: Solar Central Receiver Project. SAND 86-8249, Sandia National Laboratory, Albuquerque.

Garg, H.P., Mullick, S.C., and Bhargava, A.K. 1985. *Solar Thermal Energy Storage*. D. Reidel, Boston.

Glendenning, I. 1981. Advanced mechanical energy storage, in *Energy Storage and Transportation,* G. Beghe, Ed., pp. 50–52. D. Reidel, Boston.

Jensen, J. 1980. *Energy Storage*. Newnes-Butterworth, Boston.

Makansi, J. 1994. Energy storage reinforces competitive business practices. *Power.* 138(9):63.

Moses, P.J. and Lane, G.A. 1983. Encapsulation of PCMs, in *Solar Heat Storage: Latent Heat Materials*, Vol. II, pp. 93–152. CRC Press, Boca Raton, FL.

O'Connor, L. 1993. Energizing the batteries for electric cars. *Mech. Eng*. 7:73–75.

Sharma, S.K. and Jotshi, C.K. 1979. Discussion on storage subsystems, in *Proceedings of the First National Workshop on Solar Energy Storage*, pp. 301–308. Panjab University, Chandigarh, India.

Tomlinson, J.J. and Kannberg, L.D. 1990. Thermal energy storage. *Mech. Eng*. 9:68–72.

8.8 Nuclear Power

Roberto Pagano and James S. Tulenko

Nuclear power refers to power generated through reactions involving atomic nuclei (i.e., nuclear reactions). These reactions fall into three broad categories — fusion reactions, fission reactions, and radioisotopes. In fusion, two light nuclei (most commonly isotopes of hydrogen) combine to form a heavier nucleus (usually helium), with energy being released in the process. Nuclear fusion is the source of energy generated in the stars (our sun). In artificial applications, the technology to induce fusion reactions has been available for several decades, but such reactions have been essentially uncontrolled (the hydrogen bomb). Once initiated, fusion reactions generate huge amounts of energy, which is subsequently released explosively. Means to produce and release energy from fusion in a sustained, controlled manner are still being developed. Extensive research is ongoing, both in the United States and abroad, on the development of nuclear fusion as a controlled source of power.

Nuclear fission, in contrast, is the basis of a mature technology applied to the generation of power. Fission is the fragmentation of a heavy nucleus into two, sometimes three, lighter nuclei. Certain nuclides found in nature fission spontaneously, that is, with no external intervention. However, spontaneous fission in naturally occurring nuclides takes place at a very slow rate. Fission can be induced through a nuclear reaction. Of primary interest here is the fissioning of several specific nuclei through interactions with neutrons. Again, the fissioning of a nucleus is accompanied by the release of energy.

At present, the element of primary importance with respect to nuclear fission power is uranium. Naturally occurring uranium consists of three isotopes — ^{238}U, ^{235}U, and ^{234}U. In a mixture of isotopes of an element, the abundance of any one is usually expressed as the number of atoms of that isotope present per 100 atoms of the mixture, abbreviated as atom percent a/o or weight percent w/o. Natural uranium consists of 99.2745 a/o ^{238}U, 0.7200 a/o ^{235}U, and 0.0055 a/o ^{234}U.

Radioisotope power is the third form of nuclear energy. When radioisotopes decay, high-energy electrons (beta particles), helium atoms (alpha particles), and gamma rays (photons) are emitted. When the energy of these radiations is stopped and converted to heat, a power source is created. Radioisotopes decay energies range from 0.01 to 10 MeV. Radioisotopes are generally separated from radioactive wastes produced from nuclear power plants. The most common radioisotopes are polonium-210 (alpha emitter of 5.3 MeV), plutonium-238 (alpha emitter of 5.46 MeV), cesium-144 (beta emitter of 1.25 MeV), and strontium-90 (beta emitter of 1.10 MeV).

The Fission Process

Consider first the fission of a nucleus of ^{235}U caused by an interaction with a neutron. A compound nucleus of ^{236}U is initially formed. If fission occurs, it does so within a very short time. Normally with thermal reaction, 85% of the interaction leads to fission. Alternatively, the compound nucleus dissipates energy by emitting a gamma photon, no fission occurs and the nucleus remains as ^{236}U. This latter process occurs in 20% of the interaction of ^{235}U with a neutron.

The fissioning of a nucleus produces fission fragments called fission products, a number of neutrons and gamma photons. Most frequently, the number of neutrons is 2 or 3, ranging in extreme cases from 0 to 8. In the fissioning of ^{235}U, the average number of neutrons released, designated by υ, has a value of 2.42. This value applies strictly if the fission is induced by a neutron of relatively low kinetic energy, called a thermal neutron.

In a nuclear reactor, which is a special material medium in which ^{235}U is dispersed for the reactor to work, one of the neutrons liberated in the fissioning of a nucleus must go on to induce a fission in another nucleus. This leads to the idea of a self-sustaining chain reaction or, more specifically, a **critical configuration** in which a self-sustaining chain reaction can be maintained indefinitely. To this end, an adequate supply of ^{235}U must be on hand and replenished as needed. Further, the configuration must be

such that the likelihood that any particular neutron ultimately induces a fission is adequately high to ensure that on average one neutron will induce a fission.

The energy liberated in fission results from Einstein's equation $E = Mc^2$, which says that mass and energy are equivalent. A summation of the masses of the fission fragments and the neutrons resulting from fission shows that the combined mass of the products of a fission is less than the mass of the compound nucleus before fission occurs. It is found that the energy released is equal to $E = \Delta Mc^2$ when ΔM is the difference in the masses. This nuclear energy is traditionally expressed in units of electron volts (eV), with the equivalence of 1 eV = 1.602×10^{-19} J. The single fission of a single uranium atom releases approximately 200×10^6 eV, or 200 MeV, of energy. When one realizes that the combusion of a single carbon atom ($C + O_2 \rightarrow CO_2$) releases 4 eV, a quantity 50 million times smaller, one gets a true appreciation of the concentrated power of nuclear energy.

Most of the energy liberated in a fission appears as the kinetic energy of the fission fragments (168 MeV, or 84%) and the kinetic energy of the neutrons (5 MeV, or 2.5%). The remainder is distributed among the gamma photons appearing instantaneously with the fission and the energy associated with the radioactive decay of the fission fragments. These fragments are readily stopped in the reactor. Their range is of the order of 0.01 to 0.001 mm. Thus, the major portion of the energy from a fission is deposited within a very short distance from the site of the fission.

In the largest power reactors in operation in the United States today, heat is generated at the rate of 3800 MW. At 200 MeV per fission, fissioning in such reactors must occur at the rate of 1.2×10^{20} fissions/sec to produce the power. In terms of ^{235}U, this requires the fissioning of all the nuclei contained in 0.047 g of ^{235}U, or the fissioning of approximately 4 kg per day. Thus, as a rule of thumb, the fissioning of all the nuclei present in 1 g of ^{235}U is sufficient to generate 1 MW day of thermal energy. In contrast, the generation of the same amount of energy from coal requires the combustion of 4 tons of coal of typical heating value. With the combustion of coal there is the associated release of a large quantity of carbon dioxide (~14 tons) to the atmosphere with its effects on global warming.

Cross Sections

A measure of the probability of a particular nuclide to interact with a neutron is provided by a quantity known as a **cross section**. Numerical values of cross sections are determined experimentally and are expressed in units of barns (b), with 1 b defined as 10^{-24} cm^2, or 10^{-28} m^2.

As a quantity, a cross section may be interpreted as a target area — the larger the cross section, the more likely the interaction of the nucleus with a neutron in its vicinity. For example, the cross section for fission of ^{235}U, denoted by σ_f^{235}, has a value of 582 b if the interacting neutron is traveling at the velocity associated with thermal energy (2200 m/sec). If the neutron is traveling at high energy, the cross section may drop to a value of approximately 2 b. With respect to the radiative capture of a neutron in ^{235}U leading to the formation of ^{236}U, the cross section is given by $\sigma_c^{235} = 99$ b, if the neutron is thermal. In summary, a cross section is a property specific to a given nuclide, but it is a property whose value depends on the energy of the interacting neutron.

Cross sections are additive. Thus, the cross section for the absorption of a thermal neutron in ^{235}U — whether the absorption gives rise to a fission or a radiative capture — is given by $\alpha_a = \alpha_f + \alpha_c = 582$ b + 99 b = 681 b. Further, the probability of a fission occurring as a result of a thermal neutron being absorbed in ^{235}U is given by $\alpha_f/\alpha_a = 582$ b/681 b = 0.85. Fission is, therefore, the more likely outcome of an interaction between a ^{235}U nuclide and a thermal neutron.

On average, the neutrons arising from the fissioning of ^{235}U have a kinetic energy of 2 MeV, corresponding to a speed of 2×10^7 m/sec. These neutrons are four orders of magnitude greater than the speed at which a neutron is considered to be thermal (2200 m/sec).

Categories of Nuclear Reactors

A prerequisite for a self-sustaining chain reaction is that sufficient ^{235}U be present in the medium to ensure that the absorption of a neutron in a nucleus of ^{235}U is a likely occurrence. If the population of neutrons present in the medium at any instant consists predominantly of slow neutrons, a far lesser amount of ^{235}U is needed to ensure criticality than would be the case if the population were to consist of fast neutrons. This comes about because of the difference in the values of the cross sections mentioned previously.

There is, from this particular standpoint, an incentive to slow down the neutrons originating in fission in order to reduce the inventory of ^{235}U needed to maintain criticality. In the power reactors operating today, means are provided to slow down the neutrons. The slowing down is effected through multiple elastic scatterings of the neutrons with the nuclei of light elements deliberately present in the medium acting as so-called **moderators**. Notable among such elements are hydrogen present in water, deuterium in heavy water, and carbon in the form of graphite.

All of the reactors in which substantive moderation of the neutrons occurs are categorized as **thermal reactors**. This term stems from the distinguishing feature that the neutron population is in, or near, thermal equilibrium with the nuclei of the moderator. As a consequence, there is no net exchange of energy between the neutron population and its surroundings. The neutrons are then referred to as thermal neturons.

In a population of **thermal neutrons**, the distribution of the speeds of the neutrons is characterized, adequately in many cases, by the Maxwell-Boltzmann distribution, originally formulated to apply to the molecules of an ideal gas. According to this distribution, the most probable speed of the neutrons at the reference temperature of 20°C is 2200 m/sec and the kinetic energy corresponding to the most probable speed is 0.025 eV.

Reactors that are not thermal reactors fall in the category of **fast reactors**. In these reactors, the moderation of neutrons is much reduced for reasons discussed later.

Nuclear Fuel

In light-water reactors (LWR), the type of power reactors most commonly in service today, the nuclear fuel is uranium with a content of 2 to 4% of ^{235}U. This fuel is produced by enriching natural uranium in ^{235}U by one of several technologies, principally gaseous diffusion and gaseous centrifugation (Benedict et al., 1981). Neutrons of all energies, down to and including thermal energies, can induce fission in ^{235}U. For this reason, ^{235}U is said to be fissile.

In contrast, ^{238}U, present to the extent of 96 to 98% in the fuel, can be fissioned to a significant extent by neutrons with energies in excess of a threshold of roughly 2 MeV. Fissions of ^{238}U, referred to as fast fissions, play only a slight role in the chain reaction in an LWR. However, ^{238}U absorbs neutrons radiatively to yield ^{239}U. This nuclide is radioactive and decays to ^{239}Np which, in turn, decays to ^{239}Pu, a **fissile nuclide**. Thus, in LWR fuel ^{239}Pu, produced from ^{238}U, is available for fissioning by neutrons of all energies and contributes to the chain reaction. Because of its ability to form fissile ^{239}Pu, ^{238}U is termed a **fertile nuclide**.

Conversion and Breeding

To characterize the unique capability of nuclear fuel simultaneously to produce and consume fissile material, a figure of merit known as the **conversion ratio** (CR) is informative. It is defined by the relation:

$$\text{CR} = \frac{\text{number of fissile nuclei produced from fertile nuclei}}{\text{number of fissile nuclei consumed}}$$

In fuel irradiated in an LWR, the conversion ratio typically has a value of 0.5. If the appropriate combination of materials, design, and operating parameters could be found to raise the conversion ratio

to a value greater than unity, a reactor would become a breeder reactor, that is, one that produces more fissile material than it consumes in its operation.

To illustrate the possibility of breeding, consider a parameter known as the reproduction factor and given by

$$\eta = \upsilon \frac{\text{number of neutrons causing fission in fuel}}{\text{total number of neutrons absorbed in fuel}} = \nu \frac{\sigma_f^{\text{fuel}}}{\sigma_a^{\text{fuel}}}$$

In the case of ^{235}U and thermal neutrons, the value of η is given by $\eta_{235} = 2.42 \times 582/(589 + 99) = 2.42 \times 0.85 = 2.07$.

If a chain reaction is to be self-sustaining in a reactor, the condition $\eta > 1$ must apply. To achieve breeding requires that $\eta > 2$. In other words, one neutron from fission would be available to sustain the chain reaction and another to produce a fissile nucleus from a fertile nucleus. Practical considerations indicate that the value of η must be substantially greater than 2, since neutrons will be lost by absorption in structural materials, heat removal medium, fission fragments, the moderator, if present, and by escaping from the physical confines of the reactor.

As shown, ^{235}U has a value of η slightly above 2 with neutrons at thermal energies. Breeding or near-breeding conditions could arise, in principle, if very judicious choices of materials and parameters prevail. A more attractive fuel from the standpoint of breeding is ^{233}U. This isotope of uranium is produced artificially by placing the naturally occurring nuclide ^{232}Th in a reactor. A radiative capture of a neutron in ^{232}Th leads to the formation of the radioactive nuclide ^{233}Th. Two successive radioactive decays yield ^{233}U. In a thermal reactor, the value of η with ^{233}U is 2.29, approaching the level where breeding might be contemplated. Intermediate between the two fissile isotopes of uranium is ^{239}Pu, which at thermal energies yields a value of η of 2.15.

Figure 8.8.1 shows the behavior of η as the energy of the neutrons inducing fission increases. A little above thermal energies the value of η for ^{239}Pu and ^{235}U drops below 2, indicating that breeding is impossible at such energies. As energy increases, the values of η for both reach the threshold of 2 and continue to increase steadily, with ^{239}Pu clearly the more attractive fuel from the standpoint of breeding. The value of ^{239}Pu for ^{235}U is relatively insensitive to increases in energy and remains continuously above 2. Again, at higher energies, η is the more attractive fuel.

Research on the development of **breeder reactors** has focused on the ^{239}Pu fuel cycle, both in the U.S. and abroad. Representative of these reactors is the liquid metal fast breeder reactor (LMFBR) in which liquid sodium is the heat-removal fluid and provides the small amount of moderation needed. Breeder reactors with ^{233}U as fuel, represented by an adaptation of the high-temperature gas-cooled reactor (HTGCR), in which the heat-removal fluid is helium and the moderator is graphite, although less attractive, in principle, as breeders, might with further research and development prove to be viable alternatives to the LMFBR.

LWR Fuel

Nuclear fuel in light water is in the form of small cylindrical pellets of the ceramic UO_2, with the uranium enriched to 2 to 4% in ^{235}U, as mentioned previously. These pellets are stacked vertically in tubes and the ends of the tubes are sealed off. The dimensions and further details given here apply strictly to the more common type of LWR, known as the pressurized water reactor (PWR), but may be taken as generally representative of LWRs.

The tubes containing the fuel pellets are referred to as fuel rods. They are 4.3 to 4.7 m in length and 0.0095m in outside diameter. An array typically of 17 × 17 rods constitutes a fuel assembly, as shown in Figure 8.8.2. Certain fuel rods within the assembly are replaced by guide sheaths in which absorber rods can be moved vertically. These rods absorb neutrons, thus providing one of the means of controlling the chain reaction as the rods are inserted or withdrawn. Within the fuel assembly the fuel rods are placed on a pitch of 0.0127 m, leaving vertical passages through which water can flow. A total of

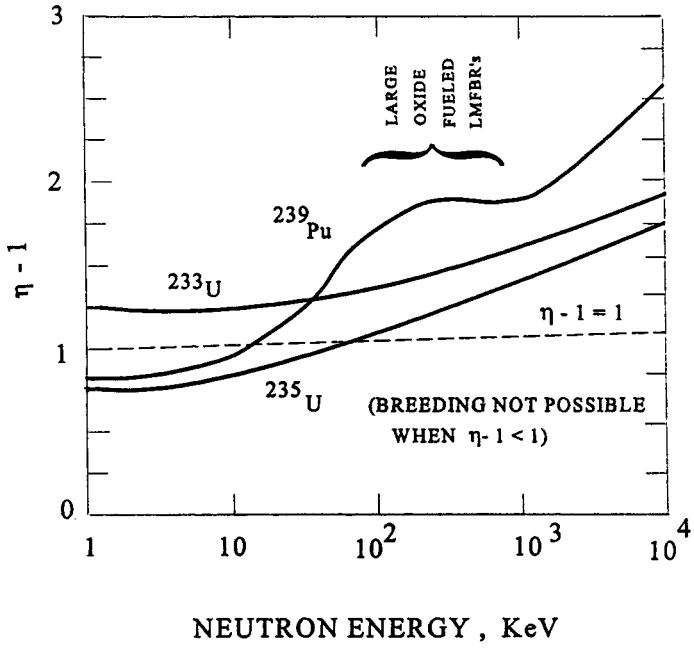

FIGURE 8.8.1 Dependence of reproduction factor of neutron energy.

approximately 200 fuel assemblies, juxtaposed to form a roughly cylindrical configuration constitute the core of the reactor. Water is circulated through the core where the water serves both to moderate the neutrons and to remove the heat generated by fissions in the nuclear fuel.

Light-Water Reactors

LWRs currently make up the largest portion of the installed nuclear generating capacity throughout the world. Among these, the PWRs are more numerous. By operating at a sufficiently high pressure, bulk boiling of the reactor coolant is suppressed in a PWR. In contrast, the coolant is allowed to boil in a boiling water reactor (BWR) and a portion of the coolant is converted to steam as it circulates through the core.

Pressurized Water Reactors

A schematic of a PWR system is shown in Figure 8.8.3. At the heart of the system is the core made up of fuel assemblies and associated control rods. The core is contained in a reactor vessel, or pressure vessel, designed to operate at a pressure typically of 15.5 mPa. Water is circulated through the core where it acts as a moderator and also removes the heat generated through fission. Typical operating temperatures at full power are 295°C at the inlet and 330°C at the outlet, an increase of 35°C as a result of the water passing through the core.

From the reactor vessel, the coolant is circulated to steam generators and returned to the reactor vessel to complete the so-called primary loop. This loop constitutes the nuclear steam supply (NSS). Steam emerging from the steam generators is directed toward the secondary loop, or balance of plant, consisting of turbine generator, condenser, and feedwater pumps. Extremely small quantities of radioactive contaminants may be present in the steam generated in PWRs, and all releases to the environment from the secondary side of the plant are carefully monitored and controlled. Otherwise, steam from the NSS differs from steam generated in fossil fueled plants only inasmuch as its grade is inferior.

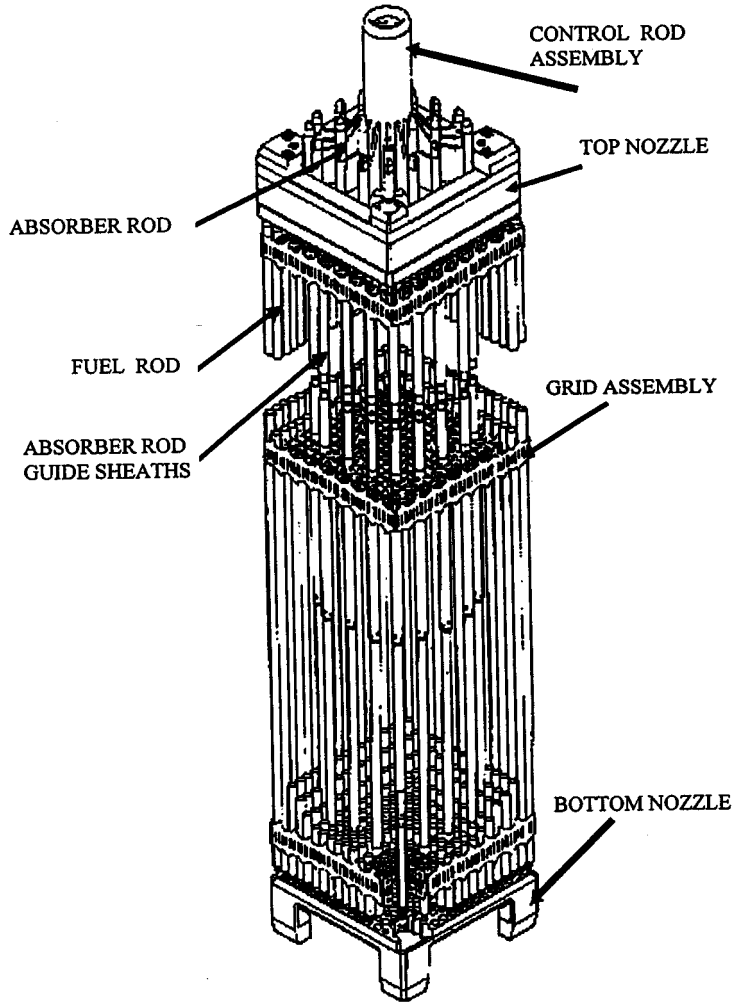

FIGURE 8.8.2 PWR fuel assembly.

Boiling Water Reactors

Figure 8.8.4 is a schematic of a BWR system. A reduced operating pressure of 7.2 MPa causes a portion of the coolant to flash to steam. Steam separators and driers allow dry steam to emerge from the reactor vessel, thus eliminating the need for separate steam generators and a secondary loop. Steam from the reactor vessel flows through a turbine generator and condenser, from which circulating pumps return the condensate to the reactor. Large quantities of radioactive contamination may be present in the steam produced by a BWR because of the direct cycle, so releases must be carefully monitored. A distinguishing feature of the BWR are the jet pumps, typically 24 in number, placed along the periphery of the core. These pumps augment the flow of coolant through the core.

Defining Terms

Breeder reactors: Reactors in which the conversion ratio is greater than unity.

Conversion ratio: The ratio of the number of fissile nuclei produced in a reactor to the number of fissile of nuclei consumed.

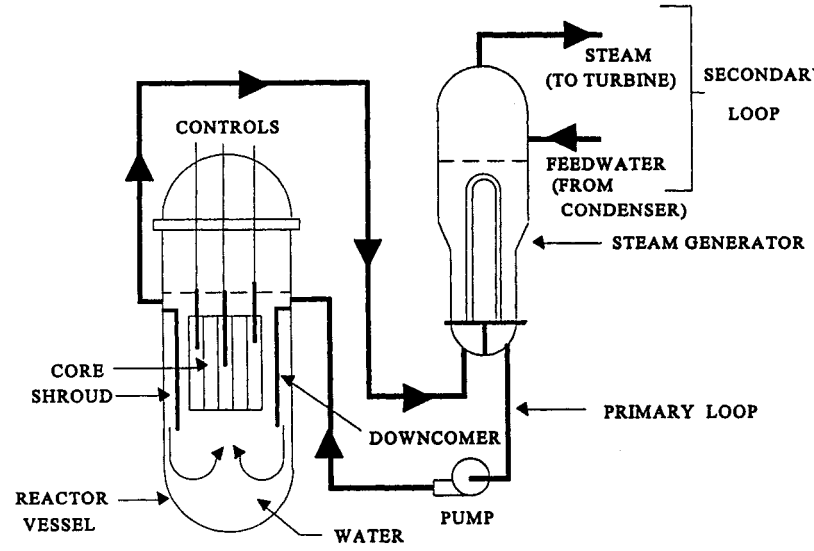

FIGURE 8.8.3 Schematic of a pressurized water reactor.

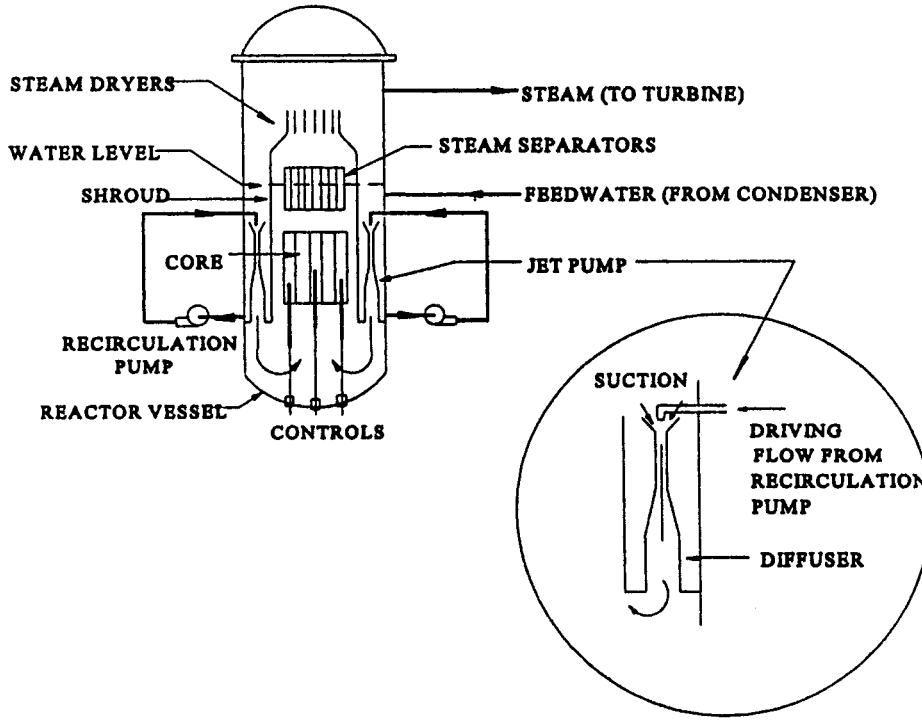

FIGURE 8.8.4 Schematic of a boiling water reactor.

Critical configuration: A medium containing nuclear fuel in which a self-sustaining chain reaction can be maintained.

Cross section: A numerical quantity, determined experimentally, related to the probability that a specific nuclide will undergo a given nuclear reaction.

Fast reactors: Reactors in which little moderation of the neutrons occurs and the neutron populations consist of neutrons of relatively high speeds.

Fertile nuclide: A nuclide that, through the absorption of a neutron and subsequent radioactive decays, can produce a fissile nuclide.

Fissile nuclide: A nuclide that can be fissioned by neutrons of all energies, down to and including thermal energies.

Moderator: A component of a reactor present expressly to slow down neutrons and produce a population of thermal neutrons.

Thermal neutrons: A population of neutrons in, or near, thermal equilibrium with the nuclei of a medium in which the populations exists.

Thermal reactors: Reactors in which the neutron populations consist predominantly of thermal neutrons.

References

Benedict, M., Pigford, T.H., and Levi, H.W. *Nuclear Engineering,* 2nd ed., McGraw-Hill, New York, 1981.

Further Information

Glasstone, S. and Sesonske, A. *Nuclear Reactor Engineering,* 3rd ed., Van Nostrand Reinhold, New York, 1981.

8.9 Nuclear Fusion

Thomas E. Shannon

Introduction

Nuclear fusion holds the promise of providing almost unlimited power for future generations. If the process can be commercialized as envisioned by reactor design studies (Najmabadi et al., 1994), many of the problems associated with central electric power stations could be eliminated. Fusion power plants would not produce the pollution caused by the burning of fossil fuel and would eliminate the concern for meltdown associated with nuclear fission. The amount of radioactive waste material produced by a fusion reactor will be much less than that of a fission reactor since there is essentially no radioactive ash from the fusion reaction. If **low activation advanced materials** such as silicon carbide composites can be developed for the reactor structural material, the problem of disposal of activated components can also be eliminated.

Fusion Fuel

Although a number of different atomic nuclei can combine to release net energy from fusion, the reaction of **deuterium and tritium** (D-T) is the basis of planning for the first generation of fusion reactors. This choice is based on considerations of reactor economy. The D-T reaction occurs at the lowest temperature, has the highest probability for reaction, and provides the greatest output of power per unit of cost (Shannon, 1989). The disadvantages of D-T as a fusion fuel are twofold. Tritium does not occur naturally in nature and must be bred in the fusion reactor or elsewhere. Second, tritium is a radioactive isotope of hydrogen with a relatively long **half-life** of 12.3 years. Since tritium can readily combine with air and water, special safety procedures will be required to handle the inventory necessary for a fusion reactor. There is hope that a less reactive fuel, such as deuterium alone (D-D) will eventually prove to be an economically acceptable alternative (Shannon, 1989).

Confinement Concepts

Magnetic fusion, based on the tokamak concept, has received the majority of research funding for fusion energy development. However, other magnetic fusion concepts, such as the stellarator, the spherical torus, reversed-field pinch, and field-reversed configurations, are being developed as possible alternatives to the tokamak (Sheffield, 1994). It may also be possible to develop fusion power reactors by inertial confinement concepts (Waganer et al., 1992). Research on these concepts has been done primarily in support of weapons development; therefore, the level of scientific understanding for power reactor applications is significantly less than that of magnetic fusion. The remainder of this discussion on reactor development, fusion energy conversion, and transport will consider only the tokamak magnetic fusion concept.

Tokamak Reactor Development

The tokamak device has proved to be the most effective means of producing the conditions necessary for magnetic fusion energy production. In 1994, researchers at the Princeton Plasma Physics Laboratory achieved in excess of 10 MW of D-T fusion power in a research tokamak, the Tokamak Fusion Test Reactor (TFTR). This accomplishment, coupled with worldwide progress in 40 years of magnetic fusion research, has established the scientific feasibility of the tokamak concept. The next major step, the International Thermonuclear Experimental Reactor (ITER) is being carried out under an international agreement among Europe, Japan, Russia, and the United States (Conn et al., 1992). A drawing of the ITER tokamak is shown in Figure 8.9.1. If the project is approved for construction, it will be in operation

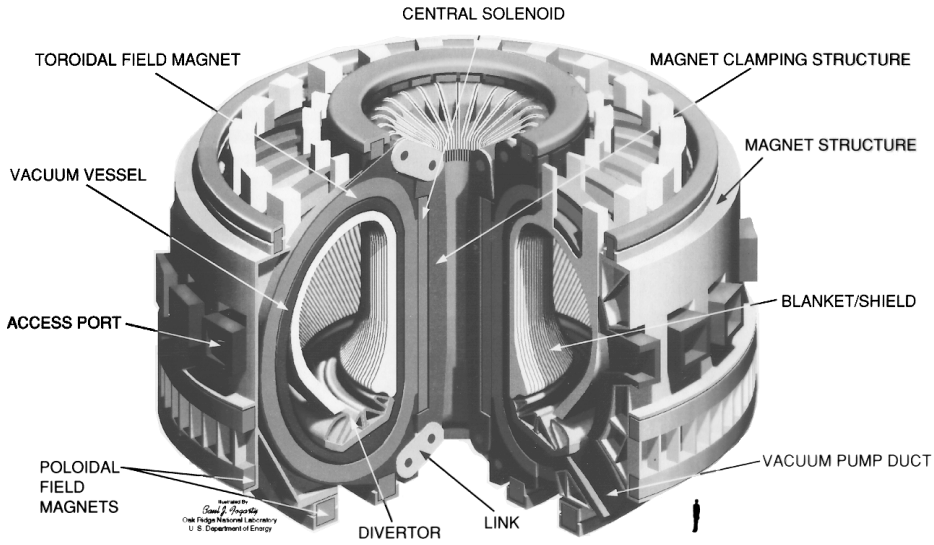

FIGURE 8.9.1 The International Thermonuclear Experimental Reactor (ITER).

around 2005. The ITER is being designed to produce a fusion power in excess of 1000 MW. This will be a significant step on the path to commercial fusion power.

The U.S. Department of Energy has proposed a strategy, shown in Figure 8.9.2, which will lead to a demonstration power reactor by the year 2025. Supporting research and development programs necessary to achieve this goal are shown in this figure.

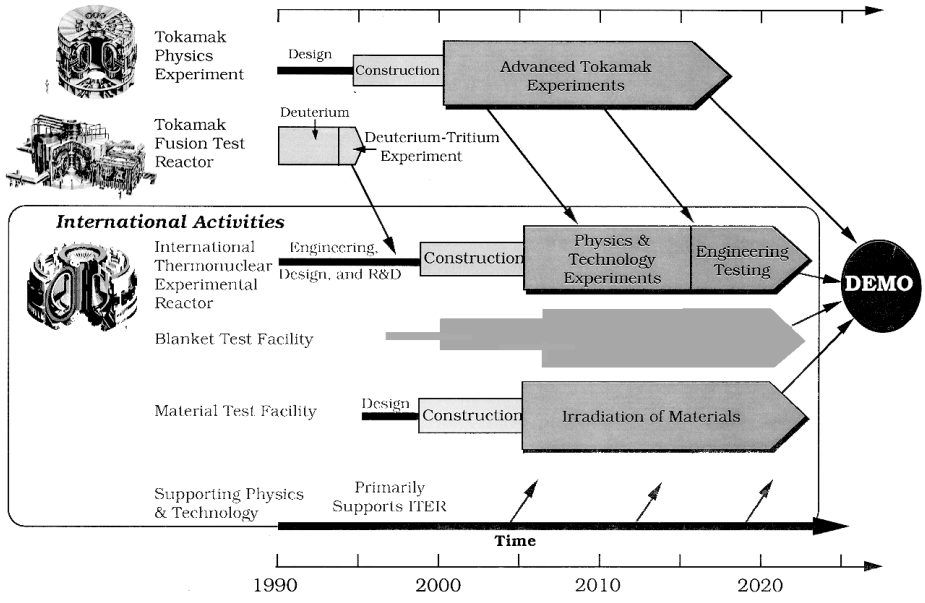

FIGURE 8.9.2 The U.S. Department of Energy magnetic fusion energy strategy.

Fusion Energy Conversion and Transport

The energy from fusion is created in the form of charged particles and neutrons. The D-T reaction produces a neutron with an energy of 14.1 MeV and an alpha particle (helium) with an energy of 3.5 MeV in the reaction

$$D + T \rightarrow He^4\ (3.5\ MeV) + n(14.1\ MeV)$$

In the tokamak device, the reaction will take place in the toroidal vacuum vessel as previously shown in the ITER drawing, Figure 8.9.1. The D-T fuel, in the form of a **plasma**, will absorb energy from the positively charged alpha particles to sustain the temperature necessary for the reaction to continue. The neutron, having no charge, will escape from the plasma and pass through the wall of the vessel and penetrate into the surrounding blanket/shield structure. The kinetic energy of the alpha particles from the fusion reaction is eventually deposited on the wall of the vacuum vessel by radiation and conduction heat transfer from the plasma while the neutron deposits most of its energy within the cross section of the blanket/shield. The resulting thermal energy is transferred by a coolant such as water to a steam generator where a conventional steam to electric generator system may be used to produce electricity. An overall schematic diagram of the energy conversion and heat-transport system is shown in Figure 8.9.3.

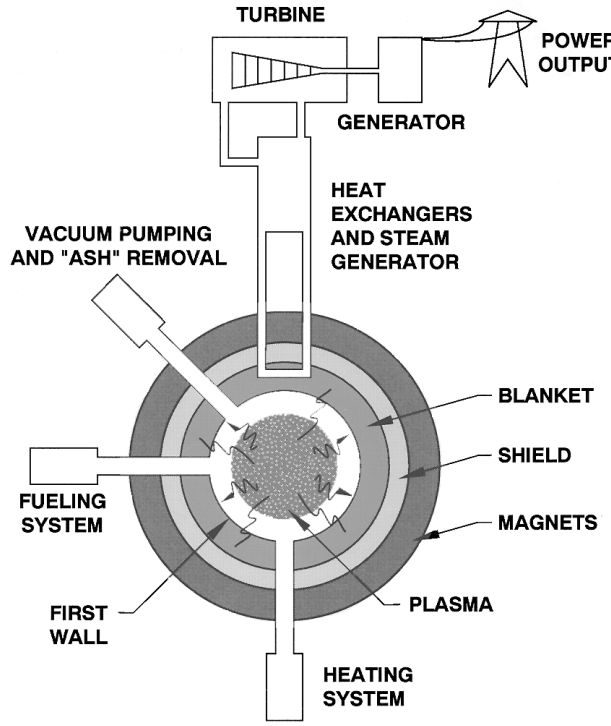

FIGURE 8.9.3 Schematic Diagram of a Magnetic Fusion Reactor Power Plant.

Defining Terms

Deuterium and tritium: Isotopes of hydrogen as the fuel for fusion reactors.
Half-life: The time required for half of the radioactive material to disintegrate.
Low activation advanced materials: Structural materials that significantly reduce the radioactivity induced by exposure to fusion neutrons.

Plasma: A gas such as a mixture of deuterium and tritium raised to a very high temperature at which the electrons and the nuclei of the atoms separate. The plasma, consisting of electrons and ions, can conduct electricity and react to magnetic fields.

References

Conn, R.W., Chuyanov, V.A., Inoue, N., and Sweetman, D.R. 1992. The International Thermonuclear Experimental Reactor, *Sci. Am.* 266(4).

Najmabadi, F. et al. 1994. The ARIES-II and -IV Second Stability Tokamak Reactors, University of California, Los Angeles, report UCLA-PPG-1461.

Shannon, T.E. 1989. Design and cost evaluation of a generic magnetic fusion reactor using the D–D fuel cycle. *Fusion Technol.* 15(2), Part 2B, 1245–1253

Sheffield, J. 1994. The physics of magnetic fusion reactors. *Rev. Mod. Phy.* 66(3).

Waganer, L. et al. 1992. Inertial Fusion Energy Reactor Design Studies. U.S. Department of Energy Report. Vol. I, II, and III, DOE/ER-54101 MDC 92E0008.

Further Information

The U.S. Department of Energy, Office of Fusion Energy maintains a home page on the World Wide Web. The address http://wwwofe.er.doe.gov provides an excellent source of up-to-date information and access to information from most institutions involved in fusion research.

8.10 Solar Thermal Energy Conversion

D. Yogi Goswami

Introduction

Solar thermal energy applications such as space and water heating have been known for a long time. Researchers over the past few decades have developed a number of additional solar thermal applications, such as industrial process heat, refrigeration and air-conditioning, drying and curing of agricultural products, and electric power production by solar thermal conversion. This section will cover solar thermal energy conversion including solar thermal collectors and conversion systems.

Solar Thermal Collectors

A simple **solar thermal collector** consists of (1) an absorber surface (usually a dark, thermally conducting surface), (2) some insulation behind the surface to reduce heat loss, (3) a trap for thermal reradiation from the surface such as glass, which transmits the shorter-wavelength solar radiation but blocks the longer-wavelength radiation from the absorber, and (4) a heat-transfer medium such as air, water, etc. High-temperature collectors require reflectors of sunlight that concentrate solar radiation on the absorber. The technology of solar collectors is developed to achieve temperatures as high as 1000°C or even higher. The design of a solar collector and the choice of working fluids depend on the desired temperature and the economics of the application. Table 8.10.1 lists the types of solar thermal collectors based on their temperature range.

TABLE 8.10.1 Types of Solar Collectors and Their Typical Temperature Range

Type of Collector	Concentration Ratio	Typical Working Temperature Range (°C)
Flat plate collector	1	≤70
High-efficiency flat plate collector	1	60–120
Fixed concentrator	2–5	100–150
Parabolic trough collector	10–50	150–350
Parabolic dish collector	200–2000	250–700
Central receiver tower	200–2000	400–1000

Source: Compiled from Goswami, D.Y., *Alternative Energy in Agriculture,* Vol. 1, CRC Press, Boca Raton, FL, 1980.

Flat Plate Collectors

Flat plate collectors may be designed to use liquids (water, oil, etc.) or air as the heat-transfer fluid. Figure 8.10.1 shows a typical liquid-type flat plate collector. The choice of materials for glazing and absorber needs special attention.

Glazing. The purpose of **glazing** is to (1) transmit the shorter-wavelength solar radiation, but block the longer-wavelength reradiation from the absorber plate, and (2) reduce the heat loss by convection from the top of the absorber plate. Glass is the most widely used glazing material. Transmittance of low iron glass in the visible and near infrared wavelength range can be as much as 91%, while for the longer-wavelength radiation (>3 μm) its transmittance is almost zero. Other materials than can be used as glazings include certain plastic sheets such as polycarbonates (Lexan® and Tuffac® — transmittance ~75%), acrylics (Plexiglass® and Lucite® — transmittance ~92%), and thin plastic films such as polyethylene. A major advantage of the plastics is that they are shatterproof; however, they scratch easily and lose transparency over time.

Absorbers. Copper is the most common material used for absorber plates and tubes because of its high thermal conductivity and high corrosion resistance. For low-temperature applications such as swimming pool heating, a plastic material called ethylene propylene polymer (trade names EPDM, HCP,

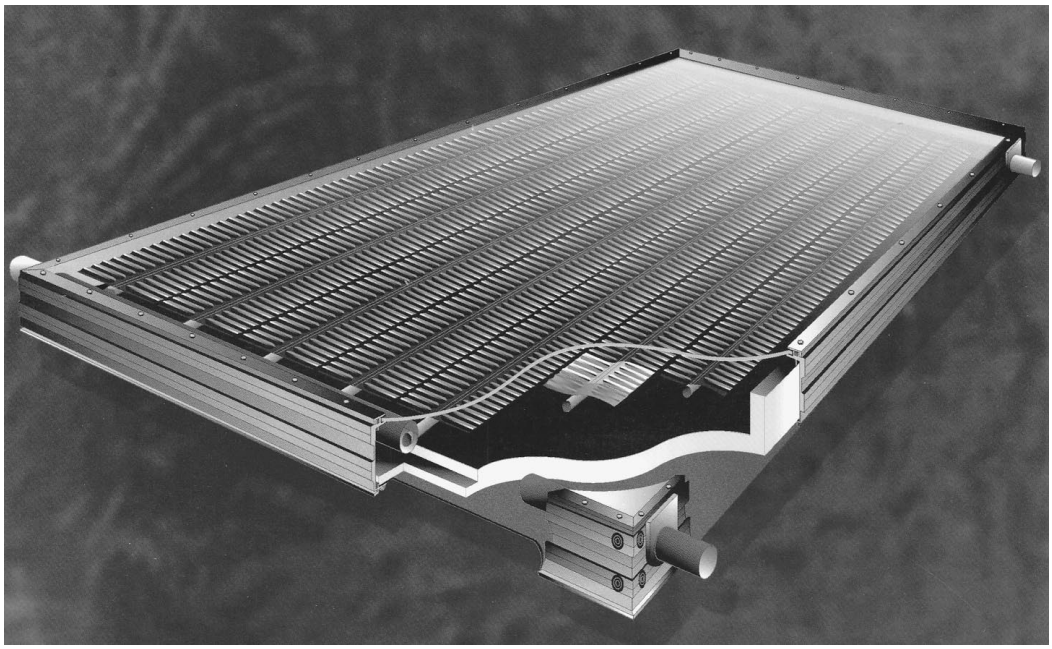

FIGURE 8.10.1 A typical liquid flat plate collector. (Courtesy of American Energy Technologies, Green Cove Springs, FL.)

etc.) can be used to provide inexpensive absorber material. To compensate for low thermal conductivity of these materials, a large surface area is provided for heat transfer. In order to increase the absorption of solar radiation and to reduce the emission from the absorber, the metallic absorber surfaces are painted or coated with flat black paint or some selective coating. Absorptivities and emissivities of some common **selective surfaces** are given in Table 8.10.2.

TABLE 8.10.2 Absorptivity and Emissivity of Common Selective Surfaces

Surface	Absorbtivity	Emissivity
Black chrome	0.95	0.1
Black nickel	0.9	0.08
Copper oxide	0.9	0.17
Lead sulfide	0.89	0.2
Flat black paint	0.98	0.98

Source: Compiled from Duffie, J.A. and Beckman, W.A., *Solar Engineering of Thermal Processes*, John Wiley and Sons, New York, 1980.

Evacuated Tube Collectors. Evacuated tube collectors have essentially a vacuum between the absorber and the glazing tube. This eliminates most of the heat loss by conduction and convection. Therefore, these collectors give a very high efficiency at higher temperatures. Evacuated tube collectors are typically used in the temperature range of 80 to 140°C

Concentrating Collectors. Concentrating collectors use reflectors or lenses to focus solar radiation from a large area onto a small area, thereby creating higher temperatures. Such collectors are usually used for temperatures higher than 100°C. Figure 8.10.2 shows schematics of some of the concentrating collectors.

Nontracking Concentrators. The simplest concentrating collector can be made by using flat wall reflectors to concentrate the solar radiation on a flat plate collector. Concentration ratios of two to three can be

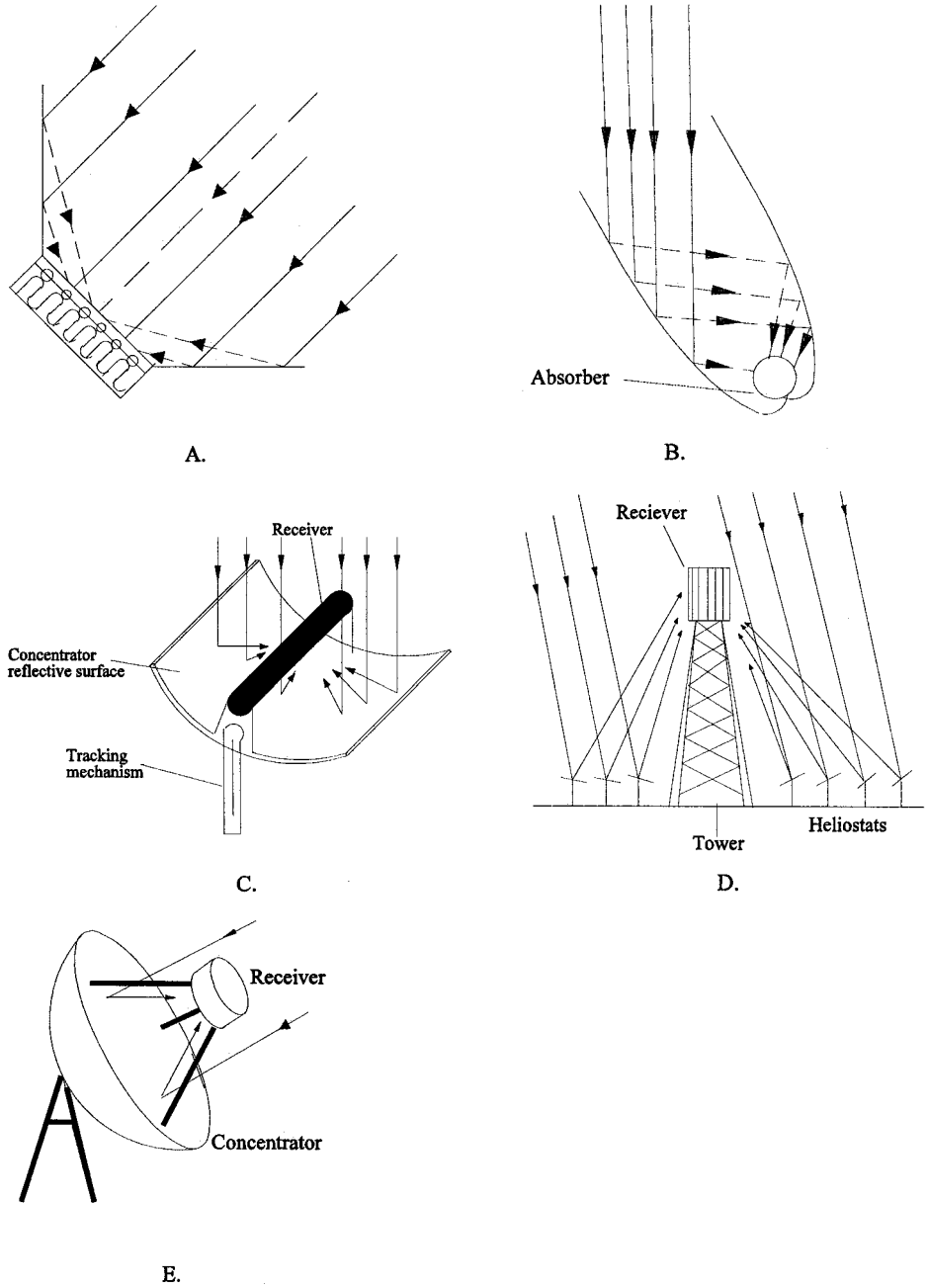

FIGURE 8.10.2 Types of concentrating collectors. (A) Flat plate collector with reflective wings; (B) Compound parabolic concentrator; (C) parabolic trough; (D) central receiver; (E) parabolic dish.

achieved this way. For slightly higher concentration ratios, a novel design, developed by Roland Winston, called a "compound parabolic concentrator" (CPC) can be used (Winston, 1974).

Tracking Concentrators. For temperatures up to 350°C, cylindrical parabolic trough collectors are used. These collectors focus solar radiation on a line focus where the absorber is located. These collectors usually require tracking on one axis only with seasonal adjustment on the other axis. A reflecting spherical or paraboloidal bowl is used when temperatures of the order of 250 to 500°C are needed. These collectors

require two-axis tracking. In some cases, the dish is kept stationary while the receiver is moved to track the focus of the reflected solar radiation. Finally, for extremely high temperatures (500 to 1000°C) needed for large-scale thermal power generation, a large field of tracking flat mirrors (called heliostats) is used to concentrate solar radiation on a receiver that is located on top of a central tower.

Collector Thermal Performance

The instantaneous efficiency of a collector is given by

$$\eta = \frac{\text{Useful energy collected}}{\text{Incident solar energy}} = \frac{Q_u / A}{I} \tag{8.10.1}$$

where

$$Q_u = mC_p\left(T_o - T_i\right) \tag{8.10.2}$$

and A = area of the collector, I = incident solar energy per unit area, m, C_p, T_i, and T_o are the mass flow rate, specific heat, and inlet and outlet temperatures of the heat-transfer fluid.

The efficiency of a flat plate solar collector can also be written by the Hottel–Whillier–Bliss equation:

$$\eta = F_R(\tau\alpha)_e - F_R U_L \frac{\left(T_i - T_{\text{amb}}\right)}{I} \tag{8.10.3}$$

where F_R, called the collector heat-removal factor, is a convenient parameter that gives the ratio of the actual useful energy gain of a flat plate collector to the useful gain if the whole collector surface were at the inlet fluid temperature; $(\tau\alpha)_e$ = effective transmittance absorptance product; and U_L = collector heat-loss coefficient.

Equation 8.10.2 suggests that if the efficiency, η, is plotted against $(T_i - T_{\text{amb}})/I$, the resulting curve will have a y intercept equal to $F_R\,(\tau\alpha)_e$ and a slope of $F_R U_L$. A linear curve usually gives an adequate approximation. Figure 8.10.3 shows an example of a performance curve for a water-heating flat plate collector, which is a linear least square curve fit to the actual test data.

Solar Ponds

A solar pond combines collector and energy storage in one unit. Solar radiation that enters the pond travels some distance through the water before being totally absorbed, thus increasing the temperature of the water at that depth. The heat thus collected can be stored in the pond by creating a stagnant, transparent, insulating layer in the top part of the pond. The most common method is by the addition of a salt into the pond to increase the density of water in the lower section of the pond. This type of pond is called a **salt gradient solar pond**. Reid (1987) reviewed the progress in the design and applications of salt gradient solar ponds. Figure 8.10.4 shows a schematic of a salt gradient pond along with a density profile in the pond.

The theory of salt gradient solar ponds has been described by Tabor (1981). The most important aspect of such ponds is the creation and maintenance of the salt gradient. Theory shows that the condition for maintaining stability is

$$\frac{\partial S}{\partial Z} > -1.14\frac{\partial \rho}{\partial T} \times \frac{\partial T}{\partial Z}\frac{\partial \rho}{\partial S} \tag{8.10.4}$$

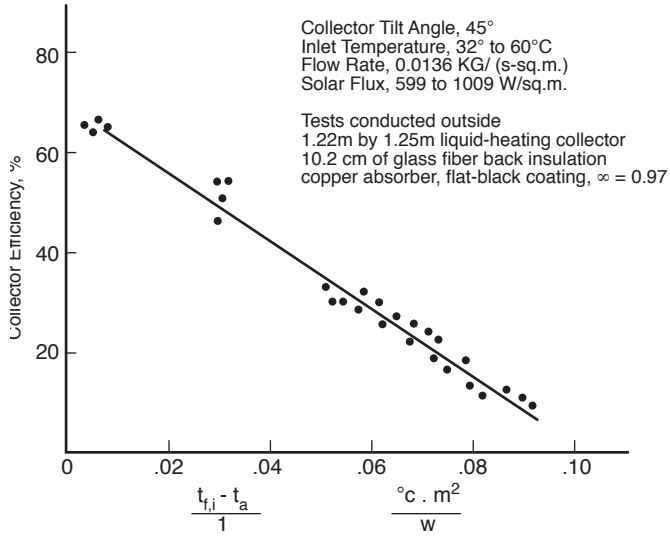

FIGURE 8.10.3 Thermal efficiency curve for a double-glazed flat plate liquid-type of solar collector. (Reprinted by permission of the American Society of Heating, Refrigerating and Air-Conditioning Engineers, Inc., Atlanta, GA, from ASHRAE Standard 93-77, *Methods of Testing to Determine the Thermal Performance of Solar Collectors*, 1977.)

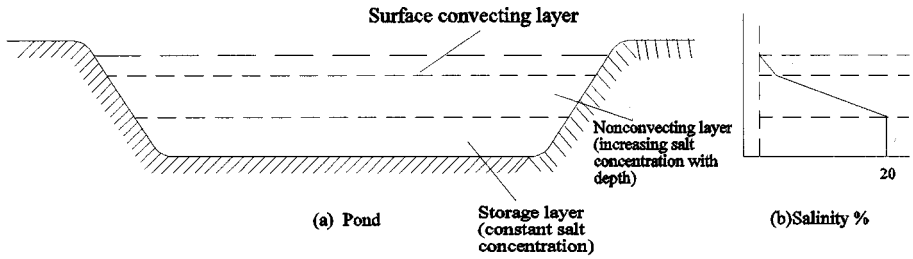

FIGURE 8.10.4 Schematic of a salt gradient solar pond.

where S is the salt concentration in kilograms per cubic meter, Z is the depth from the surface in meters, ρ is the density in kilograms per cubic meter, and T is the temperature in Kelvin. The two most common salts considered for solar pond applications are NaCl and $MgCl_2$. According to the above criteria, there is no difficulty in obtaining stability with $MgCl_2$ and it is somewhat difficult but possible to get stability with NaCl.

Solar Water-Heating Systems

Solar water-heating systems represent the most common application of solar energy at the present time. Small systems are used for domestic hot water applications while larger systems are used in industrial process heat applications. There are basically two types of water-heating systems: **natural circulation or passive solar system** (thermosyphon) and **forced circulation or active solar system**.

Natural Circulation

Figure 8.10.5 shows a schematic of a natural circulation solar water-heating system. It is also called a thermosyphon or passive solar water heater because it does not require a pump to circulate water. The storage tank is located above the collector. When the water in the collector gets heated, it rises into the tank, because of density change, setting up a circulation loop.

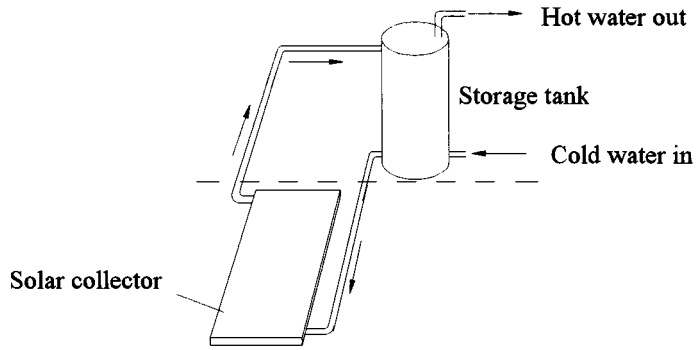

FIGURES 8.10.5 Schematic of a thermosyphon solar water-heating system.

Forced Circulation

Figure 8.10.6 shows three configurations of forced circulation systems: (1) open loop, (2) closed loop, and (3) closed loop with drainback. In an open loop system, the collectors are empty when they are not providing useful heat and the storage tank is at atmospheric pressure. A disadvantage of this system is the high pumping power required to pump the water to the collectors every time the collectors get hot. This disadvantage is overcome in the pressurized closed loop system (Figure 8.10.6B) since the pump has to overcome only the resistance of the pipes. Because water always stays in the collectors of this system, antifreeze (propylene glycol or ethylene glycol) is required for locations where freezing conditions can occur. During stagnation conditions (in summer), the temperature in the collector can become very high, causing the pressure in the loop to increase. This can cause leaks in the loop unless some fluid is allowed to escape through a pressure-relief valve. In both cases, air enters the loop causing the pump to run dry. This disadvantage can be overcome in a closed loop drainback system (Figure 8.10.6C). In this system, when the pump shuts off, the water in the collectors drains back into a small holding tank, which can be located where freezing does not occur. The holding tank can be located at a high level to reduce pumping power.

Industrial Process Heat Systems

For temperatures of up to about 100°C, required for many industrial process heat applications, forced circulation water-heating systems described above can be used. The systems, however, will require a large collector area, storage and pumps, etc. For higher temperatures, evacuated tube collectors or concentrating collectors must be used.

Space-Heating Systems

Solar space-heating systems can be classified as active or passive depending on the method utilized for heat transfer. A system that uses pumps and/or blowers for fluid flow in order to transfer heat is called an *active system*. On the other hand, a system that utilizes natural phenomena for heat transfer is called a *passive system*. Examples of passive solar space-heating systems include direct gain, attached greenhouse, and storage wall (also called Trombe wall).

Active space-heating systems store solar collected heat in water or rocks. Heat from water storage can be transferred to the space by convertors or by fan-coil units. A system using a fan-coil unit can be integrated with a conventional air system as shown in Figure 8.10.7. Heat from rock storage can be transferred to air by simply blowing air over the rocks.

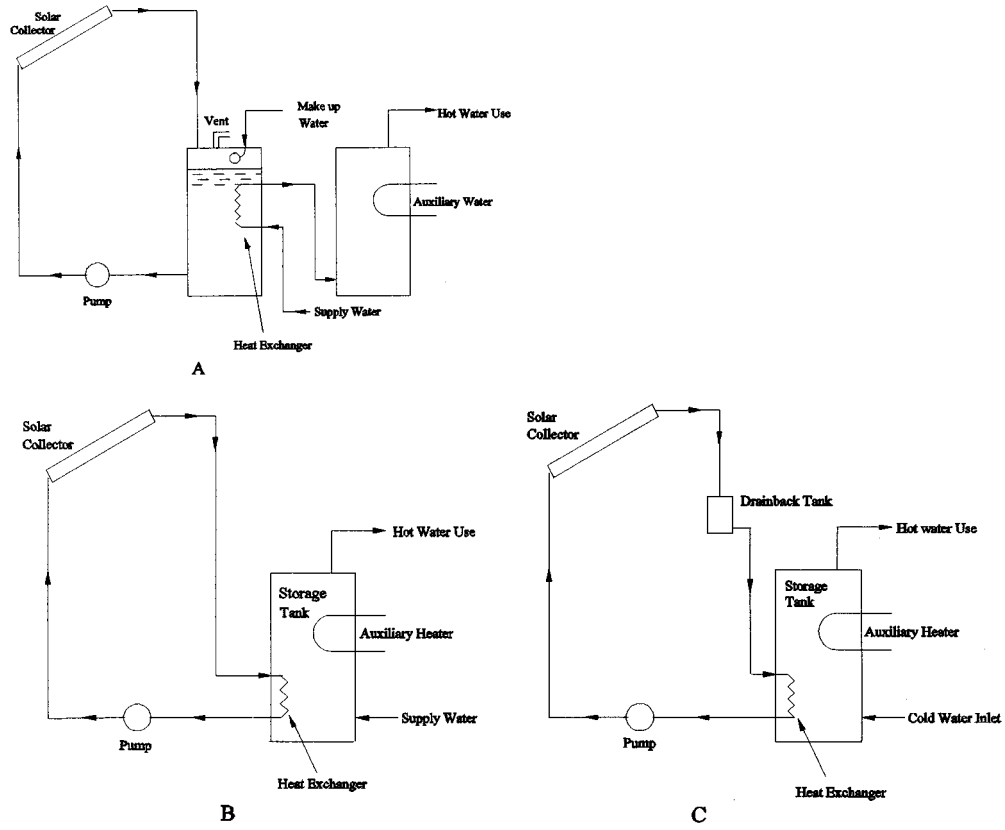

FIGURE 8.10.6 Typical configurations of solar water-heating systems: (A) open loop system, (B) closed loop system, (C) closed loop drainback system. (Adapted from Goswami, D.Y., *Alternative Energy in Agriculture,* Vol. 1, CRC Press, Boca Raton, FL, 1986.)

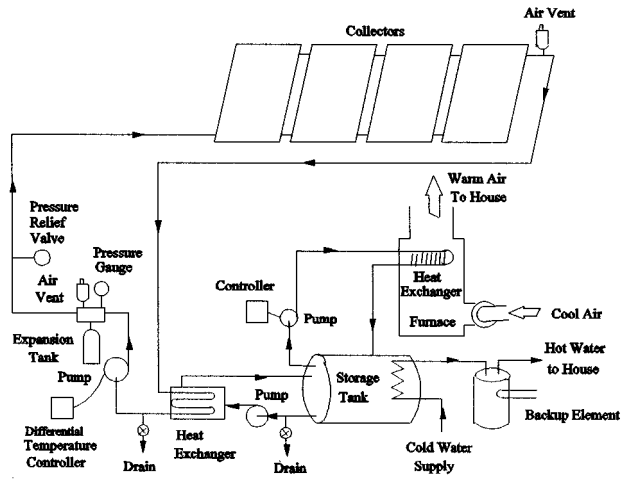

FIGURE 8.10.7 Schematic of an active solar space-heating system.

Solar Thermal Power

Solar thermal energy can be used to produce electrical power using conventional thermodynamic power cycles such as Rankine, Stirling, and Brayton cycles. The choice of power cycle and the working fluids depends on the temperature obtainable in the solar system, which depends on the type of solar collectors used. At present, developed solar thermal power systems include

Parabolic trough systems
Central receiver systems
Parabolic dish-Stirling engine system

Parabolic Trough Systems

Parabolic trough systems are simple in concept and, therefore, the most developed commercially. In 1984, Luz Company installed a Solar Electric Generating System (SEGS I) of 14 MW_e capacity in Southern California, utilizing parabolic trough solar collectors and natural gas fuel for superheat and backup. From 1984 to 1991, Luz Company installed eight additional plants, SEGS II to SEGS IX, with the total capacity of the nine plants being 354 MW_e. With each successive SEGS plant the technology was improved and the cost reduced. The cost of electricity was reduced from about 30¢/kWhr for the first plant to about 8¢/kWhr for the last plant. A schematic of the SEGS IX is shown in Figure 8.10.8, and some important data for the system are given in Table 8.10.3.

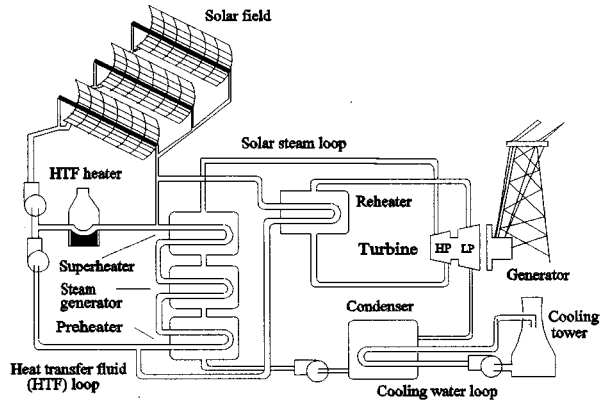

FIGURE 8.10.8 Schematic of SEGS IX power plant.

TABLE 8.10.3 Plant Characteristics — SEG IX

Power Block		Solar Field	
Gross power	88 MWe	Number of collectors	888
Net power	80 MWe	Aperature area	483,960 m^2
Steam inlet pressure	100 bar	Inlet temperature	293°C
Steam inlet temperature	371°C	Outlet temperature	390°C
Reheat pressure	17.2 bar	Annual thermal efficiency	50%
Reheat temperature	371°C	Peak optical efficiency	80%
Conversion efficiency	37.6%	Heat-transfer fluid (HTF)	Oil (VP-1)
Annual gas use	25.2×10^9 m^3	HTF volume	1289 m^3

Source: DeLaquil, P. et al., in *Renewable Energy Sources for Fuel and Electricity*, Island Press, Washington, D.C., 1993. With permission.

It has been recognized that this design does not utilize the energy of the natural gas efficiently. It has been suggested that energy of natural gas can be better utilized by combining the solar system with a natural gas turbine combined-cycle power plant (DeLaquil et al., 1993; Washom et al., 1994). Such a

hybrid system would use the exhaust of a natural gas turbine for superheating and preheating of water, while the solar field would be used for steam generation. Such a hybrid system can achieve conversion efficiency as high as 60%. A schematic of a **solar hybrid combined cycle** is shown in Figure 8.10.9.

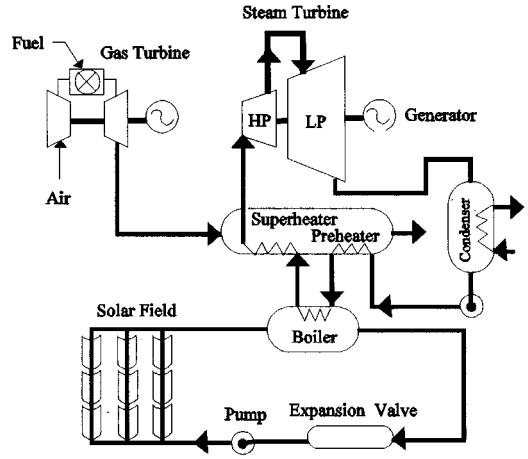

FIGURE 8.10.9 Solar hybrid combined cycle. (Adapted from Washom, B. et al., paper presented at the 1994 ASES Annual Conference, San Jose, CA, 1994.)

Central Receiver System

A central receiver system can potentially operate at very high temperature and therefore can have much higher efficiency than parabolic trough systems. However, the system can be economical only at larger capacities, such as 100 MW and above. The central receiver absorber can heat the working fluid or an intermediate fluid to a temperature as high as 600 to 1000°C which can be used to drive a Rankine cycle or Brayton cycle.

Solar One, a 10-MW_e central receiver power plant started operating in 1982 in Barstow, California. This plant generated superheated steam at 510°C and 10.3 MPa in the receiver absorber, which was used to drive a simple steam Rankine power cycle. The plant operated successfully for 6 years and provided a good learning experience. The plant has now been redesigned as Solar Two in which molten sodium nitrate is used as the heat-transfer fluid as well as for storage. Use of molten salt allows operation of the receiver absorber at much lower pressures The constraint is that the salt must always be above its melting point (220°C). Figure 8.10.10 shows a schematic of the Solar Two power plant.

Parabolic Dish Systems

Parabolic dish systems can achieve very high temperatures. The high temperatures produced by parabolic dishes can be used to drive Rankine, Stirling, and Brayton power cycles. So far, Rankine and Stirling cycles have been successfully demonstrated with parabolic dishes for electrical power production.

Early versions of parabolic dishes were made from die-stamped aluminum petals made reflective using a metallized polymer film. Later designs used simpler flat mirror facets fixed on a structure in such a way as to approximate a parabolic dish. The latest designs use a polymer film stretched on a circular frame (Mancini, 1994). The film is given a slight concave curvature by providing a vacuum behind it. These stretched polymer films are fixed on a structure to approximate a parabolic dish. Because of the low weight of the polymer film, the dish structure can be made out of light tubular members, thereby reducing the cost of the dish considerably. Parabolic dishes require two-axis tracking.

McDonnell Douglas Corporation successfully demonstrated a 25-KW_e parabolic dish system using a Stirling engine and a generator assembly fixed at the focal point of the dish in 1985 (Gupta, 1987). The concept is very attractive because it provides a modular design of stand-alone power plants for small

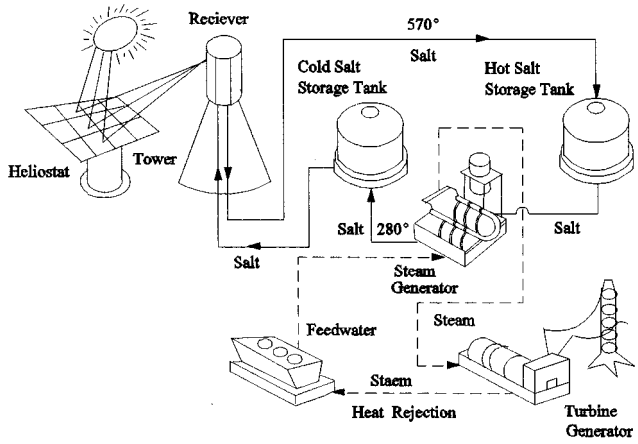

FIGURE 8.10.10 Schematic of Solar Two.

communities and independent power applications. Cummins Power Generation Company, in Indiana, has developed this concept further (Mancini, 1994). The Cummins system uses stretched polymer film facets for a parabolic dish, a heat pipe receiver absorber, a free-piston Stirling engine, and a linear alternator, resulting in a very compact power generation system. Figures 8.10.11 shows the latest version of the Cummins Dish Stirling power system. A detailed discussion of Stirling engines is given in Section 8.5.

Nomenclature

A = area of collector
C_p = specific heat
m = mass flow rate
T = temperature
I = incident solar radiation
Qn = useful heat collected
F_R = collector heat-removal factor
U_L = collector heat-loss coefficient
S = salt concentration
Z = depth

Greek Symbols

α = absorptance
τ = transmittance
η = efficiency
ρ = density

Subscripts

i = inlet
o = outlet
amb = ambient
e = effective

Defining Terms

Forced circulation or active solar system: A solar thermal system that uses active means, such as pumps, for fluid flow and heat transfer.

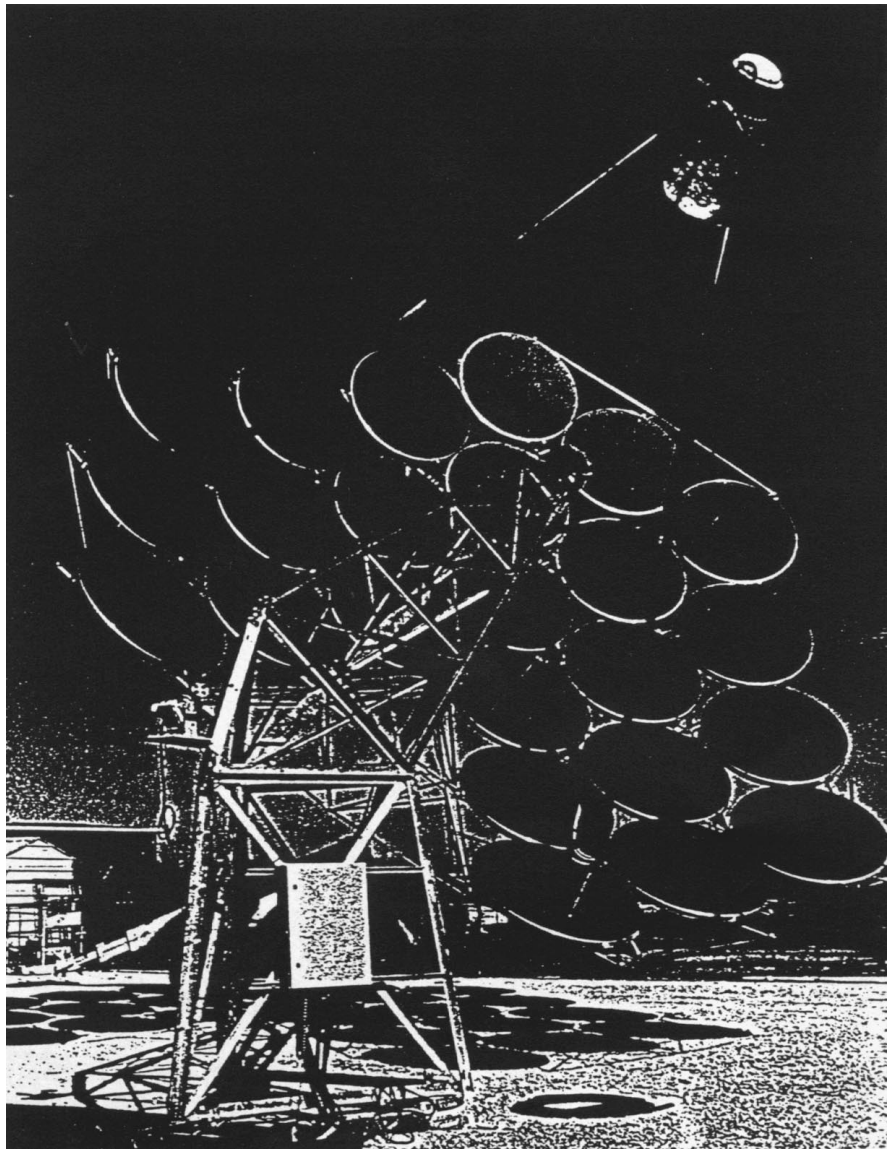

Figures 8.10.11 A parabolic dish — Stirling Engine Power System.

Glazing: A material used in a solar collector that transmits short-wavelength solar radiation and blocks longer-wavelength reradiation from the absorber plate.

Natural circulation passive solar system: A solar thermal system that uses natural means, such as the thermosyphon effect, for fluid flow and heat transfer.

Salt gradient solar pond: A solar pond that uses high salt concentration in the lowest layer and a concentration gradient in the middle layer to make those layers nonconvective.

Selective surface: A surface that has high absorptance in short wavelengths and low emittance in longer wavelengths.

Solar hybrid combined cycle: A hybrid of solar and natural gas turbine combined cycle.

Solar thermal collector: A solar collector that absorbs sunlight and converts it to heat.

References

ASHRAE. 1977. ASHRAE Standard 93-77, *Method of Testing to Determine the Thermal Performance of Solar Collectors*, ASHRAE, Atlanta, GA.

DeLaquil, P., Kearney, D., Geyer, M., and Diver, R. 1993. Solar thermal electric technology, Chapter 5 in *Renewable Energy Sources for Fuel and Electricity*, T.B. Johansson, M. Kelly, A.K.N. Reddy, and R.H. Williams, Eds., Island Press, Washington, D.C.

Duffie, J.A. and Beckman, W.A. 1980. *Solar Engineering of Thermal Processes*, John Wiley & Sons, New York.

Goswami, D.Y. 1986. *Alternative Energy in Agriculture,* Vol. I, CRC Press, Boca Raton, FL.

Gupta, B.P. 1987. Status and progress in solar thermal research and technology, in *Progress in Solar Engineering*, Ed. D.Y. Goswami, Hemisphere Publishing, Washington, D.C.

Mancini, T.R. 1994. The DOE solar thermal electric program, in *Proceedings of the 1994 IECEC*, pp. 1790–1975. AIAA, Washington, D.C.

Reid, R.L. 1987. Engineering design of salt gradient solar pond for thermal and electric energy, in *Progress in Solar Engineering*, Ed. D.Y. Goswami, Hemisphere Publishing, Washington, D.C.

Tabor, H. 1981. Solar ponds. *Solar Energy*, 27(3), 181.

Washom, B., Mason, W., Schaefer, J.C., and Kearney, D. 1994. Integrated Solar Combined Cycle Systems (ISCCS) Utilizing Solar Parabolic Trough Technology — Golden Opportunities for the 90s, paper presented at the 1994 ASES Annual Conference, San Jose, CA.

Winston, R. 1974. Principles of solar concentrators of novel design. *Solar Energy*, 16(2), 89.

Further Information

For solar heating and cooling:

Solar Engineering of Thermal Processes, by J.A. Duffie and W.A. Beckman, John Wiley & Sons, New York, 1980.

Principles of Solar Engineering, by F. Kreith and J.F. Kreider, Hemisphere Publishing, a division of Taylor and Francis, Washington, D.C., 1978.

For solar thermal power:

Solar Energy Fundamentals and Design, by W.B. Sine and R.W. Harrigan, John Wiley & Sons, New York, 1985.

8.11 Wind Energy Conversion*

Dale E. Berg

Introduction

Wind energy conversion machines have evolved over the past 2000 years, mostly by trial and error. Although there are many different configurations of wind machines, most of them can be classified as either horizontal-axis wind turbines (HAWTs), which utilize rotors that rotate about a horizontal axis parallel to the wind, or vertical-axis wind turbines (VAWTs), which have rotors that rotate about a vertical axis. Figure 8.11.1 illustrates the main features of both HAWTs and VAWTs. Figure 8.11.2 shows both types of turbines in a wind farm in the Altamont Pass area of California. HAWTs have all of their drivetrain equipment located on a tower, which makes servicing somewhat difficult, their blades are subjected to cyclic stresses due to gravity as they rotate, and they must be oriented with respect to the wind. However, they may be placed on tall towers to access the stronger winds typically found at greater heights. VAWTs, on the other hand, have most of their drivetrain on the ground, do not experience cyclic gravitational stresses, and do not require orientation with the wind. VAWTs, however, cannot be placed on tall towers to exploit the stronger winds at greater height, and their blades are subject to severe alternating aerodynamic loading due to rotation. The most common type of modern HAWT is the propeller-type machine, and these machines are generally classified according to the rotor orientation (upwind or downwind of the tower), blade articulation (rigid or teetering), and number of blades (generally two or three). The most common types of modern VAWTs are the Darrieus, with curved blades that are fixed in pitch, and the fixed-pitch, straight-bladed machines. The following discussion will focus on these types of turbines.

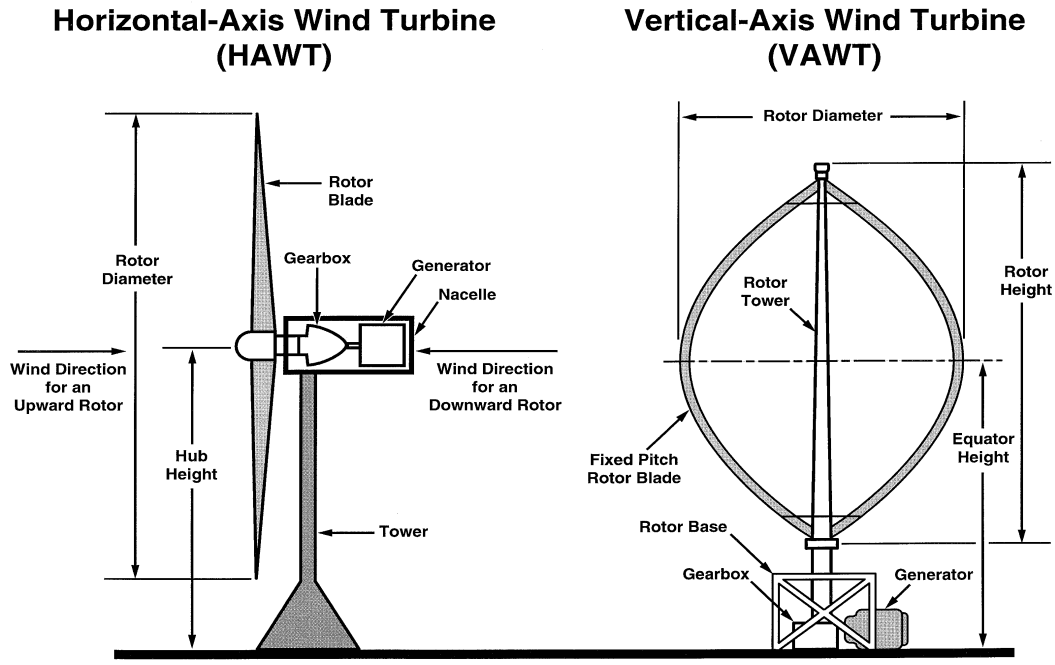

FIGURE 8.11.1 Wind turbine configurations.

* This work was supported by the United States Department of Energy under Contract DE-AC04-94AL 85000.

FIGURE 8.11.2 Wind farm both horizontal-axis and vertical-axis turbines.

While small and even medium-sized machines have been developed primarily through trial and error, developing larger, more-complex, and highly efficient machines this way becomes very expensive and time-consuming. A large cost-effective machine can be developed at a reasonable cost only if the designers can accurately predict the performance of conceptual machines and investigate the effects of design alternatives. In the past two decades numerous techniques to predict the aerodynamic and structural dynamic performance of wind turbines have been developed. These analytical models are not, in general, amenable to simple approximations, but must be solved with the use of computer codes of varying complexity. These models and codes will be summarized in the following sections.

Wind Turbine Aerodynamics

Items exposed to the wind are subjected to both drag (in the direction of the wind) and lift (perpendicular to the wind) forces. The earliest wind machines used drag to produce power. The European and American windmills discussed in Section 7 of Chapter 7 were primarily drag devices, but they did make some use of lift. Modern wind turbines rely on airfoil-shaped blades that generate large amounts of lift to produce power more efficiently than the drag machines. Let us consider how efficient these machines are at extracting energy from the wind.

Figure 8.11.3 illustrates the flow field about a translating drag device. The drag results from the relative velocity between the wind and the device, and the power that is generated by the device (the product of the drag force and the translation velocity) is given by

$$P = Dv = \left[0.5\rho(U - v)^2\right] C_D clv \tag{8.11.1}$$

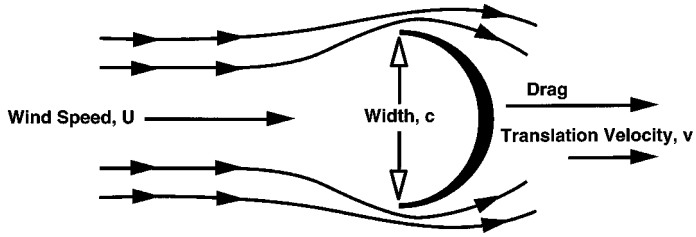

FIGURE 8.11.3 Schematic of translating drag device.

where

P = power extracted in watts
D = drag force per unit spanwise length in n/m
l = length of device (distance into the page) in m
v = translation velocity in m/sec
ρ = air density in kg/m^3
U = steady free-stream wind velocity in m/sec
C_D = drag coefficient; function of device geometry function
c = width of device (perpendicular to wind) in m

The velocity of the device must always be less than the wind velocity, or no drag is generated. The **power coefficient** (the ratio of the power extracted to the power available in the area occupied by the device) for this machine is

$$C_p = \frac{P}{0.5\rho U^3 cl} = \frac{v}{U}\left[1 - \frac{v}{U}\right]^2 C_D \tag{8.11.2}$$

Now consider a device that utilizes lift to extract power from the wind. Figure 8.11.4 illustrates an airfoil that is translating at right angles to the wind direction and is subject to both lift and drag forces. The relative velocity across this surface is the vector sum of the free-stream wind velocity and the wind speed induced by translation. The angle between the direction of the relative velocity and the chord line of the airfoil is termed the angle of attack α. In this case, the power is given by

$$P = 0.5\rho U^3 cl \frac{v}{U}\left[C_L - C_D \frac{v}{U}\right]\sqrt{1 + \left(\frac{v}{U}\right)^2} \tag{8.11.3}$$

where c = airfoil chord length in m and C_L, C_D = lift and drag coefficients, respectively; functions of airfoil shape and α. The power coefficient then is

$$C_p = \frac{v}{U}\left[C_L - C_D \frac{v}{U}\right]\sqrt{1 + \left(\frac{v}{U}\right)^2} \tag{8.11.4}$$

Figure 8.11.5 compares Equations (8.11.2) and (8.11.4) using $C_L = 1.0$ and $C_D = 0.10$ for the airfoil (easily achieved with modern airfoils) and a maximum drag coefficient of 2.0 for the drag machine. The airfoil has a maximum power coefficient of 15, compared with 0.3 for the drag device, or 50 times more power per unit of projected area. Moreover, operating a lifting device at velocities well in excess of the wind velocity is easily achieved with rotating machines.

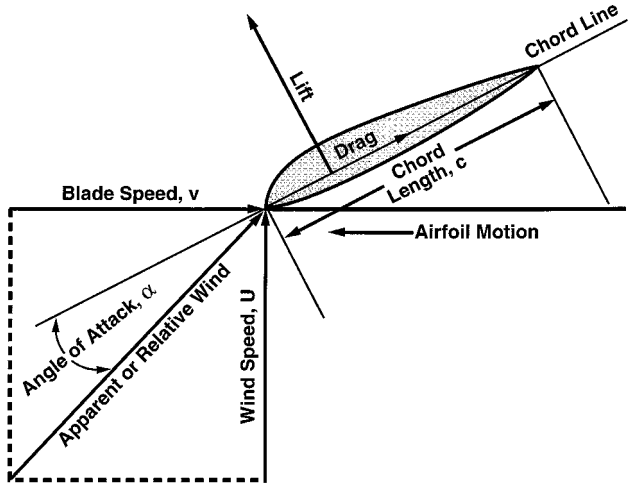

FIGURE 8.11.4 Schematic of translating lift device.

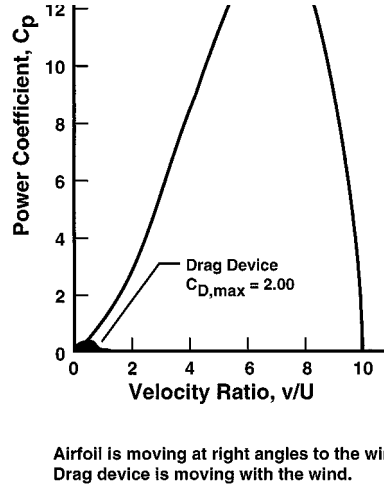

FIGURE 8.11.5 Comparison of power coefficients for a translating airfoil and a translating drag device. The airfoil is moving at right angles to the wind direction. The drag device is moving in the wind direction.

Machines discussed in this section utilize lift-producing blades to capture wind energy.

Aerodynamic Models

The aerodynamic analysis of a wind turbine has two primary objectives: (1) to predict the power produced by of the turbine and (2) to predict the detailed aerodynamic loads which will act on the turbine rotor blades. In general, the same models are used to accomplish both objectives. The aerodynamics of wind turbines are far too complex to model with simple formulas that can be solved with hand-held calculators; computer based models ranging from very simplified to very complex are required. The various models commonly used today are described below.

Momentum Models

The simplest aerodynamic model of a wind turbine is the actuator disk model or **momentum theory** in which the turbine is modeled as a single porous disk. In this model the axial force acting on the rotor or disk is equated to the time rate of change of momentum of the airstream passing through the rotor

or disk. By utilizing the conservation of mass, the conservation of axial momentum, the Bernoulli equation, and the first law of thermodynamics and by assuming isothermal flow, the power produced by the turbine (the product of the axial force and the air velocity at the disk) may be found to be

$$P = 2\rho AV^3 a(1-a)^2 \tag{8.11.5}$$

where V is the freestream wind velocity, $a = (V - v)/V$ and v is the wind velocity at the disk. The power coefficient for the turbine becomes

$$C_p = 4a(1-a)^2 \tag{8.11.6}$$

This is maximized for $a = {}^1/_3$, and we get $C_{p,\max} = 16/27 = 0.593$, the **Betz limit**, as the maximum fraction of available energy that can be extracted from the wind by a turbine.

The typical performance of various types of wind machines is compared with the Betz limit in Figure 8.11.6 where the variation of the turbine power coefficients with the **tip–speed ratio** (the ratio of the speed of the blade tip to the free-stream wind speed) are presented. Even though the maximum performance of modern HAWTs and VAWTs is well above that of the older machines, it still falls more than 10% below the Betz limit.

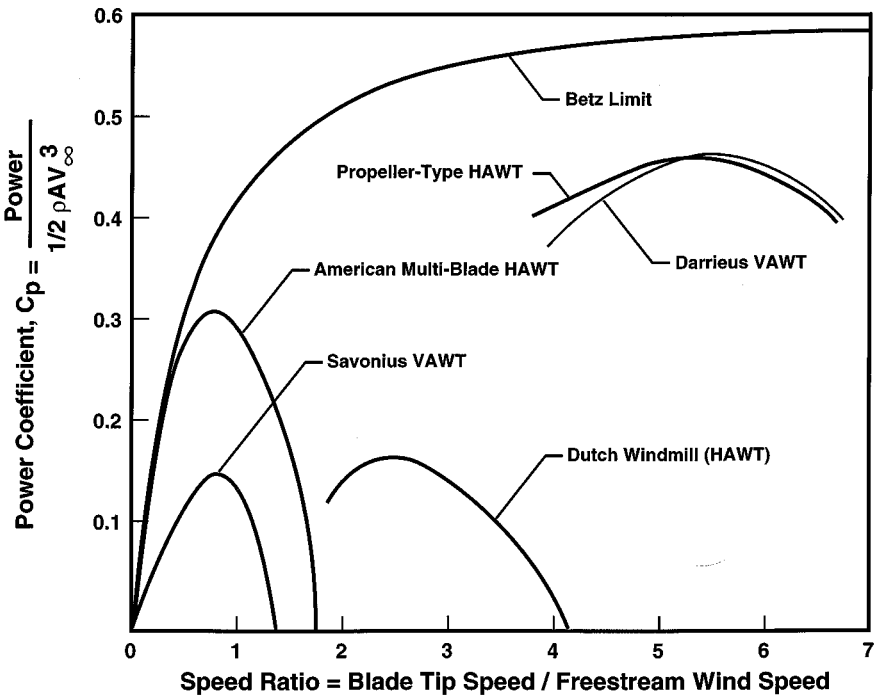

FIGURE 8.11.6 Typical performance of various types of wind turbines.

For HAWTs, momentum theory can be expanded to the blade element or strip theory, which includes the effects of blade lift and drag, wake rotation, and number and type of blades. Numerous corrections are applied to account for the three-dimensional flow near blade tips, the thick blade sections near the root, and gaps along the blade span. Additional information on these models may be found in Hansen and Butterfield (1993) and Wilson (1994).

Momentum theory may also be expanded for vertical-axis turbines into the multiple streamtube and the double-multiple streamtube theories that are the VAWT equivalent of the HAWT blade element theory. Additional information on these models may be found in Touryan et al. (1987) and Wilson (1994).

Wind shear and local Reynolds number variations may be readily accounted for with both the blade element and multiple streamtube methods. These models are extremely popular with wind turbine designers because they are simple, fast, and fairly accurate for performance prediction. However, they are very approximate methods based upon the assumption of steady flow and streamtubes that are fixed in time and space. More-complex models such as vortex and local circulation models are needed for the analysis of yawed flow, unsteady aerodynamics, and other complex flows, all of which can have large impacts on turbine performance and loads.

Vortex Models

Vortex models, based on the vorticity equation, can use either lifting line or lifting surface formulations for the blades with either free-wake or fixed- (or prescribed-) wake models, although there are a number of variations of these models. The three-dimensional, lifting-surface, free-wake formulation is the most physically realistic model, but a computer program implementing such a model will require a tremendous amount of computer resources and time. The problem with vortex codes is one of finding a balance between model simplification (and limitation) and computation time. Additional information on vortex models may be found in Strickland et al. (1981) and Kocurek (1987).

Local Circulation Method

The local circulation method (LCM) utilizes a balance between the force on the blade and the change in wind momentum as it passes through the rotor, similar to what is done with the momentum models. The blade, however, is represented as a superposition of imaginary blades of different spans with elliptical circulation distributions. Unlike the streamtube models, LCM models may be formulated to analyze unsteady flow, and are able to yield detailed flow field velocity and blade-loading information. The LCM yields better answers than the momentum models, avoids the convergence problems of the vortex models, and, with an appropriate wake model, requires far less computer time than the vortex models. However, this model has not been widely used. Additional information may be found in Nasu and Azuma (1983), Masse (1986), and Oler (1989).

Common Model Limitations

All of the aerodynamic models in use today use airfoil section characteristic tables (lift and drag coefficients as functions of angle of attack and Reynolds number) to determine the blade loading and turbine performance. Static two-dimensional wind tunnel test results or two-dimensional static airfoil design code predictions are modified with empirical, semiempirical, or analytic methods and used to estimate blade loads under three-dimensional, dynamic conditions. The greatest difficulty in obtaining accurate load predictions with any performance code is the determination of the appropriate airfoil section characteristics.

Additional information and references on turbine aerodynamics may be found in Hansen and Butterfield (1993) and Wilson (1994) for HAWTs and in Touryan et al. (1987) and Wilson (1994) for VAWTs.

Wind Turbine Loads

Wind turbine aerodynamic loads are of two types — the narrowband harmonic or cyclic loads resulting from the steady atmospheric wind, wind shear, rotor rotation, and other steady effects; and the broadband random loads resulting from nonuniformity or turbulence in the wind. The prediction of these loads is more complicated than the prediction of the aerodynamic performance and requires the use of computer-based models. The harmonic loads are generally predicted with the same codes that are used to predict wind turbine performance. The random loads are typically estimated with empirical relations, although a few analysts do utilize a performance code with a nonuniform wind model to predict them. A wind

turbine will experience hundreds of millions of loading cycles in a 30-year lifetime, and small errors that lead to underpredicting component loads can result in costly short-term component failure.

Accurate prediction of turbine performance does not guarantee accurate prediction of detailed aerodynamic loads — the performance predictions result from the integration of loads over the entire turbine, and significant errors may be present in the detailed loads but balance out in the performance predictions. While there is a considerable body of data showing good agreement of predicted performance with measured performance, there are very few data available against which to compare detailed aerodynamic load predictions.

Wind Turbine Dynamics

Horizontal-Axis Turbines

Horizontal-axis turbine designs usually use fairly rigid, high-aspect-ratio blades, cantilevered from a rigid hub and main shaft, although they may sometimes use relatively slender, quite flexible blades, attached to a less rigid hub and/or main shaft. This assembly rotates and yaws about a tower which may be flexible. These structures have many natural vibration modes, and some of them may be excited by the wind or the rotation frequency to cause a **resonance** condition in which the vibrations are amplified and cause large stresses in one or more components. Careful structural analysis during the design can ensure that the turbine that is built is dynamically stable under turbine operating conditions. Ignoring the structural analysis or failing to properly conduct parts of it will likely result in a machine that experiences resonances and fails very quickly. Relatively rigid systems are less likely to experience these stability problems than are very flexible, highly dynamic systems.

Detailed analysis of the structural response of a turbine is a rather daunting task requiring the formulation and solution of the full governing equations of motion, usually performed with a finite-element structural model. Those equations must account for the interaction between the blades and the steady centrifugal forces, the time-dependent gravitational forces, the steady and oscillatory aerodynamic forces, and the Coriolis forces. They must also model nonsteady airflow, the yaw motion of the nacelle, pitch control of the blades, teetering blades, the interaction between the rotor and the supporting tower, starting and braking sequences, etc. The rotor must be modeled in a rotating coordinate frame with time-dependent coefficients, while the tower must be modeled in a fixed coordinate frame, with the exciting forces arising from the nonlinear, time-dependent coupling of the rotor and the time-dependent loading of the wind.

Malcolm and Wright (1994) provide a list of some of the available HAWT dynamics codes that have been developed, together with their limitations.

Vertical-Axis Turbines

Darrieus turbine designs normally use relatively slender, high-aspect-ratio structural elements for the blades and supporting tower. The result is a very flexible, highly dynamic structure, with many natural modes of vibration which, again, must be carefully analyzed to ensure that the turbine is dynamically stable under all operating conditions. Typically, the guy cables and turbine support structure can be analyzed with conventional methods, but the tower and blades require a more refined analysis, usually performed with a finite-element structural program.

The blades and tower must be modeled in the rotating coordinate frame with time-independent coefficients. The equations of motion are determined by the steady centrifugal and gravitational forces, the steady and oscillatory aerodynamic forces, and the Coriolis forces, together with the turbine physical properties. Detailed information on the modeling may be found in Lobitz and Sullivan (1983).

Aerodynamic Loads/Blade Motion Coupling

The blades themselves are driven by aerodynamic as well as structural dynamic forces. The motion of slender, high-aspect-ratio blades may couple with the aerodynamic loads acting on them. This coupling may increase the motion of the blades, creating a potentially fatal condition known as flutter instability,

or it may decrease the motion of the blades, creating a beneficial condition known as aerodynamic damping.

Stochastic Wind Effects

The wind is **stochastic** in nature, with significant short-term variations in both direction and velocity. As turbines become larger, the relative extent of these variations becomes smaller than the size of the turbine, and the effects become more pronounced. Analysis of the effect of fluctuating wind loads on the response of the turbine shows an increase in the broadband response, accompanied by a decrease in the magnitude of the dominant narrowband responses at multiples of the rotation frequency. This increase in broadband response can include excitation of turbine vibration modes that are close to a narrowband response frequency, but that are not predicted to be excited by a uniform wind (Lobitz, 1984).

Wind Turbine Controls

In general, wind turbines are designed to operate when the incident wind is high enough to generate electricity and to shut down when the wind speeds exceed 25 to 30 m/sec. In spite of the tremendous amount of power which is present in the high winds, the amount of energy that can be captured is usually more than offset by the fatigue damage that is sustained by the turbine.

Brakes

Most turbines utilize mechanical brakes, frequently in conjunction with aerodynamic brakes, to stop the rotor and to keep it from rotating when the turbine is not generating electricity. A few turbines rely solely on aerodynamic braking devices to accomplish this. Whatever type of braking system is used, it should be a fail-safe design that will automatically activate to slow or stop the rotor in the event of an electrical system failure.

Yaw Systems

Virtually all upwind and a few downwind HAWT turbines incorporate an active yaw control system, using wind-direction sensors and electric or hydraulic drive motors, to orient the rotor with respect to the wind. VAWTs do not require yaw systems.

Peak Power Regulation

All turbines incorporate some method of limiting the peak power produced. This enables the generator to operate near its design power rating, where it is most efficient, over a range of wind speeds. The increase in generator efficiency at lower wind speeds, together with the lower cost of the drivetrain, more than offset the energy that is lost as a result of power limiting. Most horizontal-axis turbines use one of three common techniques to limit peak power — stall regulation with fixed-pitch blades (passive control), full- or partial-span pitch control, or partial-span control surfaces such as ailerons and/or flaps. With stall regulation, the blades are designed so that airfoil **stall**, which creates decreased lift and increased drag, limits the power output in high winds. However, rotor drag loads continue to increase as the wind speed increases. Another disadvantage is the difficulty of controlling aerodynamic loads in deep stall. With full- or partial-span blade pitch control, peak power is controlled by decreasing blade pitch angle as wind speed increases, limiting peak power and decreasing rotor drag loads. A major disadvantage of pitch control is the poor peak power control during high-wind stochastic (or turbulent) conditions — power excursions can exceed twice the rated power levels before the pitch-control system can respond. Partial-span control surfaces limit the peak power by decreasing the lift and increasing the drag of a portion of the airfoil. They can respond to wind changes somewhat faster than full-span pitch control systems can. Sample power curves for both stall and pitch-regulated turbines are shown in Figure 8.11.7.

Several other methods of pitch control have also been used, but on a limited basis. Passive pitch-control techniques automatically adjust the blade pitch angle using cams activated by centrifugal loads or using tailored blade materials that permit the blade to twist as the aerodynamic loads increase. The

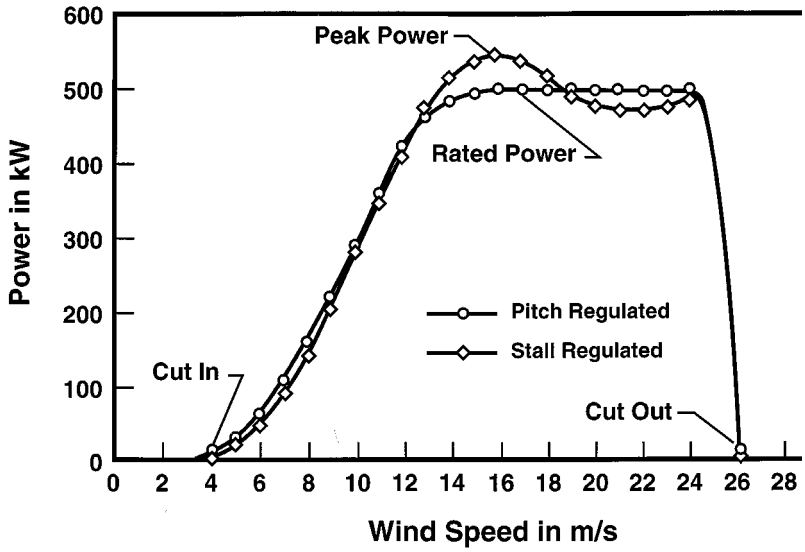

FIGURE 8.11.7 Sample power curves for stall-regulated and pitch-regulated wind turbines.

Italian Gamma 60 turbine utilizes a novel means to control peak power — it is the only large-scale turbine that yaws a fixed-pitch rotor out of the wind to limit rotor power.

Virtually all VAWTs utilize stall regulation with fixed-pitch blades to control peak power.

Controller

Every wind turbine contains a controller, usually a microprocessor-based system, to control turbine operations. The basic turbine controller will start and stop the machine and connect or disconnect the generator output lines to the grid, as needed; control the operation of the brake system; control the operation of the yaw and pitch systems, if present; perform diagnostics to monitor the operation of the machine; and perform normal or emergency shutdown of the turbine as required. However, the controller can incorporate many other functions as well, functions such as recording turbine performance characteristics and controlling the operating state of a variable-speed machine.

Wind Turbine Electrical Generators

Once a wind turbine has converted the kinetic energy in the wind into rotational mechanical energy, the energy is usually converted into electricity which can be readily transported to where it is needed. While small wind turbines may utilize permanent magnet alternators to generate electricity, most grid-connected turbines today use either synchronous or induction electrical generators. Induction machines are cheaper than synchronous machines, are easier to control, and provide some power train damping, but they require reactive power that must be supplied by the grid. This can cause problems, but those problems can be usually be solved fairly quickly and at low cost.

Generator efficiency drops off rapidly as the generated power falls below the rated generator capacity, and single-generator systems tend to be very inefficient at low wind speeds where there is little power available in the wind. Some systems address this by having a second, smaller generator which is used for low-wind operation, where it operates close to its rated power. At higher winds, the smaller generator is disconnected and the larger generator is used. Similar results can be obtained with a single generator utilizing pole switching or dual windings. The two-generator operation may yield a sizeable increase in energy capture, but the additional costs of the smaller generator or the generator modification and additional controls must be balanced against the increased energy capture to determine if this is cost-effective.

While most turbines operate at a single fixed rotational speed, some operate at two or more fixed rotational speeds, and some operate anywhere within a range of speeds. Variable-speed turbine operation offers two major advantages over fixed-speed operation:

1. The aerodynamic efficiency of the rotor at low to moderate wind speeds may be improved by more closely matching the rotor speed to the short-term average wind speed. At higher wind speeds, the blades are either in stall or are pitched to control peak power, so matching rotor speed to wind speed is less important.
2. System dynamic loads are attenuated by the "flywheel" action of the rotor as it speeds up and slows down in response to wind gusts.

In addition, variable speed permits the operation of the turbine in a variety of modes, including operation at maximum efficiency for all wind speeds to maximize energy capture or operation to minimize fatigue damage. However, certain rotational speeds within the operating-speed range will likely excite turbine vibration modes, causing resonance and increased rates of fatigue damage. These rotational speeds must be avoided during operation, and turbine control can become quite a complicated issue.

Variable-speed operation, in general, generates variable-frequency power. Most applications, including interfacing with power grids, require high-quality power at a reference frequency. Sophisticated power electronics may be used to accomplish this interface (Smith, 1989).

Wind-Diesel Systems

Wind turbines are increasingly being coupled with diesel engine-powered generators to create **wind-diesel systems**. In these systems, the diesel engine provides dependable, consistent power and the wind turbines generate some of the power, reducing the engine fuel consumption and the system cost of energy. A large variety of wind-diesel systems and concepts have been investigated over the past decade (Infield, et. al., 1992). Although quite a few of these have been technically successful, very few of them have been commercially successful. While the potential market for wind-diesel systems appears to be very large, it has yet to materialize, for the reliability of the technology has not yet been well proven.

Water-Pumping Applications

The multibladed, mechanical windmill (the so-called "American" windmill) with a mechanical piston pump has been used for over a century to pump water in remote areas. Over the past few years some changes to improve operation in low wind speeds have been made to the design of these machines.

Researchers at the U.S. Department of Agriculture facility at Bushland, Texas have reported considerable success in using variable-voltage, variable-frequency electricity produced by small stand-alone wind turbines to directly power submersible water pumps. Clark (1994) compares the pumping performance of one of these wind–electric systems and that of the traditional American windmill with a piston pump. He found that the wind–electric system performed significantly better than the mechanical system, even though the price of the two systems was nearly identical. The wind–electric system offers another advantage as well — while the windmill for the mechanical pump must be mounted directly over the well, the wind turbine for a wind–electric system may be mounted some distance away, at a better wind location.

Defining Terms

Betz limit: Maximum fraction of available wind energy that can be extracted by a wind turbine rotor, according to momentum theory.
Momentum theory: A method of estimating the performance of a turbine by equating the time rate of change of air stream momentum through the turbine to the force acting on turbine blades.
Power coefficient: The ratio of captured energy to the energy available in the reference area.

Resonance: A vibration of large amplitude caused by a relatively small excitation at or near a system natural frequency.

Stall: A condition in which an airfoil experiences a decrease in lift and a large increase in drag.

Stochastic: Containing variations from a smooth, uniform flow.

Tip-speed ratio: The ratio of the speed of the blade tip to the free-stream wind speed.

Wind–diesel system: An electrical-generation system that utilizes both diesel engine–powered generators and wind turbines to create a dependable, consistent power system.

References

Clark, R.N. 1994. Wind-electric water pumping systems for rural domestic and livestock water, in *Proceedings of the 5th European Wind Energy Association Conference and Exhibition,* Macedonia, Greece, pp. 1136–1140.

Hansen, A.C. and Butterfield, C.P. 1993. Aerodynamics of horizontal-axis wind turbines, *Ann. Rev. Fluid Mech.,* 25, 115–149.

Infield, D., Scotney, A., Lunsager, P., Binder, H., Uhlen,K., Toftevaag, T., and Skarstein, O. 1992. Wind diesel systems — design assessment and future potential, paper presented at Sixth International Wind–Diesel Workshop, Prince Edward Island, Canada.

Kocurek, D. 1987. Lifting surface performance analysis for horizontal axis wind turbines, *SERI/STR*-217, 3163.

Lobitz, D.W. 1984. NASTRAN-based software for the structural dynamic analysis of VAWTs and HAWTs, paper presented at European Wind Energy Conference, Hamburg, p. 385

Lobitz, D.W. and Sullivan, W.N. 1983. A comparison of finite element prediction and experimental data for forced response of DOE 100 kW VAWT, in *Proceedings of the Sixth Biennial Wind Energy Conference and Workshop*, Minneapolis, MN, pp. 843–853.

Malcolm, D.J. and Wright, A.D. 1994. The use of ADAMS to model the AWT-26 prototype, in *Proceedings of 1994 ASME Wind Energy Symposium*, New Orleans, LA, pp. 125–132

Masse, B. 1986. A local-circulation model for Darrieus vertical-axis wind turbines, *J. Propulsion Power,* 2 (March-April) 135–141.

Nasu, K. and Azuma, A. 1983. An experimental verification of the local circulation method for a horizontal axis wind turbine, paper presented at 18th Intersociety Energy Conversion Engineering Conference, Orlando, FL.

Oler, J.W. 1989. A discrete local circulation model for Darrieus turbines, in *Proceedings of the Eighth ASME Wind Energy Symposium,* Houston, TX, pp. 65–69.

Smith, G.A. 1989. Electrical control methods for wind turbines, *Wind Eng.,* 13(2), 88–98.

Strickland, J.H., Smith, T., and Sun, K. 1981. A vortex model of the Darrieus turbine: an analytical and experimental study, SAND81-7017, Sandia National Laboratories, Albuquerque, NM.

Touryan, K.J., Strickland, J.H., and Berg, D.E. 1987. Electric power from vertical-axis wind turbines, *J. Propulsion Power,* 3(6), 481–493.

Wilson, R.E. 1994. Aerodynamic behaviour of wind turbines, in *Wind Turbine Technology, Fundamental Concepts of Wind Turbine Engineering,* D. Spera, Ed., ASME Press, New York, 215–282.

Further Information

Excellent summaries of HAWT and VAWT aerodynamics, together with extensive reference lists, are presented by Craig Hansen and Sandy Butterfield in their paper "Aerodynamics of Horizontal-Axis Wind Turbines" in the *Annual Review of Fluid Mechanics*, 1993, and by Ken Touryan, Jim Strickland, and Dale Berg in their paper "Electric Power from Vertical-Axis Wind Turbines" in the *Journal of Propulsion,* Volume 3, Number 6, 1987.

The latest developments in the field of wind energy in the U.S. and Europe may be found in the following:

Proceedings of the ASME Wind Energy Symposium, published annually by the American Institute of Aeronautics and Astronautics, 1801 Alexander Bell Drive, Suite 500, Reston, VA 20191–4344.

Proceedings of Windpower, the annual American Wind Energy Association (AWEA) conference, published annually by AWEA, 122 C St. NW, 4th Floor, Washington, D.C. 20001.

Proceedings of the European Wind Energy Association, published annually by EWEA, Eaton Court, Maylands Avenue, Hemel Hempstead, Hertforshire HP2 7TR, England.

8.12 Energy Conversion of the Geothermal Resource

Carl J. Bliem and Gregory L. Mines

This section discusses the uses of the geothermal resource. The primary use of the energy from geothermal resources to date has been in the production of electrical energy. Other applications, such as process heat and space conditioning, have also been made and will be discussed under the topic of direct use. This section begins with a discussion of the geothermal resource as it applies to the use of the energy. Then discussion of the three types of electrical generating facilities presently in use: — the **direct steam system**, the **flashed steam system**, and the **binary system** — is given. Finally, some discussion of direct-use applications is given.

Geothermal Resource Characteristics Applicable to Energy Conversion

Geothermal energy as defined here applies to hot fluids under pressure found at a reasonable depth (1 to 2 km) in the earth's crust. If one disregards the complex geological details relating to the formation of such naturally occurring reservoirs of hot fluids, Figures 8.12.1 and 8.12.2 present schematic representations of these reservoirs. High-temperature fluid (200 to 300°C) is created by the convection of water through the porous rock. As the water circulates, it dissolves various amounts of minerals containing sodium, potassium, calcium, silica, carbonates, and chlorides and gases such as nitrogen and carbon dioxide. In **geopressured resources** of the Gulf of Mexico, high pressures and significant amounts of dissolved methane are seen.

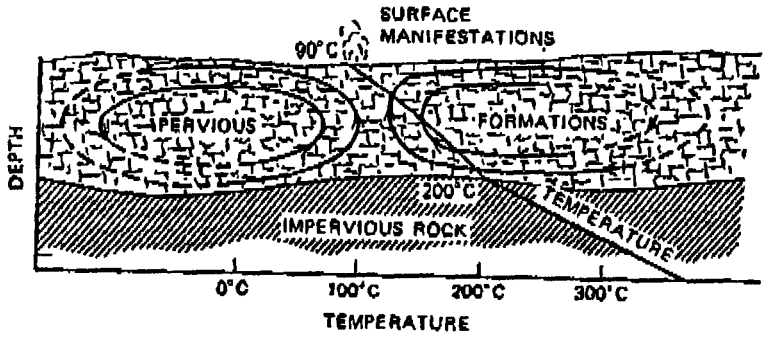

FIGURE 8.12.1 Schematic diagram of the convective cells in a geothermal reservoir. (From Kestin, J., Ed., Sourcebook on the Production of Electricity from Geothermal Energy, U.S. DOE, DOE/RA/4051-1, Washington, D.C., 1980).

The convective cells operate over large horizontal distances of as much as 30 km. The time in which the transfer of energy from the magma to the water takes place is of the order of 10^5 to 10^6 years. At the present time, it is difficult to say whether or not the resource can be considered "renewable." If natural circulation or the injection of spent geothermal liquid into the reservoir can make up for the liquid extracted during the energy conversion process, the reservoir can be considered at least of a very long life. (Individual wells generally have a life of about 10 years.)

The resources considered in this section are said to be **hydrothermal**. (Work is being done on creating artificial reservoirs by injecting water into hot dry rock, but this development is in its early stages and will not be considered here. The geopressured resource will not be considered either.)

As the geofluid is extracted from a reservoir, it flows to a region of lower static pressure. If this pressure falls below the saturation pressure for the temperature of the geofluid (close to but not equal to the saturation pressure of pure water because of the presence of the dissolved solids and gases), the

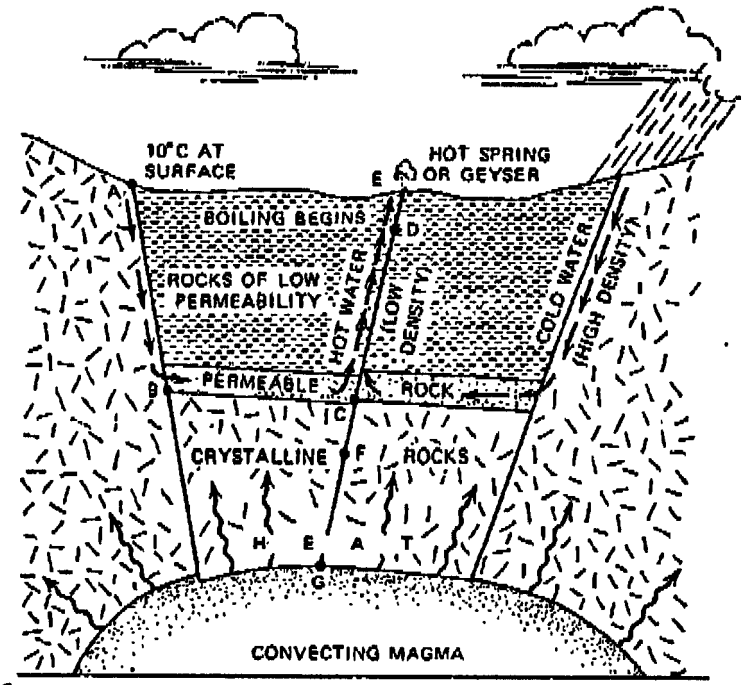

FIGURE 8.12.2 Schematic diagram of a characteristic geothermal reservoir. (From Kestin, J., Ed., Sourcebook on the Production of Electricity from Geothermal Energy, U.S. DOE, DOE/RA/4051-1, Washington, D.C., 1980).

geofluid will flash into steam. Therefore, the person using this energy source may have a number of different physical forms to consider:

1. Wet steam from a *vapor-dominated resource*;
2. Superheated or saturated steam from a vapor-dominated resource;
3. Liquid at a pressure above the saturation pressure from a *liquid-dominated resource*;
4. A mixture of liquid and vapor at a relatively low quality from a liquid-dominated resource.

Electrical Energy Generation from Geothermal Resources

The type of energy conversion system used to produce electrical power depends on the type and quality (temperature) of the geothermal resource. Vapor-dominated resources use systems where steam is expanded directly through a turbine, similar to conventional fossil fuel steam plants. Liquid-dominated resources use flash steam systems and binary systems, with binary systems predominantly used for the lower-quality resources. The term **binary system** is used to describe a power cycle where the geothermal fluid provides the source of thermal energy for a closed-loop Rankine cycle using a secondary working fluid. In this closed loop, the working fluid is vaporized using the energy in the geofluid, expanded through a turbine, condensed, and pumped back to the heater completing the closed loop.

Hydrothermal resources typically contain varying amounts of numerous dissolved minerals and dissolved gases. In power cycles where steam is extracted from the geothermal resource directly (vapor dominated) or indirectly (flashing liquid dominated) and expanded through a condensing turbine, the design and operation of the power cycle must account for the removal of the noncondensable gases. If the gases are not removed from the condenser, they will accumulate in the condenser, raising the turbine back pressure and decreasing the power output. In systems where the liquid geofluid is handled (binary cycle heat exchangers and piping and flash steam flash tanks and piping), measures must be taken to

prevent the precipitation of the dissolved solids and/or to provide a means of removal of the resulting scale.

Direct Steam Systems — Vapor-Dominated Resources

For a geothermal resource producing a superheated or saturated vapor steam (Case 2), the vapor from the geothermal production well is sent to a conventional steam turbine as shown in Figure 8.12.3. (This is done after appropriate removal of rocks and debris and possibly after scrubbing with water to remove corrosive substances.) Normally, the turbine is a condensing type, as shown in the figure, although in some applications a back-pressure turbine is used, exhausting the steam to the atmosphere. The back-pressure turbine is typically used for small systems with the possible later addition of another turbine and a condenser to increase the power generated by the geofluid flow from the wells.

Figure 8.12.3 shows a system with a direct-contact condenser and a wet cooling tower. In this type of system, the condensate from the condenser is more than enough to make up the evaporation and blowdown from the cooling tower. Therefore, the figure shows some of the condensate being injected into the reservoir. In many cases, direct-contact condensers are not feasible because of the hydrogen sulfide in the steam which would be released in the cooling tower exhaust. When hydrogen sulfide is in the steam, the majority of it appears as noncondensable and the noncondensable gas from the condensers must be treated. For these systems, surface condensers are normally used in conjunction with wet cooling towers. The actual hardware configuration is dictated by the process for removal of the sulfur. Again, some of the condensate can be used for cooling tower makeup if the sulfur is removed from the process. A number of processes have been developed to remove sulfur from the process.

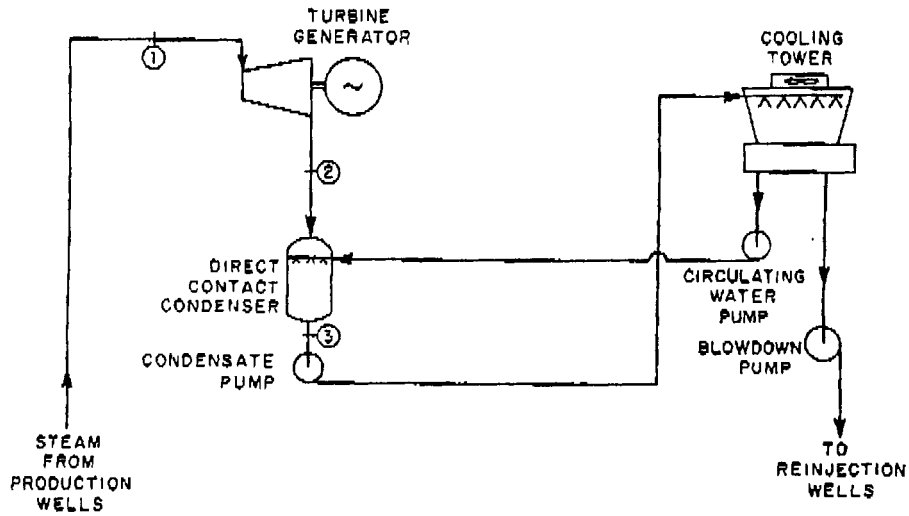

FIGURE 8.12.3 Schematic diagram of a direct dry-steam plant. (From Kestin, J., Ed., Sourcebook on the Production of Electricity from Geothermal Energy, U.S. DOE, DOE/RA/4051-1, Washington, D.C., 1980).

Figure 8.12.4 depicts a system which is similar to the one described above, but one which receives wet steam (Case 1). Here, the liquid is separated from the vapor prior to the entry of the vapor into the turbine. Otherwise, the system is the same as the one in Figure 8.12.3 and the same comments apply.

Flash Steam Systems — Liquid Dominated Resources

When the geofluid is flashed before it leaves the well, flash steam systems are generally used. This indicates that the resource is at a relatively high temperature. Figures 8.12.5 and 8.12.6 depict single- and dual-flash systems schematically. The single-flash system in Figure 8.12.5 is quite similar to the system in Figure 8.12.4. The only difference is that the geofluid pressure is dropped further before the steam is separated and sent to the turbine. An optimum flash pressure exists because the lower the flash

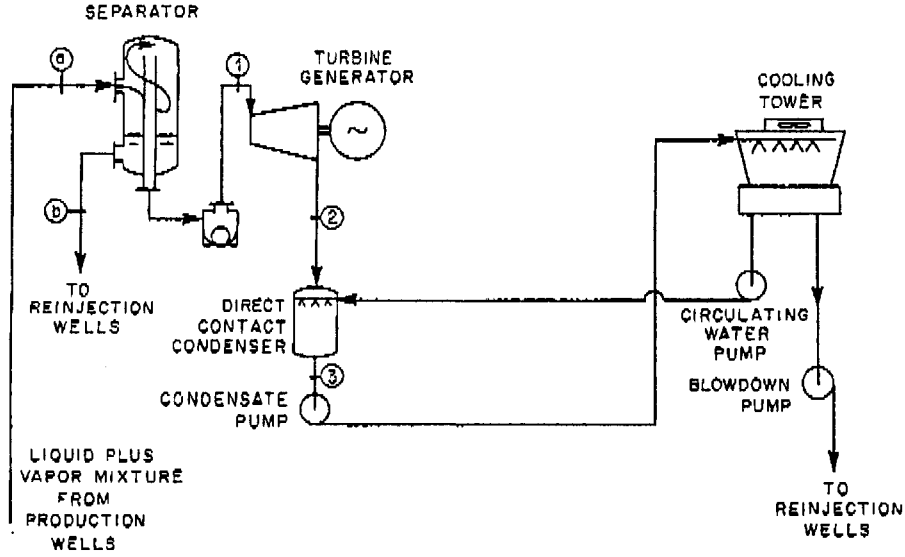

FIGURE 8.12.4 Schematic diagram of a plant using a two-phase resource. (From Kestin, J., Ed., Sourcebook on the Production of Electricity from Geothermal Energy, U.S. DOE, DOE/RA/4051-1, Washington, D.C., 1980).

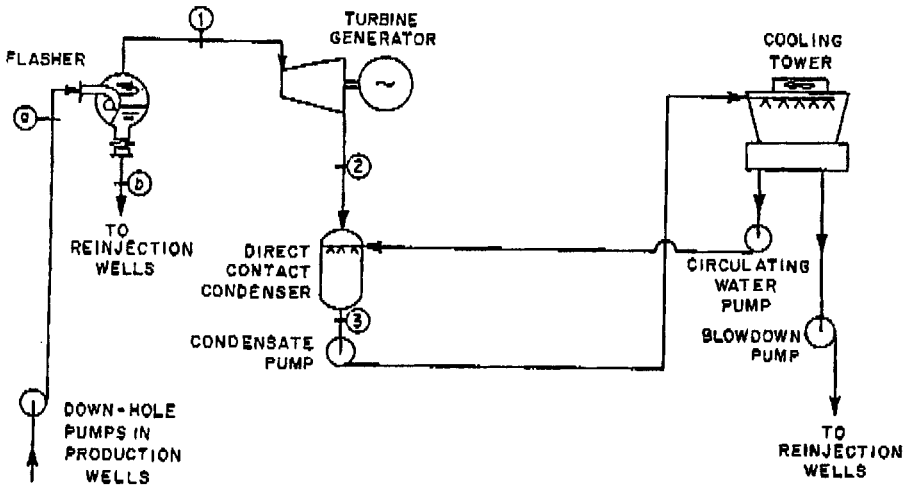

FIGURE 8.12.5 Schematic diagram of a single-flash plant. (From Kestin, J., Ed., Sourcebook on the Production of Electricity from Geothermal Energy, U.S. DOE, DOE/RA/4051-1, Washington, D.C., 1980).

pressure, the more steam which is evolved. However, the work done per unit mass of steam flowing through the turbine will also decrease with the lower flash pressure. For a given set of geofluid conditions entering the plant, a flash pressure exists that will maximize the energy produced per unit mass of geofluid and also minimize the levelized energy cost (LEC). The performance and cost optima will be near, but not generally at the same pressure.

The flash steam system can also be utilized in applications where the fluid enters the plant as a liquid (single phase). In these systems, the geothermal fluid is throttled with an expansion valve to the desired flash pressure. This flashing process can be considered adiabatic, where the amount of steam evolved can be determined from energy and mass balances of a simple throttling calculation.

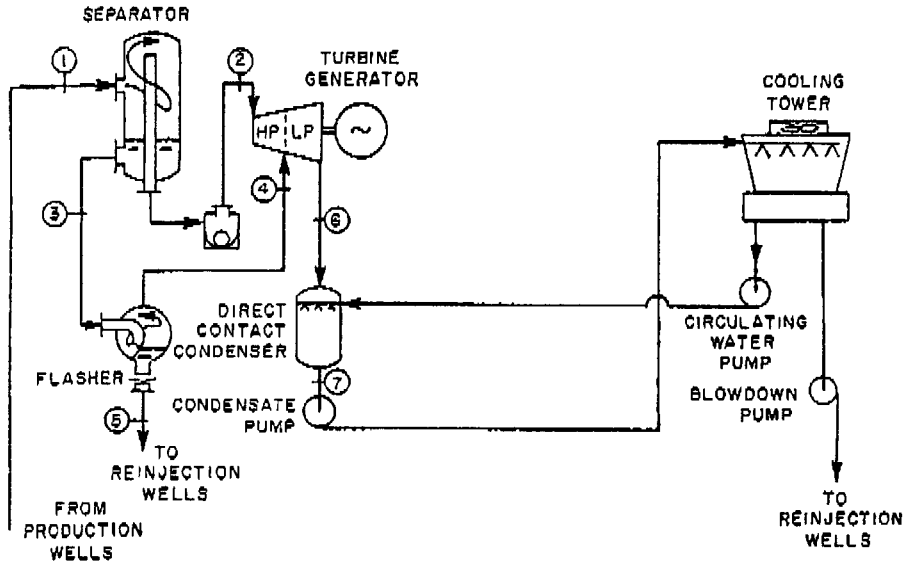

FIGURE 8.12.6 Schematic diagram of a dual-flash plant. (From Kestin, J., Ed., Sourcebook on the Production of Electricity from Geothermal Energy, U.S. DOE, DOE/RA/4051-1, Washington, D.C., 1980).

Most successful flash systems are dual flash. The first flash is generally near the well-head pressure and the second flash near atmospheric pressure. The low-pressure flash is normally kept above atmospheric pressure to prohibit leakage of air into the system in the flasher. Some recent studies have indicated that for low-temperature resources, a subatmospheric second flash would produce a cost-effective system. Again, optimization of the two flash pressures is necessary to minimize the LEC. In cases in which the geofluid has a high dissolved solid content, flash crystallizers are used to remove the precipitated dissolved solids. The flashing process releases carbon dioxide dissolved in lowering the geofluid pH, which causes the precipitation of insoluble carbonates. The solubility of silica is temperature dependent; lowering the geofluid temperature causes the precipitation of silica.

None of the steam cycles depicted provides for the removal of the noncondensable gases from the condenser. This removal is typically accomplished with steam ejectors or compressors which continuously remove the small stream of vapor from the condenser. Some steam is lost in this process of removing the noncondensable gases.

Binary Systems — Liquid-Dominated Resources

Recent studies have shown that for resources below 200°C, current technology binary systems have lower LEC than flash steam plants for liquid-dominated resources. Figure 8.12.7 shows a typical binary system with an evaporative heat-rejection system. This type of heat-rejection system has been replaced by air-cooled condensers in most applications. In the areas where the geothermal resource exists, there is little excess water for makeup in the cooling tower, as shown in Figure 8.12.7. All of the cooled geofluid in a binary system is typically injected back into the reservoir. This provides an environmentally acceptable means of disposal of the fluid and, more important, provides a recharge of the reservoir to maintain the reservoir productivity.

The binary cycle is an attempt to reduce the scaling potential of the geofluid. Carbonates are precipitated when the pressure of the geofluid is reduced and carbon dioxide comes out of solution as the geofluid flashes. With downhole pumps in the wells, this can be eliminated by keeping the fluid pressurized. Some resources do not require pumps to maintain the flow and pressure necessary to eliminate flashing (artesian flow). Similarly, if the exit temperature of the geofluid remains above some minimum value, silica will not be precipitated. These two operational strategies limit the scaling in a binary plant. Any constraint imposed on the geofluid exit temperature will impact the design of the

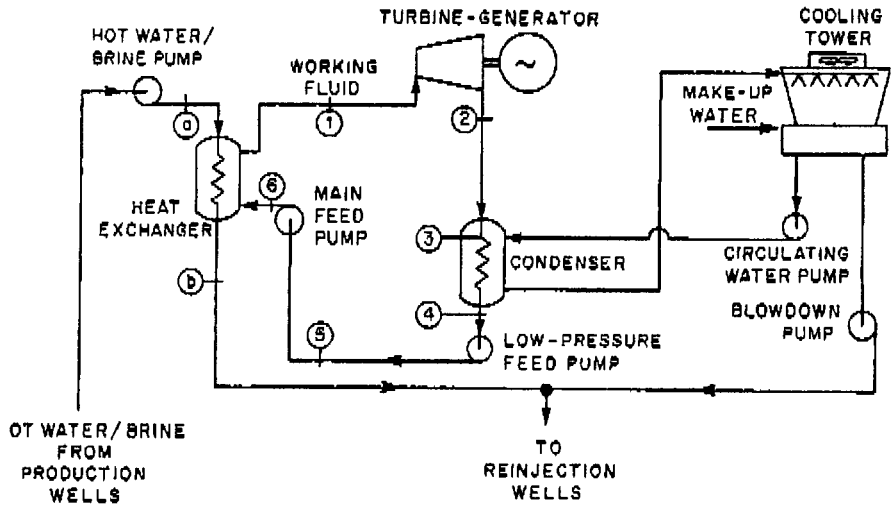

FIGURE 8.12.7 Schematic diagram of a binary plant. (From Kestin, J., Ed., Sourcebook on the Production of Electricity from Geothermal Energy, U.S. DOE, DOE/RA/4051-1, Washington, D.C., 1980).

binary plant, affecting the selection of turbine inlet conditions as well as the possible choice of working fluid.

The binary cycle consists of a closed loop of a working fluid normally performing a Rankine cycle. Most existing binary cycles use isobutane, pentane, or isopentane as working fluids. Studies have indicated that mixtures of hydrocarbons, e.g., 96% isobutane/4% hexane, will produce better utilization of a 180°C resource and in some instances lower LEC.

The performance of the binary system depends on a number of factors. Some plant designs incorporate multiple or staged boiling cycles, where the working fluid flow is split and boiling occurs at multiple pressures. In these cycles, multiple or staged turbines are required. The advantage of these cycles is the fact that the working fluid heat-addition process more closely matches the sensible cooling of the liquid geofluid (as shown on the T-Q or T-h diagram). This lowers temperature differences through the cycle, reducing cycle irreversibilities and increasing performance. The same effect can be achieved by heating the working fluid at supercritical pressures (pressures above the critical pressure). While the supercritical cycle will have higher component, material, and pumping costs because of higher operating pressures, they have fewer components because they are less complex than multiple boiling cycles. (In many cases, the maximum pressure can be kept below 600 psi with hydrocarbons such as isobutane.) Lowering the mean temperature difference in heat exchangers tends to require larger units so that capital costs are increased. In general, the LEC is reduced because the effects of increased performance more than outweigh the increase in capital cost.

The choice of the working fluid for the power cycle will also impact the cycle performance. In general, as resource temperature decreases, the more volatile fluids will produce more power per unit mass of geofluid. Power cycles using the more volatile fluids typically operate at higher pressures and have higher associated material and equipment cost. These higher costs may offset the gains in performance and produce higher LECs in some cases.

Working fluid mixtures have been shown to provide superior performance to the single component or pure working fluids. This performance improvement is due to the nonisothermal phase changes of this type of fluid at constant-pressure (both boiling and condensing), which allows the working fluid to match more closely the sensible cooling of the geofluid. More importantly in the reduction of irreversibilities, the desuperheating and condensing process more closely matches the sensible heating of cooling water or air in the heat-rejection process.

One additional type of binary cycle that has been proposed uses an ammonia-water mixture for the working fluid. A great deal of recuperative preheat of the working fluid is accomplished by splitting the duty of the geofluid, turbine exhaust, and preheated liquid flows through a more complex heat-transfer train than is shown in Figure 8.12.7. These systems are known as **Kalina systems**. In general, these systems do not change the composition of the mixture in the cycle as the Kalina cycle for applications such as is the case for gas turbine bottoming.

There is some consideration of using a binary cycle as a bottoming cycle for a flash steam or direct steam system. Similarly, a binary cycle could be used to bottom another binary system, perhaps with a different working fluid.

Design Considerations

The selection of the working fluid in binary cycles imposes safety considerations to be considered in the design of the power plant. Equipment and facility designs must take into account the flammable characteristic of the hydrocarbon working fluids.

The selection of materials of construction for the piping and components exposed to the geofluid will be resource specific. Typically, carbon steel is used for piping and pressure vessels. Turbines that use the steam directly may have stainless steel components, although the use of stainless may be limited by the presence of chlorides and the potential for stress cracking. The standard design for heat exchangers in binary cycles is for the geofluid to be on the tube side. This facilitates the cleaning of the exchanger if scaling or fouling occurs on the surfaces exposed to the geofluid. If the geofluid has a high scaling potential, components and piping should be designed to allow for periodic cleaning.

Direct Use of the Geothermal Resource

A number of direct-use applications of the heat in a geothermal resource have been successfully implemented. These include

1. Space conditioning (heating with the resource or a secondary fluid and cooling with heat pumps);
2. Heating of greenhouses;
3. Aquaculture;
4. Process heating (drying vegetable products);
5. Ground coupled heat pumps.

Although the United States is one of the world leaders for the production of electrical power from geothermal energy, other nations take the lead for the direct use of this energy source. In Iceland, over 85% of the buildings are supplied with heat and domestic hot water from geothermal systems (Ragnorson, 1995).

Typical direct-use applications are either closed systems with produced fluids being injected back into the geothermal reservoir or systems where the produced water is pure enough for beneficial use or disposal to surface waterways. Experience has shown that it is usually worthwhile to inject as much of the cooled fluid as possible back into the reservoir to maintain pressure and production rates.

Defining Terms

Binary system: A binary system that uses thermal energy from the geofluid to vaporize a secondary working fluid in a Rankine cycle.

Direct steam system: A geothermal energy conversion system that utilizes steam directly from a geothermal well.

Flashed steam system: A geothermal energy conversion system that utilizes steam flashed from the liquid geofluid.

Geopressurized resource: Naturally occurring reservoirs of hot pressurized fluid created by convection of water through hot porous rock.

Hydrothermal resource: Artificial reservoirs created by injecting water into hot dry rock in the earth's core.

Kalina system: A binary system using a mixture of ammonia and water as the working fluid in the power cycle.

Reference

Ragnorson, A. Iceland country update, in *Proceedings of the World Geothermal Congress, 1995*, Florence, Italy, May 1995, 145–161.

Further Information

Kestin, J. Ed., *Sourcebook on the Production of Electricity from Geothermal Energy,* U.S.DOE, DOE/RA/4051-1, Washington, D.C., 1980.

Lienau, Paul J. and Ben C. Lunis, Eds., *Geothermal Direct Use Engineering and Design Guidebook,* USDOE, Idaho Falls, ID, 1991.

Transactions of the Geothermal Resources Council, Vol. 1–19, (1977–1995), Geothermal Resources Council, Davis, CA.

8.13 Direct Energy Conversion

Solar Photovoltaic Cells

Kitt C. Reinhardt

Introduction

Solar photovoltaic cells convert sunlight directly into electrical energy via the collection of solar photon-generated semiconductor charge carriers. The collection of charge carriers within the cell produces a voltage across the terminals of the cell, called the **photovoltaic effect**, that can drive an external electrical circuit or charge a storage battery. Photovoltaic cells are useful in both space and terrestrial power applications. Silicon, Si, photovoltaic cells have provided the main source of electrical power to virtually all Earth-bound satellites since the advent of the space program in the late 1950s. In the early 1970s, photovoltaics generated a significant amount of interest for use in terrestrial power systems when oil supplies to the industrial world were disrupted. Today, while photovoltaic power remains the primary energy source for most communication and surveillance satellites, issues concerning system efficiency, reliability, and cost currently prevent its widespread use in residential and power utility applications. For example, in the United States the average price for conventional utility electricity is 6¢/kWhr, compared with ~35¢/kWhr for terrestrial photovoltaic electricity (Zweibel, 1995). Thus, the cost of photovoltaic power must be reduced by a factor of ~6 for it to become economically viable. At present, photovoltaic power is generally only cost-competitive for use in remotely located systems where conventional power is cost-prohibitive, such as in remote water-pumping and communications stations, signal and emergency lighting, and for village power. Factors that influence photovoltaic system energy costs include cell panel efficiency, total system lifetime, and cost per unit area. The present discussion will focus on issues concerning photovoltaic cells and panels. Detailed literature on power conditioning electronics and energy storage systems can be found elsewhere. A large number of different photovoltaic cell designs have been demonstrated by researchers over the years. However, the most common and practical cell designs are fabricated using single-crystal Si. Consequently, Si will be used to describe basic principles of semiconductors and photovoltaic cell operation.

Introduction to Semiconductors

We begin with a description of the concept of covalent bonding, valence electrons, and energy bands, which relates to conduction in semiconductors (Sze, 1981). The crystalline structure of Si is diamond, where each Si atom in the lattice is covalently bonded to four equidistant nearest neighbors that lie at the corners of a tetrahedron. Each Si atom has four electrons in its outer orbit, called valence electrons, and each atom shares these electrons with its four neighbors to form four covalent bonds. The atomic configuration of the 14 electrons of Si is $1s^2 2s^2 2p^6 3s^2 3p^2$. At practical temperatures, only the $3s^2 3p^2$ valence electrons contribute to the electrical conductivity; the $1s^2 2s^2 2p^6$ core electrons are too tightly bounded to the nucleus to participate. In a simplified model, as N Si atoms are brought together at 0 K to form a crystal, two distinct and nearly continuous bands of electronic energy levels form that are separated by an energy gap called the semiconductor **band gap, E_g**. The resulting upper **conduction band** contains 4N states, as does the lower **valence band**. The 4N electrons that come from the Si $3s^2 3p^2$ states completely fill the 4N states in the valence band at 0 K, and the conduction band states are completely empty. Since there are no unoccupied states in the valence band for electrons to move and the conduction band is empty, Si is a perfect insulator at 0 K.

As the temperature of the crystal increases, electrons in the valence band gain sufficient thermal energy ($>E_g$) to be excited across the band gap into the conduction band, leaving holes (missing electrons) behind in the valence band. When current conduction in a semiconductor is dominated by thermally generated electrons and holes, it is called intrinsic. In this case, the resulting number of electrons per unit volume in the conduction band, n, equals the number of holes per volume in the valence band, p, that is $n = p = n_i$, where n_i is called the intrinsic carrier concentration. In the presence of an electric

field, intrinsic electrons and holes gain kinetic energy and conduct electricity. However, since at room temperature n_i for Si is only 1.45×10^{10} cm^{-3}, compared with a free-electron density of more than 10^{22} cm^{-3} in metals, Si behaves as a very good insulator, i.e., electrical conductivity, σ, is given by $\sigma = q(n\mu_n + p\mu_p)$, where q is the electronic charge and μ is the respective carrier mobility.

In order to increase the conductivity to values useful for solid-state devices, the level of n and p can be increased by purposely adding impurity atoms into the crystal, called doping, that liberate extra electrons or holes. In the case of Si, which is in column IV of the periodic table, and hence has four valence electrons for bonding, doping is achieved using either column III elements (boron, aluminum, gallium, or indium), which have three valence electrons, or column V elements (phosphorus, arsenic, or antimony), which have five valence electrons. When an arsenic atom with five valence electrons replaces (substitutes) an Si atom, four of its electrons are used to form covalent bonds with the four neighboring Si atoms. The fifth electron is loosely bound to the arsenic nucleus, and at room temperature is ionized and "donated" to the conduction band. Arsenic is therefore called a donor, and Si becomes an n-type (mostly electrons) semiconductor. Similarly, when a boron atom with three valence electrons substitutes for an Si atom, one of the boron four covalent bonds becomes deficient of one electron. Boron can then accept one electron from the valence band to satisfy the bond requirement, which creates a positively charged hole in the valence band. Boron is therefore called an acceptor, and Si becomes a p-type (mostly holes) semiconductor. In this way the electrical conductivity of semiconductors can be precisely controlled by varying the concentration of donor and acceptor impurities. In practical solid-state devices, typical values of n and p range between 10^{15} and 10^{19} cm^{-3}.

The p-n Junction Diode

The p-n junction is a basic structure used for solid-state device rectification, amplification, and switching, as well as for photocarrier collection in photovoltaic cells. A p-n junction is formed when a p-type semiconductor is metallurgically joined with an n-type semiconductor (Streetman, 1980). Before they are joined, the p-material has a large concentration of holes and very few electrons, whereas the converse is true for the n-material. Upon joining the two materials, holes instantaneously diffuse from the p-side into the n-side and electrons diffuse from the n-side into the p-side. The transport of these carriers constitutes a "diffusion" current from the p-side to n-side; electron current is opposite in direction to electron flow by convention. As shown in Figure 8.13.1, negative acceptor ions are left behind as holes leave the p-side of the junction, creating a negative space-charge region (SCR), and positive donor ions are left behind as electrons leave the n-side of the junction, creating a positive SCR. Consequently, an electric field directed from the positive SCR to the negative SCR results that opposes the further diffusion of electrons and holes; i.e., the electric field creates a drift component of current from the n-side to p-side that opposes the diffusion component. In the absence of any external fields a condition of equilibrium is established, and the net current flow across the junction is zero. As will be discussed, the p-n junction electric field is also responsible for separating and collecting photon-generated carriers in photovoltaic cells.

When a voltage is applied across a p-n junction, the balance between the electron and hole drift and diffusion currents is disturbed and a net current results. Under forward bias, a positive voltage is applied to the p-side relative to the n-side, and the electric field across the junction is reduced; i.e., the electric field associated with the applied voltage subtracts from the zero-bias field. The reduced field enhances hole diffusion from the p-side to the n-side and electron diffusion from the n-side to the p-side, thereby increasing the "positive" current; the transport of current from the p-side to the n-side is positive by convention. Conversely, under reverse bias a negative voltage is applied to the p-side relative to the n-side, and the electric field across the junction increases. Consequently, the diffusion component of current decreases relative to the drift component, and a net "negative" current results across the junction.

The dark current-voltage (I-V) characteristics for an Si p-n junction are generally well described by the ideal Shockley diode equation (Sze, 1981),

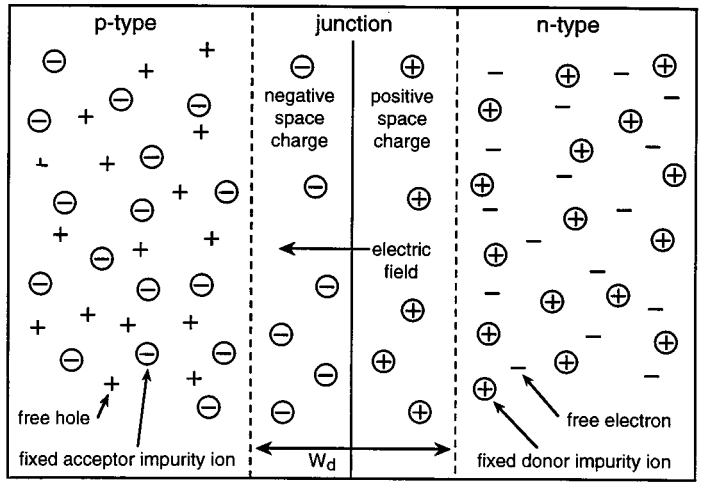

FIGURE 8.13.1 Schematic diagram illustrating an abrupt p-n junction with a unifiorm concentration of donor impurities in the n-region and acceptor impurities in the p-region.

$$I_D = I_o\left[\exp\left(qV/nkT\right) - 1\right] \tag{8.13.1}$$

where I_D is the junction dark current, I_o is the reverse saturation current, V is the forward-bias voltage, n is the diode ideality factor, and T is the absolute temperature. The value of n is ~1.0 when the current is dominated by carrier diffusion, but increases and approaches values of ~2 or greater when other current mechanisms become important, such as carrier recombination or tunneling. In high-quality Si p-n junction photovoltaic cells, the value of n is ~1.0 near the relevant operating voltage. The parameter I_o varies with T and E_g according to

$$I_o = qA\left[D_n n_p/L_n + D_p p_n/L_p\right] \propto T^3 \exp\left(-E_g/kT\right) \tag{8.13.2}$$

where A is the junction area and D_n and D_p, n_p and p_n, and L_n and L_p are the diffusion coefficients, minority carrier densities, and diffusion lengths for electrons and holes, respectively. The value of I_o decreases strongly as E_g increases, which, as will be shown, increases the photovoltage obtainable from a photovoltaic cell.

Cell Operation and Efficiency

Cell Operation. Photovoltaic energy conversion in a p-n junction is a two-step process where free electrons and holes (photocarriers) are generated in the semiconductor via the absorption of solar energy and then simultaneously collected across the junction (Fahrenbruch and Bube, 1983). Consider the schematic of a typical photovoltaic cell shown in Figure 8.13.2 which consists of a p-n junction formed very close to the top surface of the cell. Front metal ohmic contact grid fingers allow solar energy to pass into the absorber layers. The entire top surface is covered with an antireflection coating to minimize reflective losses, and the entire back surface is covered with an ohmic contact. The ohmic contacts form n and p region terminals that transfer (conduct) current from the semiconductor to the external circuit with a negligible amount of voltage drop.

When the photovoltaic cell is exposed to solar radiation, photons with energies greater than E_g (super-band-gap photons) are absorbed in the n and p layers, and free electrons and holes are generated via the breaking of covalent bonds. These electron-hole pairs, or **photocarriers**, are shown in Figure 8.13.1. The energy of the free photocarriers is converted directly into a current and voltage via photocarrier collection by the junction. The absorbed photons effectively contribute an energy E_g to the cell output,

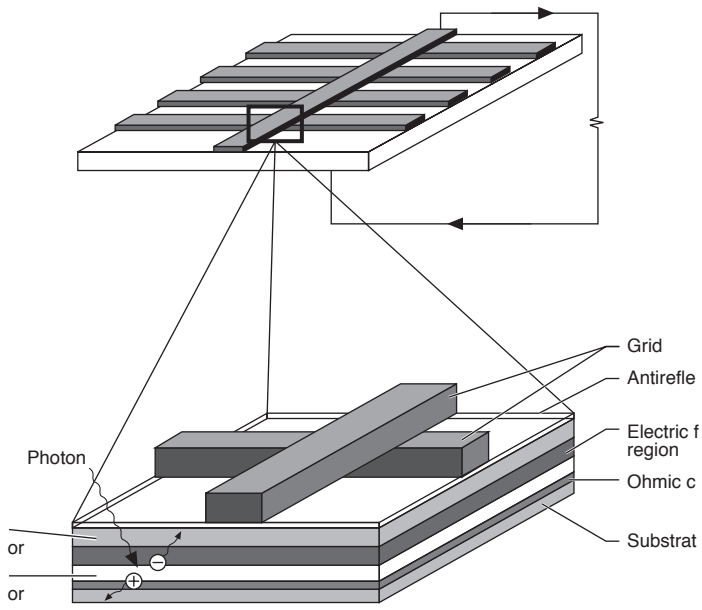

FIGURE 8.13.2 Schematic diagram of a typical p-n junction photovoltaic cell.

and energy greater than E_g is lost as heat. Photons with energies less than E_g (sub-band-gap photons) are transmitted through the cell. After generation, minority photocarriers, that is, holes on the n-side and electrons on the p-side, diffuse toward the edges of the junction due to a gradient of carriers that exists there. If the minority carriers are generated within a diffusion length, L, of the junction, they will reach it and be swept across it by the electric field of the junction. Hence, electrons are swept from the p-side to the n-side and holes from the n-side to the p-side, and thus they are separated. The minority carrier gradient present at the edges of the junction is due to the depletion of minority carriers that results from their transfer across the junction. The diffusion flux of minority carriers toward and across the junction constitutes a light-generated current, I_L, or photocurrent, that is directed from the n-side to the p-side of the cell. The build-up of positive holes on the p-side and negative electrons on the n-side gives rise to a **photovoltage** across the junction. The polarity of both the photovoltage and photocurrent is identical to that of a battery, and power is delivered from the junction to the external circuit.

Cell Efficiency. In order to derive the solar conversion efficiency, it is convenient to model the photovoltaic cell as an ideal p-n diode in parallel with a **light-generated** (constant) **current** source, I_L, as shown in the equivalent circuit of Figure 8.13.3. Parasitic series and shunt resistance losses, R_s and R_{sh}, respectively, are also shown, where R_s is due to ohmic contact and semiconductor resistances, and R_{sh} is due to defect-related carrier recombination and/or tunneling phenomena (Stirn, 1972). A qualitative expression for I_L is given by Tada et al. (1982):

$$I_L = qAG\left(L_n + W_d + L_p\right) \tag{8.13.3}$$

where G is the photocarrier generation rate in carriers/cm^3-sec due to solar photon absorption, which depends on E_g and the photon energy (wavelength) and intensity (concentration), and W_d is the sum of the negative and positive SCR widths. As mentioned, I_L is directed from the n-side to the p-side. In

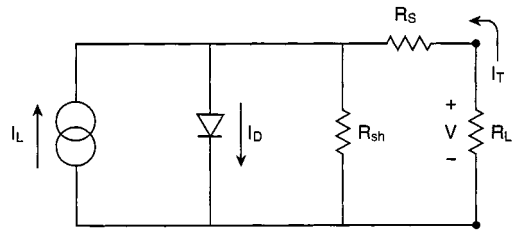

FIGURE 8.13.3 Schematic of equivalent circuit model for a p-n photovoltaic cell.

contrast, the dark diode current given by Equation (8.13.1) is directed oppositely from the p-side to the n-side. The **dark current** is due to the forward-bias photovoltage that appears across the cell p-n junction when it is illuminated. Thus, the dark current opposes the light current. In the ideal case, that is, when $R_s = 0$ and $R_{sh} = \infty$, the total forward current, I_T, is given by

$$I_T = I_D - I_L = I_o\left[\exp(qV/nkT) - 1\right] - I_L \tag{8.13.4}$$

A plot of dark and light current-voltage (I-V) curves resulting from Equations (8.13.1) and (8.13.4), respectively, is shown in Figure 8.13.4 for a typical p-n solar cell. Under illumination, the forward-bias dark I-V curve is displaced downward into the fourth quadrant by the **photocurrent**, $\boldsymbol{I_L}$. It is noted from Figure 8.13.3 that the voltage drop across the load resistance, R_L, is $V = -I_T R_L$. Under short-circuit conditions, that is, when the n and p terminals are tied to each other, R_L is negligible. The resulting voltage drop across the p-n junction will also be negligible, and from Equation (8.13.1), $I_D \approx 0$. As shown in Figure 8.13.4, the resultant current is termed the **short-circuit current**, $\boldsymbol{I_{sc}}$, or $I_T = -I_{sc} = -I_L$. As the value of R_L increases, a voltage appears across the junction, $V = -I_T R_L$, called the **photovoltage**, and I_D increases in accordance with Equation 8.13.1. Under this condition the cell is operating in the fourth quadrant of the I-V characteristic (i.e., the junction voltage is positive and the current is negative), and, consequently, the cell delivers power (product of the current and voltage) to R_L. As the value of R_L continues to increase, so too does V and I_D. When the value of R_L approaches infinity, that is, under open-circuit conditions, I_D approaches I_L and I_T goes to zero. The resulting **open-circuit voltage**, $\boldsymbol{V_{oc}}$, is shown in Figure 8.13.4. V_{oc} can be obtained by setting $I_T = 0$ in Equation (8.13.4) and solving for V. For $V \gg kT/q$,

$$V_{oc} = nkT/q\ln\left[I_L/I_o\right] \tag{8.13.5}$$

Thus, the operating point on the I-V curve in the fourth quadrant can be swept from (I_{sc}, 0) to (0, V_{oc}) by varying the value of R_L. When the optimum load is chosen (i.e., $R_L \approx V_{oc}/I_{sc}$), approximately 80% of the product $I_{sc}V_{oc}$ can be extracted as useful power as shown by the shaded maximum-power rectangle in Figure 8.13.4. Also shown in Figure 8.13.4 are the parameters I_m and V_m, which correspond to values of current and voltage, respectively, that yield the maximum cell power, P_m, where $P_m = I_m V_m$. The knee that appears at P_m is due to the parasitic effects of R_s and R_{sh}. The curvature of the knee at P_m is described by the **fill factor**, **FF**, where

$$\text{FF} = I_m V_m / I_{sc} V_{oc} \tag{8.13.6}$$

The photovoltaic cell **conversion efficiency**, η, is defined as

$$\eta = I_m V_m / P_{in} A$$

or

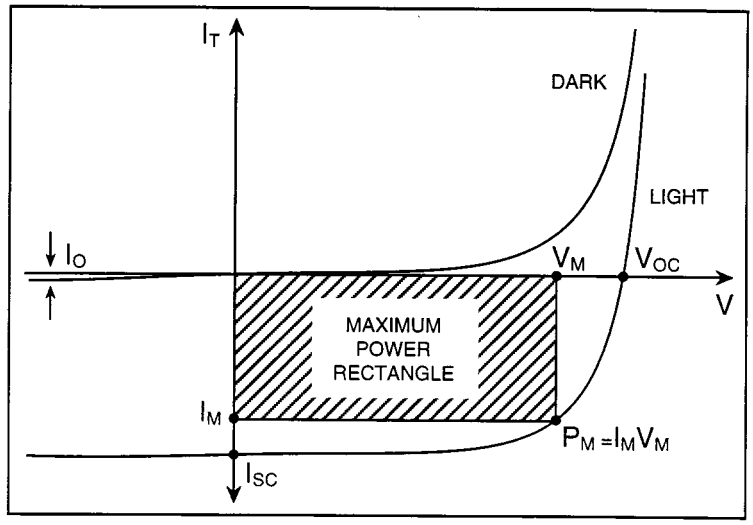

FIGURE 8.13.4 Typical dark and light current-voltage characteristics for a p-n photovoltaic cell.

$$\eta = FF\, I_{sc} V_{oc} / P_{in} \tag{8.13.7}$$

where P_{in} is the incident power in W/m^2 equal to the sum in energy of the incident photons per time per area. Values for V_{oc}, I_{sc}, FF, and η can be obtained in the laboratory under various air mass conditions from light *I-V* curves measured using a carefully controlled (calibrated) light source to illuminate the cell.

Cell Material vs. Efficiency

The optimum value of material E_g for solar photovoltaic conversion is ~1.0 to 1.5 eV. To understand how the choice of cell material affects conversion efficiency, an ideal expression can be derived using Equation 8.13.4 for the theoretical conversion efficiency. The output power can be expressed as (Henry, 1980)

$$P = IV = I_o V\left[\exp\left(qV/nkT\right) - 1\right] - I_L V \tag{8.13.8}$$

The maximum output power is obtained when $dP/dV = 0$, and an expression for I_m and V_m can be obtained from Equation (8.13.8) and multiplied to give P_m, where

$$P_m = I_m V_m \approx I_L\left[V_{oc} - kT/q \ln\left(qV_m/kT + 1\right) - kT/q\right] \tag{8.13.9}$$

In practical cells, values for V_m and V_{oc} are typically $^1/_2E_g/q$ to $^2/_3E_g/q$. Thus, for materials with $E_g \sim 1 - 2$ eV, the quantity in the large brackets of Equation (8.13.9) becomes $\sim V_{oc}$, and the factors that determine I_L and V_{oc} also determine P_m. From Equations (8.13.2) and (8.13.5), it is clear that V_{oc} increases with E_g through the reduction in I_o. In contrast, as E_g increases, I_L decreases because a smaller portion of the solar spectrum is energetic enough to be absorbed; i.e., I_L is the product of q and the number of available photons with energy greater than E_g. Hence, for a given solar spectrum there is an optimum value of E_g that maximizes the product of V_{oc} and I_L. A plot of ideal AM1 conversion efficiency vs. E_g is shown in Figure 8.13.5 for "one sun" (925 W/m^2) and "1000 suns" (925 kW/m^2) concentrations (Henry, 1980). The efficiency curves were obtained using Equations (8.13.1) through (8.13.7) at 300 K. A maximum in efficiency occurs for $E_g \sim 1.0 - 1.5$ eV.

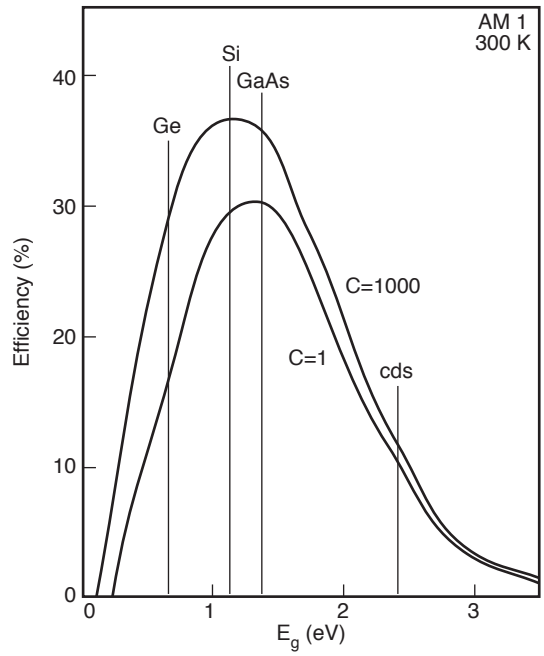

FIGURE 8.13.5 Theoretical AM1 efficiency vs. semiconductor band gap E_g for an ideal photovoltaic cell under 1 sun and 1000 suns concentrations.

Manufacture of Cells and Panels

There are basically five important solar cell design concepts, and each offers a trade-off between efficiency and cost: (1) Large-area single-crystal planar cells, typically 1 × 1 cm² to 6 × 6 cm², yield high efficiencies under normal light conditions, 2) single-crystal small-area concentrator cells, typically less than 1 × 1 cm², are potentially less costly and yield higher efficiencies under concentrated light, i.e., concentration ratios of 20 to 1000 are typical; (3) more-complex single-crystal multijunction cells yield the highest efficiencies measured to date, but are substantially more expensive; (4) cells made from polycrystalline materials are less expensive than single-crystalline cells, but are less efficient; and (5) cells made from thin film amorphous materials provide the lowest-cost approach yet, but are generally less efficient than polycrystalline cells.

A typical 15% 4 × 4 cm² photovoltaic cell produces only ~0.25 W under AM1.5 conditions. Therefore, individual cells must be electrically wired together to form larger submodules or panels to increase the total output power. The cells can be connected in series to increase the total voltage or in parallel to increase the current. The modular nature of photovoltaic power allows the design of systems that can deliver electrical power from a few watts to many megawatts. In terrestrial applications the cells are typically supported and held in place with a rigid substrate, i.e., typically aluminum, Plexiglas, fiberglass, or glass, and are encapsulated with glass or a polymeric material; in space applications the support structure may be rigid or flexible, and the cells are protected from the space environment with quartz cover slides. The electrical power generated by the cells is conducted to an electrical load or storage battery. Metal interconnects soldered to the ohmic contacts of the cells conduct electrical current from one cell to the next. Current is then conducted from the network of series- and parallel-connected cells by wires to a distribution terminal "bus" that transfers the power to either the load or battery.

Single-Crystal Cells. The p-n photovoltaic cells made from **single-crystal** Si dominate in space and terrestrial applications because of their high efficiency and reliability. The formation of single-crystal p-

type Si results from the selective cooling of pure molten Si to form large cylindrical crystal ingots, called boules, from which thin wafers are sliced and polished. The p-type impurities, usually boron, are added to the melt, to give the desired impurity concentration. A large-area p-n junction is then formed by diffusion of n-type impurity atoms, usually phosphorus. Front and back metal ohmic contacts and an antireflection coating are then formed using standard photolithography thermal evaporation or sputtering techniques (Sze, 1985). The resulting cell structure is shown in Figure 8.13.2, and typical cell areas range from 1 to 36 cm^2. Different semiconductors absorb sunlight more efficiently than others, described by a factor called the absorption coefficient. Si has a relatively small absorption coefficient compared with other materials, such as InP, GaAs, and amorphous-Si, and consequently requires an absorption layer thickness of ~100 μm to maximize conversion efficiency. Conventional Si cells have a thickness on the order of 250 μm, but can be chemically or mechanically polished to a thickness of 100 μm.

Single-crystal III-V photovoltaic cells, such as InP and GaAs, are made from elements in the III and V columns of the periodic table. The band gaps of these cells, 1.35 and 1.42 eV, respectively, are close to the optimum value. These materials involve the growth of single-crystal semiconductor layers upon a single-crystal semiconductor substrate. This technique is called epitaxy and it provides a method to produce both n-type and p-type layers to form the p-n junction. Epitaxial growth of n and p layers is required for InP and GaAs because diffusion of impurities at high temperatures is confounded by the high vapor pressure of the material. The formation of ohmic contacts and antireflection coating employ the same techniques as used for Si cells. The required absorption layer thickness for these cells is only a few microns because of their large absorption coefficients. However, issues concerning yield and mechanical strength limit their minimum thickness to ~100 μm The best reported efficiencies for single-crystal Si, GaAs, and InP cells under AM1.5 conditions are 24, 25, and 22%, respectively (Green et al., 1995).

Polycrystalline Cells. In the case of **polycrystalline** Si cells, molten Si is directly deposited into either cylindrical or rectangular ingots. As the material solidifies, individual crystalline regions form that are separated by grain boundaries which contain large numbers of structural defects. When the cell is illuminated, these defects capture a portion of the light-generated electron-hole pairs through recombination processes before they can reach the junction and be collected. Thus, the grain boundaries diminish the light-generated current and overall efficiency of the cell. However, polycrystalline silicon cells are sufficiently inexpensive to be commercially viable (Stone, 1993). An area that requires improvement is the slicing of polycrystalline ingots, where yields as low as 50% are common. An approach that eliminates the expense of sawing and polishing altogether is the growth of polycrystalline Si directly into the form of thin ribbons using a technique called edge-defined film-fed growth (EFG) (Fahrenbruch and Bube, 1983). In this approach, a carbon die with a slot-shaped aperture is immersed in a crucible of molten Si. The liquid Si wets the die and flows through the slot where it cools and is pulled to form a thin ribbon. This material also has high crystalline defect densities, but has good overall yields. An additional approach involves the growth of films of nearly single-crystal quality, where two parallel supporting dendrites form the boundaries of a web or ribbon pulled from a supercooled melt of Si. The best efficiency for polycrystalline Si cells under AM1.5 conditions is ~18%; that for Si cells grown by the EFG technique is 14%; and that for Si dendritic web cells is 15.5% (Stone, 1993). It is important to note that although these lower-cost films yield lower cell efficiencies compared with single-crystal cells, the cost of cells depends on the cost of the starting material and the cost per watt is more important than efficiency (Zweibel, 1995).

Thin Film Cells. Thin films cells provide an even lower-cost (and lower-efficiency) approach because they require a very small amount of semiconductor. An excellent review on thin film photovoltaic technologies, particularity on present and future cost issues, is given by Zweibel (1995). The general approach involves depositing only a few microns of material on a low-cost substrate using various vacuum deposition techniques, although a multitude of other deposition techniques have also been demonstrated. The top thin film cell candidates are amorphous Si, a-Si, cadmium telluride, CdTe, and copper indium diselenide, CIS (and related alloys). The highest reported thin film AM1.5 efficiencies

are 17% for CIS, followed by 15.8% for CdTe, and ~11% for a-Si (Zweibel, 1995). However, the relative level of maturity of each design for commercial application must be put into perspective. While the best CIS cell efficiency is quite high, the best CIS square foot panel efficiency reported back in 1988 was, and still is today, only 11%. Significant manufacturing problems have plagued the CIS cell, and currently it is still not commercially available. CdTe is believed to be the easiest of the thin film cells to fabricate, and probably represents the closest to large-scale commercialization. Two U.S. companies have publicly announced CdTe manufacturing plants, and commercial efficiencies are likely to be in the range of 6 to 8% in the first plants. The future of a-Si cells is currently believed to be limited if it cannot overcome a 10% efficiency at the module level. Development problems include electrochemical instability to light that results in a 20 to 40% degradation. However, it appears that the use of multijunction thin film a-Si layers may solve the problem, and modules of 7 to 9% are expected in the near term.

Concentrator Cells. Photovoltaic modules are typically either of the flat plate or concentrator configuration. Flat plate modules can be fixed with respect to the sun or mounted to track the sun in one or two axis. Concentrator modules use large-area mirrors or lenses to concentrate sunlight onto smaller-area cells. Concentrator cells operate at higher efficiencies. However, concentrator modules require one- or two-axis tracking which adds system complexity and cost that generally offsets the module efficiency and lower area cost benefits. The increase in conversion efficiency with illumination intensity is shown in the 1000-sun concentration curve of Figure 8.13.5. Values for I_L increase linearly with concentration through the factor G in Equation (8.13.3) and V_{oc} increases logarithmically with concentration through I_L in Equation (8.13.5). Under solar concentration of "20 suns" or greater, a significant amount of cell heating can occur. While J_{sc} increases slightly with increasing temperature, values of V_{oc} and FF drop strongly. Thus, on adequate heat sink or active cooling is required at high concentrations. The reported AM1.5 efficiency for Si cells increases from 24 to 26.5% under a concentration of 255; and that for GaAs cells increases from 25 to 27.6% under a concentration of 140 (Green et al., 1995).

Multijunction Cells. Another approach to increase photovoltaic cell efficiency is through the use of multijunction tandem cells. The simplest multijunction cell is a two-junction, two-terminal device. In this design, a high-band-gap (E_{g1}) p-n junction is vertically stacked (mechanically) or epitaxially grown atop a bottom lower-band-gap (E_{g2}) p-n junction as shown in Figure 8.13.6. The top junction absorbs photons with energy $\geq E_{g1}$, and the bottom junction absorbs photons with energy E, where $E_{g1} > E \geq E_{g2}$, that passed through the top cell. This increases the utilization of the solar spectrum, since the excess energy of the high-energy photons is not wasted. The values of E_{g1} and E_{g2} must be chosen to achieve maximum solar absorption and current matching; i.e., the two cells must generate equal currents when illuminated. The band gap combinations of ~0.7 and 1.4, 1.0 and 1.4, 1.1 and 1.4, and 1.4 and 1.9 eV are current matched, where E_g for GaSb, $CuInSe_2$, Si, GaAs, AlGaAs, and $GaInP_2$ are ~0.7, 1.0, 1.1, 1.4, and 1.9 eV, respectively. Multijunction concentrator cells have reported efficiencies in excess of 30% (Green, 1995).

Design of a Photovoltaic Generating System

A schematic diagram depicting the basic components of a typical photovoltaic power generation system is shown in Figure 8.13.7 (Pulfrey, 1978). The system includes a photovoltaic array that consists of many smaller submodules, each containing many hundreds or thousands of photovoltaic cells. The DC output power from the array is controlled by a power conditioning unit that contains an inverter for developing AC power and an input power tracking device to maintain the optimal array load to achieve maximum output power. Power is directly fed to the electrical load and/or storage system by the conditioning unit. The storage system is needed to save energy when power is generated in excess of the immediate demand, or when the load demand exceeds the immediate generation level. Total photovoltaic power system efficiency is the product of the efficiencies of the individual components. Typical efficiencies for the power conditioning unit (determined by the inverter) and energy storage system are about 95% and 50-80%, respectively. Thus, an array efficiency of 10% would result in a total system

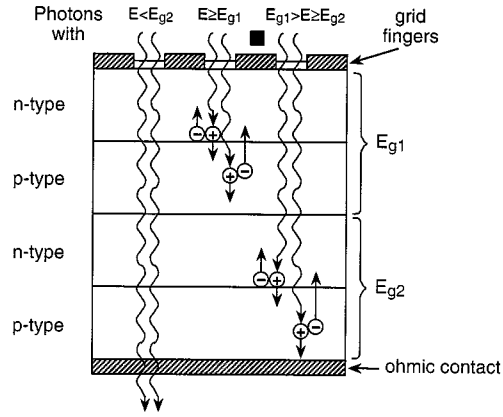

FIGURE 8.13.6 Schematic diagram of a multijunction (two-junction) photovoltaic cell under illumination.

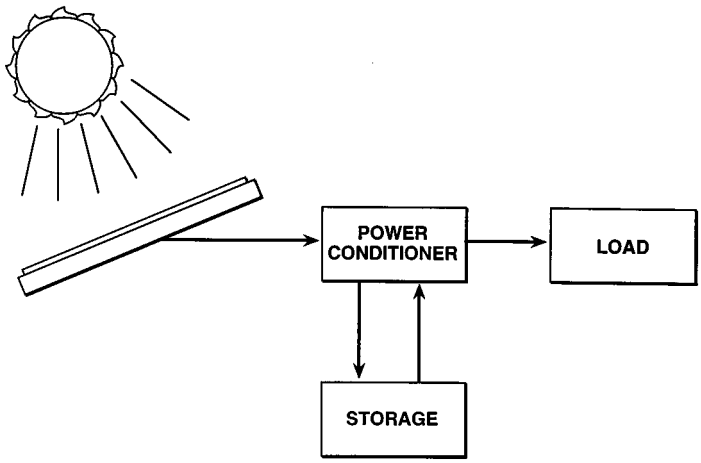

FIGURE 8.13.7 Schematic diagram depicting the basic components of a typical photovoltaic power system.

efficiency of about 5 to 8%, and a total system efficiency of 10% would require an array efficiency in excess of 13%.

Defining Terms

Band gap (E_g): The difference in energy between the energy level of the bottom of the conduction band and the energy level of the top of the valence band.

Conduction band: A range of allowable energy states in a solid in which electrons can move freely.

Conversion efficiency (η): The ratio of the available power output photovoltaic cell to the total incident radiant power.

Dark current: Any current that flows through the p-n junction in the absence of external irradiation.

Fill factor (ff): The ratio of the maximum photovoltaic cell output power to the product of the open-circuit voltage and short-circuit current.

Light-generated current (I_L): The electrical current obtained from an illuminated p-n junction resulting from the collection of photocarriers across the junction.

Open-circuit voltage (V_{oc}): The voltage obtained across the terminals of an illuminated p-n photovoltaic cell under open-circuit conditions.

Photocarriers: Electrons and holes generated within a semiconductor via the absorption of photon energy.

Photocurrent: Synonymous with light-generated current.

Photovoltaic effect: The production of a voltage difference across a p-n junction resulting from the absorption of photon energy.

Photovoltage: The voltage resulting from the photovoltaic effect.

Polycrystalline: A material characterized by an array or agglomerate of small single-crystal sections of various crystal orientations separated from one another by grain boundaries, which are localized regions of very severe lattice disruptions and dislocations.

Short-circuit current (I_{sc}): The electrical current measured through the terminals of an illuminated p-n photovoltaic cell under short-circuit conditions.

Single crystal: A material characterized by a perfect periodicity of atomic structure; the basic arrangement of atoms is repeated throughout the entire solid.

Valence band: A range of allowable energy states in a solid crystal in which lie the energies of the valence electrons that bind the crystal together.

References

Fahrenbruch, A.L. and Bube, R.H. 1983. *Fundamentals of Solar Cells — Photovoltaic Solar Energy Conversion,* Academic Press, New York.

Green, M.A., Emery, K., Bucher, K., and King, D.L. 1995. *Short communication: solar cell efficiency tables (version 5), Prog. Photovoltaics Res. Dev.*, 3, 51–55.

Henry, C.H. 1980. Limiting efficiency of ideal single and multiple energy gap terrestrial solar cells, *J. Appl. Phys.,* 51, 4494.

Pulfrey, D.L. 1978. *Photovoltaic Power Generation,* Van Nostrand Reinhold, New York.

Stirn, R.J. 1972. *Junction characteristics of Si solar cells,* in Proceedings of the 9th IEEE Photovoltaics Specialists Conference, p.72.

Stone, J.L. 1993. Photovoltaics: unlimited electrical power from the sun, *Phys. Today*, Sepember, 22–29.

Streetman, B.G. 1980. *Solid State Electronic Devices,* Prentice-Hall, Englewood Cliffs, NJ.

Sze, S.M. 1981. *Physics of Semiconductor Devices,* 2nd ed., John Wiley & Sons, New York.

Sze, S.M. 1985. *Semiconductor Devices: Physics and Technology,* John Wiley & Sons, New York, 341–457.

Tada, H.Y., Carter, J.R., Anspaugh, B.E., and Downing, R.G. 1982. *Solar Radiation Handbook*. JPL Publication 82-69, 2-11

Zweibel, K. 1995. *Thin Films: Past, Present, Future*. NREL/IP-413-7486 Publication (DOE UC Category 1260 DE95004084).

Further Information

An excellent presentation of the basic theory of the various photovoltaic cell designs is given in *Fundamentals of Solar Cells: Photovoltaic Solar Energy Conversion*, by Alan L. Fahrenbruch and Richard H. Bube. This text covers the basics of solar insolation, semiconductors, p-n junctions, and single-crystal, polycrystalline, thin film, and concentrator photovoltaic cells.

An excellent review of the progress achieved in terrestrial and space photovoltaics can be traced in the *Proceedings of the IEEE (Institute of Electrical and Electronics Engineers) Photovoltaics Specialists Conference* (PVSC) that dates back to 1961. These proceedings include thousands of papers that address nearly every aspect of photovoltaic cell development: basic theory, design, fabrication, and application.

The monthly journal *Solar Energy Materials and Solar Cells* covers many aspects of improving device efficiency, reducing costs, and testing and applications.

The monthly journal *Progress in Photovoltaics* documents recent results of research work conducted in photovoltaics worldwide. This journal is an excellent source for currently reported cell conversion efficiencies.

Proceedings of the conference *Space Photovoltaics Research and Technology* is an excellent source for the reader interested in the development of photovoltaics for use in space.

Fuel Cells

D. Yogi Goswami

Introduction

A *fuel cell* is an electrochemical device in which a fuel and an oxidant react in such a controlled manner that the chemical energy of reaction is converted directly into electrical energy. Ordinarily, a fuel reacts violently with an oxidant in a combustion reaction resulting in the release of heat of combustion. The heat of combustion can, then, be converted into electrical energy via mechanical work with the constraint of the second law of thermodynamics. The overall efficiency of the series of conversion processes is of the order of 40%. A fuel cell bypasses these processes resulting in potential efficiencies of the order of 80%. As an example, when hydrogen is burned in an atmosphere of oxygen it results in the following reaction:

$$H_2 + \frac{1}{2}O_2 \rightarrow H_2O + \Delta H \quad (\text{heat of reaction}) \tag{8.13.10}$$

In this reaction, two hydrogen atoms bond with an oxygen atom by sharing their electrons with the outermost orbit of oxygen, which becomes full, resulting in a stable structure.

The reactants H_2 and O_2 may be combined to form the same product (H_2O) by first stripping the electrons away from the hydrogen atoms and allowing the electrons to pass through an external circuit before combining with oxygen. Table 8.13.1 gives typical electrochemical reactions in fuel cells.

$$H_2 \rightarrow 2H^+ + 2e^- \quad (\text{electrons}) \tag{8.13.11}$$

$$2H^+ + O + 2e^- \rightarrow H_2O \tag{8.13.12}$$

Figure 8.13.8 shows a schematic of an arrangement that would allow the above reaction to proceed.

TABLE 8.13.1 Electrochemical Reactions in Fuel Cells

Fuel Cell	Anode Reaction	Cathode Reaction	Overall Reaction
Proton exchange	$H_2 \rightarrow 2H^+ + 2e^-$	$^1/_2O_2 + 2H^+ + 2e^- \rightarrow H_2O$	$H_2 + {}^1/_2O_2 \rightarrow H_2O$
Alkaline	$H_2 + 2(OH)^- \rightarrow 2H_2O + 2e^-$	$^1/_2O_2 + H_2O + 2e^- \rightarrow 2(OH)^-$	$H_2 + {}^1/_2O_2 \rightarrow H_2O$
Phosphoric acid	$H_2 \rightarrow 2H^+ + 2e^-$	$^1/_2O_2 + 2H^+ + 2e^- \rightarrow H_2O$	$H_2 + {}^1/_2O_2 \rightarrow H_2O$
Molten carbonate	$H_2 + CO_3^- \rightarrow H_2O + CO_2 + 2e^-$ $CO + CO_3^- \rightarrow 2CO_2 + 2e^-$	$^1/_2O_2 + CO_2 + 2e^- \rightarrow CO_3^-$	$H_2 + {}^1/_2O_2 + CO_2$ (cathode) $\rightarrow H_2O + CO_2$ (anode)
Solid oxide	$H_2 + O^- \rightarrow H_2O + 2e^-$ $CO + O^- \rightarrow CO_2 + 2e^-$ $CH_4 + 4O^- \rightarrow 2H_2O + CO_2 + 8e^-$	$^1/_2O_2 + 2e^- \rightarrow O^-$	$H_2 + {}^1/_2O_2 \rightarrow H_2O$ $CO + {}^1/_2O_2 \rightarrow CO_2$ $CH_4 + 2O_2 \rightarrow H_2O + CO_2$

Source: Hirschenhofer, J.H. et al., *Fuel Cells, A Handbook*, rev. 3, Gilbert/Commonwealth, Morgantown, WV, 1994. With permission.

In order for the above reactions to occur according to the schematic of Figure 8.13.8:

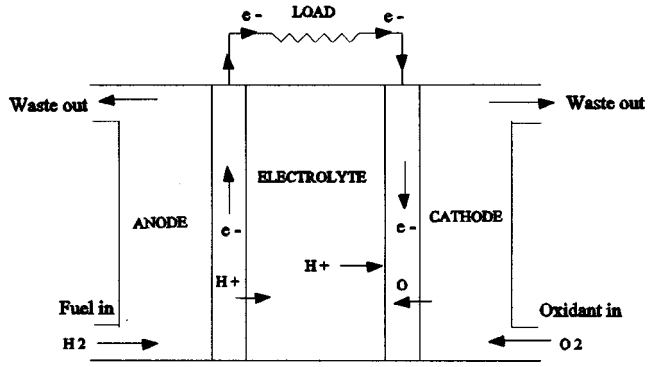

FIGURE 8.13.8 Conceptual schematic of a hydrogen fuel cell.

1. Electrodes must be porous to let the fuel and electrolyte penetrate.
2. The electrolyte must be permeable to H^+ and $(OH)^-$ ions.
3. Electrode materials must be catalysts for the reaction (Pt, Ni, etc.).

In 1839, William Grove, an English investigator, constructed a chemical battery in which he noticed that the water-forming reaction of hydrogen and oxygen generated an electrical current. However, it was not until 50 years later that two English chemists, Ludwig Mond and Carl Langer, developed a device they actually called a fuel cell (Angrist, 1982). There has been a strong resurgence in research and development of fuel cells in the last four decades.

Thermodynamic Performance

The energy released or needed in any chemical reaction (ΔH) is equal to the difference between the enthalpy of formation of the products and the reactants.

$$\Delta H = \sum (\Delta H)_{\text{products}} - \sum (\Delta H)_{\text{reactants}} \tag{8.13.13}$$

In an exothermic reaction the change in enthalpy of formation (ΔH) is negative. Table 8.13.2 gives values of ΔH for various compounds at 25°C at 1 atm. All naturally occurring elements have a ΔH value of zero.

TABLE 8.13.2 Enthalty of Formation ΔH^0 and Gibbs Free Energy ΔG^0 of Compounds at 1 atm and 298 K

Compound or Ion	Enthalpy of Formation, ΔH^0, J/kg · mol	Gibbs Free Energy ΔG^0, J/kg · mol
CO	-110.0×10^6	-137.5×10^6
CO_2	-394.0×10^6	-395.0×10^6
CH_4	-74.9×10^6	-50.8×10^6
Water	-286.0×10^6	-237.0×10^6
Steam	-241.0×10^6	-228.0×10^6
C, H_2, O_2	0	0
O(g)	$+249.2 \times 10^6$	$+231.8 \times 10^6$
H(g)	$+218.0 \times 10^6$	$+203.3 \times 10^6$

Source: Adapted from Wark, K., *Thermodynamics*, McGraw–Hill, New York, 1988. With permission.

In a combustion reaction all of the change in the enthalpy of formation (ΔH) is converted to heat and is, therefore, called the higher heating value (HHV).

$$-(\Delta H)_{\text{reaction}} = \text{HHV of fuel} \tag{8.13.14}$$

For example, for complete combustion of hydrogen according to the following reaction:

$$H_2 + \frac{1}{2}O_2 \rightarrow H_2O \quad (\text{liquid}) \tag{8.13.15}$$

Change in the enthalpy of formation is

$$\Delta H = \Delta H_{H_2O} - \Delta H_{H_2} - \frac{1}{2}\left(\Delta H_{O_2}\right) = \left(-286 \times 10^6\right) - 0 - 0 = -286 \times 10^6 \ \text{J/kg} \cdot \text{mol } H_2 \tag{8.13.16}$$

In a fuel cell, most of ΔH can be converted to electricity directly. The part that cannot be converted to work directly gets converted into heat. The minimum amount that must be converted to heat is represented by reversible heat transfer $\int T\,dS$. If a fuel cell operates isothermally, the maximum amount of electrical work (W_e) produced is given by

$$W_e, \max = \Delta H - T\Delta S \tag{8.13.17}$$

In an irreversible reaction

$$W_e, \max < \Delta H - T\Delta S \tag{8.13.18}$$

Gibbs free energy, G, is given by:

$$G = H - TS \tag{8.13.19}$$

Therefore, in a reversible isothermal process

$$\Delta G = \Delta H - T\Delta S = W_e, \max \tag{8.13.20}$$

The actual electrical work in a fuel cell is given by

$$W_e \leq \Delta G \quad (\text{change in Gibbs free energy for the reaction}) \tag{8.13.21}$$

$$\Delta G_{\text{reaction}} = \sum (\Delta G)_{\text{products}} - \sum (\Delta G)_{\text{reactants}} \tag{8.13.22}$$

The electrical work, W_e, is associated with the work of electrons passing through an external resistance. 1 g · mol of electrons is equal to Avogadro's number (6.022×10^{23}) and the charge of these electrons is equal to 96,439 C which is called a **faraday** (F). If n g · mols of electrons are generated and E is the internal reversible cell voltage, then the maximum electrical work is given by

$$W_e, \max = \Delta G = -nFE \tag{8.13.23}$$

denoting values under standard conditions (25°C, 1 atm) by superscript 0, we have

$$\Delta G^0 = -nFE^0 \tag{8.13.24}$$

Values of G^0 for various compounds are given in Table 8.13.2. For fuel cell reactions as below:

$$aA + bB \rightarrow cC + dD \tag{8.13.25}$$

if the reactants (A and B) and the products (C and D) are assumed to be ideal gases with partial pressures P_A, P_B, P_C, and P_D the change in Gibbs free energy ΔG and the internal reversible cell voltage, E, are given by

$$\Delta G = \Delta G^0 + RT \ln \frac{(P_C)^c (P_D)^d}{(P_A)^a (P_B)^b} \tag{8.13.26}$$

$$E = E^0 + RT \ln \frac{(P_A)^a (P_B)^b}{(P_C)^c (P_D)^d} \tag{8.13.27}$$

Equation 8.13.27 is also called the Nernst equation.

Table 8.13.3 gives Nernst equations for the electrochemical reactions listed in Table 8.13.1.

TABLE 8.13.3 Fuel Cell Reactions and the Corresponding Nernst Equations

Cell Reactions	Nernst Equation
$H_2 + {}^1/_2O_2 \rightarrow H_2O$	$E = E^0 + (RT/2F)\ln[P_{H_2}(P_{O_2})^{1/2}/P_{H_2O}]$
$H_2 + {}^1/_2O_2 + CO_2(c) \rightarrow H_2O + CO_2(a)$	$E = E^0 + (RT/2F)\ln[P_{H_2}(P_{O_2})^{1/2}(P_{CO_2})_c/(P_{H_2O}(P_{CO_2})_a]$
$CO + {}^1/_2O_2 \rightarrow CO_2$	$E = E^0 + (RT/2F)\ln[P_{CO}(P_{O_2})^{1/2}/P_{CO_2}]$
$CH_4 + 2O_2 \rightarrow H_2O + CO_2$	$E = E^0 + (RT/8F)\ln[P_{CH_4}(P_{O_2})^2/P^2_{H_2O}P_{CO_2}]$

Note: (a) = anode; (c) = cathode; E = equilibrium potential.

Source: Hirschenhofer, J.H. et al., *Fuel Cells, A Handbook,* Gilbert/Commonwealth, Morgantown, WV, 1994. With permission.

The maximum conversion efficiency of a fuel cell is given by

$$\eta_{max} = \frac{W_e,\max}{\Delta H} = \frac{\Delta G}{\Delta H} = 1 - \frac{T\Delta S}{\Delta H} = \frac{-nFE}{\Delta H} \tag{8.13.28}$$

As current is drawn through an external circuit, the actual voltage drop (V) will be less than the internal cell voltage (E). Therefore, the actual conversion efficiency of a fuel cell will be lower than above and may be calculated as

$$\eta_{actual} = \frac{-nFV}{\Delta H} = \frac{ItV}{\Delta H} \tag{8.13.29}$$

where I is the current drawn through an external circuit for a period of time, t.

Types of Fuel Cells

Fuel cells are primarily classified by type of electrolyte, since many other characteristics, particularly operating temperatures, are limited by the electrolyte properties (Hirschenhofer et al., 1994). Major fuel cells under active development at this time are the **phosphoric acid fuel cell (PAFC)**, the **molten carbonate fuel cell (MCFC)**, the **solid oxide fuel cell (SOFC)**, the **polymer electrolyte fuel cell (PEFC)**, and the **alkaline fuel cell (AFC)**.

Phosphoric Acid Fuel Cell. PAFC uses concentrated phosphoric acid (H_3PO_4) as the electrolyte, hydrogen as the fuel, and oxygen (from air) as the oxidant. Table 8.13.4 provides information on the electrodes and other materials for PAFC as well as other fuel cells.

The reactions take place at the porous electrodes on highly dispersed electrocatalyst Pt particles supported on carbon black and a polymeric binder, usually polytetrafluoroethylene (PTFE) (about 30 to 50% by weight) (Kinoshita et al., 1988; Hirschenhofer et al., 1994). A porous carbon paper substrate provides structural support for the electrocatalyst and serves as the current collector. A typical carbon paper electrode impregnated with the electrocatalyst has a porosity of about 60%, consisting of micropores of about 34 Å diameter and macropores of 3 to 50 μm diameter.

Dipolar plates (usually graphite) are used to separate the individual cells and electrically connect them in series in a fuel cell stack. In PAFC stacks, provisions are included to remove the waste heat, by liquids (usually water) or gases (usually air) which flow through channels provided in the cell stack.

Molten Carbonate Fuel Cells. MCFCs use as electrolytes mixtures of molten carbonates of lithium (Li_2CO_3), potassium (K_2CO_3), and sodium (Na_2CO_3) in proportions as shown in Table 8.13.4. The operating temperature of the cell (~650°C) is higher than the melting temperature of the carbonate electrolytes. Besides H_2 (fuel) and O_2 (oxidant from air) the cell uses CO_2 which transfers from the cathode to the anode according to the reactions in Table 8.13.1.

According to the reactions, 1 g · mol of CO_2 is transferred along with 2 g · mol of electrons ($2F$). The reversible potential for an MCFC, taking into account the transfer of CO_2, is given by the Nernst equation in Table 8.13.3.

It is usual practice to recycle the CO_2 generated at the anode to the cathode where it is consumed. An early process used to fabricate electrolyte structures involved hot processing mixtures of $LiAlO_2$ and alkali carbonates at temperatures slightly below the melting point of carbonates. These electrolyte structures had problems of void spaces, nonuniformity of microstructure, poor mechanical strength, and high iR drop. To overcome these problems, processes have been developed recently that include tape casting (Man et al., 1984; Hirschenhofer et al., 1994) and electrophoretic deposition (Baumgartner et al., 1985; Hirschenhofer et al., 1994).

Increasing the operating pressures results in enhanced cell voltages. Increasing the operating temperature above 550°C also enhances the cell performance. However, beyond 650°C the gains are diminished and the electrolyte loss and material corrosion are increased. Therefore, 650°C is about the optimum operating temperature.

Solid Oxide Fuel Cell. SOFCs offer a number of advantages over MCFCs for high-temperature operation, since there is no liquid electrolyte. Solid electrolyte allows flexibility in cell shape design based on application. Cells of several shapes, as shown in Figure 8.13.9, are being developed. Because of the high temperature of operation (~1000°C) carbon monoxide (CO) and hydrocarbons such as methane (CH_4) can be used as fuels. At 1000°C, these fuels can easily produce H_2 that is used at the anode by steam reforming and water-gas reactions as

$$CO + H_2O \rightarrow CO_2 + H_2 \quad (\text{water-gas}) \tag{8.13.30}$$

$$CH_4 + H_2O \rightarrow CO + 3H_2 \quad (\text{steam reforming}) \tag{8.13.31}$$

Because of very high operating temperatures the choice of cell materials is limited by (1) chemical stability in oxidizing and reducing atmosphere; (2) chemical stability of contacting materials; and (3) conductivity and thermomechanical compatibility. A detailed description of the current status is given by Minh (1991; 1993) and Appleby and Foulkes (1989). Present SOFC designs make use of thin film wall concepts where films of electrodes, electrolyte, and interconnect material are deposited on each other and sintered to form cell structure. Electrochemical vapor deposition (EVD) is now used to deposit thin layers.

TABLE 8.13.4 Cell Components for Various Fuel Cells

Component	PAFC	MCFC	SOFC[b]	PEFC	AFC
Anode	• PTFE-bonded Pt/C • Vulcan XC-72[a] • 0.1 mg Pt/cm^2	• Ni-10 wt% Cr • 3–6 μm pore size • 50–70% initial porosity • 0.5–1.5 mm thickness • 0.1–1 m^2/g	• Ni/ZrO_2 cermet[c] (30 mol% Ni) • Deposit slurry • 12.5 × 10^{-6} cm/cm °C • ~150 μm thickness • 20–40% porosity	• 10% Pt thin film	• Dual Porosit Ni • 16 μm max pore on electrolyte side • 30 μm pore on gas side
Cathode	• PTFE-bonded Pt/c • Vulcan XC-72[a] • 0.5 mg Pt/cm^2	• Lithiated NiO • 7–15 μm pore size • 60–65% after lithiation and oxidation • 70–80% initial porosity • 0.5–0.75 mm thickness • 0.5 m^{2}g	• Sr-doped lanthanum manganite (10 mol% Sr) • Deposit slurry, sinter • ~1 mm thickness • 12 × 10^{-6} cm/cm °C expansion from room temperature to 1000°C[d] • 20–40% porosity	• 10% Pt thin film	• Porous lithinated NiO
Electrode support	• Carbon paper	—	—	• Carbon paper with Teflon coating on one side	
Electrolyte support	• PTFE-bonded SiC	• γ-$LiAlO_2$ • 0.1–12m^2/g • 0.5 mm thickness	—	—	—
Electrolyte[a]	• 100% H_3PO_4	• 62 Li-38 K • 50 Li-50 Na • 50 Li-50 K • Tape cast • 0.5 mm thickness	• Yttria-stabilized ZrO_2 (8 mol% Y) • EVD[d] • 10.5 × 10^{-6} cm/cm °C expansion from room temperature to 1000°C[d] • ~40 μm thickness	• Proton conducting membrane of perfluoro sulfonic acid polymer	• KOH (45% to 85%)

[a] Conductive oil furnace black, product of Cabot Corp. Typical properties: 002 d-spacing of 3.6 Å by X-ray diffusion, surface area of 220 m^2/g by nitrogen adsorption, and average particle size of 30 μm by electron microscopy.

[b] Specifications for Westinghouse SOFC.

[c] Y_2O_3 stabilized ZrO_2.

[d] EVD = electrochemical vapor deposition.

Source: Hirschenhofer, J.H. et al., *Fuel Cells, Handbook,* Gilbert/Commonwealth, Morgantown, WV, 1994. With permission.

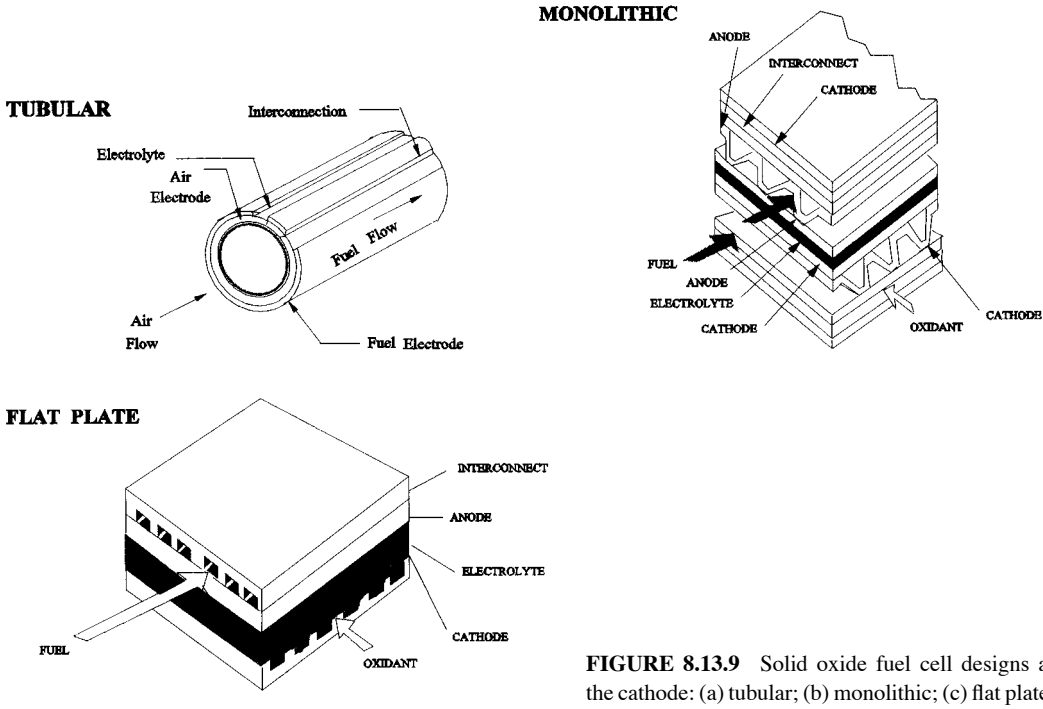

FIGURE 8.13.9 Solid oxide fuel cell designs at the cathode: (a) tubular; (b) monolithic; (c) flat plate.

Increasing pressure and temperature enhances the performance of SOFC.

Polymer Electrolyte Fuel Cell. The basic cell consists of a proton-conducting membrane such as perfluoro sulfonic acid polymer sandwiched between two Pt-impregnated porous electrodes. The backs of the electrodes are made hydrophobic by coating with Teflon®, which provides a path for gas to diffuse to the catalyst layer.

The electrochemical reactions for PEFC are similar to PAFC as given in Table 8.13.1.

The protons from the anode diffuse through the membrane with the help of water molecules soaked in the membrane. The cell operates at low temperature (80°C) and can have very high current densities. Therefore, the cell can be made very compact and can have fast start. There are no corrosive fluids (acids or alkalis) in the cell. Because of these attributes the cell is particularly suited for vehicle-power operation. Present research includes investigation of using methanol and natural gas as the fuel for the cell.

Alkaline Fuel Cell. Alkaline electrolytes have faster kinetics, which allows the use of non-noble metal electrocatalysts. However, AFCs suffer a drastic performance loss if CO_2 is present in the fuel or the oxidant, for example, air. Therefore, AFCs are restricted for use where pure H_2 and O_2 can be used. They have been used in the past in the space program.

Fuel Cell Performance

The performance of fuel cells is affected by the operating variables (e.g., temperature, pressure, gas composition, reactant utilization, and current density) and other factors that influence the reversible cell potential (impurities) and the magnitude of the irreversible voltage losses (polarization, contact resistance, exchange current).

The cell voltage (V_{cell}) is given by

$$V_{cell} = E - iR - \mu_p \tag{8.13.32}$$

where i is the current through the cell, R is the cell resistance, and μ_p is the polarization loss.

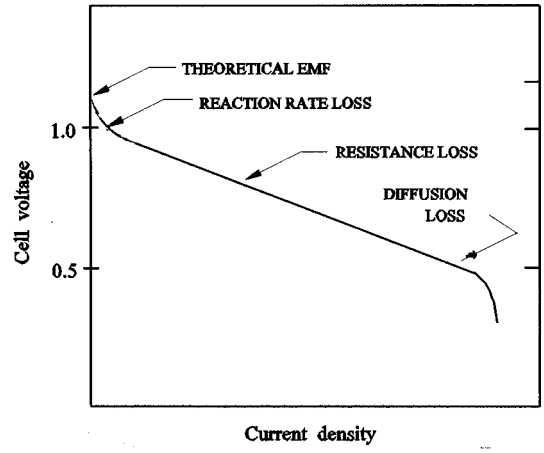

FIGURE 8.13.10 Losses affecting current-voltage characteristics.

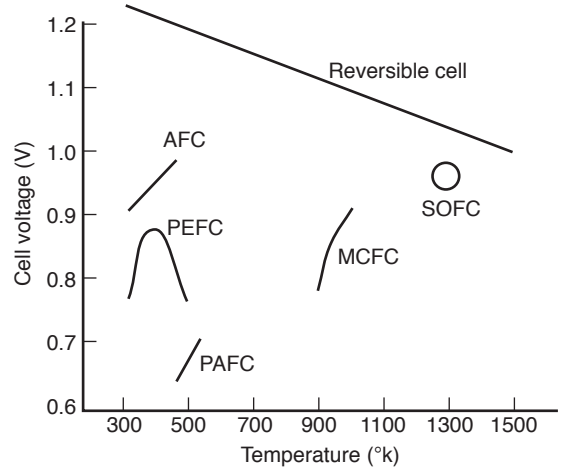

FIGURE 8.13.11 Dependence of the initial operating cell voltage of typical fuel cells on temperature. .

Current Density. Current density has a major impact on the cell voltage. Figure 8.13.10 shows how various losses affect the current-voltage characteristics.

Temperature and Pressure. Increase in pressure generally has a beneficial effect on the cell performance. Increased reactant pressure increases gas solubility and mass transfer rates. In addition, electrolyte loss due to evaporation is decreased.

Theoretically, the reversible potential of an H_2/O_2 fuel cell decreases with an increase in temperature. The practical effect of temperature is mixed, as shown in Figure 8.13.11.

Fuel Cell Power Systems

A general fuel cell power system consists of a fuel processor, fuel cell stack, power conditioner, and possibly a cogeneration or bottoming system to utilize the rejected heat. A schematic of a basic system is shown in Figure 8.13.12.

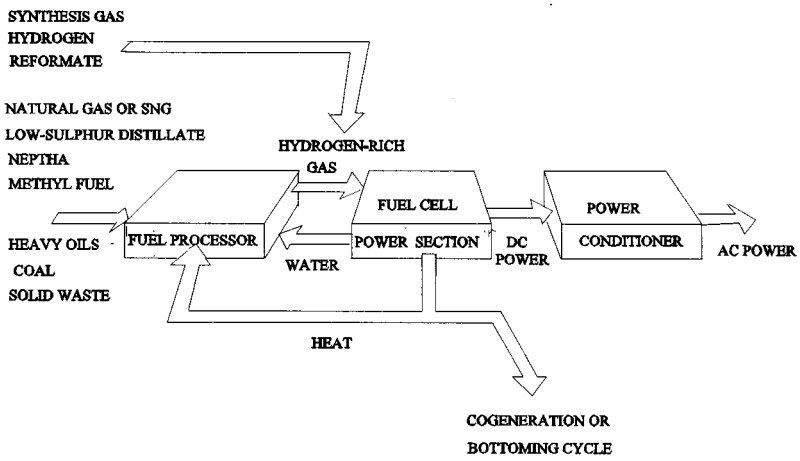

FIGURE 8.13.12 Basic fuel cell power system.

Fuel Processors. If pure hydrogen is available, no additional fuel processor is needed. However, in most applications hydrogen needs to be generated from other fuels, such as natural gas, methane, methanol, etc.

Natural Gas Processing. Natural gas is mostly methane (CH_4) with small amounts of other hydrocarbons. It can be converted to H_2 and CO in a steam-reforming reactor according to Equation (8.13.31). Fuels are typically steam reformed at temperatures of 760 to 980°C.

Liquid Fuel Processing. Liquid fuels such as distillate, naphtha, diesel oil, and fuel oil can be reformed by noncatalytic partial oxidation of the fuel by oxygen in the presence of steam with flame temperatures of 1300 to 1500°C.

Nomenclature

E = internal cell voltage
F = faraday, charge of 1 g-mol of electrons
G = Gibbs free energy
H = enthalpy
ΔH = heat of reaction, enthalpy of formation
I = current
n = number of g-mol
P = Pressure
R = gas constant
S = entropy
t = time
T = temperature
V = voltage drop
W_e = electrical work

Superscript

0 = values under standard conditions — 25°C, 1 atm

Defining Terms

Alkaline fuel cell (AFC): A fuel cell using KOH as the electrolyte.
Faraday: Change of 1 g · mol of electrons, which equals 96,439 C.
Molten carbonate fuel cell (MCFC): A fuel cell using molten carbonate as the electrolyte.

Phosphoric acid fuel cell (PAFC): A fuel cell using phosphoric acid as the electrolyte.
Polymer electrolyte fuel cell (PEFC): A fuel cell using Zerconia as the electrolyte.
Solid oxide fuel cell (SOFC): A fuel cell using potassium as the electrolyte.

References

Angrist, S.W. 1982. Chapter 8, in *Direct Energy Conversion*. Allyn and Bacon, Boston.
Appleby, A.J. and Foulkes, F.R. 1989. *Fuel Cell Handbook,* Van Nostrand Reinhold, New York.
Baumgartner, C.E., DeCarlo, V.J., Glugla, P.G., and Grimaldi, J.J. 1985. *J. Electrochem. Soc,* 132, 57.
Farooque, M. 1990. ERC, Development on Internal Reforming Carbonate Fuel Cell Technology, Final Report, prepared for United States DOE/METC, DOC/MC/23274-2941, pp. 3–19, October.
Hirschenhofer, J.H., Stauffer, D.B., and Engleman, R.R. 1994. *Fuel Cells, A Handbook,* rev. 3. Prepared by Gilbert/Commonwealth, Inc., under U.S. DOE Contract No. DE-AC01-88FE61684, United States Department of Energy, Office of Fossil Energy, Morgantown, WV.
Kinoshita, K., McLarnon, F.R., and Cairns, E.J. 1988. *Fuel Cells, A Handbook*. Prepared by Lawrence Berkeley Laboratory for the United States DOE under contract DE-AC03765F00098.
Maru, H.C., Paetsch, L., and Piegeaud, A. 1984. In *Proceedings of the Symposium on Molten Carbonate Fuel Technology,* R.J. Selman and T.D. Claar, Eds., The Electrochemical Society, Pennington, NJ, p. 20.
Minh, N.Q. 1991. High-temperature fuel cells, Part 2: The solid oxide cell, *Chem. Tech.,* 21, February.
Minh, N.Q. 1993. Ceramic fuel cells, *J. Am. Ceram. Soc.,* 76(3), 563–588.
Pigeaud, A., Skok, A.J., Patel, P.S., and Maru, H.C. 1981. *Thin Solid Films,* 83, 1449.
Wark, K. 1988. *Thermodynamics*, McGraw-Hill, New York, p. 873.

Further Information

Information presented in this section borrows heavily from Hirschenhofer et al. (1994) which lists original references of works published by thousands of researchers across the world. For those references and further information, readers are referred to the *Fuel Cell* handbooks by Hirschenhofer, Stauffer, and Engleman (1994), and Appleby and Foulkes (1989), listed in the References section.

Thermionic Energy Conversion

Mysore L. Ramalingam

Introduction

Thermionic energy conversion (TEC) is the process of converting heat directly to useful electrical work by the phenomenon of thermionic electron emission. This fundamental concept can be applied to a cylindrical version of the planar converter, considered the building block for space nuclear power systems (SNPS) at any power level. Space nuclear reactors based on TEC can produce power in the range of 5 kWe to 5 MWe, a spectrum that serves the needs of current users such as National Aeronautics and Space Administration (NASA), United States Air Force (USAF), United States Department of Energy (USDOE), and Ballistic Missile Defense Organization (BMDO). Electrical power in this range is currently being considered for commercial telecommunication satellites, navigation, propulsion, and planetary exploration missions.

The history of thermionic emission dates back to the mid-1700s when Charles Dufay observed that electricity is conducted in the space near a red-hot body. Although Thomas Edison requested a patent in the late 1800s, indicating that he had observed thermionic electron emission while perfecting his electric light system, it was not until the 1960s that the phenomenon of TEC was adequately described theoretically and experimentally (Hatsopoulos and Gryftopoulos, 1973). These pioneering activities have led to the development of thermionic SNPS that could potentially be augmented by Brayton and Stirling

cycle generators to produce additional power from waste heat in NASA manned lunar and martian exploration missions (Ramalingam and Young, 1993).

Principles of Thermionic Energy Conversion

Figure 8.13.13 represents a schematic of the essential components and processes in an elementary thermionic converter (TC). Electrons "boil-off" from the emitter material surface, a refractory metal such as tungsten, when heated to high temperatures (2000 K) by a **heat source**. The electrons then traverse the small interelectrode gap, to a colder (1000 K) collector surface where they condense, producing an output voltage that drives the current through the electrical load and back to the emitter. The flow of electrons through the electrical load is sustained by the temperature difference and the difference in **surface work functions** of the electrodes.

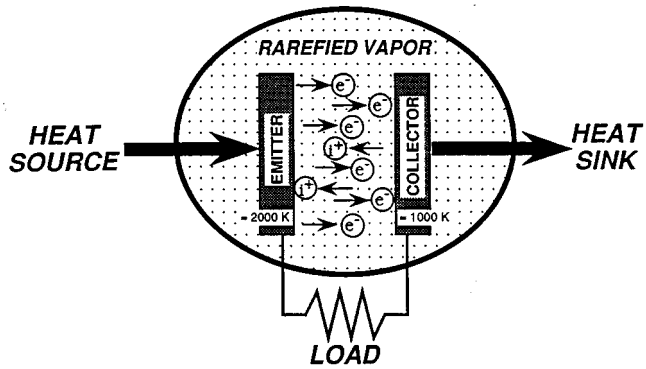

FIGURE 8.13.13 Schematic of an Elementary TEC.

Surface Work Function. In a simple form, the energy required to separate an electron from a metal surface atom and take it to infinity outside the surface is termed the electron work function or the work function of the metal surface. The force experienced by an electron as it crosses an interface between a metal and a rarefied vapor can be represented by the **electron motive**, Ψ, which is defined as a scalar quantity whose negative gradient at any point is a measure of the force exerted on the electron at that point (Langmuir and Kingdon, 1925). At absolute zero the kinetic energy of the **free electrons** would occupy quantum energy levels from zero to some maximum value called the Fermi level. Each energy level contains a limited number of free electrons, similar to the electrons contained in each electron orbit surrounding the nucleus of an atom. Fermi energy, μ, corresponds to the highest energy of all free electrons at absolute zero. At temperatures other than absolute zero some of the free electrons begin to experience energies greater than that at the Fermi level. Thus, the electron work function Φ, would be defined as

$$\Phi = \Psi_T - \mu \tag{8.13.33}$$

where Ψ_T represents the electron motive or energy at some temperature, T, above absolute zero.

Interelectrode Motive Distribution. Figure 8.13.14 provides a schematic representation of the electron motive distribution in the interelectrode space of a thermionic converter. Under ideal conditions of particle transport, the motive varies linearly from Ψ_{EM}, the motive just outside the emitter, to Ψ_{CO}, the motive outside the collector surface. The magnitudes of the Fermi energies of the emitter and collector relative to Ψ_{EM} and Ψ_{CO} are clearly indicated. The internal voltage drop of the converter is defined as;

$$\Delta V = \left(\Psi_{EM} - \Psi_{CO}\right)/e \tag{8.13.34}$$

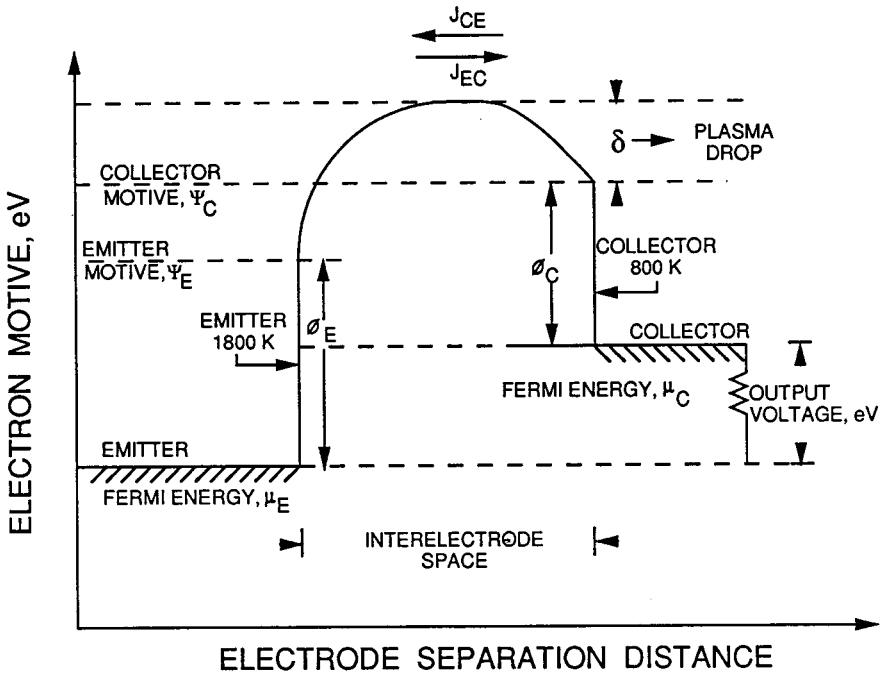

FIGURE 8.13.14 Electron motive distribution in the interelectrode gap.

In a conventional thermionic converter, the emitter and collector are not at the same temperature, but to a good approximation, the output voltage, neglecting **lead losses** and **particle interaction losses**, can be represented by the relationship.

$$V = \left(\mu_{CO} - \mu_{EM}\right)/e \tag{8.13.35}$$

Since a real thermionic converter has an ionizing medium to improve its performance, a similar motive distribution can be defined for the ions. It is sufficient to state that the ion interelectrode motive has a slope equal and opposite to the corresponding electron interelectrode motive. The ions are, therefore, decelerated when the electrons are accelerated and vice versa.

Electron Saturation Current. In the absence of a strong influence from an external electrical source, the electron current ejected from a hot metal at the emitter surface into the vacuum ionizing medium is termed the *electron saturation current*. As this quantity depends on the number of free electrons $N(\varepsilon_x)$, Fermi-Dirac statistics provide the means to compute the number of free electrons, $N(\varepsilon_x)\,d\varepsilon_x$, incident on a unit area within the metal in unit time with energies corresponding to the motion normal to the area, between ε_x and $\varepsilon_x + d\varepsilon_x$. For energies greater than the Fermi energy, the functional dependence of $N(\varepsilon_x)$ on ε_x is given by (Fowler, 1955)

$$N\left(\varepsilon_x\right) \approx \left[4\pi m_e kT/h^2\right]\left[\exp\left\{-\varepsilon_x - \mu/kT\right\}\right] \tag{8.13.36}$$

where m_e is the mass of the electron = 9.108×10^{-28} g and h is Planck's constant = 4.140×10^{-15} eV · sec.

The electron saturation current density, J_{sat}, for a uniform surface, is found by integrating $N(\varepsilon_x)$ in the range of ε_x from Ψ_T to infinity for all $\Psi_T - \mu > kT$, which is the case for almost all materials and practical temperatures. The result of the integration yields

$$J_{sat} = AT^2 \exp\left[-\left(\Psi_T - \mu\right)/kT\right] \tag{8.13.37}$$

or

$$J_{sat} = AT^2 \exp\left[-\left(\Phi\right)/kT\right] \tag{8.13.38}$$

where A is the Richardson constant ≈ 120 A/cm$^2 \cdot$ K^2.

Equation (8.13.38), which is the most fundamental and important relationship for the design of a thermionic converter, is called the Richardson-Dushmann equation (Richardson, 1912). On similar lines, the ion saturation current density for a converter with an ionizing medium is given by the relationship (Taylor and Langmuir, 1933):

$$J_{isat} = ep_g \left[\left(2\pi m_g kT_g\right)^{0.5}\left(1 + 2\exp\left\{\left(V_i - \Phi/kT\right)\right\}\right)\right] \tag{8.13.39}$$

where p_g, T_g, m_g, and V_i are the pressure, temperature, mass, and first ionization energy, respectively, of the ionizing medium.

Types of Thermionic Converters

Thermionic converters can be broadly classified as vacuum thermionic converters and vapor thermionic converters, depending on the presence of an ionizing medium in the interelectrode gap. In vacuum thermionic converters the interelectrode space is evacuated so that the space is free of particles other than electrons and the two electrodes are placed very close together, thereby neutralizing the negative space charge buildup on the electrode surface and reducing the total number of electrons in transit. Due to machining limitations, vacuum converters have been all but completely replaced by vapor-filled thermionic converters. In vapor-filled thermionic converters, the interelectrode space is filled with a rarefied ionizing medium at a vapor pressure generally on the order of 1 to 10 torr. The vapor generally used is cesium as it is the most easily ionized of all stable gases and this can be provided through an external two-phase reservoir or an internal graphite reservoir (Young et al., 1993). The vapor neutralizes the negative space charge effect by producing positive ions at the electrode surfaces and gets adsorbed on the surfaces, thereby altering the work function characteristics.

Converter Output Characteristics

Figure 8.13.15 represents the output current-voltage characteristics for various modes of operation of the vacuum and vapor-filled thermionic converters. Characteristics obtained by not considering particle interactions in the interelectrode gap are generally considered ideal output characteristics. The figure essentially displays three types of converter output current-voltage characteristics, an ideal characteristic, an ignited mode characteristic, and an unignited mode characteristic. For an ideal converter in the interelectrode space the net output current density consists of the electron current density, J_{EMCO} flowing from emitter to collector diminished by the electron current density J_{COEM} flowing from collector to emitter and the ion-current density J_{iEMCO} flowing from emitter to collector. Thus,

$$J_{net} = J_{EMCO} - J_{COEM} - J_{iEMCO} \tag{8.13.40}$$

By expressing the individual terms as functions of ϕ, T, and V,

$$\begin{aligned} J_{net} = {} & AT_{EM}^2 \exp\left[-\left(\Phi_{EM}/kT_{EM}\right)\right] - AT_{CO}^2 \exp\left[-\left(\Phi_{EM} - eV\right)/kT_{CO}\right] \\ & - J_{EMS} \exp\left[-\left(\Psi_{EM} - \Psi_{CO}\right)kT_{EM}\right] \end{aligned} \tag{8.13.41}$$

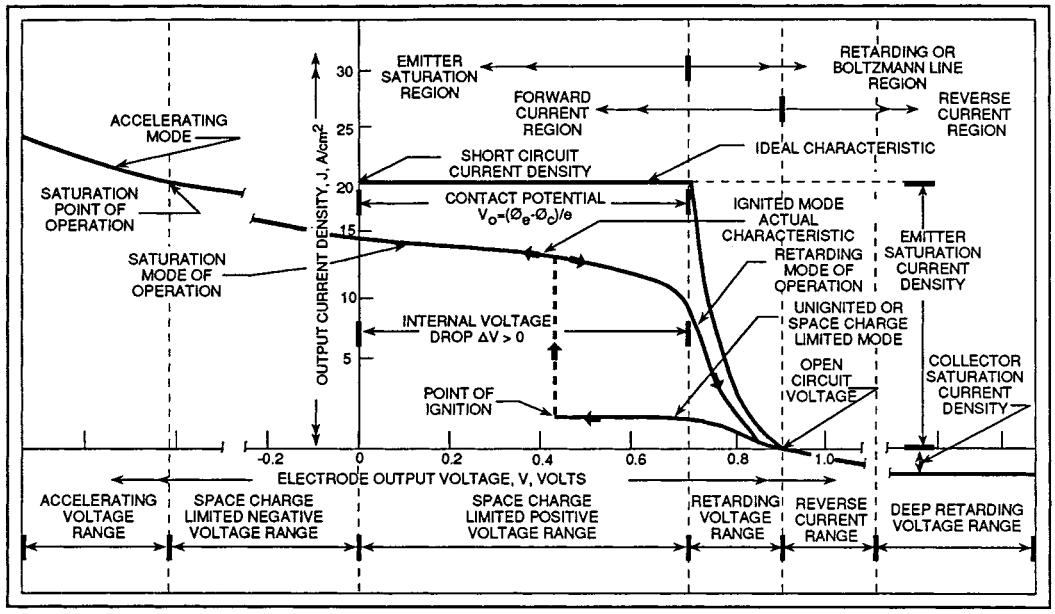

FIGURE 8.13.15 Thermionic diode output current density characteristics and nomenclature.

$$\text{for} \quad eV < \Phi_{EM} - \Phi_{CO}$$

Similar relationships can be generated for various types of thermionic converters.

Thermodynamic Analysis

In thermodynamic terms a thermionic converter is a heat engine that receives heat at high temperature, rejects heat at a lower temperature, and produces useful electrical work while operating in a cycle analogous to a simple vapor cycle engine. Based on the application of the first law of thermodynamics to the control volumes around the emitter (Houston, 1959; Angrist, 1976),

$$\text{Energy In} = \text{Energy Out} \tag{8.13.42}$$

i.e.,

$$q_{CB} + q_{JH} + q_{HS} = q_{EC} + q_{WB} + q_{CD} + q_{RA} \tag{8.13.43}$$

where, by using the terminology in Figure 8.13.14, each of the terms in Equation (8.13.43) can be elaborated as follows:

(a) Energy supplied by back emission of the collector:

$$q_{CB} = J_{COEM}\left[\Phi_{CO} + \delta + V + \left(2kT_{CO}/e\right)\right] \tag{8.13.44}$$

(b) Energy supplied by joule heating of lead wires and plasma:

$$q_{JH} = 0.5\left[J_{EMCO} - J_{COEM}\right]^2\left(R_{LW} + R_{PL}\right) \tag{8.13.45}$$

(c) Energy dissipated by electron cooling:

$$q_{EC} = J_{EMCO}\left[\Phi_{CO} + \delta + V - \Phi_{EM} + \left(2kT_{EM}\right)/e\right] \tag{8.13.46}$$

(d) Energy dissipated due to phase change by electron evaporation:

$$q_{WB} = J_{EM}\Phi_{EM} \tag{8.13.47}$$

(e) Energy dissipated by conduction through the lead wires and plasma:

$$q_{CD} = \Delta T\left[\left(K_{LW}A_{LW}/A_eL_{LW}\right) + \left(K_{PL}A_{PL}/A_eL_{IG}\right)\right] \tag{8.13.48}$$

Here, K represents thermal conductivity, LW = lead wires, PL = plasma, and IG = interelectrode gap.

(f) Energy dissipated by radiation from emitter to collector:

$$q_{RA} = 5.67 \times 10^{-12}\left(T_{EM}^2 - T_{CO}^4\right)\left(\varepsilon_{EM}^{-1} + \varepsilon_{CO}^{-1} - 1\right)^{-1} \tag{8.13.49}$$

Substitution for the various terms in Equation (8.13.42) yields q_{Hs}, the energy supplied to the emitter from the heat source.

The thermal efficiency of the thermionic converter is now expressed as

$$\eta_{TH} = \left[V\left(J_{EMCO} - J_{COEM}\right)/q_{HS}\right] \tag{8.13.50}$$

Design Transition to Space Reactors — Concluding Remarks

All the fundamentals discussed so far for a planar thermionic converter can be applied to a cylindrical version which then becomes the building block for space power systems at any power level. In a thermionic reactor, heat from the nuclear fission process produces the temperatures needed for thermionic emission to occur. The design of a thermionic SNPS is a user-defined compromise between the required output power and the need to operate reliably for a specified lifetime. Based on the type of contact the emitter has with the nuclear fuel, the power systems can be categorized as "in-core" or "out-of-core" power systems. At this stage it suffices to state that the emitter design for in-core systems is extremely complex because of its direct contact with the hot nuclear fuel.

Defining Terms

Electron motive: A scalar quantity whose negative gradient at any point is a measure of the force exerted on an electron at that point.

Free electrons: Electrons available to be extracted from the emitter for thermionic emission.

Heat source: Electron bombardment heating of the emitter.

Lead losses: Voltage drop as a result of the built-in resistance of the leads and joints.

Particle interaction losses: Voltage drop in the interelectrode gap as a result of particle collisions and other interactions.

Surface work function: A measure of the electron-emitting capacity of the surface.

Thermionic energy conversion: Energy conversion from heat energy to useful electrical energy by thermionic electron emission.

References

Angrist, S.W. 1976. *Direct Energy Conversion,* 3rd ed., Allyn and Bacon, Boston.
Fowler, R.H. 1955. *Statistical Mechanics,* 2nd ed., Cambridge University Press, New York.
Hatsopoulos, G.N. and Gyftopoulos, E.P. 1973. *Thermionic Energy Conversion,* Vol. 1, MIT Press, Cambridge, MA.
Houston, J.M. 1959. Theoretical efficiency of the thermionic energy converter, *J. Appl. Phys.,* 30:481–487.
Langmuir, I. and Kingdon, K.H. 1925. Thermionic effects caused by vapors of alkali metals, *Proc. R. Soc. London, Ser. A,* 107:61–79.
Ramalingam, M.L. and Young, T.J. 1993. The power of thermionic energy conversion, *Mech. Eng.,* 115(9):78–83.
Richardson, O.W. 1912. Some applications of the electron theory of matter, *Philos. Mag.,* 23:594–627.
Taylor, J.B. and Langmuir, I. 1933. The evaporation of atoms, ions and electrons from cesium films on tungsten, *Phys. Rev.,* 44:423–458.
Young, T.J., Thayer, K.L., and Ramalingam, M.L. 1993. Performance simulation of an advanced cylindrical thermionic fuel element with a graphite reservoir, presented at 28th AIAA Thermophysics Conference, Orlando, FL.

Further Information

Hatsopoulos, G.N. and Gryftopoulos, E.P. 1979. *Thermionic Energy Conversion,* Vol. 2, MIT Press, Cambridge, MA.
Cayless, M.A. 1961. Thermionic generation of electricity, *Br. J. Appl. Phys.,* 12:433–442.
Hernquist, K.G., Kanefsky, M., and Norman, F.H. 1959. Thermionic energy converter, *RCA Rev.,* 19:244–258.
Rasor, N.S. 1960. Figure of merit for thermionic energy conversion, *J. Appl. Phys.,* 31:163–167.
Ramalingam, M.L. 1993. The Advanced Single Cell Thermionic Converter Program, WL-TR-93-2112, USAF Technical Report, Dayton, OH.

Thermoelectric Power Conversion

Jean-Pierre Fleurial

Introduction

The advances in materials science and solid-state physics during the 1940s and 1950s resulted in intensive studies of thermoelectric effects and related applications in the late 1950s and through the mid-1960s (Rowe and Bhandari, 1983). The development of semiconductors with good thermoelectric properties made possible the fabrication of thermoelectric generators and refrigerators. Being solid-state devices, thermoelectric systems offer some unique advantages, such as high reliability, long life, small-size and no-vibrations refrigerators, and can be used in a wide temperature range, from 200 to 1300 K. However, because of their limited conversion efficiencies, these devices have remained confined to specialized applications. As the following sections will emphasize, the performance of those devices is closely associated with the magnitude of the **dimensionless figure of merit**, *ZT*, of the thermoelectric semiconductor.

ZT represents the relative magnitude of electrical and thermal cross-effect transport in materials. State-of-the-art thermoelectric materials, known since the early 1960s, have been extensively developed. Although significant improvements of the thermoelectric properties of these materials have been achieved, a maximum *ZT* value close to 1 is the current approximate limit over the whole 100 to 1500 K temperature range (Figure 8.13.16). To expand the use of thermoelectric devices to a wide range of applications will require improving *ZT* by a factor of two to three. There is no theoretical limitation on

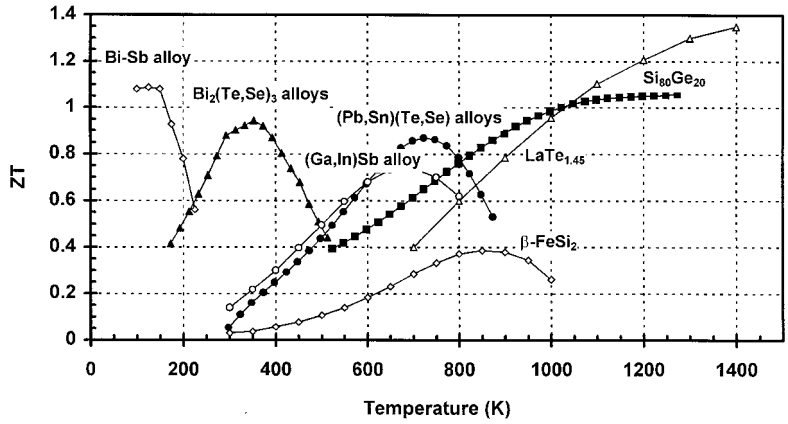

FIGURE 8.13.16 Typical temperature variations of *ZT* of state-of-the-art n-type thermoelectric alloys.

the value of *ZT*, and new promising approaches are now focusing on the investigation of totally different materials and the development of novel thin film heterostructure.

Thermoelectric Effects

Thermoelectric devices are based on two transport phenomena: the Seebeck effect for power generation and the Peltier effect for electronic refrigeration. If a steady temperature gradient is applied along a conducting sample, the initially uniform charge carrier distribution is disturbed as the free carriers located at the high-temperature end diffuse to the low-temperature end. This results in the generation of a back emf which opposes any further diffusion current. The open-circuit voltage when no current flows is the Seebeck voltage. When the junctions of a circuit formed from two dissimilar conductors (n- and p-type semiconductors) connected electrically in series but thermally in parallel are maintained at different temperatures T_1 and T_2, the open-circuit voltage V developed is given by $V = S_{pn}(T_1 - T_2)$, where S_{pn} is the Seebeck coefficient expressed in $\mu V \cdot K^{-1}$.

The complementary Peltier effect arises when an electrical current I passes through the junction. A temperature gradient is then established across the junctions and the corresponding rate of reversible heat absorption $\dot{Q}$ is given by $\dot{Q} = \Pi_{pn} I$, where Π_{pn} is the Peltier coefficient expressed in $W \cdot A^{-1}$ or V. There is actually a third, less-important phenomenon, the Thomson effect, which is produced when an electrical current passes along a single conducting sample over which a temperature gradient is maintained. The rate of reversible heat absorption is given by $\dot{Q} = \beta I(T_1 - T_2)$, where β is the Thomson coefficient expressed in $V \cdot K^{-1}$. The three coefficients are related by the Kelvin relationships:

$$S_{pn} = \frac{\Pi_{pn}}{T} \quad \text{and} \quad \frac{dS_{pn}}{dT} = \frac{\beta_p - \beta_n}{T} \tag{8.13.51}$$

Thermoelectric Applications

The schematic of a thermoelectric device, or module, on Figure 8.13.17, illustrates the three different modes of operation: power generation, cooling, and heating. The *thermoelectric module* is a standardized device consisting of several p- and n-type legs connected electrically in series and thermally in parallel, and bonded to a ceramic plate on each side (typically alumina). The modules are fabricated in a great variety of sizes, shapes, and number of thermoelectric couples and can operate in a wide range of currents, voltages, powers, and efficiencies. Complex, large-scale thermoelectric systems can be easily designed and built by assembling various numbers of these modules connected in series or in parallel depending on the type of applications.

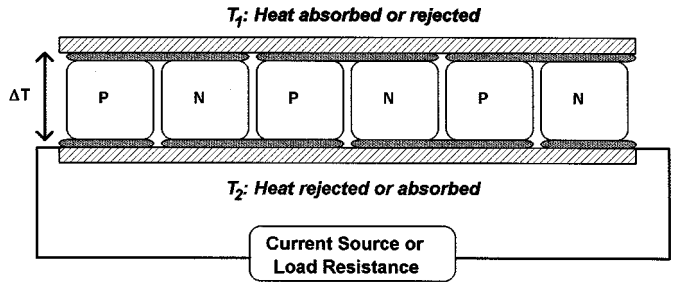

FIGURE 8.13.17 Schematic of a thermoelectric module.

Power Generation. When a temperature gradient is applied across the thermoelectric device, the heat absorbed at the hot junction (Figure 8.13.17, hot side $T_h - T_1$ and cold side, $T_c - T_2$) will generate a current through the circuit and deliver electrical power to the load resistance R_L (Harman and Honig, 1967). The conversion efficiency η of a thermoelectric generator is determined by the ratio of the electrical energy, supplied to the load resistance, to the thermal energy, absorbed at the hot junction, and is given by

$$\eta = \frac{R_L I^2}{S_{\text{pn}} I T_h + K\left(T_h - T_c\right) - \frac{1}{2} RI^2} \tag{8.13.52}$$

where K is the thermal conductance in parallel and R is the electrical series resistance of one p-n thermoelectric couple. The electrical power P_L generated can be written as

$$P_L = \frac{S_{\text{pn}}\left(T_h - T_c\right)^2 R_L}{\left(R_L + R\right)^2} \tag{8.13.53}$$

The thermoelectric generator can be designed to operate at maximum power output, by matching the load and couple resistances, $R_L = R$. The corresponding conversion efficiency is

$$\eta_P = \frac{T_h - T_c}{\frac{3}{2}T_h + \frac{1}{2}T_c + \frac{1}{4}Z_{\text{pn}}^{-1}} \tag{8.13.54}$$

where Z_{pn} is the figure of merit of the p-n couple given by

$$Z_{\text{pn}} = \frac{S_{\text{pn}}^2}{RK} \tag{8.13.55}$$

The figure of merit can be optimized by adjusting the device geometry and minimizing the RK product. This results in Z_{pn} becoming independent of the dimensions of the **thermoelectric legs**. Moreover, if the p- and n-type legs have similar transport properties, the figure of merit, $Z_{\text{pn}} = Z$, can be directly related to the Seebeck coefficient S, electrical conductivity σ or resistivity ρ, and thermal conductivity λ of the thermoelectric material:

$$Z = \frac{S^2}{\rho\lambda} = \frac{S^2\sigma}{\lambda} \tag{8.13.56}$$

The maximum performance η_{max} of the generator is obtained by optimizing the load-to-couple-resistance ratio, leading to the maximum energy conversion efficiency expressed as

$$\eta_{max} = \frac{T_h - T_c}{T_h} \frac{\sqrt{1 + Z_{pn} T_{av}} - 1}{\sqrt{1 + Z_{pn} T_{av}} + \frac{T_c}{T_h}} \tag{8.13.57}$$

It must be noted that the maximum efficiency is thus the product of the Carnot efficiency, less than unity, and of a material-related efficiency, increasing with increasing Z_{pn} values as illustrated in Figure 8.13.18.

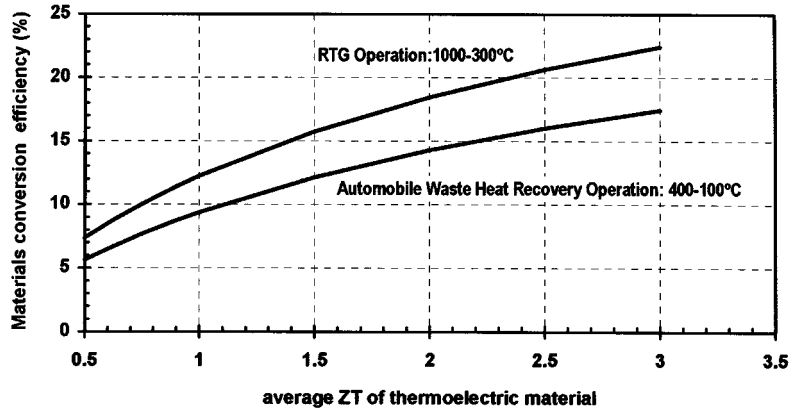

FIGURE 8.13.18 Maximum conversion efficiency η_{max} as a function of the average material figure of merit *ZT,* calculated using Equation (8.13.57) for two systems operating in different temperature ranges: the radioisotope generator (RTG) used for deep space missions and an automobile waste heat recovery generator.

Refrigeration. When a current source is used to deliver electrical power to a thermoelectric device, heat can be pumped from T_1 to T_2 and the device thus operates as a refrigerator (Figure 8.13.17, hot side $T_h = T_2$ and cold side, $T_c = T_1$). As in the case of a thermoelectric generator the operation of a thermoelectric cooler depends solely upon the properties of the p-n thermocouple materials expressed in terms of the figure of merit Z_{pn} and the two temperatures T_c and T_h (Goldsmid, 1986). The conversion efficiency or **coefficient of performance**, COP, of a thermoelectric refrigerator is determined by the ratio of the cooling power pumped at the cold junction to the electrical power input from the current source and is given by

$$\text{COP} = \frac{S_{pn} T_c I - \frac{1}{2} RI^2 - K(T_h - T_c)}{S_{pn}(T_h - T_c) I + RI^2} \tag{8.13.58}$$

There are three different modes of operation which are of interest to thermoelectric coolers. A thermoelectric cooler be designed to operate at maximum cooling power, Qc_{max}, by optimizing the value of the current:

$$I_{Qc_{max}} = \frac{S_{pn} T_c}{R} \text{ and } Qc_{max} = \frac{1}{2} \frac{(ST_c)^2}{R} - K(T_h - T_c) \tag{8.13.59}$$

Similarly, the conditions required for operating at maximum efficiency, COP_{max}, across a constant temperature gradient, are determined by differentiating Equation (8.13.58) with respect to I, with the solution:

$$I_{COP_{max}} = \frac{K(T_h - T_c)_c}{S_{pn} T_{av}} \left(1 + \sqrt{1 + Z_{pn} T_{av}}\right) \tag{8.13.60}$$

$$COP_{max} = \frac{T_c}{T_h - T_c} \frac{\sqrt{1 + Z_{pn} T_{av}} - \frac{T_h}{T_c}}{\sqrt{1 + Z_{pn} T_{av}} + 1} \tag{8.13.61}$$

By reversing the input current to the device, the thermoelectric refrigerator can become a heat pump, with T_1 being the hot junction temperature. The expression of the maximum conversion efficiency of the heat pump is very similar to Equation (8.13.61) because of the following relationship:

$$\left(COP_{max}\right)^{\text{heat pump}} = 1 + \left(COP_{max}\right)^{\text{refrigerator}} \tag{8.13.62}$$

The maximum COP expression in Equation (8.13.61) is similar to the one derived for the conversion efficiency η of a thermoelectric generator in Equation (8.13.57). However, there is a major difference between the COP_{max} and η_{max} parameters. Clearly, η_{max} increases with increasing ΔT values but is limited by the Carnot efficiency (Equation 8.13.54) which is less than 1, while COP_{max} in Equation (8.13.52) increases with decreasing ΔT values and can reach values much larger than 1. Figure 8.13.19 represents the variations of the COP_{max} of a thermoelectric cooling device optimized for working voltage and geometry as a function of average ZT values and temperature differences (hot junction temperature at 300 K). The average ZT value for current state-of-the-art commercially available materials (Bi_2Te_3-based alloys) is about 0.8. For example, it can be seen that a COP_{max} of 4 is obtained for a $(T_h - T_c)$ difference of 10 K, meaning that to pump 8 W of thermal power only 2 W of electrical power needs to be provided to the thermoelectric cooling device. This also means that 10 W of thermal power will be rejected at the hot side of the cooler.

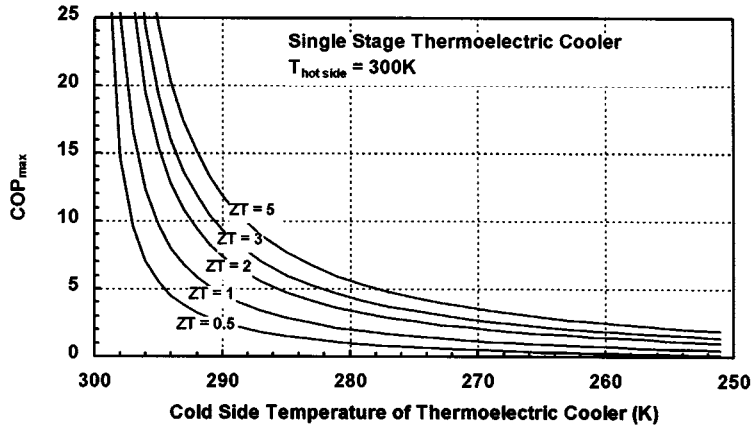

FIGURE 8.13.19 Maximum material coefficient of performance COP_{max} of a single-stage thermoelectric cooler calculated using Equation (8.13.61) as a function of the cold-side temperature (hot-side temperature of 300 K). Curves corresponding to various values of the average material figure of merit are displayed.

The operation of a thermoelectric refrigerator at maximum cooling power necessitates a substantially higher input current than the operation at maximum efficiency. This is illustrated by calculating the variations of the maximum COP and cooling power with the input current and temperature difference which have been plotted in Figures 8.13.20 and 8.13.21. The calculation was based on the properties of a thermoelectric cooler using state-of-the-art Bi_2Te_3-based alloys, and the arbitrary units are the same for both graphs. It can be seen that $I_{COP_{max}}$ increases while $I_{Qc_{max}}$ decreases with increasing ΔT. Also, it is possible to operate at the same cooling power with two different current values.

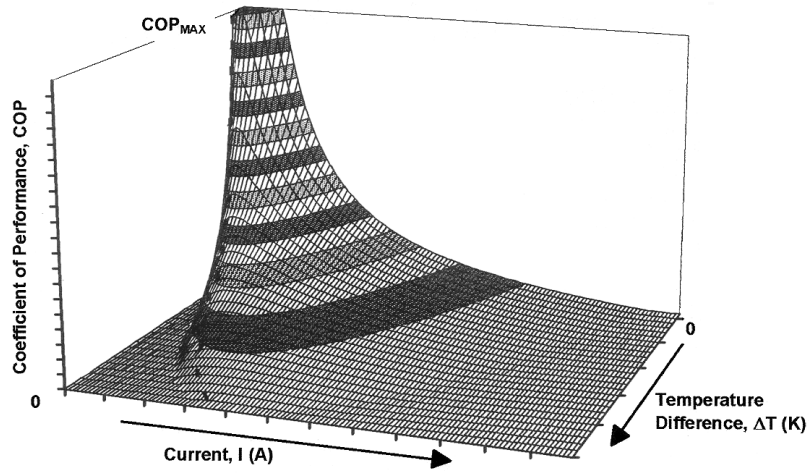

FIGURE 8.13.20 Three-dimensional plot of the variations of the COP of a thermoelectric cooler as a function of the operating current and the temperature difference.

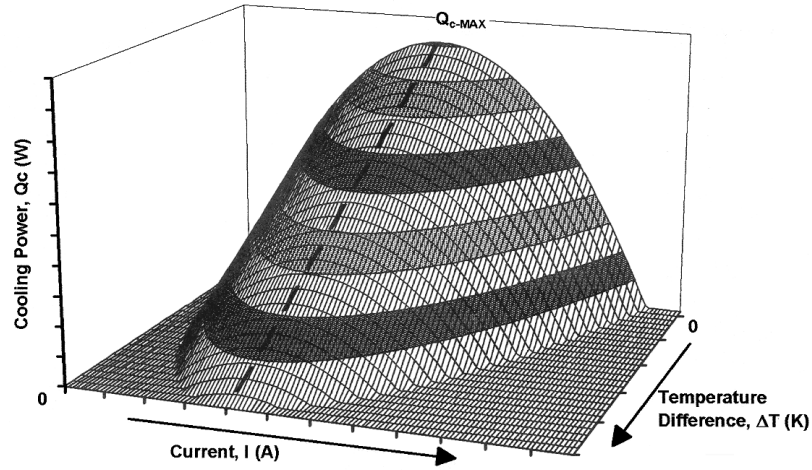

FIGURE 8.13.21 Three-dimensional plot of the variations of the cooling power of a thermoelectric cooler as a function of the operating current and the temperature difference.

Finally, the third problem of interest for thermoelectric coolers is to determine the maximum temperature difference, ΔT_{max}, that can be achieved across the device. As shown on Figure 8.13.21, by operating at maximum cooling power and extrapolating Equation (8.13.59) to $Qc_{max} = 0$, ΔT_{max} is given by

$$\Delta T_{\max} = \frac{1}{2} Z_{\text{pn}} T_c^2 \quad \text{and} \quad T_{c\,\min} = \frac{\sqrt{1 + 2Z_{\text{pn}} T_h} - 1}{Z_{\text{pn}}} \tag{8.13.63}$$

where $T_{c\,\min}$ corresponds to the lowest cold-side temperature achievable. If the cooler operates at a ΔT close to $\Delta T_{\max}$ or higher, it becomes necessary to consider a cascade arrangement with several **stages**. The COP of an n-stage thermoelectric cooler is optimized if the COP of each stage, COP_i, is the same, which requires $\Delta T_i / T_{i-1}$ to be the same for each stage. The overall maximum COP is then expressed as

$$\text{COP}_{\max} = \frac{1}{\left(\prod_{i=1}^{n} \left(1 + \frac{1}{\text{COP}_i} \right) - 1 \right)} \tag{8.13.64}$$

Additional Considerations

When considering the operation of an actual thermoelectric device, several other important parameters must be considered. The thermal and electrical contact resistances can substantially degrade the device performance, in particular for short lengths of the thermoelectric legs. For example, the conversion efficiency of a radioisotope generator system is about 20% lower than the value calculated in Figure 8.13.18 for the thermoelectric materials only. The electrical contact resistance arises from the connection (see Figure 8.13.17) of all the legs in series. Typical values obtained for actual generators and coolers are 10 to 25 $\mu\Omega \cdot \text{cm}^2$. The thermal contact resistance is generated by the heat-transfer characteristics of the ceramic plates and contact layers used to build the thermoelectric module. The heat exchangers and corresponding heat losses should also be taken into account.

In addition, the transport properties of the thermoelectric materials vary with temperature, as illustrated in Figure 8.13.16. When a thermoelectric device is operating across a wide temperature range, these variations should be factored in the calculation of its performance.

Nomenclature

COP	coefficient of performance
$\text{COP}_{\max}$	maximum coefficient of performance
COP_i	coefficient of performance of the *i*th stage of a multistage thermoelectric cooler
I	current intensity
$I_{\text{COP}_{\max}}$	current intensity required to operate a thermoelectric cooler at maximum conversion efficiency
$I_{Qc_{\max}}$	current intensity required to operate a thermoelectric cooler at maximum cooling power
K	thermal conductance
Q	rate of reversible heat absorption
R	electrical resistance
R_L	load resistance
P_L	electrical power delivered to the load resistance
S	Seebeck coefficient
S_{pn}	Seebeck coefficient of a p-n couple of thermoelements
T_1	temperature
T_2	temperature
T_{av}	average temperature across the thermoelectric device
T_c	cold-side temperature of a thermoelectric device
$T_{c\,\min}$	minimum cold-side temperature which can be achieved by a thermoelectric cooler
T_h	hot-side temperature of a thermoelectric device
V	voltage; open-circuit voltage
Z	thermoelectric figure of merit

Z_{pn} thermoelectric figure of merit of a p-n couple of thermoelements
ZT dimensionless thermoelectric figure of merit
β Thomson coefficient
β_p Thomson coefficient for the p-type thermoelement
β_n Thomson coefficient for the n-type thermoelement
ΔT temperature difference across a thermoelectric device
ΔT_{max} maximum temperature difference which can be achieved across a thermoelectric cooler
η thermoelectric conversion efficiency
η_{max} maximum thermoelectric conversion efficiency
λ thermal conductivity
Π_{pr} Peltier coefficient
ρ electrical resistivity

Defining Terms

Coefficient of performance: Electrical to thermal energy conversion efficiency of a thermoelectric refrigerator, determined by the ratio of the cooling power pumped at the cold junction to the electrical power input from the current source.

Dimensionless figure of merit: The performance of a thermoelectric device depends solely upon the properties of the thermoelectric material, expressed in terms of the dimensionless figure of merit *ZT*, and the hot-side and cold-side temperatures. *ZT* is calculated as the square of the Seebeck coefficient times the absolute temperature divided by the product of the electrical resistivity to the thermal conductivity. The best *ZT* values are obtained in heavily doped semiconductors, such as Bi_2Te_3 alloys, PbTe alloys, and Si-Ge alloys.

Stage: Multistage thermoelectric coolers are used to achieve larger temperature differences than possible with a single-stage cooler composed of only one module.

Thermoelectric leg: Single thermoelectric element made of n-type or p-type thermoelectric material used in fabricating a thermoelectric couple, the building block of thermoelectric modules. The geometry of the leg (cross-section-to-length ratio) must be optimized to maximize the performance of the device.

Thermoelectric module: Standardized device consisting of several p- and n-type legs connected electrically in series and thermally in parallel, and bonded to a ceramic plate on each. The modules are fabricated in a great variety of sizes, shapes, and number of thermoelectric couples.

References

Goldsmid, H.J. 1986. *Electronic Refrigeration,* Pion Ltd., London.

Hannan, T.C. and Honig, J.M. 1967. *Thermoelectric and Thermomagnetic Effects and Applications,* McGraw-Hill, New York.

Rowe, D.M and Bhandari, C.M. 1983. *Modern Thermoelectrics,* Reston Publishing, Reston, VA.

Further Information

The *Proceedings of the Annual International Conference on Thermoelectrics* are published annually by the International Thermoelectric Society (ITS). These proceedings provide the latest information on thermoelectric materials research and development as well as thermoelectric devices and systems. The ITS also publishes a semiannual newsletter. For ITS membership or questions related to thermoelectrics, you may contact the current ITS secretary: Dr. Jean-Pierre Fleurial, Jet Propulsion Laboratory, MS 277-212, Pasadena, CA 91109. Phone (818)-354-4144. Fax (818) 393-6951. E-mail jean-pierre.fleurial@jpl.nasa.gov.

Also, the *CRC Handbook of Thermoelectrics,* edited by D.M. Rowe was published by CRC Press Inc., Boca Raton, FL, became available in 1996. This handbook covers all current activities in thermoelectrics.

Magnetohydrodynamic Power Generation

William D. Jackson

Introduction

The discipline known as magnetohydrodynamics (MHD) deals with the interactions between electrically conducting fluids and electromagnetic fields. First investigated experimentally by Michael Faraday in 1832 during his efforts to establish the principles of electromagnetic induction, application to energy conversion yields a heat engine which has its output in electrical form and, therefore, qualifies as a direct converter. This is generally referred to as an MHD generator, but could be better described as an electromagnetic turbine as it operates on a thermodynamic cycle similar to that of a gas turbine.

The operating principle is elegantly simple, as shown in Figure 8.13.22. A pressurized, electrically conducting fluid flows through a transverse magnetic field in a channel or duct. Electrodes located on the channel walls parallel to the magnetic field and connected through an external circuit enable the motionally induced "Faraday electromotive force" to drive an electric current through the circuit and thus deliver power to a load connected into it. Taking the fluid velocity as **u** and the magnetic flux density as **B**, the intensity of the motionally induced field is $\mathbf{u} \times \mathbf{B}$. The current density, **J**, in the channel for a scalar conductivity σ is then given by Ohm's law for a moving conductor as

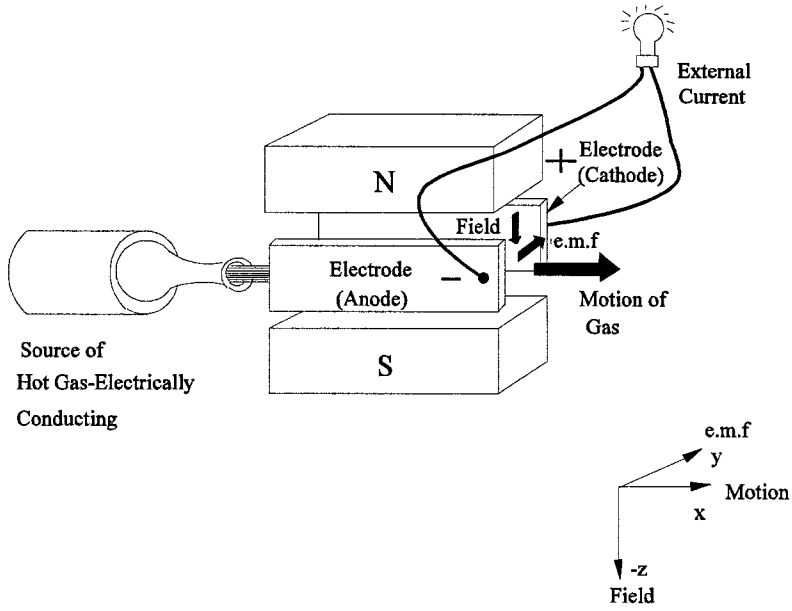

FIGURE 8.13.22 Principle of electromagnetic turbine or MHD generator.

$$\mathbf{J} = \sigma[\mathbf{E} + \mathbf{u} \times \mathbf{B}]$$

By taking the coordinates of Figure 8.13.22 and assuming that the quantities are constant, the power density flow from the MHD generator is, using $\mathbf{E} \cdot \mathbf{J}$

$$w_e = \sigma u_x^2 B^2 k(1-k)$$

where $k = Ez/u \times B$ is the "loading factor" relating loaded electric field to open circuit induction and is used in the same manner as the regulation of an electrical machine is applied to its terminal voltage.

It is instructive at this point to determine the power density of an MHD generator using values representative of the most commonly considered type of MHD generator. Combustion gas with $\sigma = 10$ S/m, a flow velocity of 800 m/sec and an applied field of 5 T for maximum power transfer ($k = 0.5$) yields w_e as 40 MW/m^3. This value is sufficiently attractive to qualify MHD generators for bulk power applications. An intensive, worldwide development effort to utilize this and other MHD generator properties has been conducted since the late 1950s. However, this has not yet led to any significant application of MHD generators. To understand how this has come about and what still needs to be accomplished to make MHD attractive will now be summarized.

Electrical Conductivity Considerations

Two approaches have been followed to obtain adequate ionization and, therefore, conductivity in the working fluid. What may be termed the mainline approach to achieving electrical conductivity is to add a readily ionizable material to "seed" the working fluid. Alkali metals with ionization potentials around 4 V are obvious candidates, although a lower value would be highly desirable. A potassium salt with an ionization potential of 4.09 eV has been widely used because of low cost but cesium with a 3.89-eV value is the preferred seed material when the running time is short or the working fluid is recycled. There are two methods of ionization:

1. Thermal ionization in which recombination ensures a common temperature for electrons, ions, and neutrals; the mass action law (Saha equation) is followed; and the heat of ionization in electron volts is the ionization potential; and
2. Extrathermal or nonequilibrium ionization where electrons and heavy particles are at different temperatures and the concept of entwined fluids (electron, ion, and neutral gases) is involved.

The former is applicable to diatomic combustion gases while the latter occurs in monatomic (noble) gases but is also observed in hydrogen. Only a small amount of seed material is required and is typically around 1% of the total mass flow for maximum conductivity.

The existence of mutually perpendicular **E** and **B** fields in an MHD generator is of major significance in that the electrons are now subjected to the Hall effect. This causes electrons and, therefore, electric currents to flow at an angle with respect to the **E** field in the collision-dominated environment of the MHD generator. The presence of a significant Hall effect requires that the electrical boundary conditions on the channel be carefully selected and also introduces the possibility of working fluid instabilities driven by force fluctuations of electrical origin. A further source of fluctuations and consequent loss of conductivity occurs when nonequilibrium ionization is employed due to current concentration by Joule heating. This latter effect is controlled by operating only in a regime where, throughout the channel, complete ionization of the seed material is achieved.

Generator Configurations and Loading

The basic consequence of the Hall effect is to set up **E** fields in both transverse and axial directions in the generator channel and these are generally referred to as the Faraday and Hall fields, respectively. The direction of the Faraday field depends on the magnetic field; the Hall field depends on the Hall parameter and is always directed toward the upstream end of the channel. These considerations, in turn, lead to the MHD generator having the characteristics of a gyrator — a two-terminal pair power-producing device in which one terminal pair (Faraday) is a voltage source and the other (Hall) is a current source dependent in this case on the Hall parameter. Electric power can be extracted from either the Faraday or Hall terminals, or both.

This has resulted in several electrical boundary conditions being utilized with the axial flow channel as shown in Figure 8.13.23. These are most readily understood by treating each anode-cathode pair as a generating cell. The segmented Faraday configuration (Figure 8.13.23a) is then simply a parallel operation of cells which leads to the apparently inconvenient requirement of separate loading of individual

cells: the Hall connection (Figure 8.13.23b) utilizes a single load by series connection but depends on the Hall parameter for its performance; and the diagonal connection (Figure 8.13.23c) connects the cells in series-parallel and so avoids Hall parameter dependence while retaining the single load feature. In all three linear configurations, the channel walls are electrically segmented to support the Hall field, and experience has shown that this must be sufficiently finely graded so that no more than 50 V is supported by the interelectrode gaps to avoid electrical breakdown.

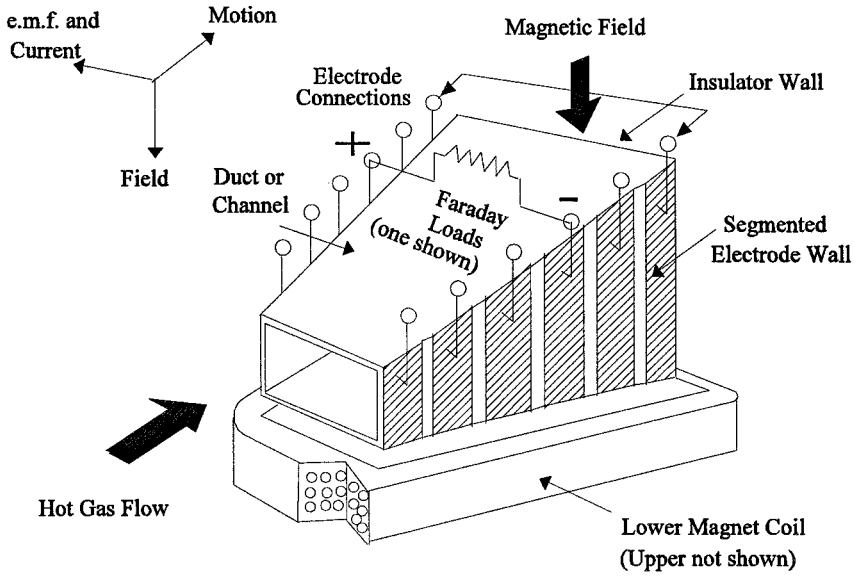

FIGURE 8.13.23 Basic Faraday linear MHD generator.

The MHD generator is a linear version of the homopolar machine originally demonstrated by Faraday and is, as a practical matter, confined to DC generation. Accordingly, some form of DC-AC conversion using power electronics is required for the vast majority of applications. The single load feature loses significance in this situation as the "power conditioning" can readily be arranged to combine (consolidate) the individual cell outputs before conversion to the required AC system conditions. Indeed, to maximize power extraction while limiting interelectrode voltages and controlling electrode currents (to ensure adequate lifetime), the power conditioning is arranged to extract power from both Faraday and Hall terminal pairs.

An alternative geometry is to set up a radial flow (usually but not necessarily outward) with the disk configuration of Figure 8.13.23d. The result is a Hall generator, which is generally favored for nonequilibrium ionization as it avoids the inevitable nonuniformities associated with electrode segmentation with their proclivity for promoting ionization instabilities. A measure of Faraday performance is achievable through the introduction of swirl, and additional ring electrodes enable power conditioning to control (and optimize) the radial electric field.

Components

An MHD generator per se requires several components to make up a complete powertrain. In addition to the power conditioning needed for DC-AC conversion these include a magnet, seed injector, combustor with fuel and oxidizer supply or an input heat exchanger, nozzle, compressor, diffuser, exhaust gas-cleaning system (for once-through systems), and controls. The need to accommodate a channel between the poles of a magnet qualifies the MHD generator as a large-air-gap machine.

Systems

Power systems incorporating MHD generators are either of the once-through (open-cycle) or working fluid recycle (closed-cycle) type, and the complete MHD system described in the previous section can either be stand-alone or incorporated into a more complex configuration such as a binary cycle. In the latter case, the high-temperature operation of the MHD unit makes it a topping cycle candidate and it is in this mode that MHD has received most system consideration. An MHD generator operated directly on ionized combustion gas is usually associated with an open cycle while nonequilibrium ionization with seeded noble gases and LMMHD are invariably considered for closed-cycle operation. An exception is nonequilibrium ionization in cesium-seeded hydrogen which has received some attention for open-cycle operation.

Heat Sources, Applications, and Environmental Considerations

A heat source capable of providing from 1000 K for LMMHD to over 3000 K for open-cycle systems for power production is a candidate. Rocket motor fuels, all fossil fuels, high-temperature nuclear reactors cooled with hydrogen and biomass are suitable for open cycles, while closed cycles can be driven through a heat exchanger by any of these combustion sources. A high-temperature nuclear reactor, probably helium cooled, is also a feasible source for MHD and in the early stages of development of the process received much attention. With the abandonment of efforts to develop commercial reactors to operate at temperatures above 1200 K, attention has focused on high-energy fuels for pulse power (few seconds) operation and coal for utility power generation.

While the debate over the role of fossil energy in the long-term electricity generation scenario continues, it is established that coal is a major resource which must be utilized at maximim efficiency to limit CO_2 production and must be combusted in a manner which reduces SO_2 and NO_x effluents to acceptable levels. The use of MHD generators significantly advances all of these objectives. Briefly, it was first observed that the "electromagnetic turbine" has the major advantage that it cannot only provide the highest efficiency of any known converter from the Carnot viewpoint but that its operation is not adversely affected by coal slag and ash. Indeed, slag provides an excellent renewable coating for the channel walls and increases lifetime.

System calculations have shown that, when coupled as a topping cycle to the best available steam plant technology, a thermal efficiency with coal and full environmental control is 52.5%. When coupled into a ternary cycle with either a gas turbine or fuel cells and a steam turbine, efficiencies upward of 60% are possible.

Technology Status

A pulse-type MHD generator was successfully built and operated by Avco (now Textron Defense Industries) in 1963 and a complete natural gas-fired pilot plant with a nominal 20-MW MHD generator was commissioned in the U.S.S.R. on the northern outskirts of Moscow in 1971. In the decade of the 1980s, development was focused on coal firing as a result of the oil crises of the 1970s and in the U.S. progressed to the point where the technology base was developed for a demonstration plant with a 15-MW MHD generator.

Future Prospects

The two particular attributes of the MHD generator are its rapid start-up to multimegawatt power levels for pulse power applications and its ability to provide a very high overall thermal efficiency for power plants using coal while meeting the most stringent environmental standards. The first has already been utilized in crustal exploration, and the second must surely be utilized when coal is the fuel of choice for electric power production. In the meantime, MHD has been established as a viable technology on which further development work will be conducted for advanced applications such as the conversion system for thermonuclear fusion reactors.

Further Information

The following proceedings series contain a full and complete record of MHD generator and power system development:

1. *Proceedings of the Symposia for the Engineering Aspects of Magnetohydrodynamics*, held annually in the U.S. since 1960 (except for 1971 and 1980).
2. *Proceedings of 11 International Conferences on Magnetohydrodynamic Electrical Power Generation*, held in 1962, 1964, 1966, 1968, 1971 , 1975, 1980, 1983, 1986, 1989, and 1992. The 12th conference will be held in Yokahama, Japan in October 1996.

8.14 Ocean Energy Technology

Desikan Bharathan and Federica Zangrando

The ocean contains a vast renewable energy potential in its waves and tides, in the temperature difference between cold, deep waters and warm surface waters, and in the salinity differences at river mouths (SERI, 1990; WEC, 1993; Cavanagh et al., 1993). Waves offer a power source for which numerous systems have been conceived. Tides are a result of the gravity of the sun, the moon, and the rotation of the Earth working together. The ocean also acts as a gigantic solar collector, capturing the energy of the sun in its surface water as heat. The temperature difference between warm surface waters and cold water from the ocean depths provides a potential source of energy. Other sources of ocean energy include ocean currents, salinity gradients, and ocean-grown biomass.

The following sections briefly describe the status and potential of the various ocean energy technologies, with emphasis placed on those with a near-term applicability.

Ocean Thermal Energy Conversion

Ocean thermal energy conversion (OTEC) technology is based on the principle that energy can be extracted from two reservoirs at different temperatures (SERI, 1989). A temperature difference as little as 20°C can be exploited effectively to produce usable energy. Temperature differences of this magnitude prevail between ocean waters at the surface and at depths up to 1000 m in many areas of the world, particularly in tropical and subtropical latitudes between 24° north and south of the equator. Here, surface water temperatures typically range from 22 to 29°C, while temperatures at a depth of 1000 m range from 4 to 6°C. This constitutes a vast, renewable resource, estimated at 10^{13} W, for potential baseload power generation.

Recent research has been concentrated on two OTEC power cycles, namely, **closed-cycle** and **open-cycle**, for converting this thermal energy to electrical energy (Avery and Wu, 1994). Both cycles have been demonstrated, but no commercial system is yet in operation. In a closed-cycle system, warm seawater is used to vaporize a working fluid such as ammonia flowing through a heat exchanger (evaporator). The vapor expands at moderate pressures and turns a turbine. The vapor is condensed in another heat exchanger (condenser) using cold seawater pumped from the ocean depths through a cold-water pipe. The condensed working fluid is pumped back to the evaporator to repeat the cycle. The working fluid remains in a closed system and is continuously circulated. In an open cycle system, the warm seawater is "flash" evaporated in a vacuum chamber to make steam at an absolute pressure of about 2.4 kPa. The steam expands through a low-pressure turbine coupled to a generator to produce electricity. The steam exiting the turbine is condensed by using cold seawater pumped from the ocean depths through a cold-water pipe. If a surface condenser is used, condensed steam provides desalinated water.

Effluent from either a closed cycle or an open cycle system can be further processed to enhance production of desalinated water through a flash evaporator/condenser system in a second stage.

For combined production of power and water, these systems are estimated to be competitive with conventional systems in several coastal markets.

Tidal Power

The energy from tides is derived from the kinetic energy of water moving from a higher to a lower elevation, as for hydroelectric plants. High tide can provide the potential energy for seawater to flow into an enclosed basin or estuary that is then discharged at low tide (Ryan, 1980). Electricity is produced from the gravity-driven inflow or outflow (or both) through a turbogenerator. The tidal resource is variable but quite predictable, and there are no significant technical barriers for deployment of this technology. Because costs are strongly driven by the civil works required to dam the reservoir, only a few sites around the world have the proper conditions of tides and landscape to lend themselves to this technology.

Although it has benefited from some recent developments in marine and offshore construction that significantly reduce construction time and costs, the economics of tidal power production still does not make it competitive with conventional energy systems.

The highest tides in the world can reach above 17 m, as in the Bay of Fundy between Maine and Nova Scotia, where it is projected that up to 10,000 MW could be produced by tidal systems in this bay alone. A minimum tidal range (difference between mean high and low tides) of 5 m is required for plants using conventional hydroelectric equipment (horizontal axial-flow water turbines housed in underwater bulbs or Straflo turbines). More recently, low-head hydroelectric power equipment has proved adaptable to tidal power and new systems for 2-m heads have been proposed.

There are a few tidal power stations operating in France, the former U.S.S.R., China, and Canada. The largest and longest-operating plant is the 240-MW tidal power station on the Rance River estuary in northern France (Banal and Bichon, 1981), which has operated with 95% availability since 1968. The 400-kW tidal plant in Kislaya Bay on the Barents Sea in the former U.S.S.R. has been operating since 1968; at this favorable site only a 50-m-wide dam was needed to close the reservoir. The 20-MW Canadian plant at Annapolis on the Bay of Fundy uses a Straflo turbine generator and has operated reliably since 1984. A number of small-bulb and Straflo turbine generator plants of up to 4 MW are also installed on the China coastline.

Wave Power

Waves contain significant power which can be harnessed by shore-mounted or offshore systems, the latter having larger incident power on the device but requiring more costly installations. A myriad of wave-energy converter concepts have been devised, transforming wave energy into other forms of mechanical (rotative, oscillating, or relative motion), potential, or pneumatic energy, and ultimately into electricity; very few have been tested at sea.

The power per unit frontal length of the wave is proportional to wave height squared and to wave period, with their representative values on the order of 2 m and 10 sec. The strong dependence on wave height makes the resource quite variable, even on a seasonal and a yearly average basis. The northeastern Pacific and Atlantic coasts have average yearly incident wave power of about 50 kW/m, while near the tip of South America the average power can reach 100 kW/m. Japan, on the other hand, receives an average of 15 kW/m. Waves during storms can reach 200 kW/m, but these large waves are unsafe for operation because of their severity, and they impose significant constraints and additional costs on the system. Overall, the amount of power that could be harvested from waves breaking against world coastlines is estimated to be on the order of the current global consumption of energy. However, total installed capacity amounts to less than 1 MW worldwide.

A commonly deployed device is the oscillating water column (OWC), which has so far been mounted on shore but is also proposed for floating plants. It consists of an air chamber in contact with the sea so that the water column in the chamber oscillates with the waves. This motion compresses the air in the chamber, which flows in and out of a Wells turbine. This turbine can be self-rectifying, i.e., it uses the airflow in both directions, and it consists of a simple rotor, with symmetrical airfoil blades attached tangentially to a central disk. Inertial energy storage (flywheels) is often used to even out the variable pneumatic energy delivered by the air.

Two of the largest wave-energy power plants were built at Toftestallen, near Bergen, Norway. A Norwegian company, Norwave A.S., built a 350-kW tapered channel (Tapchan) device in 1984, which survived a severe storm in 1989 (the 500 kW multi-resonant OWC plant built by Kvaerner Brug A.S. did not). The channel takes advantage of the rocky coastline to funnel waves through a 60-m-wide opening into a coastal reservoir of 5500 m^2, while maintaining civil engineering costs to a minimum. Wave height increases as the channel narrows over its 60-m length, and the rising waves spill over the 3-m-high channel walls, filling the reservoir. Continuous wave action maintains the reservoir level at a relatively constant elevation above sea level, providing potential energy for a low-head hydroelectric Kaplan turbogenerator. Estimates by Norwave to rebuild an identical plant at this site suggested capital

costs of $3500/kW installed, and energy costs of 8¢/kWhr, at a plant capacity factor of 25% (ASCE, 1992). In recent efforts, the National Institute of Ocean Technology has installed a 150-kW wave-energy conversion device in the southern tip of India.

Concluding Remarks

Among the many ocean energy prospects, OTEC, tides, and tapered channel wave-energy converters offer the most near-term potential and possess applicability for a large variety of sites. To realize their potential, additional research and development is required.

Defining Terms

Ocean thermal energy conversion (OTEC): A system that utilizes the temperature difference between the seawater at the surface and at depths.

Closed-cycle OTEC: Uses a working fluid in a closed cycle.

Open-cycle OTEC: Uses steam flashed from the warm seawater as the working fluid which is condensed and exhausted.

References

ASCE, 1992, *Ocean Energy Recovery, The State of the Art,* R.J. Seymour, Ed., American Society of Civil Engineers, New York.

Avery, W.H. and Wu, C. 1994, *Renewable Energy from the Ocean, a Guide to OTEC,* Oxford University Press, New York.

Banal, M. and Bichon, A. 1981. Tidal Energy in France: The Rance Estuary Tidal Power Station — Some Results after 15 Years of Operation, Paper K3, Second Symposium on Wave and Tidal Energy, Cambridge, England, September.

Cavanagh, J.E., Clarke, J.H., and Price, R. Ocean energy systems, in *Renewable Energy, Sources for Fuels and Electricity,* T.B. Johansson, H. Kelley, A.K.N. Reddy, and R.H. Williams (Eds.), Island Press, Washington, D.C., 1993, chap 12.

Ryan, P.R. 1979/80. Harnessing power from tides: state of the art, *Oceanus,* 22(4), 64–67.

SERI, 1989. *Ocean Thermal Energy Conversion: An Overview*, Solar Energy Research Institute, SERI/SP-220-3024, Golden, CO.

SERI, 1990. *The Potential of Renewable Energy: An Interlaboratory White Paper*, Solar Energy Research Institute, SERI/TP-260-3674, Golden, CO.

WEC, 1993. *Renewable Energy Resources — Opportunities and Constraints 1990–2020*, World Energy Council, London, England.

Further Information

CEC, *1992 Energy Technology Status Report*, California Energy Commission, Sacramento, CA, 1992.

Funakoshi, H., Ohno, M., Takahashi, S., and Oikawa, K. Present situation of wave energy conversion systems, *Civil Eng. Jpn.,* 32, 108–134, 1993.

8.15 Combined Cycle Power Plants

William W. Bathie

There is a considerable amount of energy available in the exhaust gases of a gas turbine engine that can be used as the energy source for another system. Table 8.15.1 lists exit temperatures and flow rates for several present-day gas turbine engines.

TABLE 8.15.1 Gas Turbine Exhaust Temperatures and Mass Flow Rates for Several Gas Turbines

Manufacturer Model	Year Available	ISO Base Rating, kW	Heat Rate, Btu/kWhr	Mass Flow, Ib/sec	Exhaust Temperature
ABB					
GT 5	1993	2,650	12,544	33.5	445°C
GT 11N	1987	83,800	10,403	699.0	505°C
GT 13D	1970	97,900	10,564	869.0	490°C
GT 26	1994	240,000	9,030	1195.0	608°C
GE Power Systems					
PG 5371 (PA)	1987	26,300	11,990	270.0	909°F
PG 6541 (B)	1978	38,340	10,780	302.0	1002°F
PG 7161 (EC)	1994	116,000	9,890	769.0	1030°F
PG 9311 (FA)	1992	226,500	9,570	1327.0	1093°F
Siemens (KWU)					
V 64.3	1990	62,200	9,720	423.0	529°C
V 84.3A	1994	170,000	8,980	1000.0	562°C
V 94.3A	1995	240,000	8,980	1410.0	562°C

Source: 1995 Handbook, Gas Turbine World, Southport, CT, 1995. With permission.

In the past two decades, several cycles which combine the gas turbine and the steam turbine have become available with good fuel utilization compared with other available power plants. The first ones in the 1970s had net plant efficiencies of about 40% with the most recent ones achieving net plant efficiencies of over 55%.

One way to utilize the energy available in gas turbine exhaust gases is as the energy source for a steam power plant. This is called a *combined cycle* and uses components from two systems which have independently proved themselves. The combined cycle power plant usually consists of one or more gas turbine engines exhausting into a heat-recovery steam generator (HRSG) where the energy is transferred from the exhaust gases to the water in the steam power plant.

The simplest arrangement for a combined cycle power plant is the single-pressure system as illustrated in Figure 8.15.1. It consists of the HRSG, a turbine, condenser, and pump. In this simplified configuration, it is assumed that no additional fuel is burned between the gas turbine and the HRSG.

The gases leaving the gas turbine engine enter the HRSG at state 4 and leave the HRSG at state 5. The water in the steam cycle portion of the combined cycle enters the HRSG economizer as a subcooler liquid (state a). The temperature of the water is increased in the economizer until it is a saturated liquid (state m). This is the point where the minimum temperature difference between the water in the steam cycle and the exhaust gases occurs and is called the *pinch point*. Typical pinch point values range from 10 to 30°C; the smaller the pinch point difference, the larger the required heat-transfer surface area. From state m to state v, the water is changed from a saturated liquid to a saturated vapor. From state v to state d, the water is superheated where it has its maximum temperature. A typical temperature-heat transfer diagram for this single-pressure steam turbine combined cycle is illustrated in Figure 8.15.2.

One should note that there is a significant difference between the desired feedwater conditions of a combined cycle power plant and a conventional steam power plant. In a combined cycle power plant, it is desirable to have the temperature of the water at as low a temperature as possible as it enters the HRSG to permit the maximum amount of energy to be transferred from the exhaust gases to the water

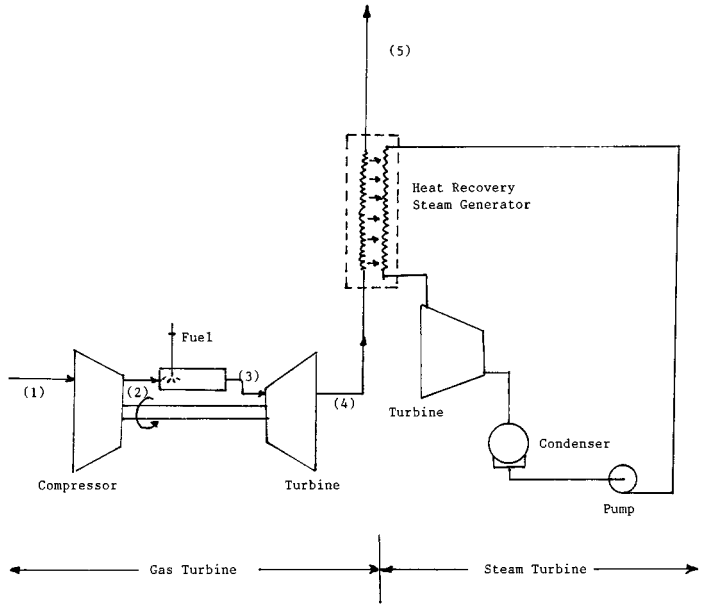

FIGURE 8.15.1 Combined cycle power plant with no supplementary firing.

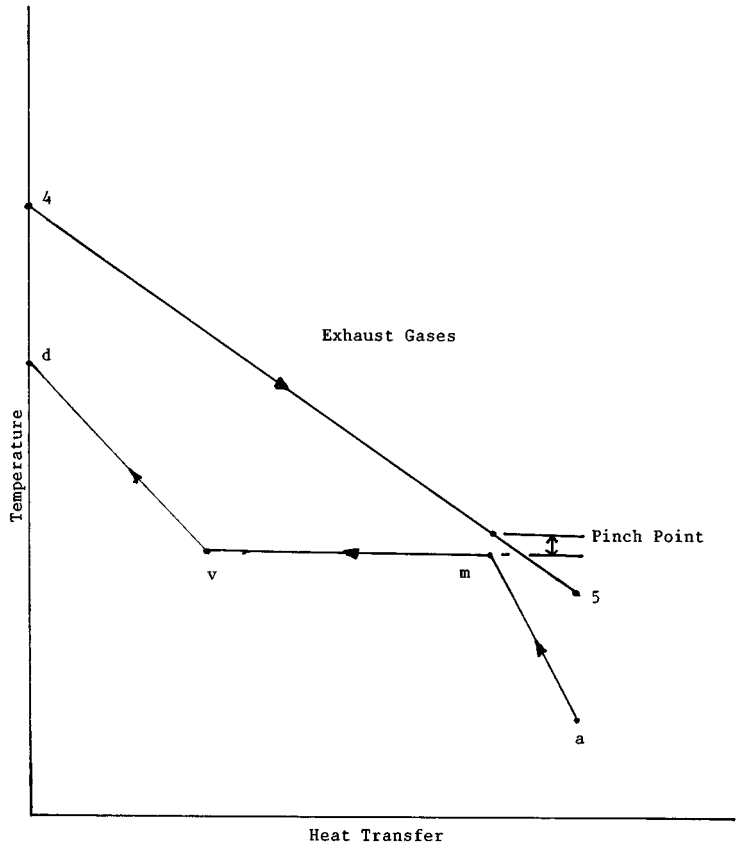

FIGURE 8.15.2 Typical temperature-heat transfer diagram for a single-pressure combined cycle power plant.

since the more energy transferred, the greater the amount of power produced by the steam turbine and the higher the combined cycle thermal efficiency or the lower the heat rate. In a conventional steam cycle power plant, the higher the feedwater temperature as it enters the steam generator (boiler), the higher the cycle thermal efficiency. Conventional steam cycle power plants achieve the higher feedwater temperature by the use of feedwater heaters.

Table 8.15.2 lists net plant output, heat rate, and net plant efficiency values for several combined cycles. One should observe for the units listed in Table 8.15.2 that

1. The size varies widely from a low of 22,800 kW to a high of 711,000 kW;
2. The heat rates vary from 7880 to 5885 Btu/kWhr. These compare with heat rate values for the gas turbines listed in Table 8.15.1 that vary from a high of 12,544 Btu/kWhr to a low of 8980 Btu/kWhr.
3. The net plant efficiency varies from a low of 42.8% to a high of 57.0%;
4. The fraction of the total net plant output from the steam turbine power plant in most cases ranges from 35 to 39%.

TABLE 8.15.2 Net Plant Output, Heat Rate, and Net Plant Efficiency for Several Combined Cycles

Manufacturer Model	Net Plant Output, kW	Heat Rate, Btu/kWhr	Net Plant Efficiency, %	Steam Turbine Power, kW
ABB				
KA 35-1	22,800	7,880	42.8	6,200
KA 8C-4	314,400	6,560	51.2	109,700
KA 11N-4	506,300	6,755	49.8	185,400
KA 24-2	501,800	5,885	57.0	182,800
GE Power Systems (60 Hz)				
S106B	59,200	7,020	48.6	22,600
S406B	240,000	6,930	49.3	93,600
S206FA	219,300	6,380	53.4	85,620
S207EC	357,700	6,415	53.2	134,400
S207FA	509,600	6,170	55.3	188,400
Siemens (KWU)				
GUD 3.64.3	275,000	6,550	52.1	98,000
GUD 3.84.2	486,000	6,560	52.0	186,000
GUD 3.94.2	711,000	6,525	52.3	269,000
GUD 2.84.3A	499,000	6,330	56.9	176,000

Source: 1995 Handbook, Gas Turbine World, Southport, CT, 1995. With permission.

One should keep in mind that only a few of the combined cycle plants currently available are listed in Table 8.15.2. The ones listed are intended to illustrate the range in net plant output and heat rate values and should not be interpreted as a list of all units currently available.

The amount of energy transferred in the HRSG is dependent on the steam pressure. This is illustrated in Figure 8.15.3. In this comparison, it is assumed in both cases that the steam exit temperature is the same and that the exhaust gas HRSG inlet temperature and flow rate are the same. One observes that the pressure of the water dictates the temperature at which evaporation occurs. The higher the evaporation temperature (and therefore steam pressure), the lower the mass flow rate of the steam, and therefore the lower the power generated by the steam power plant. It is obvious that the lower the steam pressure, the lower the flue gas temperature.

The output of an unfired single-pressure combined cycle power plant is determined by the gas turbine selected since this fixes the temperature and mass flow rate of the exhaust gases. One way to increase the steam cycle output is to introduce supplementary firing in the exhaust duct between the gas turbine exit and HRSG inlet. This is shown schematically in Figure 8.15.4. The advantages of adding supplementary firing are

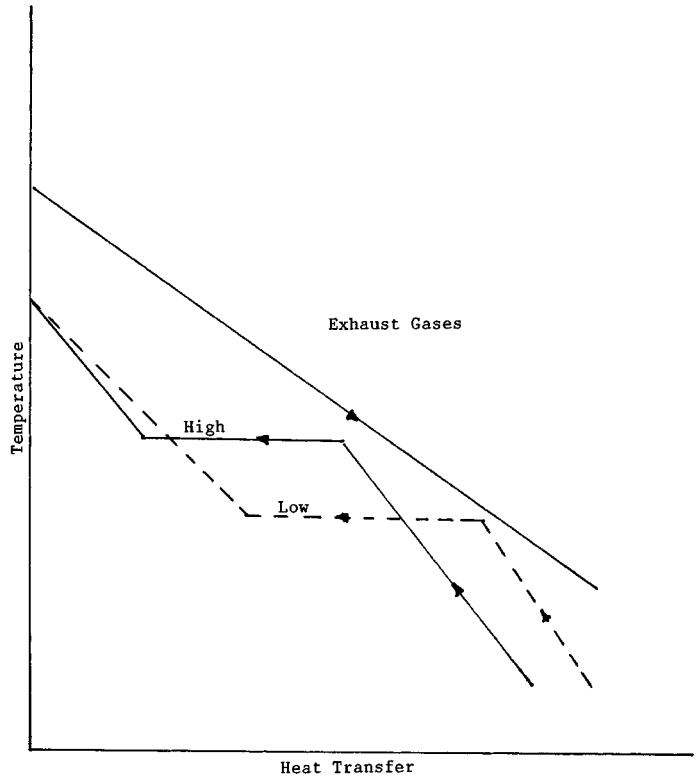

FIGURE 8.15.3 Effect of steam cycle pressure on energy transferred for a single-pressure combined cycle power plant.

1. The total output from the combined cycle will increase with a higher fraction of the output coming from the steam turbine cycle;
2. The temperature at the inlet to the HRSG can be controlled. This is important since the temperature and mass flow rate at the exit from the gas turbine are very dependent on the ambient temperature.

Figure 8.15.5 illustrates the effect on the temperature of the exhaust gases at the exit from the HRSG for unfired and supplementary fired combined cycles with the same pinch point temperature.

Combined cycle power plants with a single-pressure steam turbine do not maximize utilization of the energy in the exhaust gases. The ideal temperature-heat transfer diagram would be one where the temperature difference in the HRSG between the water (steam) and the exhaust gases is a constant.

One way to approach this constant temperature difference and improve the utilization of the energy in the exhaust gases is to use multipressures in the steam power plant cycle. Systems which have been used are

1. A dual pressure nonreheat cycle;
2. A dual-pressure reheat cycle; and
3. A triple-pressure reheat cycle.

Each system listed above has advantages and disadvantages. As new gas turbine engines enter the market with increased turbine inlet temperatures and component efficiencies, exhaust temperature from the gas turbine increases. This allows for higher superheated steam temperatures and improved combined cycle power plant efficiencies. This means that each design must be analyzed so that the selected design yields the most economical system.

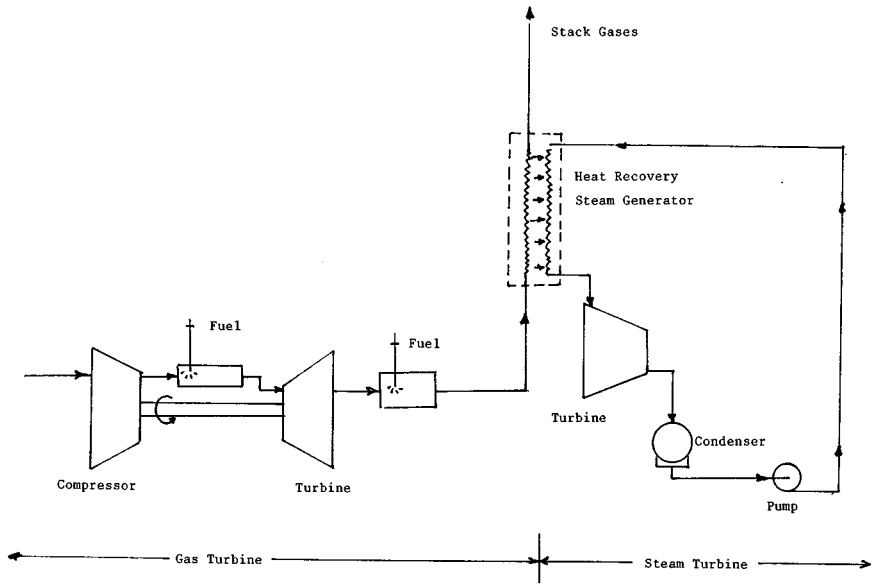

FIGURE 8.15.4 Combined cycle power plant with supplementary firing.

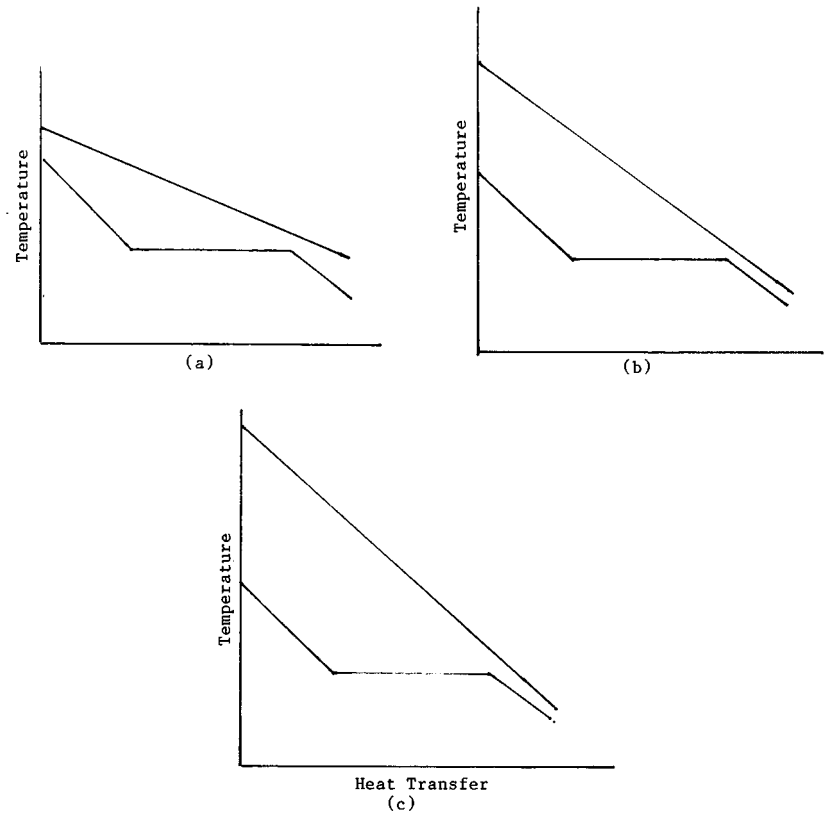

FIGURE 8.15.5 Effect of supplementary firing on exit temperature for same pinch point temperature difference. (a) No supplementary firing; (b), (c) supplementary firing.

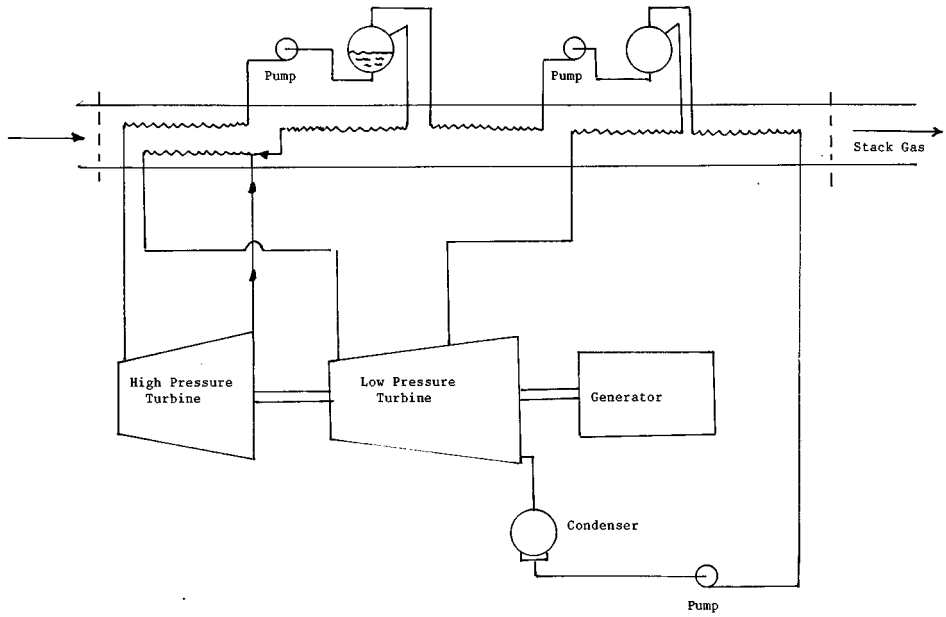

FIGURE 8.15.6 Schematic diagram for a three-pressure steam turbine combined cycle with superheating and reheat.

A simplified schematic diagram for a three-pressure combined cycle power plant is shown in Figure 8.15.6. This arrangement results in a high quality at the exit from the low-pressure steam turbine.

Reference

1995 Handbook, Gas Turbine World, Southport, CT, 1995.

Further Information

Bonzani, G. et al., Technical and economic optimization of a 450 MW combined cycle plant, in *1991 ASME Cogen-Turbo, 5th International Symposium and Exposition on Gas Turbines in Cogeneration, Repowering and Peak-Load Power Generation,* van der Linden, S. et al., Eds., pp. 131–143, ASME, New York, 1991.

Dechamps, P.J. et al., Advanced combined cycle alternatives with advanced gas turbines, in *ASME Cogen-Turbo Power '93, 7th Congress and Exposition on Gas Turbines in Cogeneration and Utility,* Holland, H.W. et al., Eds., pp. 387–396, ASME, New York, 1993.

Gyarmathy, G. and Ortmann, P., The off design of single- and dual-pressure steam cycles in CC plants, in *1991 ASME Cogen-Turbo, 5th International Symposium and Exposition on Gas Turbines in Cogeneration, Repowering and Peak-Load Power Generation,* van der Linden, S. et al., Eds., pp. 271–280, ASME, New York, 1991.

Horlock, J.H., *Combined Power Plants Including Combined Cycle Gas Turbine (CCGT) Plants,* Pergamon Press, New York, 1992.

Kehlhofer, W., *Combined-Cycle Gas & Steam Turbine Power Plants,* Fairmont Press, Englewood Cliffs, NJ, 1991.

Maurer, R., Destec's successes and plans for coal gasification combined cycle (CGCVC) power systems, in 1992 *ASME Cogen-Turbo, 6th International Conference in Cogeneration and Utility,* Cooke, D.H. et al., Eds., pp. 75–85, ASME, New York, 1992.

8.16 EMERGY Evaluation and Transformity

Howard T. Odum

EMERGY (spelled with an "m") evaluation is a method of energy analysis that puts all inputs and products on a common basis of what was previously required directly and indirectly to make each from one form of energy.

> EMERGY is the available energy of one kind previously used up directly and indirectly to make a service or product.

Its unit is the *emjoule,* defined to measure availability already used up. If average solar insolation at the earth's surface is chosen as the common base for the convenience of evaluating environmental and technological energy flows, then evaluations are made in units of solar emjoules, abbreviated sej.

In every energy transformation, available energy is used up to produce a smaller amount of energy of another kind. The EMERGY of one kind required directly and indirectly to make one unit of energy of another kind is defined as *transformity* (Odum, 1988).

> Solar transformity is the solar EMERGY of the inputs divided by the energy of the output.

$$\text{energy (J)} \times \text{transformity (sej/J)} = \text{EMERGY (sej)}$$

If all energy flows are expressed in solar EMERGY, then all kinds of energy may be compared according to their solar transformity. The more successive energy transformations there are, the higher the transformity. The higher the transformity, the more energy flows have converged in the process. Since many energy flows of one kind are usually required to support a smaller energy flow of another type, it is appropriate to describe the converging process as an *energy hierarchy.* The more transformations there are, the higher the transformity and the higher the position in a universal energy hierarchy. Figure 8.16.1 shows an environmental food chain with more energy flow but lower quality units (lower transformity) on the left and small total energy flow through high transformity units on the right. A land example is sunlight-grass-sheep-people. An aquatic series is sunlight-phytoplankton-zooplankton-small fish-large fish.

In environment, engineering, and economics the selective process of self organization generates higher quality energy capable of amplifying other processes. Thus observed transformitites are a measure of energy quality. Tables of solar transformity have been prepared based on previous EMERGY analysis (Odum, 1996). See sample in Table 8.16.1

Empower is the EMERGY used per unit time, for the United States about 8.5 E24 solar emjoules per year, a measure of the nation's processing of real wealth. By dividing the gross economic product ($6.5 trillion per year) the *EMERGY/money ratio* results (1.3 trillion solar emjoules per dollar). This is real wealth buying power of a dollar.

After an EMERGY evaluation is made, the solar EMERGY of each item can be divided by the *EMERGY*/money ratio to determine the *emdollars*, the buying power contributed by that item.

> *Emdollars are defined as the dollars of gross economic product due to that much real wealth measured as EMERGY.*

Because it puts all forms of available energy on a common basis, EMERGY may be the correct way to evaluate useful work. If real wealth comes from work, maximizing EMERGY production and use maximizes the real wealth of an economy. Selecting alternatives to maximize empower and emdollars is a new tool for engineering design and public policy.

Many energy analysis procedures add available energy as an exergy sum. However, EMERGY evaluation recognizes that each form of energy is different in its quality and the quantity of energy of other kinds required to make it. As shown in the EMERGY evaluation example (Table 8.16.2), each energy value is multiplied by its transformity so as to convert all items to solar EMERGY.

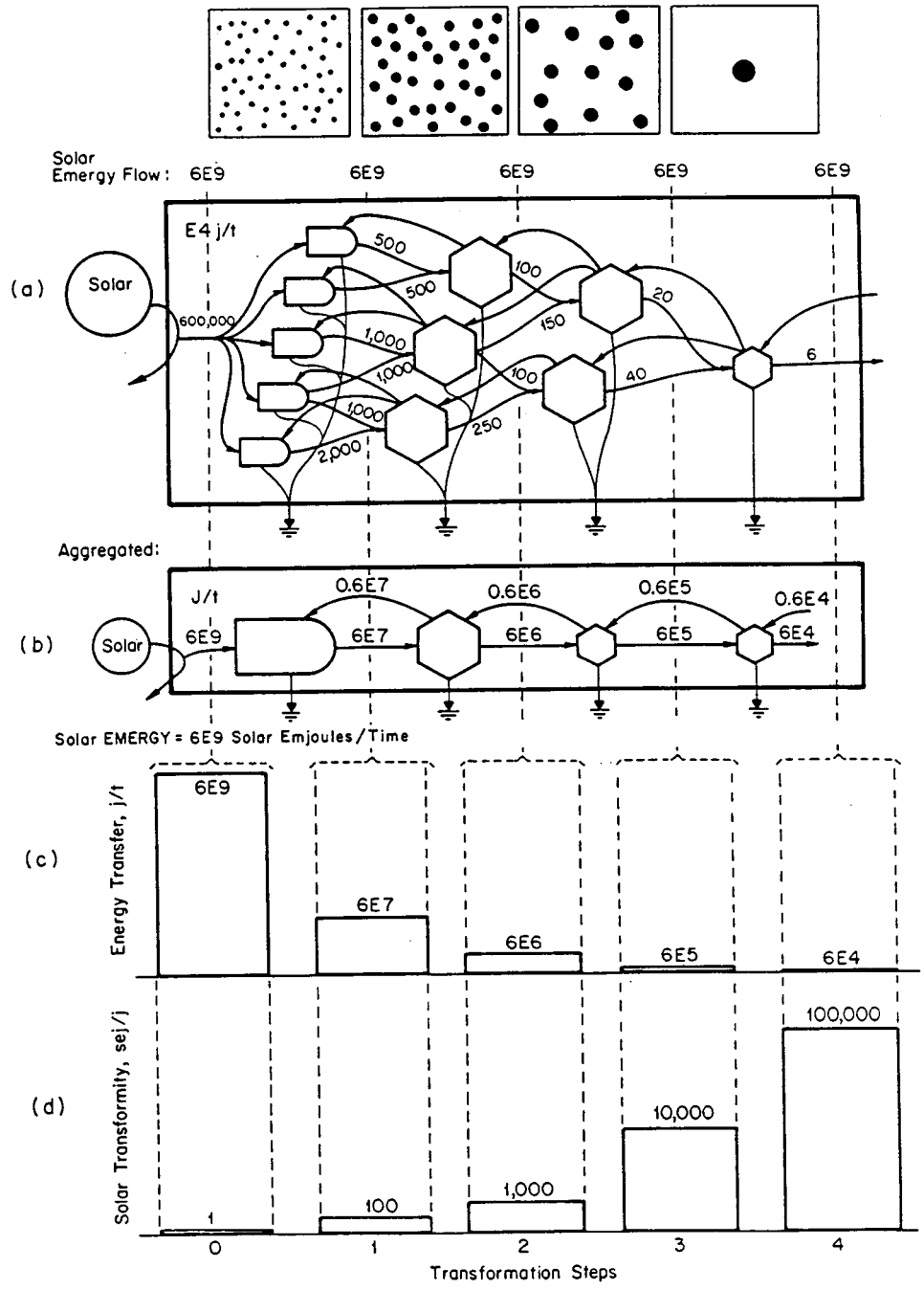

FIGURE 8.16.1 Energy transformation hierarchy: (a) spatial view of units, their sizes, and territories; (b) systems diagram of energy flow web; (c) web aggegated into an energy transformation chain; (d) energy flows between hierarchical levels; (e) transformitites of flows between levels.

TABLE 8.16.1 Typical Solar Transformities

Form of Energy	Solar Transformity sej/J
Solar insolation	1
Chemical energy in rain transpired over land[#]	18,000
Mined coal	40,000
Electric power	174,000
Human service, college graduate	343,000,000

sej/J = solar emjoules per Joule

[#] Gibbs energy relative to sea water salt concentration in leaves, the main energy basis for land plants.

TABLE 8.16.2 EMERGY Evaluation of Lignite Processing in Texas[*]

Note	Item	Data Units/Day J, G, or $	Solar EMERGY/Unit sej/unit	Solar Empower E17 sej/day	Em$ 1995$ Thsd $/yr#
1	Diverted env. product.	7.10 E11 J	1.5 E4/J	0.11	8.5
2	Topsoil lost	5.04 E12 J	6.3 E4/J	3.18	244
3	Fuel used	6.38 E10 J	5.0 E4/J	0.032	2.5
4	Electricity used	3.11 E11 J	1.6 E5/J	0.50	38.5
5	Equipment support	13.8 E6 g	5.7 E9/g	0.79	60.8
6	Goods & service costs	2.8 E5 $	2.2 E12/$	6.2	477
				6.2	477
7	Sum of inputs			10.8	830
8	Lignite yield	2.0 E14 J	3.68 E4/J	73.6	5661

[*] Analysis of Big Brown Plant, Fairfield, Texas (Odum et al., 1987, revised).

[#] Solar empower in Column 5 divided by 1.3 E12 sej/$ for U.S.A., 1995. Net EMERGY ratio = Yield/Inputs = 73.6/10.8 = 6.8

An Example of EMERGY Evaluation, Lignite

The evaluation procedure starts with an aggregated systems diagram to relate inputs, outputs, and main processes. This is used to identify line items in an evaluation table. An example is the analysis of lignite processing at the Big Brown Mine in Fairfield, Texas. Line items for the EMERGY evaluation in Table 8.16.2 were identified from the summarizing systems diagram in Figure 8.16.2. The net EMERGY ratio relates the EMERGY yield to the EMERGY required for the processing. The net EMERGY ratio of 6.8 (Table 8.16.2) means that 6.8 times more real wealth was contributed to the economy than required in the processing. The operation contributed 5.6 million emdollars per day to the economy as lignite yield, almost 12 times more than the economic value of $477,000 dollars per day.

Defining Terms

EMERGY: Available energy of one kind previously required directly and indirectly to make a product or service (unit: emjoules). Example: solar emjoules (abbreviation: sej).

Transformity: EMERGY per unit available energy (units: emjoules per joule). Example: solar emjoules per joule (abbreviation: sej/J).

Empower: EMERGY flow per unit time (units: emjoules per time). Example: solar emjoules per year (abbreviation: sej/yr).

Emdollars: EMERGY divided by EMERGY/money ratio. (abbreviation Em$).

Net EMERGY ratio: Yield EMERGY/EMERGY of purchased inputs.

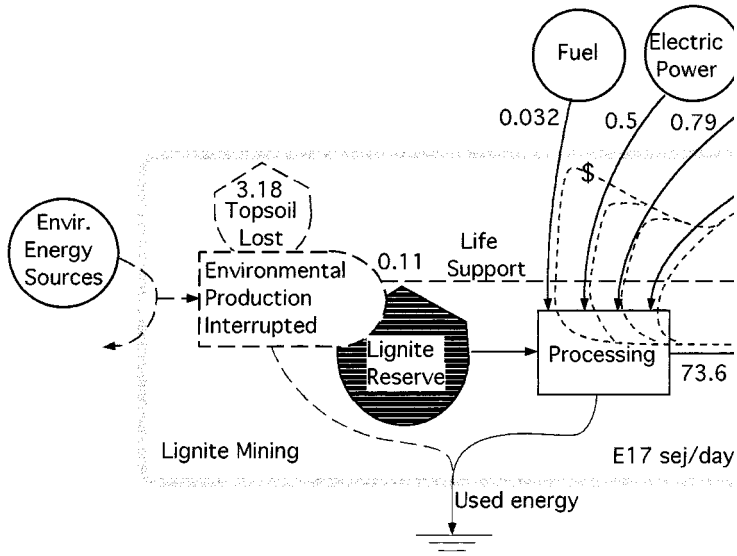

FIGURE 8.16.2 Energy systems diagram and emergy flows of a lignite mining operation evaluated in Table 8.16.2.

References

Odum, H.T., Odum, E.C., and Blissett, M. 1987. Ecology and Economy: "EMERGY" Analysis and Public Policy in Texas. Policy Research Project Report #78, Lyndon B. Johnson School of Public Affairs, The University of Texas, Austin, 178 pp.

Odum, H.T. 1988. Self organization, transformity, and information. *Science* 242, 1132–1139.

Odum, H.T. 1996. *Environmental Accounting, EMERGY and Decision Making*. John Wiley & Sons, New York, 276 pp.

Further Information

Hall, C.A.S., Ed. 1995. *Maximum Power.* University Press of Colorado, Niwot, CO, 393 pp.